Modifications to Dissolved Organic Matter and Disinfection Byproduct Formation during Solar Chlorine Photolysis and Related Oxidative Treatment, as Applied to Drinking Water Treatment

Tessora Young

A dissertation

submitted in partial fulfillment of the

requirements for the degree of

Doctor of Philosophy

University of Washington

2019

Reading Committee:

Michael C. Dodd, Chair

Gregory Korshin

Edward Kolodziej

Silvio Canonica

Program Authorized to Offer Degree:

Civil and Environmental Engineering

University of Washington

Abstract

Modifications to Dissolved Organic Matter and Disinfection Byproduct Formation during Solar Chlorine Photolysis and Related Oxidative Treatment, as Applied to Drinking Water Treatment

Tessora Young

Chair of the Supervisory Committee

Michael C. Dodd

Civil and Environmental Engineering

Chlorine is a common disinfectant used for water treatment worldwide, however not all pathogens can be inactivated using chlorine alone. Solar irradiation of chlorinated waters enhances inactivation of chlorine-resistant pathogens, through in situ formation of ozone and hydroxyl radical during photolysis of free available chlorine (FAC) at UVA/UVB wavelengths of sunlight (290 – 400nm). Organic and inorganic water constituents (e.g., natural organic matter (NOM), bromide, and carbonate) are also reactive with these photooxidants and can be linked to the formation of regulated drinking water disinfection byproducts (DBP). To evaluate the feasibility of this process as a novel water treatment, a variety of relevant surface water matrixes need to be treated via solar chlorine photolysis while monitoring consequent DBP.

A suite of relevant chlorinated and brominated disinfection/oxidation byproducts (some regulated by the U.S. EPA) were monitored including oxyhalides, four trihalomethanes (THMs), and nine haloacetic acids (HAA9). Changes to NOM were characterized by monitoring spectral and redox properties, and molecular weight distributions during solar chlorine photolysis and compared to changes associated with conventional drinking water treatment (e.g., chlorination, ozonation, and advanced oxidation processes (AOP)). The results from this study show formation of DBPs vary significantly with water composition. Chlorate concentrations increased during solar photolysis of FAC (8mg/L as Cl_2) at pH 8, and bromate formation followed similar trends (1.8× increase at pH 8 vs. pH 6) with 200 μg/L bromide. Addition of NOM (Suwannee River) adds a competitor for radical and ozone species, and completely disrupted chlorate and bromate formation mechanisms; less reactive, natural waters limited oxyhalide formation to a lesser degree. Natural organic matter contributes to THM and HAA formation during chlorination and organic DBP yields increased further following solar chlorine photolysis (solar fluences > 4 J/cm^2). Control experiments showed that increased organic DBP levels were not due to direct SRNOM photolysis and subsequent dark reactions with HOCl, but to co-exposure of SRNOM to HOCl and reactive species (e.g., O_3, $HO^{\bullet}$, $Cl^{\bullet}$, $ClO^{\bullet}$) generated by FAC photolysis.

$[ABTS^{\cdot+}]^{-}$ was utilized to quantify changes in the electron donating capacity (EDC) of natural organic matter (NOM) isolates and two model compounds: phenol a model for reactive aromatic moieties, and benzoic acid a model for less reactive aromatic moieties. Low exposures of FAC ($CT_{FAC} = \int[FAC]dt$) significantly decreased the measurable EDC of NOM and phenol, potentially due to rapid halogenation or oxidation of reactive aromatic groups. Once these fast-reacting sites were depleted, the EDC decreased slowly with increasing chlorine exposure. Chlorination resulted in moderate decreases in UV absorbance of the bulk NOM and negligible

changes in fluorescence EEM intensity ($CT_{FAC} \leq 400$ (mg/L as Cl_2)×min). Reactive oxygen species such as ozone and hydroxyl radical (independently or in combination with FAC during solar chlorine photolysis) yielded loss of UV absorbance in the bulk NOM. Pre-treatment of DOM with low exposures of hydroxyl radical (UV/H_2O_2, X-ray radiolysis, or O_2^{-}/O_3) led to increased EDC for NOM and benzoic acid, and increased THM and HAA formation after dark chlorination for NOM, benzoic acid, and phenol, likely due to hydroxylation of aromatics during pretreatment. Radical scavengers (50mM *tert*-butanol) suppressed EDC formation and hindered THM and HAA formation. Exposure to O_3 itself (with radical scavengers added) actually appears to lead primarily to oxidation and/or ring cleavage, rather than hydroxylation which appears to occur due to $HO^{\bullet}$ generated via O_3 decay. X-ray irradiation of hypochlorite at pH 10 (favoring $ClO^{\cdot}$ from reaction between $HO^{\bullet}$ and OCl^{-}) decreased EDC and spectral properties while increasing DBP yields, similar to sunlight-driven chlorine photolysis. Based on these findings, exposure of NOM to ozone, reactive oxygen and halogen species (e.g., $HO^{\bullet}$, $Cl^{\bullet}$, $ClO^{\bullet}$), and FAC during sunlight-driven chlorine photolysis involves hydroxylation of slow reacting aromatic moieties as a key pathway contributing to (a) increased electron donating capacity in aromatic components of the bulk NOM, and (b) increased reactivities toward FAC (and potentially other halogenating agents) to form halogenated organic DBPs. These findings provide an improved understanding of the processes leading to increased formation of DBP precursors during low to moderate exposures of ozone and reactive oxygen or halogen species, and could help identify strategies to minimize organic DBP formation during solar chlorine photolysis or other combinations of chlorine and ROS (such as UVC chlorine photolysis or sequential AOP/FAC treatment) likely to be applied during water and wastewater treatment.

ACKNOWLEDGEMENTS

First and foremost, I would like to express immense gratitude to Michael Dodd, my primary research advisor. His guidance and mentorship was invaluable during my studies at the University of Washington, and taught me as much about myself as the field of environmental engineering. His dedication to teaching students, in the classroom and laboratory, is consistently above and beyond what is expected. He continually strives for excellence and betters those around him. I appreciate the time he devoted to this work, including long hours mulling over new data and gentle guidance when I have felt uncertain or impeded. I am forever thankful to have had this experience working with him the past five years.

I would also like to thank my Ph.D. committee members, Gregory Korshin, Edward Kolodziej, and Silvio Canonica for their input and guidance while completing this dissertation. In particular, I like to thank Silvio for being a superb advisor during my time at Eawag in Dübendorf; his insight and experienced feedback taught me so much. From picking me up to dropping me off at the airport, he was so generous with his time and willing to lend a hand to help; I always felt supported. I also appreciated our group lunches and coffee breaks, they created a sense of home when I was so far from family. I would like to recognize Urs von Gunten, even though we were rarely in the same time zone, he made every effort to provide guidance and mentorship during my visit to Eawag.

I appreciate those who have helped train me in the laboratory, this work would be incomplete without their help. I would like to give thanks to Peiran Zhou for laying the groundwork for this dissertation and training me my first year; to J. Sean Yeung for being a great lab manager at the University of Washington; to Elisabeth Salhi for training me at Eawag and being an excellent lab manager; to Jakov Bolotin for training me to use GC-MS; to Jacqueline

Traber for assisting me with SEC analysis; and to Gordon Getzinger and Kris McNeill for helping me access equipment at ETH Zürich.

I would like to thank my fellow graduate students at the University of Washington: Huan He (it was a pleasure sharing the lab with you for 5 years!), Sin-Yi Liou, Peiran and Nicolette Zhou, Kyle Shimabuku, Siamak Modarresi, Khaled Salam, Bolun Wang, Nick Waldo, and Christina Urbanczyk for building a community and supporting me. I would also like to thank my Eawag colleagues: Sung Lim, Stephanie Remke, Caitlin Proctor, and Caroline Saul for their kindness, friendship and patience with my terrible attempts to speak Swiss German.

Finally, I would like to give thanks to my friends and family. To Eric Brauser, a dedicated partner that has supported me long-distance and in person for seven years; I truly don't think I could have done this without him. To all my current and previous ultimate frisbee teammates for helping me find balance outside of graduate school. To my family for their unconditional love, always believing me and encouraging me to continue through difficult times. I would like to dedicate this work to my mother, Julie Holman, for teaching me to be strong and persevere, and to my father, George Young, for fostered a sense of curiosity and encouraging me to pursue science. Both shared their love of nature and the environment and that has influenced my interest in environmental engineering. In loving memory of my father, you are deeply missed.

TABLE OF CONTENTS

LIST OF FIGURES AND SCHEMES

LIST OF TABLES

Chapter 1. Introduction

1.1. Overview

Chlorine is the most commonly used chemical disinfectant worldwide[1] because it is relatively inexpensive, provides persistent disinfection to many microorganisms (e.g., *Vibrio cholerae* or *Salmonella typhi*), and is safe to consume at low concentrations.[2] Even though chlorination has advanced public health, some important waterborne pathogens are chlorine-resistant and persist after disinfection with chlorine alone. For instance, highly chlorine-resistant oocysts of the protozoan parasites *Cryptosporidium hominis* and *Cryptosporidium parvum* are a frequent cause of waterborne illness in the United States and worldwide.[3, 4] *Cryptosporidiosis* was a leading cause of diarrhea morbidity and mortality in young children (according to the Global Burden of Diseases, Injuries, and Risk Factors study, released 2016) and can also contribute to long term negative health impacts such as malnutrition and stunted growth.[5, 6] Ultraviolet (UV) irradiation and ozonation are both recognized alternative disinfection strategies that can be applied to inactivate of protozoan (oo)cysts and other chlorine-resistant microorganisms; nevertheless, monetary and energy expenses may prevent their use in small-scale drinking water treatment applications.[7, 8]

Exposing chlorinated water to sunlight has been reported to dramatically enhance inactivation of chlorine-resistant *Bacillus subtilis* endospores and highly-chlorine resistant *Cryptosporidium* oocysts when compared to chlorination alone.[9, 10] Photolysis of free chlorine by solar wavelengths of UV light (i.e., UVB/UVA wavelengths from 290-400 nm) produces hydroxyl radical ($HO^{\bullet}$), chlorine atom ($Cl^{\bullet}$), and, if dissolved oxygen (O_2) is present, ozone (O_3).[9-14] O_3 and $HO^{\bullet}$ in particular are strong oxidants that can enhance disinfection during chlorination by damaging protective spore and cyst coats.[9, 10, 15, 16] Considering the low cost and widespread availability of chlorine, solar chlorine photolysis could provide a unique and

effective option for enhancing disinfection and could be utilized as a decentralized drinking water treatment similarly to conventional solar disinfection (SODIS)[17]. This treatment alternative would be especially valuable in remote areas or during periods with limited resources – for example, military operations, emergency response scenarios (e.g., natural disaster or refugee encampment), or underserved communities in developing countries.

When evaluating a novel drinking water disinfection treatment, one must also consider the formation of disinfection byproducts (DBP) before recommending or prescribing its use. Beyond microbial impacts, the oxidative and radical species formed during solar chlorine photolysis are also reactive with inorganic and organic constituents typically present in untreated surface and groundwater sources. For example, bromate has been identified as a product formed during ozonation of solutions containing bromide,[18] and is regulated by the U.S. EPA because it is likely carcinogenic to humans.[19] Free chlorine can react with naturally occurring organic matter (NOM), typically a heterogeneous mixture of vegetative and biological decay products, and form haloalkanes, such as chloroform. The occurrence of trihalomethanes and haloacetic acids in treated drinking water spurred the U.S. EPA to regularly monitor and regulate these classes of chlorinated and brominated compounds after toxicity effects were observed in mammalian cells[20, 21] and rodents.[22] However, the lifesaving benefits from disinfection should not be forgotten or compromised. A miscalculation of water treatment risks resulted in a cholera epidemic sweeping through Lima, Peru in 1991 (killing over 4,000 people) after fears of increased cancer incidence associated with disinfection byproduct formation led local water officials to cease chlorine disinfection in potable water without implementing an alternative residual disinfectant.[23] A complete evaluation of long-term and acute public health risks is essential when individuals or governing bodies make decisions regarding responsible water

treatment and management.

The objectives of this study were to (i) systematically quantify regulated disinfection byproduct formation during solar chlorine photolysis, under relevant drinking water treatment conditions, (ii) characterize changes to dissolved organic matter and model compounds during oxidation, solar irradiation, and combined exposures experienced during solar chlorine photolysis, and (iii) identify reactive species that contribute to disinfection byproduct formation, with the ultimate objective of facilitating practical implementation of solar chlorine photolysis by balancing the benefits of enhanced disinfection with the costs of toxic oxidative byproducts.

Experiments with relevant oxidants (or mixtures) and solar irradiation alone, were included in this project to evaluate their influence on water constituents during solar chlorine photolysis and relevant background information is provided for each.

1.2. Free Chlorine

Free chlorine is a well-known disinfectant that has been used for drinking water treatment in the US since 1908.[24] Chlorine can inactivate a variety of waterborne pathogenic microorganisms and its use in drinking water treatment has reduced the number of outbreaks over the past 100 years.[24] Free available chlorine (FAC) is typically introduced to water as chlorine gas (Cl_2), sodium hypochlorite solution (NaOCl), or solid calcium hypochlorite ($Ca(OCl)_2$), and each will ultimately form hypochlorous acid/hypochlorite in near-neutral aqueous solution. Temperature and pH directly impact chlorine reactivity and microbial inactivation rates. Solution pH determines the speciation of FAC; which is a weak acid with a pKa within pH ranges relevant to environmental conditions and typical drinking water treatment, Equation 1.1. The two dominant species of aqueous FAC have different redox potentials, in

which HOCl is the more effective oxidant and disinfectant (70-80× greater)[25] (Equation 1.2 and 1.3).

$$HOCl \rightleftarrows H^+ + OCl^- \quad (pK_a = 7.5, \text{ at } 25\ ^\circ C) \tag{1.1}$$

$$HOCl + H^+ + 2e^- \rightarrow Cl^- + H_2O, \quad E^0(V) = +1.482 \tag{1.2}$$

$$OCl^- + H_2O + 2e^- \rightarrow Cl^- + 2OH^-, \quad E^0(V) = +0.81 \tag{1.3}$$

Temperature will also impact chlorine reaction rates and influence prescribed chlorine exposure to incur a microbial inactivation target. The Arrhenius equation, Equation 1.4, describes the general temperature dependence of rate constants, in which chlorine reaction rate constants (and germicidal reaction rate constants) increase with increasing temperature.[26] In Equation 1.4, k is the reaction rate constant, k_0 is the frequency factor, E is the activation energy, R is the universal gas constant, and T is absolute temperature.

$$k = k_0 e^{E/RT} \tag{1.4}$$

The chlorine exposure, denoted CT_{FAC}, is estimated as the sum of the chlorine concentration over the contact time, t; the equation for which is shown in Equation 1.5.

$$CT_{FAC} = \int_0^t [FAC]dt \tag{1.5}$$

Disinfectant exposure, calculated as CT, can be used to estimate microbial inactivation kinetics as modelled by Chick-Watson Law, shown in Equation 1.6.

$$\ln(N / N_0) = -k \times CT \tag{1.6}$$

where N is the number/concentration of surviving pathogens, N_0 is the initial number/concentration of the pathogen, k is the second order rate constant for inactivation, and the disinfectant CT is calculated in Equation 1.5.

Chlorine is also an oxidant and will react with organic and inorganic constituents present in surface water or groundwater. During water treatment FAC is sometimes used to oxidize iron, manganese, and taste and odor compounds, or to bleach organic discoloration.[26] A major disadvantage for using chlorine as a disinfectant results from reactions with natural organic matter (NOM) during chlorination, leading to the formation of organic disinfection byproducts. Chlorine can also react with bromide in solution and form hypobromous acid/hypobromite ($HOBr/OBr^-$), an effective halogenating agent that can introduce brominated disinfection byproducts. Regulated halogenated organic DBPs include total trihalomethanes (TTHM) (sum of chloroform, bromodichloromethane, dibromochloromethane, and bromoform) and five haloacetic acids (HAA5) (sum of mono-, di-, and trichloroacetic acid and mono- and dibromoacetic acid). Extensive use of chlorine as a primary and/or residual disinfectant has led to increased detection of halogenated disinfection byproducts and spurred water managers to consider precursor control (e.g., NOM removal via flocculation and filtration) and alternative disinfection strategies.[25] Even before reacting with water constituents, added chlorine can introduce inorganic byproducts such as chlorate and chlorite that form during the production and storage of chlorine stock solutions.[27, 28] Using chlorine gas as a chlorine source can reduce the concentration of oxyhalide DBPs, but storage and transport of the dense toxic gas carries its own risks for operators and the surrounding areas.

Several empirically-derived models (e.g., empirical power function models) have been proposed to predict DBP formation, each typically focusing on regulated groups but some also

include unregulated groups, such as nitrogenous DBPs.[29-31] Due to time and data restrictions most models focus on a few natural water sources or prepare synthetic water matrixes (decreasing the accuracy of these models when applied to source waters outside of the selected set for model-training). However, Obolensky and Singer (2008) developed a DBP model from the Information Collection Rule (ICR) sampling dataset and was able to achieve adequate fit for many chlorine-containing DBPs.[32] Even with the ICR dataset, low yields at water treatment plants interfered with model development for bromoform and brominated HAAs.[32] Published chlorination models have used many inputs but commonly used dependent variables include temperature, chlorine/DOC concentration ratio, reaction time, pH, and bromide concentration.[29-31, 33-35] Sampling from within the distribution system adds additional uncertainty (specifically for estimating reaction time and chlorine consumption) and may require additional modelling to predict flow percentages through arms of the distribution framework.[36, 37] Chlorination of NOM in drinking water treatment has been investigated thoroughly for a range of natural sources and waste effluents, though mechanisms for organic DBP formation are still largely unknown as intermediates are still very difficult to isolate and identify.

1.3. Ozone

Ozone is a strong oxidant that is utilized in drinking water treatment as an advanced disinfectant or oxidant, e.g. for removal of taste and odor compounds or micropollutants. Ozone was first applied in water treatment in Oudshoorn, Netherlands (1893) and Nice, France (1906).[38] Ozonation at a water treatment plant begins by forming ozone gas on site via electrical corona discharge in the presence of oxygen within an ozone generator. Then the ozone/oxygen gas mixture is bubbled through water in a contact chamber. Due to the cost of generating ozone, it is

typically only applied in large drinking or waste water treatment plants, even though it is capable of inactivating chlorine-resistant pathogens such as cryptosporidium oocysts[4] and oxidizing contaminants such as algal toxins (e.g., Microcystin-LR[39]) and pharmaceuticals.[40] Ozone is strong enough to oxidize components of natural organic matter directly; additionally ozonation forms ozonide ($O_3^{\cdot-}$), superoxide ($O_2^{\cdot-}$), and hydroxyl radical ($HO^{\cdot}$) as it decays, which can also react with organic matter and other water constituents.[41, 42] Despite the many benefits of ozone water treatment, there are some drawbacks. First, ozonation of water containing bromide can result in formation of bromate (a suspected carcinogen) and hypobromous acid which can react with NOM and form brominated DBPs. Second, ozonation has been observed to breakdown NOM and increase the fraction of biodegradable dissolved organic carbon,[43] which can accelerate bacterial growth later in the treatment train or distribution system. Third, ozone is not stable in water and cannot provide continued disinfection protection. Due to the instability of ozone, chlorine or another chlorine-containing oxidant such as chloramine or chlorine dioxide is typically added in the last step of the treatment train to provide residual disinfection within the distribution system.

$$O_3 + e^- + H^+ \rightarrow O_2 + HO^{\bullet}, \quad (E^0(V) = +1.43) \tag{1.7}$$

$$O_3 + 2e^- + 2H^+ \rightarrow O_2 + H_2O, \quad (E^0(V) = +2.08) \tag{1.8}$$

Ozone is a strong, selective oxidant that can participate in one- and two-electron transfer redox reactions; the half reactions are shown in Equations 1.7 and 1.8. Ozone can oxidize organic and inorganic species via formation of an intermediate adduct (resulting in oxygen atom transfer, electron transfer, or formation of an oxyl radical) or criegee ozonolysis and ring formation.[39] Ozone is not stable in water (especially at high pH) as it can react with hydroxide

(OH^-) to form superoxide ($HO_2^{\cdot}$), which can react further with ozone to form ozonide radical ($O_3^{\cdot -}$). Ozonide radical will directly decay to produce dissolved oxygen and hydroxyl radical,[44] which can react with organic compounds. Carbon-centered radicals (from electron transfer or H-abstraction reactions with hydroxyl radical) can react with dissolved oxygen and produce more superoxide radical; completing a catalytic ozone decomposition cycle.[41] Inorganic constituents in water can also react with ozone and related reactive oxygen species (ROS), including hydroxyl radical. As previously mentioned, bromate is a regulated disinfection byproduct and it is formed via reaction of bromide with ozone and hydroxyl radical.[18] Ozone reactions with aromatic moieties in NOM often result in formation of ketones and aldehydes,[39] which are suspected disinfection byproduct precursors upon chlorination.[45] Ozone use in drinking water treatment requires monitoring and control to benefit from advanced disinfection and oxidation without forming excessive levels of disinfection byproducts.[46]

1.4. Hydroxyl Radical

Hydroxyl radical is one of the strongest oxidants used in water treatment and has the added benefit of being a non-selective oxidant, reacting via addition, electron transfer, or H-abstraction. Hydroxyl radical is produced via a variety of advanced oxidation processes (AOPs), including: H_2O_2 photolysis,[47, 48] O_3/H_2O_2 (peroxone),[42] Fenton or photo-Fenton reactions,[49] NO_3^- / NO_2^- photolysis,[50] and pulse radiolysis.[51] AOPs can be used to break down undesirable organic compounds in water such as pharmaceuticals and personal care products (PPCP), and taste and odor compounds (e.g., geosmin or 2-methylisoborneol) that are difficult to remove by other means.[52-57] However, AOPs typically require additives such as hydrogen peroxide or iron to enhance radical production during ozonation or UV irradiation treatment which may also require

additional treatment to remove any residual additive. For many utilities it may be cost-prohibitive to utilize AOPs to treat large volumes of water for drinking water and wastewater treatment as many target contaminants are only present at trace concentrations. Additionally, contaminant removal efficiency could be compromised via radical scavenging from common water constituents,[39] such as natural organic matter and bicarbonate/carbonate.[58]

The oxidation half-reaction for hydroxyl radical, shown in Equation 1.9, has the highest redox potential discussed thus far. The high reactivity of hydroxyl radical is also a potential drawback as the radical species is short-lived in solution.

$$HO^{\bullet} + e^{-} + H^{+} \rightarrow H_2O, \quad (E^0(V) = +2.70) \tag{1.9}$$

Radiation chemistry has also been studied as a radical source and has been applied to many kinetic studies; specifically X-ray and γ-radiolysis. X-ray electromagnetic radiation is capable of exciting and ionizing water and has been utilized as a radical source. When exposed to electromagnetic radiation water will dissociate and form radical species and molecular products, Equation 1.10.

$$H_2O^{*} \rightarrow e^{-}_{aq}, HO^{\bullet}, H^{\bullet}, H_2O_2, \text{ and } H_2 \tag{1.10}$$

The radical product yields in Equation 1.10 vary and are dependent on the solution conditions; with air-saturated conditions at pH 7, G values are: $H_2O^{*} = 4.3 \times 10^{-7}$ mol/J, $H^{\cdot} = 6.7 \times 10^{-8}$ mol/J, $e^{-}_{(aq)} = 2.75 \times 10^{-7}$ mol/J, $HO^{\cdot} = 2.85 \times 10^{-7}$ mol/J, and $H_2O_2 = 7.25 \times 10^{-8}$ mol/J.[59] Experimental solutions can be saturated with nitrous oxide (N_2O) and oxygen to increase hydroxyl radical yields according to Equations 1.11 and 1.12.[58, 60]

$$e^{-}_{aq} + N_2O(g) + H_2O \rightarrow HO^{\bullet} + HO^{-} + N_2(g) \tag{1.11}$$

$$H^{\bullet} + N_2O(g) \rightarrow HO^{\bullet} + N_2(g) \tag{1.12}$$

Radiolysis methods are advantageous for researching the isolated impact of hydroxyl radical with targeted compounds, but implementation for water treatment is typically unrealistic due to high energy costs and the potential safety hazards of human exposure to radiation sources.

1.5. UV and Solar irradiation

Ultraviolet (UV) light is another electromagnetic radiation source — with wavelengths spanning 100–400 nm — that can be utilized as a powerful tool to photolyze compounds or damage RNA or DNA, resulting in pathogen inactivation. These photochemical reactions are dependent on the radiation energy (inversely related to wavelength), the absorption spectra of the target molecule, and the quantum yield from the excited state of the molecule for the specific conditions. UVC (200–280nm) light is optimal for microbial disinfection; the germicidal wavelengths (245–285nm) modify DNA and RNA directly via nucleic acid absorption and dimer formation, or to a lesser degree, indirectly via damage from reactive species formed photochemically within the microorganism.[61] A contact time of seconds may be sufficient for drinking water disinfection in low turbidity water,[62] but energy costs can be significant to operate high-output UV lamps and irradiation times requirements will increase with increasing turbidity. UV irradiation also does not provide residual disinfection, so a secondary disinfectant is needed in tandem with photo-treatment to protect water from beyond the plant as some microorganisms are able to repair UV damaged DNA nucleotides and become active again.[63] .

While high energy UV lamps may be expensive to operate and maintain, solar irradiation is readily available and can be used directly via SODIS (solar disinfection). UV irradiation from sunlight (specifically UVB: 280–315 nm, and UVA: 315–400 nm) has also been observed to cause damage to DNA via ROS formation within the cell.[64] SODIS can also benefit from

infrared radiation increasing the solution thermal energy, however enhancements to the reactors may be required to improve heat retention.[17] Solar irradiation of natural waters can produce H_2O_2, $HO^{\cdot}$ and triplet state DOM ($^3DOM^*$) directly,[65] leading to other secondary radicals in solution. Solar irradiation of DOM can also photochemically generate singlet oxygen ($^1O_2$),[66] an excited state of molecular oxygen that can transform olefinic and phenolic moieties, photo-bleach NOM, and damage cells via reactions with proteins and biomolecules.[67] Hydrophobic chromophoric moieties within the natural organic matter have been identified as naturally occurring photosensitizers.[65, 67] Solar irradiation fluence requirements to target hydroxyl radical and singlet oxygen production from DOM directly are unrealistic for high throughput environmental engineering applications, but this process is very relevant in environmental systems and may contribute to solar disinfection.

1.6. Solar Photolysis of Free Chlorine

As mentioned earlier in the introduction, solar irradiation of chlorinated water (UVA/UVB irradiation 290-400 nm) results in direct photolysis of chlorine and subsequent formation of reactive oxygen and halogen species. Comparing the molar absorptivity of FAC, the spectral irradiance for simulated and natural sunlight (Figure 1.1), and the quantum yields of HOCl and OCl^- photolysis at 313 and 365 nm (Table 1.1), it can be stated that OCl^- is more efficiently photolyzed by solar light than HOCl.

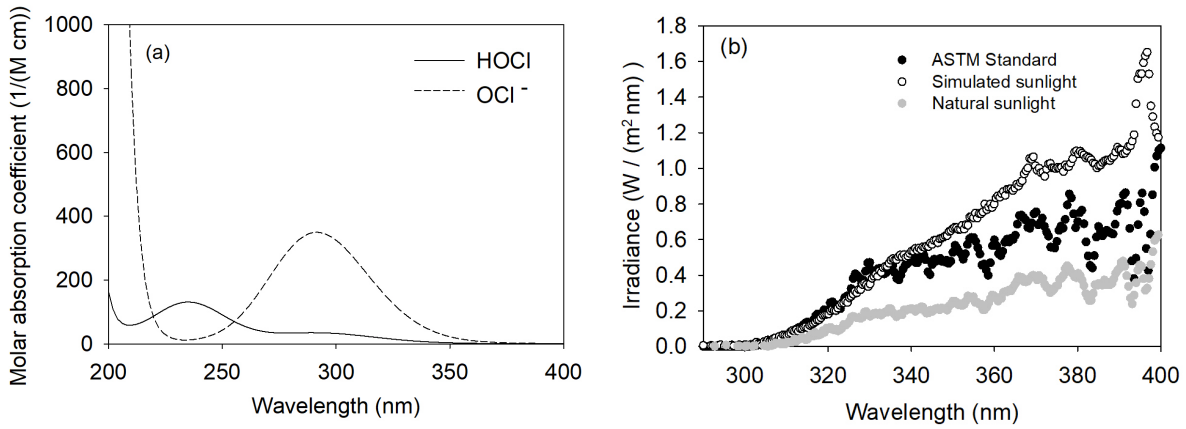

Figure 1.1. (a) Molar extinction coefficients of hypochlorous acid and hypochlorite[9]; **(b)** direct incident spectral irradiance curves between 290 and 400 nm for to the ASTM G173-03 solar irradiance standard (hemispherical on a 37º tilted surface); the Atlas SunTest Solar Simulator (with atmospheric filter and infrared radiation filter) centered and at the surface of irradiated reactor solutions, directly facing the light source; and natural sunlight on the roof of More Hall (Seattle, WA) at 3:00PM on 09/30/2016, at an angle of 45º from the horizontal facing the sun. Spectroradiometric measurements were taken using an Ocean Optics USB2000+ XR spectroradiometer equipped with a 200 μm × 2 m optical fiber and a CC-3-UV-S cosine corrector. Adapted from Young et al. (2018)[68]

Table 1.1. Summary of chlorine photolysis reactions and quantum yields

		Φ(254 nm)	Φ(313 nm)	Φ(365 nm)
$HOCl \xrightarrow{h\nu} HO^{\bullet} + Cl^{\bullet}$	(1.13a)	0.46-1.4 [69-71]	1 [72*]	N/A
$OCl^{-} \xrightarrow{h\nu} O^{\bullet -} + Cl^{\bullet}$	(1.13b)	0.278 [73]	0.127 [73]	0.08 [73]
$OCl^{-} \xrightarrow{h\nu} O(^{3}P) + Cl^{-}$	(1.14)	0.074 [73]	0.075 [73]	0.28 [73]

*at approximately 310 nm, N/A = not available

During photolysis free chlorine will undergo homolytic cleavage, forming hydroxyl radical and chlorine radical ($Cl^{\cdot}$) simultaneously (Equation 1.13).[11, 12] $Cl^{\cdot}$ is very reactive and can undergo electron transfer, H-abstraction, and addition reactions. Once formed, $Cl^{\cdot}$ contribute to formation of additional reactive chlorine species (RCS), such as reaction with chloride forming dichloride radical anion ($Cl_2^{\cdot -}$) (Equation 1.15) or reaction with hypochlorite to form chlorine

oxide radical ($ClO^{\cdot}$) (Equation 1.16).

$$Cl^{\bullet} + Cl^{-} \rightarrow Cl_2^{\bullet -} \quad (1.15)$$

$$Cl^{\bullet} + OCl^{-} \rightarrow ClO^{\bullet} + Cl^{-} \quad (1.16)$$

The formation of these RCS and hydroxyl radical during chlorine photolysis can enhance degradation of organic compounds that are recalcitrant to chlorine oxidation.[74-76] The homolytic photolysis pathway is the basis for chlorine photolysis AOPs, with UVC/chlorine treatment targeting lower wavelengths (254 nm) and slightly acidic conditions to favor HOCl photolysis.[77]

Hypochlorite also undergoes heterolytic cleavage to form atomic oxygen ($O(^3P)$) (Equation 1.14), and this photolysis pathway quantum yield is increased at higher wavelengths (Table 1.1). Atomic oxygen will react with dissolved oxygen in solution to form ozone, as seen in Equation 1.17. Hypochlorite will also compete with dissolved oxygen to react with $O(^3P)$ and produce ClO_2^- (Equation 1.18), and further reaction with ozone can form chlorine dioxide (Equation 1.19).

$$O(^3P) + O_2 \rightarrow O_3 \quad (1.17)$$

$$O(^3P) + OCl^{-} \rightarrow ClO_2^{-} \quad (1.18)$$

$$ClO_2^{-} + O_3 \rightarrow O_3^{\bullet -} + ClO_2 \quad (1.19)$$

While solar chlorine photolysis has the potential to mitigate acute health risks (enabling inactivation of chlorine-susceptible *and* chlorine-resistant pathogens)[9, 10], its possible long-term health implications (i.e. toxic disinfection byproduct formation) must also be explored before its use a drinking water treatment alternative can be recommended.

FAC and the various reactive oxygen species (ROS) and reactive chlorine species (RCS) generated during FAC photolysis also react with inorganic and organic water constituents – such as bromide and dissolved organic matter – that can serve as disinfection byproduct (DBP)

precursors. UVC photolysis of FAC has been investigated as an AOP applied to degradation of pharmaceuticals and personal care products (PPCP) with conditions favoring HOCl photolysis and hydroxyl radical formation.[78-83] Other research groups have evaluated DBP formation in DOM-containing waters during UVC-driven chlorine photolysis, however conflicting results have been reported regarding whether UVC chlorine photolysis treatment leads to *increased* DBP formation (e.g., due to precursor formation via hydroxylation and aromatic ring opening by hydroxyl radical or other radical species)[75, 78, 79, 84] or *decreased* DBP formation due to precursor degradation or DOM mineralization,[81, 85] when compared to chlorination alone.

Comparatively little information is available regarding the potential impacts of sunlight-driven FAC photolysis on DBP formation.[11, 13, 79, 86] In comparison to UVC-driven FAC photolysis, solar FAC photolysis ($\lambda > 290$ nm) proceeds to a greater extent through OCl^- heterolysis (particularly above pH 7.5) – yielding ground-state atomic oxygen (Eq. 1.11), in addition to O_3 under oxic conditions (Eq. 1.12).[14] Previous work investigating sequential exposure of DOM to O_3 and chlorine has shown that high O_3 doses can decrease DBP formation by degrading DBP precursors, whereas low O_3 doses can increase DBP formation, especially under conditions favoring $HO^\bullet$ formation.[87-89] The impact of simultaneous DOM exposure to FAC, O_3, and $HO^\bullet$ or other radicals during solar FAC photolysis is less clear, and a comprehensive evaluation of this reaction chemistry has yet to be undertaken. Several groups have noted degradation of algal toxins[90] and PPCPs,[76, 91] decreases in total organic halogens (TOX) within reclaimed water,[92] and degradation of naphthenic acids within oil sand process water[93] after sunlight-driven FAC photolysis. Others have reported increasing formation of organochlorine, trihalomethanes (THMs), and haloacetic acid (HAAs), coupled with significant degradation of chromophores and fluorophores, during treatment of organic precursors with FAC

and artificial UVA light sources (λ_{peak} ~ 350-365 nm) when compared to dark chlorination.[13, 79] However, there is limited information on formation of specific classes of DBPs during broadband simulated or natural solar irradiation of chlorinated water, or the corresponding impacts on DOM and DBP precursors during the application of this process for drinking water treatment.

1.7. References

1. WHO *Guidelines for drinking-water quality: fourth edition incorporating the first addendum*; License: CC BY-NC-SA 3.0 IGO; World Health Organization (WHO): Geneva, 2017.

2. Cheung, P. C. W., A historical review of the benefits and hypothetical risks of disinfecting drinking water by chlorination. *Journal of Environment and Ecology* **2017,** *8* (1), 73-145.

3. Painter, J. E.; Hlavsa, M. C.; Collier, S. A.; Xiao, L. H.; Yoder, J. S., Cryptosporidiosis Surveillance - United States, 2011-2012. *Mmwr Surveill Summ* **2015,** *64* (3), 1-13.

4. Medema, G. T., P., Blokker,M.; Deere,D.; Davidson,A.; Charles,P.; and Loret, J.F., Risk Assessment of Cryptosporidium in Drinking Water. Public Health and Environment: Water, S., Hygiene and Health, Ed. WHO Press: Geneva, Switzerland, 2009.

5. Sarkar, R.; Tate, J. E.; Ajjampur, S. S. R.; Kattula, D.; John, J.; Ward, H. D.; Kang, G., Burden of Diarrhea, Hospitalization and Mortality Due to Cryptosporidial Infections in Indian Children. *PLOS Neglected Tropical Diseases* **2014,** *8* (7), e3042.

6. Khalil, I. A.; Troeger, C.; Rao, P. C.; Blacker, B. F.; Brown, A.; Brewer, T. G.; Colombara, D. V.; De Hostos, E. L.; Engmann, C.; Guerrant, R. L.; Haque, R.; Houpt, E. R.; Kang, G.; Korpe, P. S.; Kotloff, K. L.; Lima, A. A. M.; Petri, W. A.; Platts-Mills, J. A.; Shoultz, D. A.; Forouzanfar, M. H.; Hay, S. I.; Reiner, R. C.; Mokdad, A. H., Morbidity, mortality, and long-term consequences associated with diarrhoea from Cryptosporidium infection in children younger than 5 years: a meta-analyses study. *The Lancet Global Health* **2018,** *6* (7), e758-e768.

7. Cho, M.; Kim, J. H.; Yoon, J., Investigating synergism during sequential inactivation of Bacillus subtilis spores with several disinfectants. *Water Res* **2006,** *40* (15), 2911-2920.

8. EPA, U. S., Technologies and Cost Document for the Final Long Term 2 Enhanced Surface Water Treatment Rule and Final Stage 2 Disinfectants and Disinfection Byproducts Rule. Water, O. o., Ed. National Service Center for Environmental Publications: 2005.

9. Forsyth, J. E.; Zhou, P. R.; Mao, Q. X.; Asato, S. S.; Meschke, J. S.; Dodd, M. C., Enhanced Inactivation of Bacillus subtilis Spores during Solar Photolysis of Free Available Chlorine. *Environ Sci Technol* **2013,** *47* (22), 12976-12984.

10. Zhou, P.; Di Giovanni, G. D.; Meschke, J. S.; Dodd, M. C., Enhanced Inactivation of Cryptosporidium parvum Oocysts during Solar Photolysis of Free Available Chlorine. *Environ Sci Tech Let* **2014,** *1* (11), 453-458.

11. Nowell, L. H.; Hoigne, J., Photolysis of Aqueous Chlorine at Sunlight and Ultraviolet Wavelengths .2. Hydroxyl Radical Production. *Water Res* **1992,** *26* (5), 599-605.

12. Nowell, L. H.; Hoigne, J., Photolysis of Aqueous Chlorine at Sunlight and Ultraviolet Wavelengths .1. Degradation Rates. *Water Res* **1992,** *26* (5), 593-598.

13. Oliver, B. G.; Carey, J. H., Photochemical Production of Chlorinated Organics in Aqueous-Solutions Containing Chlorine. *Environ Sci Technol* **1977,** *11* (9), 893-895.

14. Buxton, G. V.; Subhani, M. S., Radiation-Chemistry and Photochemistry of Oxychlorine Ions .2. Photodecomposition of Aqueous-Solutions of Hypochlorite Ions. *J Chem Soc Farad T 1* **1972,** *68*, 958-&.

15. Cho, M.; Yoon, J., Measurement of OH radical CT for inactivating Cryptosporidium parvum using photo/ferrioxalate and photo/TiO2 systems. *J Appl Microbiol* **2008,** *104* (3), 759-766.

16. Cho, M.; Yoon, J., Quantitative evaluation and application of Cryptosporidium parvum inactivation with ozone treatment. *Water Sci Technol* **2007,** *55* (1-2), 241-250.

17. McGuigan, K. G.; Conroy, R. M.; Mosler, H. J.; du Preez, M.; Ubomba-Jaswa, E.; Fernandez-Ibanez, P., Solar Water Disinfection (SODIS): A review from bench-top to roof-top. *Journal of Hazardous Materials* **2012,** *7* (53), 29-46.

18. von Gunten, U.; Oliveras, Y., Advanced Oxidation of Bromide-Containing Waters - Bromate Formation Mechanisms. *Environmental Science and Technology* **1998,** *32*, 63-70.

19. Kurokawa, Y.; Hayashi, Y.; Maekawa, A.; Takahashi, M.; Kokubo, T.; Odashima, S., Carcinogenicity of Potassium Bromate Administered Orally to F344 Rats. *Journal of the National Cancer Institute* **1983,** *71* (5), 965-972.

20. Plewa, M. J.; Wagner, E. D.; Muellner, M. G.; Hsu, K. M.; Richardson, S. D., Comparative Mammalian Cell Toxicity of N-DBPs and C-DBPs. *Disinfection by-Products in Drinking Water: Occurrence, Formation, Health Effects, and Control* **2008,** *995*, 36-50.

21. Plewa, M. J.; Simmons, J. E.; Richardson, S. D.; Wagner, E. D., Mammalian cell cytotoxicity and genotoxicity of the haloacetic acids, a major class of drinking water disinfection by-products. *Environmental and Molecular Mutagenesis* **2010,** *51*, 871-878.

22. Jorgenson, T. A.; Meierhenry, E. F.; Rushbrook, C. J.; Bull, R. J.; Robinson, M., Carcinogenicity of chloroform in drinking water to male Osborne-Mendel rats and female B6C3F1 mice. *Fundamental and Applied Toxicology* **1985,** *5* (4), 760-769.

23. Anderson, Cholera epidemic traced to risk miscalculation. *Nature* **1991,** *354* (6351), 255-255.

24. CDC Disinfection with Chlorine. (accessed 11/24/2018).

25. EPA, U. S., Alternative Disinfectants and Oxidants Guidance Manual. Water, U. S. E. P. A. E.-O. o., Ed. 1999.

26. EPA *Water Treatment Manual: Disinfection*; Environmental Protection Agency (EPA): Cincinnati, OH, 2011.

27. Garcia-Villanova, R. J.; Leite, M. V. O. D.; Hernandez-Hierro, J. M.; Alfageme, S. D.; Hernandez, C. G., Occurrence of bromate, chlorite and chlorate in drinking waters disinfected with hypochlorite reagents. Tracing their origins. *Science of the Total Environment* **2010,** *408* (12), 2616-2620.

28. Stanford, B. D., Perchlorate, Bromate, and Chlorate in Hypochlorite Solutions: Guidelines for Utilities (vol 103, pg 71, 2011). *Journal American Water Works Association* **2011,** *103* (8), 100-100.

29. Chowdhury, S.; Champagne, P.; McLellan, P. J., Models for predicting disinfection byproduct (DBP) formation in drinking waters: a chronological review. *Science of the Total Environment* **2009,** *407*, 4189-4206.

30. Chen, B.; Westerhoff, P., Predicting disinfection by-product formation potential in water. *Water research* **2010,** *44* (13), 3755-3762.

31. Sohn, J.; Amy, G.; Cho, J. W.; Lee, Y.; Yoon, Y., Disinfectant decay and disinfection by-products formation model development: chlorination and ozonation by-products. *Water Research* **2004,** *38* (10), 2461-2478.

32. Obolensky, A.; Singer, P. C., Development and interpretation of disinfection byproduct formation models using the Information Collection Rule database. *Environmental Science & Technology* **2008,** *42* (15), 5654-5660.

33. Fabbricino, M.; Korshin, G. V., Modelling disinfection by-product formation in bromide-containing waters. *Journal of Hazardous Materials* **2009,** *168*, 782-786.

34. Hong, H. C.; Liang, Y.; Han, B. P.; Mazumder, A., Modelling of trihalomethane (THM) formation via chlorination of the water from Dongjiang River. *Science of the Total Environment* **2007,** *385*, 48-54.

35. Roccaro, P.; Korshin, G. V.; Cook, D.; Chow, C.; Drikas, M., Effects of pH on the speciation coefficients in models of bromide influence on the formation of trihalomethanes and haloacetic acids. *Water Research* **2014,** *62*, 117-126.

36. Charisiadis, P.; Andra, S.; Makris, K.; Christophi, C.; Skarlatos, D.; Vamvakousis, V.; Kargaki, S.; Stephanou, E., Spatial and seasonal variability of tap water disinfection by-products within distribution pipe networks. *Science of the Total Environment* **2015,** *506*, 26-35.

37. Courtis, B.; West, J.; Bridgeman, J., Chlorine demand-based predictive modeling of THM formation in water distribution networks. *Urban Water Journal* **2009,** *6* (6), 407-415.

38. Rideal, E. K., *Ozone*. D. Van Nostrand Company: 1920.

39. von Gunten, U., Ozonation of drinking water: Part 1. Oxidation kinetics and product formation. *Water Research* **2003,** *37*, 1443-1467.

40. Huber, M. M.; Canonica, S.; Park, G.-Y.; Von Gunten, U., Oxidation of pharmaceuticals during ozonation and advanced oxidation processes. *Environmental science & technology* **2003,** *37* (5), 1016-1024.

41. Staehelin, J.; Hoigne, J., Decomposition of ozone in water in the presence of organic solutes acting as promoters and inhibitors of radical chain reactions. *Environmental Science and Technology* **1985,** *19* (12), 1206-1213.

42. Staehelin, J.; Hoigne, J., Decomposition of ozone in water: rate of initiation by hydroxide ions and hydrogen peroxide. *Environmental Science & Technology* **1982,** *16* (10), 676-681.

43. Volk, C.; Roche, P.; Joret, J.-C.; Paillard, H., Comparison of the effect of ozone, ozone-hydrogen peroxide system and catalytic ozone on the biodegradable organic matter of a fulvic acid solution. *Water Research* **1997,** *31* (3), 650-656.

44. Sehested, K.; Holcman, J.; Bjergbakke, E.; Hart, E. J., Formation of ozone in the reaction of hydroxyl with O3-and the decay of the ozonide ion radical at pH 10-13. *The Journal of Physical Chemistry* **1984,** *88* (2), 269-273.

45. Reckhow, D. A.; Singer, P. C.; Malcolm, R. L., Chlorination of humic materials: byproduct formation and chemical interpretations. *Environmental Science & Technology* **1990,** *24* (11), 1655-1664.

46. Pinkernell, U.; von Gunten, U., Bromate minimization during ozonation: Mechanistic considerations. *Environmental Science & Technology* **2001,** *35* (12), 2525-2531.

47. Dotson, A. D.; Keen, V. S.; Metz, D.; Linden, K. G., UV/H2O2 treatment of drinking water increases post-chlorination DBP formation. *Water Research* **2010,** *44* (12), 3703-3713.

48. Baxendale, J. H.; Wilson, J. A., The photolysis of hydrogen peroxide at high light intensities. *Transactions of the Faraday Society* **1957,** *53*, 344-356.

49. Zepp, R.; Faust, B.; Hoigne, J., Hydroxyl radical formation in aqueous reactions (pH 3-8) of Iron(II) with hydrogen peroxide - the Photo-Fenton Reaction. *Environmental Science and Technology* **1992,** *26*, 313-319.

50. Mack, J.; Bolton, J. R., Photochemistry of nitrite and nitrate in aqueous solution: a review. *Journal of Photochemistry and Photobiology A: Chemistry* **1999,** *128* (1-3), 1-13.

51. Westerhoff, P.; Mezyk, S. P.; Cooper, W. J.; Minakata, D., Electron pulse radiolysis determination of hydroxyl radical rate constants with Suwannee river fulvic acid and other dissolved organic matter isolates. *Environmental Science & Technology* **2007,** *41* (13), 4640-4646.

52. Liao, C.-H.; Gurol, M. D., Chemical Oxidation by photolytic decomposition of hydrogen peroxide. *Environmental Science and Technology* **1995,** *29*, 3007-3014.

53. Rosenfeldt, E. J.; Linden, K. G., Degradation of Endocrine Disrupting Chemicals Bisphenol A, Ethinyl Estradiol, and Estradiol during UV photolysis and Advanced Oxidation Processes. **2004,** *38* (20), 5476 - 5483.

54. Young, T.; Geng, M.; Lin, L.; Thagard, S., Oxidative Degradation of Bisphenol A: A Comparison between Fenton Reagent, UV, UV/H2O2 and ultrasound. *Journal of Advanced Oxidation Technologies* **2013,** *16*, 89-101.

55. Ferguson, D. W.; McGuire, M. J.; Koch, B.; Wolfe, R. L.; Aieta, E. M., Comparing PEROXONE and ozone for controlling taste and odor compounds, disinfection by-products, and microorganisms. *Journal-American Water Works Association* **1990,** *82* (4), 181-191.

56. Wols, B. A.; Hofman-Caris, C. H. M.; Harmsen, D. J. H.; Beerendonk, E. F., Degradation of 40 selected pharmaceuticals by UV/H2O2. *Water Research* **2013,** *47* (15), 5876-5888.

57. Klavarioti, M.; Mantzavinos, D.; Kassinos, D., Removal of residual pharmaceuticals from aqueous systems by advanced oxidation processes. *Environment International* **2009,** *35* (2), 402-417.

58. Buxton, G. V.; Greenstock, C. L.; Helman, W. P.; Ross, A. B., Critical-Review of Rate Constants for Reactions of Hydrated Electrons, Hydrogen-Atoms and Hydroxyl Radicals (.Oh/.O-) in Aqueous-Solution. *Journal of Physical and Chemical Reference Data* **1988,** *17* (2), 513-886.

59. Sedlak, D. L.; Hoigne, J., Oxidation of S (IV) in atmospheric water by photooxidants and iron in the presence of copper. *Environmental science & technology* **1994,** *28* (11), 1898-1906.

60. Czapski, G.; Peled, E., On the pH-dependence of G_reducing in the Radiation Chemistry of Aqueous Solutions. *Israel Journal of Chemistry* **1968,** *6* (4).

61. Qiao, Z.; Wigginton, K. R., Direct and Indirect Photochemical Reactions in Viral RNA Measured with RT-qPCR and Mass Spectrometry. *Environmental Science & Technology* **2016,** *50* (24), 13371-13379.

62. Chen, R. Z.; Craik, S. A.; Bolton, J. R., Comparison of the action spectra and relative DNA absorbance spectra of microorganisms: Information important for the determination of germicidal

fluence (UV dose) in an ultraviolet disinfection of water. *Water research* **2009,** *43* (20), 5087-5096.

63. Sinha, R.; Hader, D., UV-induced DNA damage and repair. *Photochemistry photobiology* **2002**, 225-236.

64. Cadet, J.; Sage, E.; Douki, T., Ultraviolet radiation-mediated damage to cellular DNA. *Mutation Research 0 Fundamental and molecular mechanisms of mutagenesis* **2005,** *571*, 3-17.

65. Sharpless, C. M.; Aeschbacher, M.; Page, S. E.; Wenk, J.; Sander, M.; McNeill, K., Photooxidation-Induced Changes in Optical, Electrochemical, and Photochemical Properties of Humic Substances. *Environmental Science & Technology* **2014,** *48* (5), 2688-2696.

66. Zepp, R. G.; Wolfe, N. L.; Baughman, G. L.; Hollis, R. C., Singlet oxygen in natural waters. *Nature* **1977,** *267* (5610), 421-423.

67. Latch, D. E.; McNeill, K., Microheterogeneity of singlet oxygen distributions in irradiated humic acid solutions. *Science* **2006,** *311* (5768), 1743-1747.

68. Young, T. R.; Li, W.; Guo, A.; Korshin, G.; Dodd, M. C., Characterization of disinfection byproduct formation and associated changes to dissolved organic matter during solar chlorine photolysis of free available chlorine. *Water Research* **2018,** *146* (1), 318-327.

69. Watts, M. J.; Linden, K. G., Chlorine photolysis and subsequent OH radical production during UV treatment of chlorinated water. *Water Research* **2007,** *41*, 2871-2878.

70. Jin, J.; El-Din, M.; Bolton, R. G., Assessment of the UV/Chlorine process as an advanced oxidation process. *Water Research* **2011,** *45*, 1890-1896.

71. Wang, D.; Bolton, J.; Hofmann, R., Medium pressure UV combined with chlorine advanced oxidation for trichloroethylene destruction on a model water. *Water Research* **2012,** *46*, 4677-4686.

72. Molina, M.; Ishiwata, T.; Molina, L. T., Production of OH radical from photolysis of HOCl at 307 - 309 nm. *Journal of Physical Chemistry* **1980,** *84*, 821-826.

73. Buxton, G. V.; Subhani, M. S., Radiation chemistry and photochemistry of oxychlorine ions. Part 2.—Photodecomposition of aqueous solutions of hypochlorite ions. *Journal of the Chemical Society, Faraday Transactions 1: Physical Chemistry in Condensed Phases* **1972,** *68*, 958-969.

74. Chuang, Y.-H.; Chen, S.; Chinn, C. J.; Mitch, W. A., Comparing the UV/monochloramine and UV/free chlorine Advanced Oxidation Processes (AOPs) to the UV/hydrogen peroxide AOP under scenarios relevant to potable reuse. *Environmental science & technology* **2017,** *51* (23), 13859-13868.

75. Xiang, Y.; Fang, J.; Shang, C., Kinetics and pathways of ibuprofen degradation by the UV/Chlorine advanced oxidation. *Water Res* **2016,** *90*, 301-308.

76. Cheng, S.; Zhang, X.; Song, W.; Pan, Y.; Lambropoulou, D.; Zhong, Y.; Du, Y.; Nie, J.; Yang, X., Photochemical oxidation of PPCPs using a combination of solar irradiation and free available chlorine. *Science of The Total Environment* **2019,** *682*, 629-638.

77. Bulman, D. M.; Mezyk, S. P.; Remucal, C. K., The impact of pH and irradiation wavelength on the production of reactive oxidants during chlorine photolysis. *Environmental science & technology* **2019,** *53* (8), 4450-4459.

78. Yang, X.; Sun, J.; Fu, W.; Shang, C.; Li, Y.; Chen, Y.; Gan, W.; Fang, J., PPCP degradation by UV/chlorine treatment and its impact on DBP formation potential in real waters. *Water research* **2016,** *98*, 309-318.

79. Pisarenko, A. N.; Stanford, B. D.; Snyder, S. A.; Rivera, S. B.; Boal, A. K., Investigation of the use of Chlorine Based Advanced Oxidation in Surface Water: Oxidation of Natural Organic Matter and Formation of Disinfection Byproducts. *J Adv Oxid Technol* **2013,** *16* (1), 137-150.

80. Liu, W.; Zhang, Z.; Yang, X.; Xu, Y.; Liang, Y., Effects of UV irradiation and UV/chlorine co-exposure on natural organic matter in water. *Sci Total Environ* **2012,** *414*, 576-584.

81. Wang, W. L.; Zhang, X.; Wu, Q. Y.; Du, Y.; Hu, H. Y., Degradation of natural organic matter by UV/chlorine oxidation: Molecular decomposition, formation of oxidation byproducts and cytotoxicity. *Water Res* **2017,** *124*, 251-258.

82. Guo, K.; Wu, Z.; Shang, C.; Yao, B.; Hou, S.; Yang, X.; Song, W.; Fang, J., Radical chemistry and structural relationships of PPCP degradation by UV/chlorine treatment in simulated drinking water. *Environmental science & technology* **2017,** *51* (18), 10431-10439.

83. Guo, K.; Wu, Z.; Yan, S.; Yao, B.; Song, W.; Hua, Z.; Zhang, X.; Kong, X.; Li, X.; Fang, J., Comparison of the UV/chlorine and UV/H2O2 processes in the degradation of PPCPs in simulated drinking water and wastewater: Kinetics, radical mechanism and energy requirements. *Water research* **2018,** *147*, 184-194.

84. Wang, D.; Bolton, J. R.; Andrews, S. A.; Hofmann, R., Formation of disinfection by-products in the ultraviolet/chlorine advanced oxidation process. *Sci Total Environ* **2015,** *518*, 49-57.

85. Li, T.; Jiang, Y.; An, X. Q.; Liu, H. J.; Hu, C.; Qu, J. H., Transformation of humic acid and halogenated byproduct formation in UV-chlorine processes. *Water Res* **2016,** *102*, 421-427.

86. Simard, S.; Tardif, R.; Rodriguez, M. J., Variability of chlorination by-product occurrence in water of indoor and outdoor swimming pools. *Water Res* **2013,** *47* (5), 1763-1772.

87. Mao, Y. Q.; Wang, X. M.; Yang, H. W.; Wang, H. Y.; Xie, Y. F. F., Effects of ozonation on disinfection byproduct formation and speciation during subsequent chlorination. *Chemosphere* **2014,** *117*, 515-520.

88. Riley, T. L.; Mancy, K. H., *The effect of preozonation on chloroform production in the chlorine disinfection processes*. Ann Arbor Science: Ann Arbor, MI, 1978; Vol. 2.

89. De Vera, G. A.; Stalter, D.; Gernjak, W.; Weinberg, H. S.; Keller, J.; Farre, M. J., Towards reducing DBP formation potential of drinking water by favouring direct ozone over hydroxyl radical reactions during ozonation. *Water Res* **2015,** *87*, 49-58.

90. Zhang, X.; He, J.; Lei, Y.; Qiu, Z.; Cheng, S.; Yang, X., Combining solar irradiation with chlorination enhances the photochemical decomposition of microcystin-LR. *Water research* **2019,** *159*, 324-332.

91. Sun, P.; Lee, W.-N.; Zhang, R.; Huang, C.-H., Degradation of DEET and caffeine under UV/chlorine and simulated sunlight/chlorine conditions. *Environmental science & technology* **2016,** *50* (24), 13265-13273.

92. Lv, X. T.; Zhang, X.; Du, Y.; Wu, Q. Y.; Lu, Y.; Hu, H. Y., Solar light irradiation significantly reduced cytotoxicity and disinfection byproducts in chlorinated reclaimed water. *Water Res* **2017,** *125*, 162-169.

93. Shu, Z. Q.; Li, C.; Belosevic, M.; Bolton, J. R.; El-Din, M. G., Application of a Solar UV/Chlorine Advanced Oxidation Process to Oil Sands Process-Affected Water Remediation. *Environ Sci Technol* **2014,** *48* (16), 9692-9701.

Chapter 2: Oxychloride and Bromate Detection using Ion Chromatography-Electron Spray Ionization-tandem Mass Spectrometry (IC-ESI-MS/MS) and Formation During Solar Chlorine Photolysis

Abstract

A rapid and sensitive method is outlined for measuring perchlorate, chlorate, chlorite, and bromate ions in natural and treated waters using ion chromatography with electron spray ion source and tandem mass spectrometry (IC-ESI-MS/MS). The major benefits of the newly developed IC-ESI-MS/MS include a short analysis time (12 minute) and low limits of quantification (LOQ) for bromate (0.10 μg/L), perchlorate (0.06 μg/L), chlorate (0.8 μg/L), and chlorite (0.4 μg/L). Methylamine was selected as the organic base for the mobile phase and enables pairing ion chromatography with tandem mass spectrometry without the need for a costly conductivity suppressor. The detailed isocratic method for bromate and oxychloride analysis can be modified to include a rapid transition from 80% acetonitrile 20% methylamine solution to fully aqueous (maintaining a concentration of 200 mM methylamine in the mobile phase) enabling iodate detection. Four common freshwater anions — chloride, bromide, carbonate, and sulfate — and four organic carbon sources were tested to identify possible background influences on bromate and oxychloride ion detection. Only the chlorite signal was suppressed with high chloride concentrations (> 2mM) and Suwannee River Natural Organic Matter (SRNOM) (> 2 mg/L as C). Method application confirmed that the combination of chlorine, ozone, and other reactive oxygen and halogen species formed during sunlight-driven photolysis of chlorine result in chlorate formation (+10% at pH 6 and +60% at pH 8 from chlorate introduced from the free chlorine stock). Chlorine photolysis of water containing bromide (or hypobromous acid) resulted in bromate formation, up to 20.1±1.0 μg/L and 33.8±1.0 μg/L (at pH 6 and 8, respectively). SRNOM addition disrupted bromate formation, likely by scavenging reactive oxygen or bromine species; natural water sources with less reactive NOM competed for radical species, but did not eliminate bromate and chlorate formation.

2.1. Introduction

Strong oxidants, such as ozone and chlorine dioxide, are being used more frequently in water/wastewater treatment to oxidize organic contaminants and enhance disinfection of chlorine resistant pathogens. However, ozone and chlorine dioxide will also react with halide anions (if present) and form oxyhalide disinfection byproducts (DBP).[1-3] In the past few decades, a majority of utilities have moved away from using chlorine gas (90% in 1978 to 40% in 2017) as a source of free available chlorine (FAC) and transitioned to sodium hypochlorite solutions (56% in 2017) to reduce safety hazards and security risks associated with chlorine gas storage and transport.[4] Concentrated hypochlorite stocks and on-site generated hypochlorite often contain contaminant oxyhalides, such as perchlorate, chlorate, chlorite, and bromate, and introduce these inorganic DBPs to finished water.[5-7]

Regulatory agencies have set appropriate maximum contaminant levels (MCL) or guidance limits for oxyhalides in drinking water to protect consumers. The U.S. Environmental Protection Agency (EPA) set an MCL of 10 μg/L for bromate[8] – and have classified it as a probable human carcinogen.[9] Chlorite and chlorate are not classified as carcinogenic but exposure to either has been shown to decrease red blood cells and hemoglobin[10, 11] and the U.S. EPA has set an MCL of 1.0 mg/L for chlorite.[8] There is not a specified MCL for chlorate or perchlorate in drinking water, however the U.S. EPA has set a Health Reference Level of 210 μg/L for ClO_3^- and a Drinking Water Health Advisory limit of 15 μg/L for ClO_4^- (due to ClO_4^- interference with iodide uptake and thyroid activity).[12]

With the current trends for primary and secondary disinfectants applied in water treatment, monitoring inorganic oxyhalide DBP introduced from disinfectant stocks or formed

during oxidation/disinfection processes is a concern for utilities and regulatory agencies worldwide. Many standards and published methods separate halides and oxyhalides via ion chromatography (IC), though these typically utilize ion suppressors and conductivity detectors which require careful maintenance to achieve sub-μg/L quantification and require using multiple methods and columns to quantify chlorite, chlorate, perchlorate, bromate, and iodate; detection limits are summarized in Table 2.1.[13, 14] Addition of a post-column reactor (PCR) and/or 2D-IC improved oxyhalide separation and sensitivity, specifically reliable detection of low bromate concentrations.[15-22] Trace analysis of bromate was a critical improvement for ozone treatment research and utility monitoring, however most PCR methods do not include the suite of oxychlorides.[23, 24] IC-MS has also been utilized to improve sensitivity of perchlorate (EPA Method 331 and 332),[25-27] bromate (EPA Method 557),[19] and other oxyhalide measurement;[28, 29] however these methods require a ion suppressor before MS injection. LC-MS with a Synergi Max-RP C12 column without an ion-suppressor has been applied for analysis of perchlorate, chlorate, and bromate in dilute[30] and concentrated hypochlorite solutions;[28] however this method does not include chlorite and iodate detection. Nitrate and methylamine have been applied as volatile anions in mobile phases with IonPac AG9-SC and IonPac AS21 ion chromatography columns, respectively, that are compatible with MS detection without the need for a conductivity suppressor.[31-34] Specifically, U.S. EPA Standard Method 331 describes rapid elution of perchlorate with methylamine as the hydroxide source in the mobile phase in an IC-ESI-MS/MS system with low LOD (Table 2.1). While there are a variety of published analytical methods dedicated to oxyhalide analysis, none have been capable of analyzing 5 environmentally relevant oxyhalides within one analytical method: ClO_2^-, ClO_3^-, ClO_4^-, BrO_3^-, and IO_3^-.

Table 2.1. Limit of detection (LOD) and associated injection volumes for established standard methods developed for analysis of oxyhalides (and other anions).

U.S. EPA Std. Method	Inj. Vol. µL	Perchlorate µg/L	Chlorate µg/L	Chlorite µg/L	Bromate µg/L
300.1	200	–	1.3	0.9	1.4
302	1000	–	–	–	0.18
314.2	2000	0.06	–	–	–
317	225	–	0.92	0.45	0.12
326	225	–	–	–	0.17
331	100	0.022	–	–	–
332	100	0.02	–	–	–
557	100	–	–	–	0.02

This study proposes a novel method for rapid analysis of trace concentrations of oxyhalides using a highly organic mobile phase with an IonPac AS16 column; eliminating the need for a conductivity suppressor and including detection parameters for perchlorate, chlorate, chlorite, and bromate with a modification (gradient eluent mobile phase) enabling sequential iodate analysis. Current published methods for oxyhalide analysis do not include all the listed oxyhalides, requiring additional equipment and analytical time for lab users to analyze a comprehensive oxyhalide dataset. The method was validated by quantifying oxyhalide concentrations introduced from quenched sodium hypochlorite stocks, and monitoring oxyhalide formation/degradation during solar irradiation of chlorinated water (FAC+Light) with and without natural organic matter and bromide. Solar chlorine photolysis produces reactive oxygen species in situ (including ozone and hydroxyl radical) and is being evaluated as a novel drinking water treatment. Some of these photooxidants have been identified as essential to bromate formation mechanism during ozonation.[35] The change in oxyhalide concentration has not yet been evaluated for the mixed oxidant conditions present during solar chlorine photolysis, introducing the opportunity to evaluate a novel treatment process and apply the oxyhalide method detailed in this study to natural and artificial drinking waters matrixes.

2.2. Experimental Materials and Methods

2.2.1. Materials. Sodium bromate, sodium chlorate, (> 99%, respectively), sodium chlorite (80%), and potassium iodate (>99.5%) were obtained from Sigma-Aldrich (St. Louis, MO). Sodium perchlorate (>98%) was obtained from EMD (Darmstadt, Germany). The internal standard isotope-labelled perchlorate ($Cl^{18}O_4^-$) and bromate ($Br^{18}O_3^-$) were obtained from Icon Isotopes (Summit, NJ) and isotope-labelled chlorate ($Cl^{18}O_3^-$) was obtained from EU Reference Laboratories (Stuttgart, Germany). Mass Spectrometry grade water and acetonitrile for eluents were obtained from Sigma-Aldrich (St. Louis, MO). Methylamine, ACS grade 40% in water, sodium hypochlorite, ACS grade 4.00 – 4.99% in water, and ethylene diamine (>99%) were obtained from Sigma-Aldrich (St. Louis, MO). Sodium chloride, sodium bromide, sodium sulfate, barium hydroxide, phosphate, and other buffers are the highest available purity (ACS reagent grade or higher) obtained from Sigma-Aldrich (St. Louis, MO) and were not purified further. Suwannee river natural organic matter (SRNOM), reverse-osmosis isolate 2R101N, was procured from International Humic Substances Society (St. Paul, MN). All aqueous stock and calibration standards were prepared in Milli-Q ultrapure water with resistivity ≥18.2 MΩ cm (Millipore, Billerica, MA).

2.2.2. Sample Collection and Storage. Natural samples and SRNOM stocks were filtered using 0.45μm polyethersulfone membrane filters (conditioned by flushing with 1 L of ultrapure water) prior to storage in pre-baked glassware (carbon-free) at 4 °C. Tap water was collected from More Hall at the University of Washington after flushing the faucet for 2 minutes prior to sample collection and filtered; residual chlorine was quenched with ethylene diamine (EDA) and

samples were stored for less than 24 hours prior to analysis. The experimental set up for chlorination and solar chlorine photolysis treatment is described in detail in Section 2.2.5.

2.2.3. Ion Chromatography. Analytes were separated using a 2×250 mm Dionex column packed with IonPac® AS16 hydroxide selective media (9μm particle size and 2000Å pore size) with an AG16 guard column (Bannockburn, IL). An injection volume of 100 μL was used throughout this study, but injection volumes as low as 10 μL are possible with elevated detection limits. A Shimadzu LC-20AD HPLC with binary pump was used to deliver isocratic mixture of 20% 1M methylamine in water (A) and 80% acetonitrile (B) at 0.25 mL/min. Two eluents are recommended to prevent alkaline hydrolysis of acetonitrile during storage.[36]

Method optimization also included experimentation with a 2x250 mm Dionex IonPac® AS9-HC carbonate selective media (9μm particle size and 2000Å pore size), a 2x150 mm Dionex Acclaim® Mixed Mode WAX-1 weak anion exchange column (5μm particle size and 120Å pore size), and a Supelco Ascentis C18 column (150 × 2.1 mm, 3 μm). Comparison of column performance for mixed oxyhalide analysis is summarized in Section 2.3.1.

2.2.4. Mass Spectrometry. Oxyhalides were detected using tandem mass spectrometry with an AB 4000 Q TRAP linear ion trap operated in negative ion mode with hybrid triple-quadrupole mass spectrometer (Applied Biosystems, Foster City, CA). Ions were confirmed with naturally occurring chloride and bromide isotopes, chloride masses composed of 34.969 Da – 75.78% and 36.966 Da – 24.22% and bromide masses composed of 78.91 Da – 50.69% and 80.91 Da – 49.31%. Selected reaction monitoring (SRM) was set up with precursor/product ion transitions, described in Table 2.2. Perchlorate, chlorate, and bromate concentrations were quantified using stable-isotope labeled $^{35}Cl^{18}O_4^-$, $^{35}Cl^{18}O_3^-$, and $^{81}Br^{18}O_3^-$ as internal standards.

No stable isotope is commercially available for chlorite, so concentrations were quantified using only external calibrations. The collision energy and the collision cell exit potential are listed in Table 2.2 for each oxyhalide isotope.

Table 2.2. Compound specific Selected Reaction Monitoring (SRM) MS/MS parameters, optimization in 200mM methylamine in 20% mixture of water in acetonitrile.

Compound	Precursor ion mass (m/z)	Product ion mass (m/z)	Collision energy (volts)	Collision cell exit potential (volts)
$^{81}BrO_3^-$	128.88	113.00	-34.0	-9.0
$^{79}BrO_3^-$	126.88	110.80	-48.0	-7.0
$^{37}ClO_4^-$	101.05	84.80	-34.0	-13.0
$^{35}ClO_4^-$	99.02	83.10	-34.0	-13.0
$^{37}ClO_3^-$	84.97	69.10	-34.0	-9.0
$^{35}ClO_3^-$	82.96	67.00	-28.0	-1.0
$^{37}ClO_2^-$	69.01	53.00	-20.0	-7.0
$^{35}ClO_2^-$	67.00	50.90	-18.0	-7.0
$^{81}Br^{18}O_3^-$	135.00	116.90	-30.0	-17.0
$^{79}Br^{18}O_3^-$	132.90	114.90	-32.0	-17.0
$^{37}Cl^{18}O_4^-$	109.01	91.00	-36.0	-13.0
$^{35}Cl^{18}O_4^-$	107.00	89.00	-38.0	-13.0
$^{35}Cl^{18}O_3^-$	90.975	73.00	-28.0	-5.0
$^{37}Cl^{18}O_3^-$	89.00	71.00	-28.0	-5.0
IO_3^-	174.70	158.70	-38.0	-14.0

2.2.5. Chlorination and Simulated Sunlight Experiments. Dark chlorination experiments (FAC only) were conducted in amber glass vials, thermostated at 10 deg. C. Solar chlorine photolysis experiments (FAC+Light) were undertaken under headspace-free conditions in 28-mL quartz tubes in duplicate, and thermostated at 10 °C in a circulating water bath below the simulated sunlight source. Samples were irradiated using a Suntest with 1700-W, O_3-free, Xe arc lamp with daylight filter (cutoff below 290 nm) and infrared radiation filter and sample tubes

were angled 35° from the horizontal. Phosphate buffer (10 mM) controlled pH at either pH 6.00 or 8.00±0.02 in ultrapure reagent water. DOM was sourced from SRNOM stocks, and targeted 2 mg/L as C in experiments. Bromide was added to select experiments at a concentration of 200 μg/L.

FAC only and FAC+light experiments were initiated by adding $[FAC]_0 \sim 8$ mg/L as Cl_2 to the prepared water matrix. Solutions within quartz tubes were mixed manually by inverting the tubes three times. After chlorine addition and mixing, FAC+light experiments were immediately placed within the solar simulator. FAC concentration was monitored throughout the irradiation period by means of DPD colorimetry[37]. FAC+light experiment sets were irradiated for 20 or 45 minutes (fluences equivalent to 7.2 or 16.1 J/cm^2). Irradiation times and FAC concentrations were selected to reflect conditions previously found to yield 1- to 3-$\log_{10}$ inactivation of *Cryptosporidium* spp. oocysts and/or *Bacillus subtilis* spores during sunlight-driven FAC photolysis.[38, 39] Experiments proceeded until a target cumulative FAC exposure of 400 (mg/L as Cl_2)×min was met, at which point FAC was quenched with two-fold excess ethylene diamine (EDA). Cumulative FAC exposures (CT_{FAC}, Equation 1.5) were approximated using trapezoidal Riemann summation of FAC concentrations measured at defined reaction times during the course of experiments. Quenched samples were then analyzed by IC-ESI-MS/MS for oxyhalide quantification within 24 hours.

2.3. Results and Discussion

2.3.1. Analytical Observations and Method Optimization. While other oxyhalide detection and quantification methods are published, no method simultaneously quantifies low concentrations of perchlorate, chlorate, chlorite, and bromate with rapid elution times – under 20

minutes.[15, 28, 30, 34, 40] Several columns were compared to establish one method that could separate the four oxyhalides of interest. A weak anion exchange (WAX) column was tested with varied ratios of methanol and MS grade water (containing ammonia formate or ammonia acetate), however all oxyhalides were retained on the column with this mobile phase. The WAX column was also tested with acetonitrile (replacing methanol), which facilitated oxyhalide transport through the column but yielded poor separation and broad peak shape. Adequate separation may be possible with the WAX column under different conditions, however we halted further trials with this column media. Increasing the acetonitrile percentage in the mobile phase (50-95%) resulted in enhanced retention of the oxyhalides on the C18 column and improved the measured MS signal intensity (likely due to improved ionization efficiency), but bromate, chlorate, and chlorite were poorly separated – making this an undesirable chromatography method for analyzing the suite of oxyhalides. A carbonate selective ion chromatography column (AS9-HC) was paired with a conductivity detector – tested with carbonate concentrations ranging from 9-32 mM, sourced from sodium carbonate or ammonium carbonate. The AS9-HC could effectively separate chlorite, bromate, and chlorate; however, perchlorate did not elute within 60 minutes. Ultimately the mobile phases tested on these three columns were undesirable for separation of ClO_2^-, ClO_3^-, ClO_4^-, and BrO_3^-; prompting further testing with a hydroxide selective IC column.

The Dionex AS16 column is recommended for perchlorate separation in accordance with EPA Method 314.2 (paired with an AS20 column; 2D IC-MS) and is also capable of separating polarizable and inorganic anions.[18] Initial trials with the AS16 under fully aqueous conditions (varying $[OH^-]$ between 10 – 120 mM) using a Dionex ICS-3000 equipped with a conductivity detector resulted in poor ClO_4^- detection. Perchlorate was either retained on the AS16 column media or extreme peak broadening hindered identification. Trials using the shorter 50mm AG16

guard column alone paired with a conductivity detector did facilitate faster perchlorate elution (within 5 minutes), but ClO_2^-, ClO_3^-, and BrO_3^- peaks were clustered and poorly resolved with NH_4OH concentrations ranging from 2.5 – 35 mM. Therefore, the longer column AS16 with AG16 would be necessary to separate ClO_2^-, ClO_3^-, and BrO_3^-. The LOD was high for all oxyhalides when using the conductivity detector, highlighting the demand for an MS compatible mobile phase to harness improved detector sensitivity.

Methylamine is an organic hydroxide source that increases pH without introducing salts that precipitate and interfere with ionization, making it a compatible base for MS analysis as verified by EPA Method 331.0. Combining aqueous methylamine with a high percentage of acetonitrile in the mobile phase reversed the elution order of the oxyhalides from that observed with a highly aqueous (>90% H_2O) hydroxide eluent using the same ion chromatography column[41] or reversed phase C12 column.[28, 30] The reversed elution order, as seen in Figure 2.1, may be partially due to an increase in methylamine's basicity while dissolved in a high percentage of aprotic solvent, e.g. acetonitrile.[42] It could also be partially due to altered anion interactions with the column media since column retention is driven by ion properties; such as charge density, hydrophilicity, and polarizability.[43] Acetonitrile has a high proton solvation energy relative to water and other common solvents such as methanol, resulting in a pK_a increase for all acidic analytes in acetonitrile.[44] The effective pH in the solvent-water mixture would be expected to decrease for organic base buffers such as methylamine with small additional organic solvent,[42] but with a high acetonitrile to water ratio (>70%) the pK_a of methylamine is expected to increase substantially (pK_a = 18.3 in 100% acetonitrile)[44]. With a higher pKa, a higher percentage of the methylamine will be protonated, resulting in increased hydroxide concentration in the mobile phase. With acetonitrile concentrations below 70% while maintaining a mixed

methylamine concentration of 200 mM, the retention time for the four oxyhalides increased. The analyte retention likely increased because the increased water percentage altered the proton solvation effects, resulted in a pK_a decrease for methylamine, and a lower effective hydroxide concentration with equivalent methylamine concentrations.[42, 44] Methanol and methylamine (80:20 CH_3OH:H_2O with 200 mM methylamine) was also tested with the AS16 and the resolution between ClO_2^- and ClO_3^- was poor and elution order corrected, with ClO_4^- eluting last. This provides additional support that the observed elution order reversal and oxyhalide separation is driven by altered interactions between the mobile phase, anions, and column media while in a highly aprotic organic mobile phase.

A high proportion of acetonitrile is also expected to cause swelling and impact the ion-binding sites on the column media. In effect, media swelling would decrease the number of available ion-exchange sites per area and decrease the observed retention time for all anions.[43] A high percentage of an aprotic solvent such as acetonitrile, will also inhibit ionization of the alkanol substituents on the column media, resulting in an increased positive charge density at the ion binding site.[45] This would be expected to result in enhanced retention of anions, such as oxyhalides, and that may explain the longer observed retention time for chlorite, bromate, and iodate, but does not explain the rapid elution of perchlorate which typically elutes last because of its affinity for the column media. Highly polarizable anions dissolved in some fraction of an aqueous phase will be surrounded by a hydration sphere. When mixed with a high fraction of an aprotic solvent (e.g. acetonitrile), solvent molecules will compress and organize the hydration sphere, demand more energy to rearrange the hydrogen bonding water molecules to access the anion. The organized hydration sphere shields the ion charge and hinders binding with positively-charged ion-sites on the column media.[43] Perchlorate is the most polarizable anion of

the oxyhalides included in this study, which normally contributes to enhanced retention on the ion exchange media; requiring a higher hydroxide concentration to elute. However, the rapid elution of perchlorate in this IC method could be due to charge shielding from the hydration spheres, hindering the anion attraction to the IC column media.

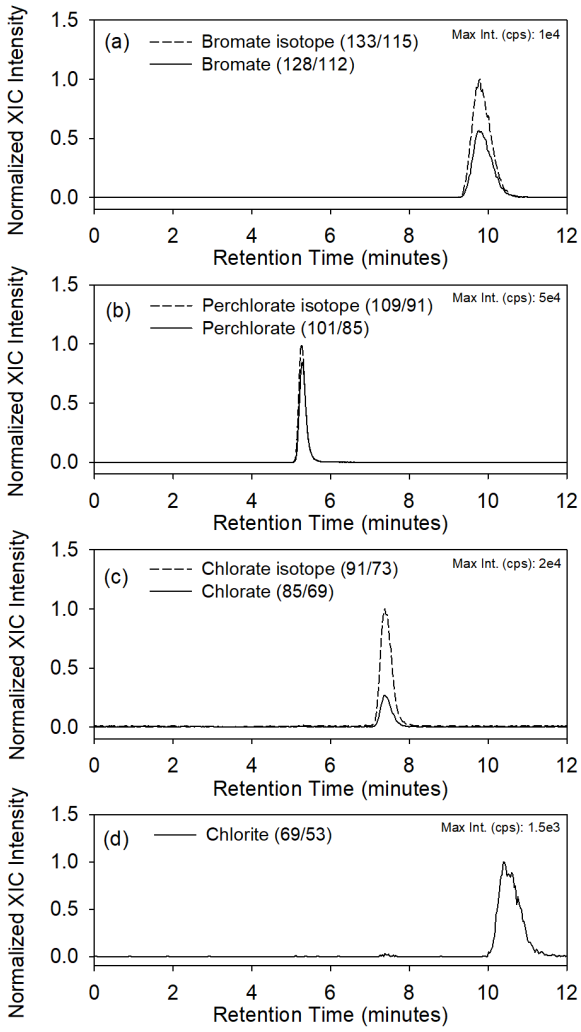

Figure 2.1. Extracted ion chromatogram (XIC) for **(a)** bromate, **(b)** perchlorate, **(c)** chlorate, and **(d)** chlorite oxyhalide standards (10 µg/L) and ^{18}O-isotope internal standards (50 µg/L) in ultrapure water.

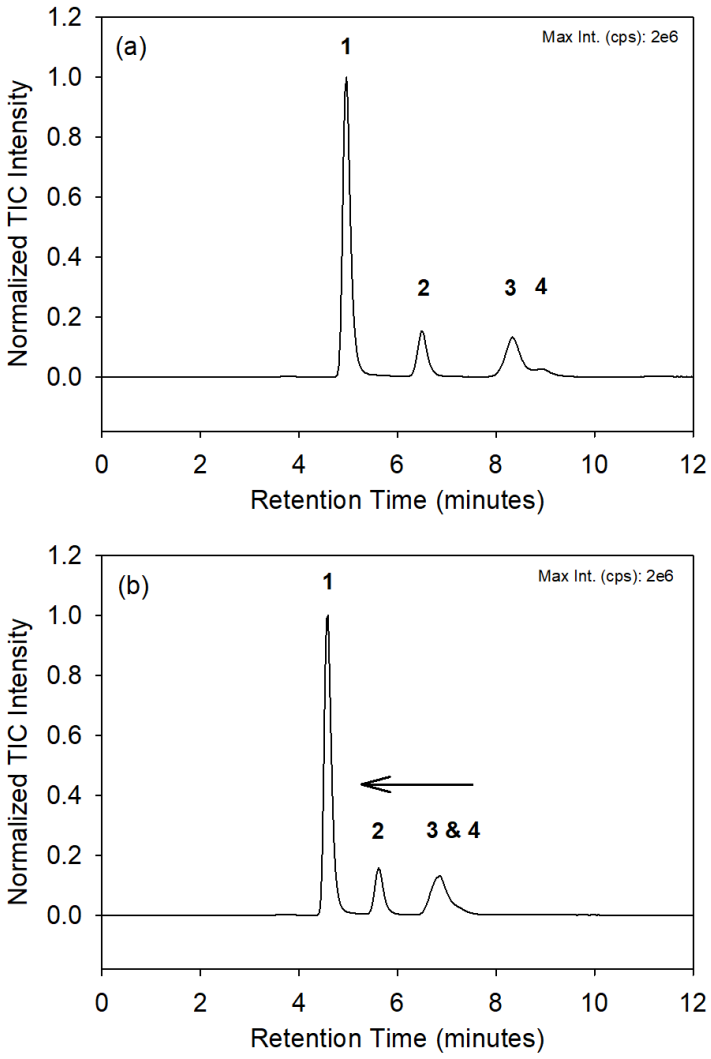

Figure 2.2. Total ion chromatogram (TIC) of oxyhalide standards (50 µg/L) and ^{18}O-isotope internal standards (50 µg/L) in **(a)** ultrapure water and, **(b)** in 10 mM phosphate buffer. The labelled peaks are: 1. perchlorate, 2. chlorate, 3. bromate, and 4. chlorite.

Table 2.3. Oxyhalide retention time (RT) after multiple injections. Standards were prepared in deionized water (DI Water), untreated 10 mM phosphate buffer at pH 8 (No Ba^{2+}), and barium treated phosphate buffer (Ba^{2+} pH 8 and Ba^{2+} pH 12). With 15 mM barium hydroxide the measured residual phosphate was less than 5 mg/L PO_4^{3-}.

Inj. no.	**Bromate RT (minutes)**				**Perchlorate RT (minutes)**				**Chlorate RT (minutes)**				**Chlorite RT (minutes)**			
	DI Water	Phosphate Buffer			DI Water	Phosphate Buffer			DI Water	Phosphate Buffer			DI Water	Phosphate Buffer		
		No Ba^{2+}	Ba^{2+} pH 8	Ba^{2+} pH 12		No Ba^{2+}	Ba^{2+} pH 8	Ba^{2+} pH 12		No Ba^{2+}	Ba^{2+} pH 8	Ba^{2+} pH 12		No Ba^{2+}	Ba^{2+} pH 8	Ba^{2+} pH 12
1	10.4	8.18	9.8	10.0	5.6	4.9	5.3	5.3	7.8	6.4	7.4	7.5	11.0	8.7	10.5	10.8
2	10.1	7.84	9.8	10.1	5.6	4.8	5.3	5.4	8.0	6.2	7.4	7.6	10.8	8.3	10.5	10.9
3	10.7	7.32	9.9	10.1	5.5	4.7	5.3	5.4	7.8	5.9	7.5	7.6	10.5	7.7	10.7	10.9
4	10.4	6.85	10.0	10.1	5.4	4.6	5.3	5.4	7.7	5.6	7.5	7.6	11.2	7.2	10.7	10.9
5	10.1	-	10.1	10.1	5.3	-	5.4	5.4	7.5	-	7.5	7.6	10.7	-	10.8	10.8

Sample solutions containing high background ion concentrations can also compete with the oxyhalides for ion-binding sites on the column media and result in retention time shifts. In particular, multiple injections of buffer solutions with high ortho-phosphate concentrations (10 mM) decreased the observed retention time, as seen in Figure 2.2b and Table 2.3 (without Ba^{2+}). The effect is most stark for bromate and chlorite which are elute last in this method. Pretreatment of 10 mM phosphate buffered samples with 15 mM barium hydroxide was sufficient to precipitate the ortho-phosphate and prevent retention time shifts after multiple injections, as seen in Table 2.3. Pretreatment of phosphate containing samples with barium, followed by filtration or centrifugation of the precipitant, was found to be a satisfactory solution that did not decreased spiked oxyhalide concentrations.

2.3.2. Iodate Modification. The described isocratic method can be modified to include the analysis of iodate following the elution of the four oxyhalides using the AS16 column. Iodate elutes quickly from the AS16 column media with 200 mM methylamine in a fully aqueous mobile phase. A simple gradient method would be optimal with a third channel (C) that is only MS grade water that replaces the acetonitrile (B) volume fraction and dilutes the 1 M methylamine (A). The first 12 minutes would remain unchanged (20% A and 80% B), then induce a rapid gradient between 12 and 13 minutes to 20% A and 80% C (maintaining a mobile phase concentration of 200 mM methylamine). Iodate elutes within 5 minutes under the aqueous conditions at a flowrate of 0.2 mL/min (see Figure 2.3). Then at 18 minutes the gradient should return to 20% A and 80% B to equilibrate before the next injection. Alternatively, the fraction of aqueous methylamine could be increased, and iodate will elute eventually. However, increasing the aqueous fraction and methylamine concentration resulted in poor separation of the other oxyhalides (bromate, perchlorate, chlorate, and chlorite). With multiple reaction monitoring,

individual oxyhalides can still be extracted and quantified, but users should be wary of possible peak overlap. See Figure S2.1 for retention time shifts with varied methylamine and acetonitrile concentrations.

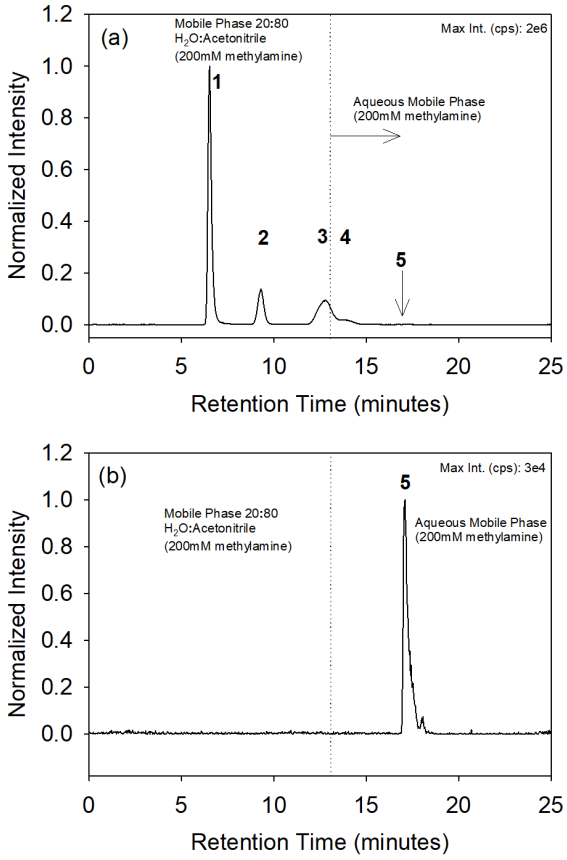

Figure 2.3. (a) TIC chromatogram with ClO_4^- (peak 1), ClO_3^- (peak 2), BrO_3^- (peak 3), ClO_2^- (peak 5), and IO_3^- (peak 5), and **(b)** extracted ion chromatogram for IO_3^- (174.7/158.7) with analysis with a modified IC-ESI-MS/MS method, including a 60 second gradient transition from 20:80 H_2O:acetonitrile (200 mM methylamine concentration) to fully aqueous with 200 mM methylamine at t = 12 minutes (gradient complete at dashed line).

2.3.3. Detection Limits. Quantification of low concentrations of contaminants such as bromate and perchlorate in drinking water samples is critical in protecting consumers. Thus, a low limit of detection (LOD) is desired, as detailed in Table 2.1 for published standard methods. Table 2.4 shows the concentrations of multiple injections of oxyhalide standards used to

determine the LOD and the limit of quantification (LOQ). In Table 2.4 the relative standard deviation (RSD) percent of low oxyhalide concentrations was calculated as (standard deviation/mean)×100. The RSD for chlorate is the highest among the oxyhalides at 17.8%, due to a noisier baseline signal, resulting in an LOD = 0.84 μg/L while LOD's for the other oxychlorides remained equal to or below 0.36 μg/L. This should not be an issue when using this method to analyze water samples treated with contaminated chlorine stocks with high final chlorate concentrations (chlorate / chlorine molar ratios ranged from 0.01 – 0.18 in hypochlorite stocks in one utility survey)[46].

Bromate detection limits are low and should be sufficient to analyze bromate in natural and treated waters. The LOD and LOQ for bromate (0.03 μg/L and 0.1 μg/L, respectively) are both orders of magnitude lower than the regulatory limit set by the EPA (10 μg/L). Perchlorate is an emerging contaminant that the EPA included on the CCL. There is not a set regulatory limit but the LOD and LOQ for perchlorate is likely low enough to identify sources in the natural and engineered environment. The LOD calculated for this method is comparable to reported values for standard methods (Table 2.1), and validates its application as an alternative when limited by instrument or time constraints.

2.3.4. Detection of Oxyhalides in Natural and Synthetic Waters. Ultrapure water with common water anions (bromide, chloride, sulfate, and carbonate) and natural waters were spiked with oxyhalide standards to determine matrix effects on oxyhalide detection. Figure 2.4 illustrates the normalized oxyhalide signal intensity (10 μg/L oxyhalide mixture in water) with varied chloride concentrations (0 – 10 mM), bromide concentrations (0 – 1 mg/L), carbonate concentrations (0 – 10 mM), and sulfate concentrations (0 – 500 mg/L). Chloride and bromide

Table 2.4. Method detection limit data for bromate, perchlorate, chlorate, and chlorite (n = 8).

Replicate No.	Oxyhalide Standard Concentration			
	0.1 µg/L BrO_3^-	**0.1 µg/L ClO_4^-**	**0.5 µg/L ClO_3^-**	**0.5 µg/L ClO_2^-**
1	0.08	0.13	0.46	0.46
2	0.11	0.13	0.43	0.47
3	0.11	0.12	0.40	0.45
4	0.11	0.13	0.54	0.49
5	0.09	0.11	0.58	0.49
6	0.09	0.12	0.51	0.53
7	0.10	0.13	0.59	0.54
8	0.11	0.13	0.71	0.57
Mean	0.10	0.12	0.53	0.50
Standard Deviation (SD)	0.011	0.006	0.093	0.040
Relative Standard Deviation (RSD) (%)	11.0%	5.1%	17.8%	7.9%
Student's t value (@ 98% n-1)	2.998	2.998	2.998	2.998
LOD = SD x Student's t value	0.03	0.02	0.28	0.12
LOQ = 3 x LOD (µg/L)	0.10	0.06	0.84	0.36

elute between 9 – 11 minutes with the outlined isocratic IC-MS method. Thus, these common halides would be expected to elute with and possibly alter the measured bromate and chlorite sensitivity. Chlorite sensitivity decreased as chloride concentration increased (>2 mM); this chloride interference could prove problematic for analysis of estuary and marine matrixes or wastewater effluent however, many freshwaters will be at or below the 70 mg/L Cl^- threshold. In Figure 2.4a, chloride concentration did not appear to alter chlorate, perchlorate, or bromate signal intensity. Bromide was not observed to affect the measured oxyhalide signal in Figure 2.4b. Similarly, there is little variation to the measured oxyhalide signal with increasing carbonate (dosed as bicarbonate) and sulfate in Figure 2.4c,d. Though users should be cautious, a perchlorate isotope ($^{37}ClO_4^-$) has similar mass transitions as two forms of isotopic sulfate ($H^{34}S^{16}O_4$ and $H^{32}S^{16}O_3{}^{18}O$), therefore high sulfate concentrations may interfere with perchlorate

analysis.[30] Sulfate could be removed from samples by pretreating with a barium or a Ba/Ag/H solid phase extraction cartridge if interference is evident.

Drinking water or wastewater samples containing free chlorine (hypochlorous acid/hypochlorite) can be quenched with ethylene diamine (EDA) prior to analysis. EDA and malonic acid do not interfere with oxyhalide detection,[28, 40] though acidic conditions are optimal for rapid chlorine quenching with malonic acid. Other chlorine quenching agents (such as sodium thiosulfate or ascorbic acid) should be avoided due to their ability to oxidize oxyhalides or interfere with MS detection.[28]

Suwannee River natural organic matter (SRNOM) isolate, two surface waters, a treated tap water sample, and two groundwaters from San Juan Island in Washington state were selected to test detection of original and spiked (0 – 25 μg/L) concentrations of bromate, perchlorate, chlorate, chlorite in a natural water matrixes (see Table 2.5 for the matrix details for the natural samples and one tap water sample). All the untreated natural water samples in Figure 2.5 did not have a detectable oxyhalide signal, and chlorate was confirmed in the treated tap water sample (likely from the chlorination source). Measured chlorate and chlorite signals appeared to deviate from the dosed oxyhalide standard concentration in the untreated groundwaters possibly due to interference from elevated chloride concentrations. Groundwater 2 also contains a high NOM concentration, and deviation between the measured and dosed oxyhalide concentrations in that matrix could be due to the carbon content. This observation prompted further analysis on the impact of natural organic matter (NOM) on oxyhalide chromatography and ionization.

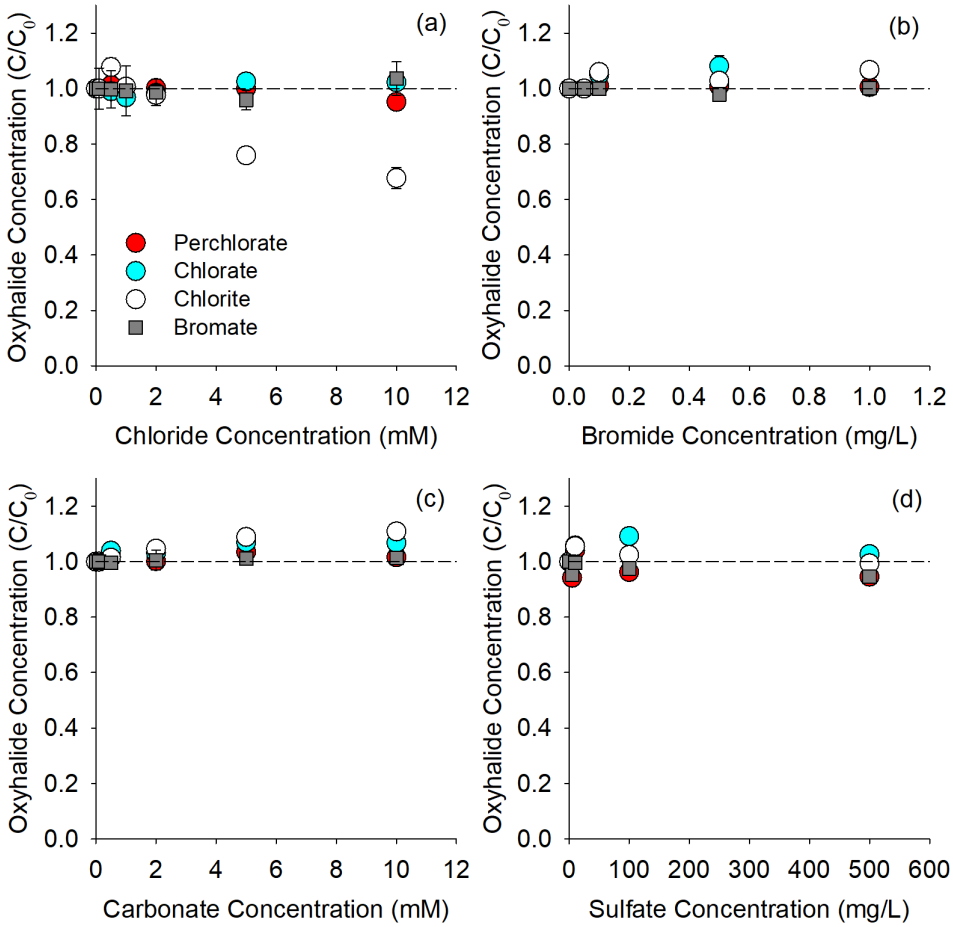

Figure 2.4. Spiked recovery of oxyhalide standards (10 µg/L mixed oxyhalide concentration) in ultrapure water with varying concentrations of **(a)** chloride, **(b)** bromide, **(c)** carbonate, and **(d)** sulfate analyzed via IC-ESI-MS/MS. Error bars are standard deviation of duplicate samples.

Table 2.5. Natural water composition

	pH	[Br^-] (µg/L)	[Cl^-] (mM)	DOC (mg/L as C)	Conductivity (µΩ/cm)
Local Reservoir (Cedar River)	8.1	24.5	0.08	0.5	
Tap water More Hall	7.6	20.0	0.14	0.4	
Groundwater 1	7.4	319.6	3.72	1.35	890
Groundwater 2	7.3	47.9	0.45	6.7	480
Lake Washington	8.1	23.7	0.07	2.4	

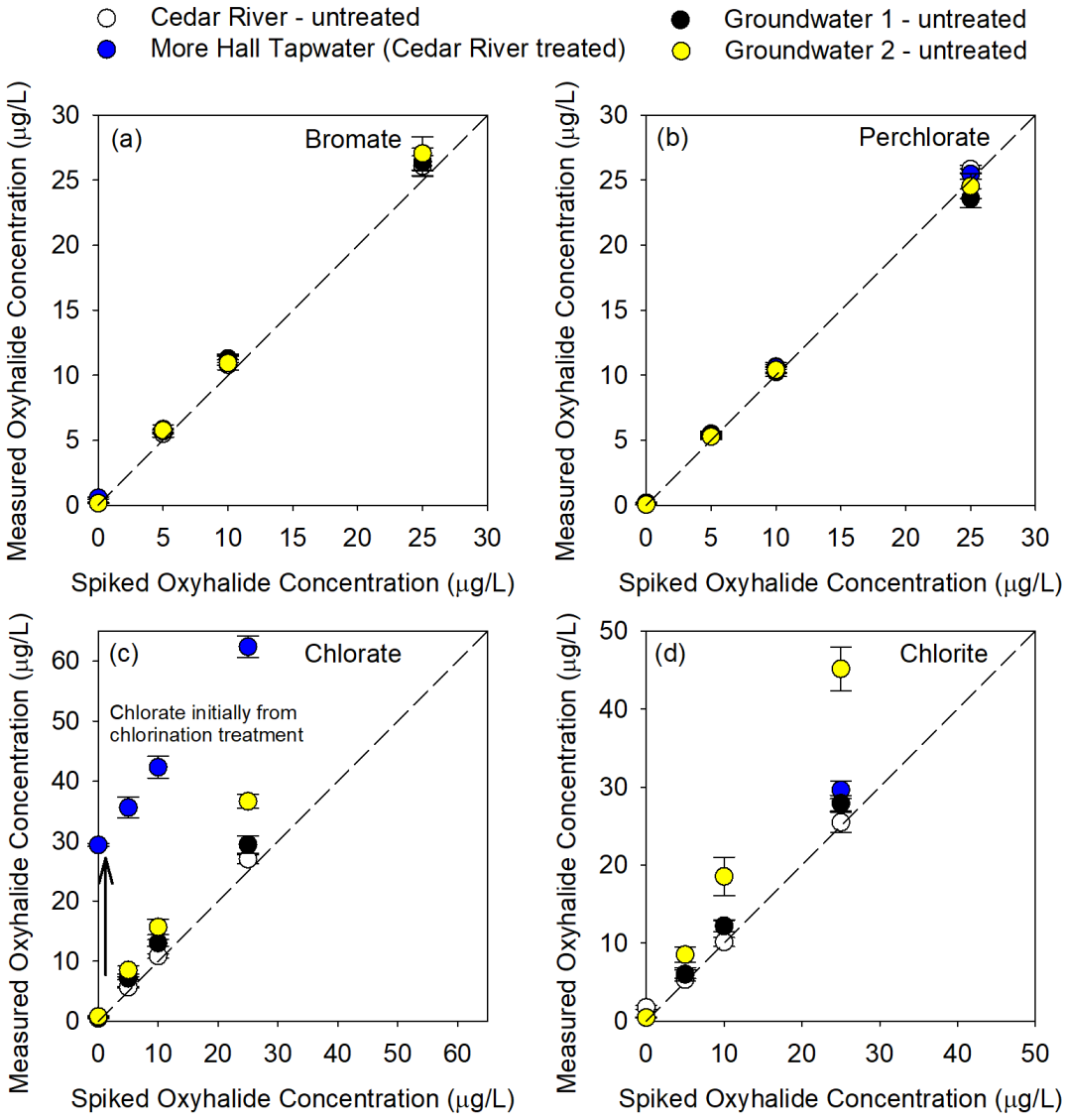

Figure 2.5. Measured **(a)** bromate, **(b)** perchlorate, **(c)** chlorate, and **(d)** chlorite concentrations in spiked natural surface-water and groundwater samples. Chlorate was detected in the tap water sample, $[ClO_3^-]_{unspiked}$ = 29.4 µg/L.

In Figure 2.6, varying concentrations of SRNOM and dilutions of groundwater 2 (with high DOC) were spiked with 10 µg/L oxyhalides and each injection was normalized by the averaged oxyhalide signal in nanopure water. Detected chlorite decreases with increasing SRNOM concentration. It is unlikely that SRNOM is affecting the signal intensity or ionization

efficiency directly but it may be reactive and reduce the dosed chlorite prior to analysis.[47, 48] However, users are typically interested in chlorite concentrations in finished water samples, after any reactions with natural organic matter. Therefore, stable chlorite concentrations should be unaffected, however if humic-rich NOM does suppress the chlorite signal, users should take care when analyzing high DOC water samples. Figure 2.6a shows that Suwannee River NOM has a minimal impact on bromate, perchlorate, and chlorate signal intensity. Similarly, the diluted ground water has a minimal effect on the detected concentrations of oxyhalides, illustrated in Figure 2.4b. Groundwater 2 was included due to its high organic content (DOC = 6.7 mg/L as organic carbon) but appears to be less reactive or aromatic than the Suwannee River NOM.

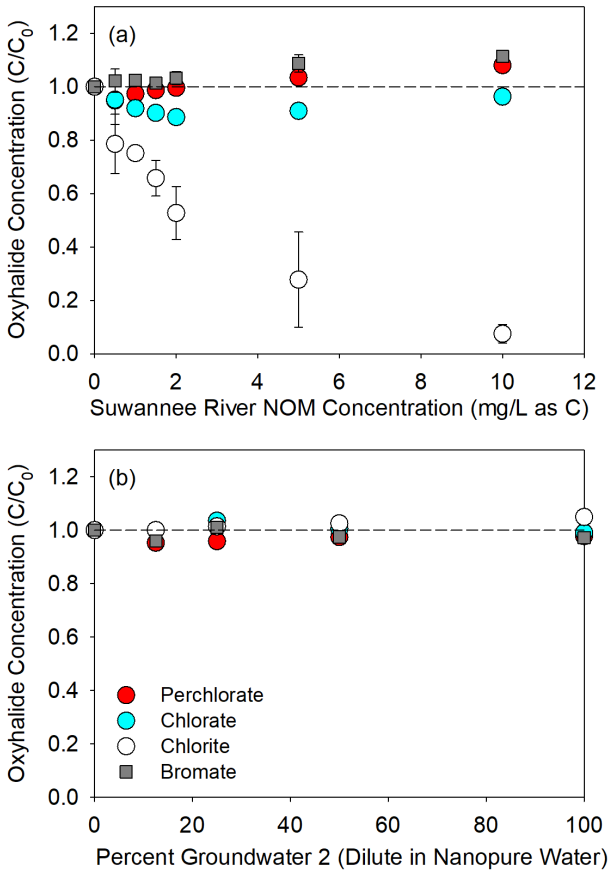

Figure 2.6. Natural water spiked with 10 µg/L oxyhalide standards, **(a)** Suwannee River natural organic matter isolate dissolved in ultrapure water; and **(b)** ground water 2 (DOC = 6.7 mg/L as C) diluted with ultrapure water.

2.3.5. Oxyhalide Formation and Degradation during Solar Chlorine Photolysis. Bromate is the only oxyhalide that is a regulated in the United States, and its formation should be evaluated in systems that expose bromide-containing waters to ozone. The formation of reactive oxygen species (e.g., O_3 and $HO^{\cdot}$) and reactive halogen species (e.g., $Cl^{\cdot}$, $Cl_2^{\cdot -}$, $ClO^{\cdot}$, $Br^{\cdot}$) during solar photolysis of chlorinated water results in increased concentrations of chlorate and bromate (with bromide addition) (Figure 2.7 and 2.8). When present, bromide will react with hypochlorous acid to form hypobromous acid, or react with hydroxyl radical to form reactive bromine species ($Br^{\cdot}$).[49] Due to the combination of bromide, hypobromous acid, hydroxyl radical, and ozone, we anticipate bromate formation to be favorable during solar chlorine photolysis with high concentrations of bromide in the untreated water (when one considers the mechanism of bromate formation).[1, 35] The data presented in Figure 2.7 confirms bromate formation can occur, and is favorable at pH 8, likely due to photolysis of hypochlorite resulting in elevated in situ ozone yields (Table 1.1). Interestingly, the addition of 2 mg/L as C SRNOM suppresses bromate formation and significantly decreases chlorate formation. This provides evidence that NOM is effectively competing for ROS and preventing progression along one (or multiple) reaction pathways that contribute to bromate and oxychloride formation.[1, 35] FAC and ozone produced during solar chlorine photolysis will oxidize bromide and producing hypobromous acid,[35, 50] and hydroxyl radical will react with bromide to produce $Br^{\cdot}$,[49] each contributing to bromate formation. However, the addition of NOM resulted in bromine incorporation from free bromine ($HOBr/OBr^-$ effectively competes with FAC to brominate active site of DOM)[51] and electron transfer reactions with $Br^{\cdot}$ (regenerating bromide), as bromine-incorporation from $Br^{\cdot}$ is unlikly.[52] Chlorite is introduced from the chlorine stock (1:55 ClO_2^-/FAC, molar basis) and is partially removed during dark reactions with NOM (FAC only)

and completely removed during FAC+Light treatment with fluences > 7.2 J/cm^2 (20 minutes irradiation in Figure 2.9). Components of SRNOM are likely reducing chlorite in the dark reactions, or the chlorite signal is suppressed in the presence of SRNOM, as discussed in Section 2.3.4. On the other hand, ozonation of chlorite, forming chlorine dioxide,[53] or oxidation of chlorite by reactive oxygen species (ROS, such as HO$^{\cdot}$ or O(^{3}P)) or reactive chlorine species (RCS, such as Cl$^{\cdot}$, $Cl_2^{\cdot -}$, or ClO$^{\cdot}$) is likely contributing to the removal of chlorite during solar chlorine photolysis. Perchlorate was not detected in the chlorine stock and formation was not observed after chlorination or solar chlorine photolysis treatment of synthetic or natural surface waters. Perchlorate is still a concern in contaminated groundwater sources and this potentially hazardous compound (due to ClO_4^- interference with iodide uptake and thyroid activity)[12] should be monitored in relevant water treatment processes. Iodate was not detected as these experiments did not include an iodide or iodine source.

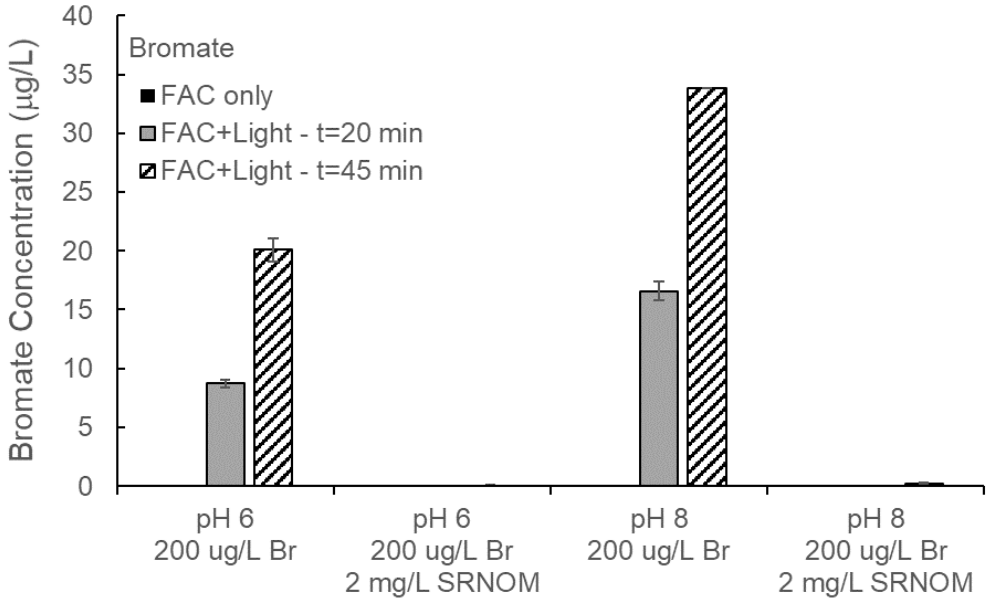

Figure 2.7. Bromate formation during chlorination only (Dark Control – black bar) with a CT_{FAC} matching the measured CT_{FAC} of the longer solar chlorine photolysis treatment, and solar chlorine photolysis for two time points (20 mins – 7.2 J/cm^2 – gray bar, 45 mins – 16.1 J/cm^2 – white striped bar). There was no bromate detected in the chlorine stock source. $[FAC]_0$ ~8 mg/L as Cl_2, 10 deg. C temp.

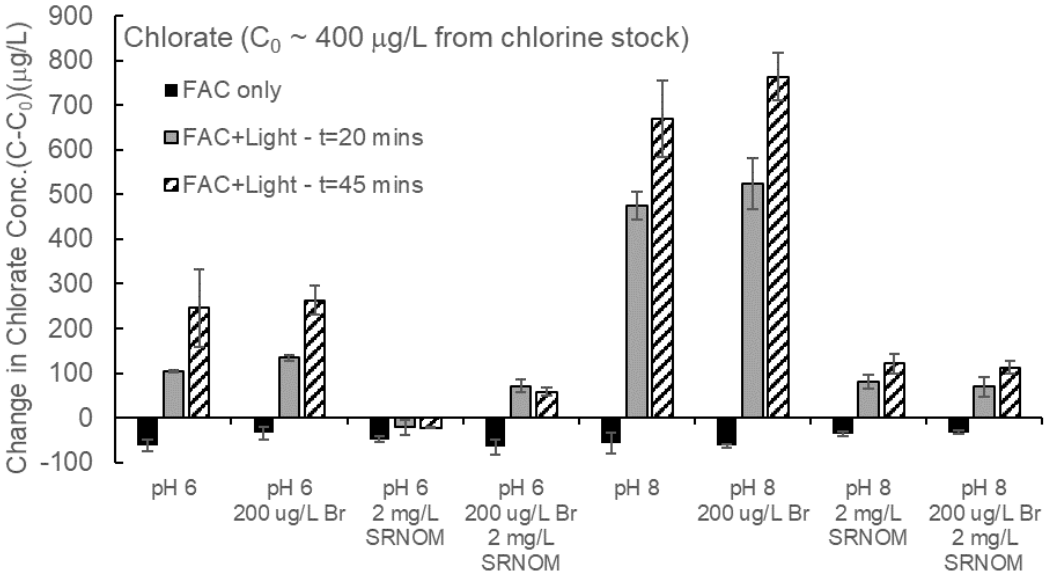

Figure 2.8. Change in chlorate concentration (C – $C_{initial}$) during chlorination only (Dark Control – black bar) with a CT_{FAC} matching the measured CT_{FAC} of the longer solar chlorine photolysis treatment, and solar chlorine photolysis for two time points (20 minutes – 7.2 J/cm^2 – gray bar, 45 minutes – 16.1 J/cm^2 – white striped bar). There was around 400 µg/L chlorate detected in the chlorine stock source. $[FAC]_0$ ~8 mg/L as Cl_2, 10 deg. C temp.

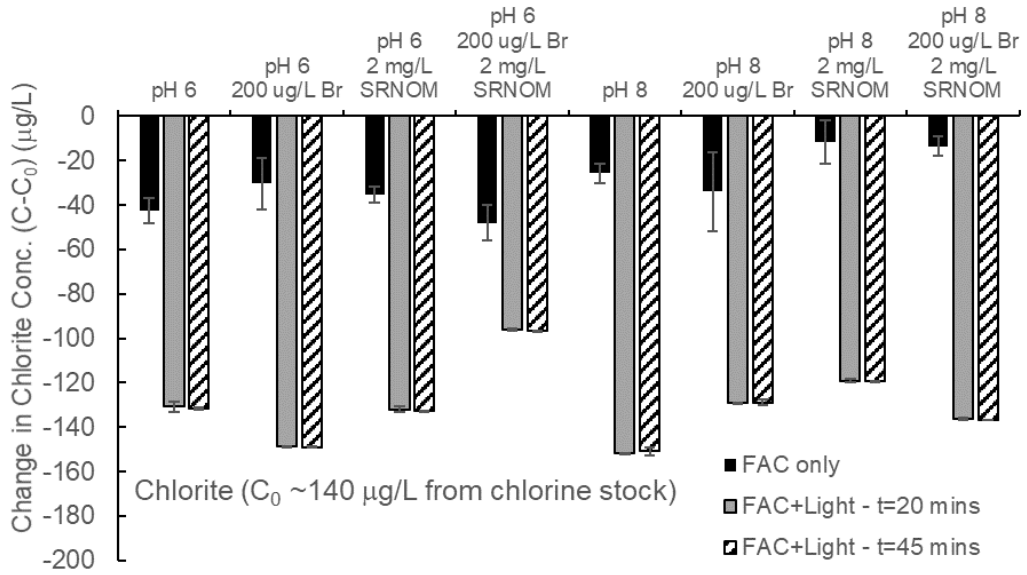

Figure 2.9. Change in chlorite concentration (C – $C_{initial}$) during chlorination only (Dark Control – black bar) with a CT_{FAC} matching the measured CT_{FAC} of the longer solar chlorine photolysis treatment, and solar chlorine photolysis for two time points (20 minutes – 7.2 J/cm^2 – gray bar, 45 minutes – 16.1 J/cm^2 – white striped bar). There was around 140 µg/L chlorite detected in the chlorine stock source. $[FAC]_0$ ~8 mg/L as Cl_2, 10 deg. C temp.

Two surface waters were also evaluated to determine oxyhalide formation in real waters with and without bromide addition during solar chlorine photolysis and chlorination controls (Figure 2.10). The two selected water samples include a high-quality surface water (Cedar River/Local Reservoir, a protected watershed) and an urban-influenced surface water (Lake Washington, between Seattle, WA and Bellevue, WA). Due to low source bromide concentrations (Table 2.5) bromate formation was only detected in samples amended with 200 μg/L bromide (Figure 2.10a). The DOM in Lake Washington appeared to decrease the yields of bromate and chlorate more effectively than the pristine reservoir source, though the DOM was clearly less reactive than SRNOM. Chlorite was effectively removed for all samples exposed to solar chlorine photolysis, providing further evidence that chlorite introduced from the free chlorine stock is degraded via photo-chemical products formed in situ during solar irradiation. The higher quality surface water (Cedar River/Local reservoir) appears to be an excellent candidate for solar chlorine photolysis treatment (low DOC, low bromide, low turbidity) but chlorate formation does occur and an increase in bromide concentration could result in bromate formation that exceeds regulatory MCLs (10 μg/L). When applying solar chlorine photolysis treatment, one would expect decreased bromate yields with NOM present as it is also reactive with hydroxyl radical and ozone species. However, oxyhalide formation could be an issue in natural waters with low DOC (or less reactive DOC) and high bromide concentration (e.g., groundwaters with seawater influence/intrusion[54, 55] and geological or anthropogenic sources of bromide[56]).

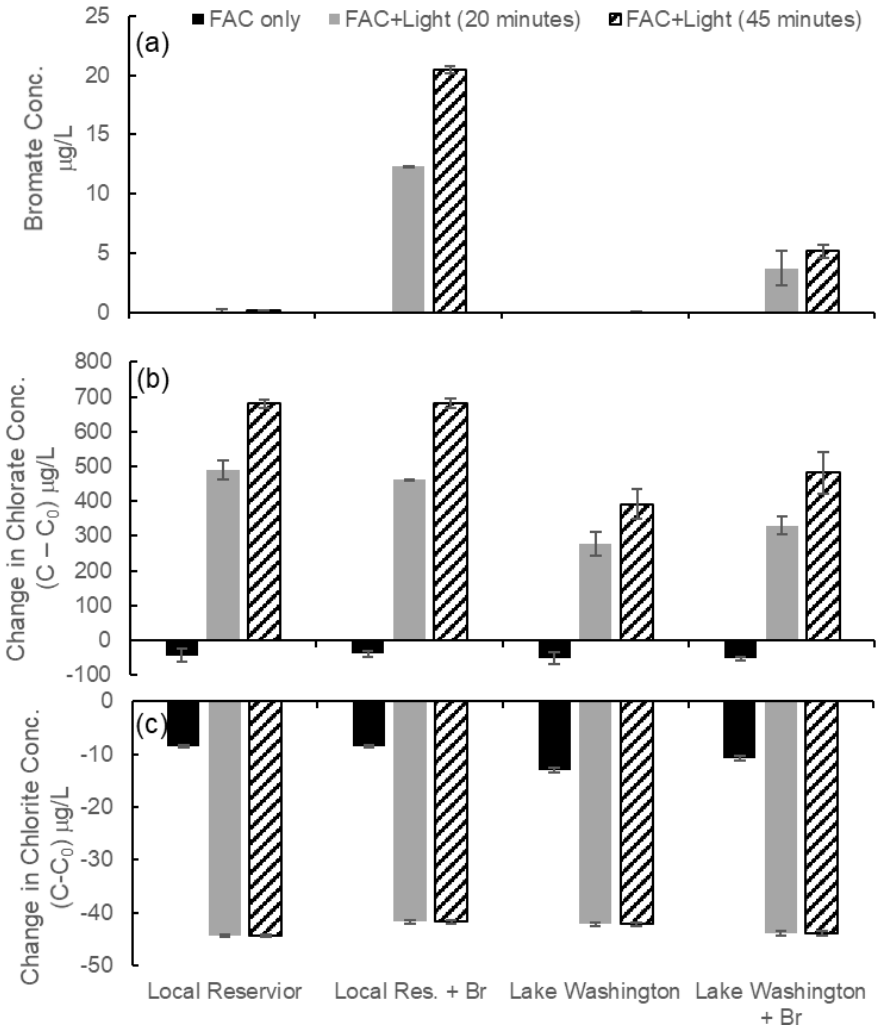

Figure 2.10. **(a)** Bromate concentration; **(b)** Change in chlorate concentration ($C - C_{initial}$); and **(c)** Change in chlorite concentration ($C - C_{initial}$) in two natural surface waters during chlorination only (Dark Control – black bar) with a CT_{FAC} matching the measured CT_{FAC} of the longer solar chlorine photolysis treatment, and solar chlorine photolysis for two time points (20 minutes – 7.2 J/cm^2 – gray bar, 45 minutes – 16.1 J/cm^2 – white striped bar). There was around ~350 µg/L chlorate and ~42 µg/L chlorite introduced from the chlorine stock. $[FAC]_0$ ~8 mg/L as Cl_2, 10 deg. C temp, and bromide addition (+ Br in x-axis) included amending samples with 200 µg/L Br^-, in addition to bromide concentrations naturally occurring in these samples.

2.4. Summary

The method described here is a rapid and sensitive method capable of simultaneously monitoring four oxyhalides of interest in a variety of aqueous mixtures, with the capability to

modify and extend the method to analyze iodate. Sample analysis is complete in less than 15 minutes, saving the user significant time required to run multiple, time-consuming methods to analyze all four analytes. The oxychloride separation is clear, the SRM detection of all analytes enables sub-μg/L detection, and injection volumes are relatively low (100 μL). Chlorite was the analyte most susceptible to retention time shifts from phosphate, signal interference from chloride, and interference or reactivity with natural organic matter. Sulfate has been reported to interfere with perchlorate SRM analysis, but sulfate concentrations included in this study did not have a discernable effect on perchlorate detection. High ortho-phosphate concentrations are capable of occupying ion-binding sites within the column and shorten the retention times for all the oxyhalides, though barium pretreatment can effectively precipitate phosphate and eliminate this effect.

The method confirmed formation of chlorate and bromate (when bromide is present) during solar chlorine photolysis, though introducing 2 mg/L as C SRNOM significantly decreased formation of these two oxyhalides. Chlorite introduced from sodium hypochlorite stock may be reduced by natural organic matter, and in situ ozone, ROS, and RCS production during solar chlorine photolysis is suspected to oxidize chlorite directly. Overall, this IC-MS/MS method is fast and sensitive enough to be used for low-concentration quantification of oxyhalides introduced during conventional and novel water treatment without the need for a conductivity suppressor.

Acknowledgements

This material is based upon work supported by the National Science Foundation under Grant No.

CBET-1236303. Additional support for T.R.Y. from a National Science Foundation Graduate Research Fellowship (ID: 2015177669) and the China Scholarship Council Scholarship for W.L. is gratefully acknowledged.

2.5. References

1. Pinkernell, U.; von Gunten, U., Bromate minimization during ozonation: Mechanistic considerations. *Environ Sci Technol* **2001,** *35* (12), 2525-2531.
2. Peeters, J. E.; Mazas, E. A.; Masschelein, W. J.; Dematurana, I. V. M.; Debacker, E., Effect of Disinfection of Drinking-Water with Ozone or Chlorine Dioxide on Survival of Cryptosporidium-Parvum Oocysts. *Appl Environ Microb* **1989,** *55* (6), 1519-1522.
3. Lee, Y.; von Gunten, U., Oxidative transformation of micropollutants during municipal wastewater treatment: Comparison of kinetic aspects of selective (chlorine, chlorine dioxide, ferrate(VI), and ozone) and non-selective oxidants (hydroxyl radical). *Water Res* **2010,** *44* (2), 555-566.
4. AWWA *2017 Water Utility Disinfection Survey Report*; American Water Works Association: 2018.
5. AWWA *The Potential Regulatory Implications of Chlorate*; AWWA: 2014.
6. Aranda-Rodriguez, R.; Lemieux, F.; Jin, Z. Y.; Hnatiw, J.; Tugulea, A. M., (Yet more) challenges for water treatment plants: potential contribution of hypochlorite solutions to bromate, chlorate, chlorite and perchlorate in drinking water. *J Water Supply Res T* **2017,** *66* (8), 621-631.
7. Garcia-Villanova, R. J.; Leite, M. V. O. D.; Hernandez-Hierro, J. M.; Alfageme, S. D.; Hernandez, C. G., Occurrence of bromate, chlorite and chlorate in drinking waters disinfected with hypochlorite reagents. Tracing their origins. *Sci Total Environ* **2010,** *408* (12), 2616-2620.
8. EPA, U. S. *Occurrence Assessment for the Final Stage 2 Disinfectants and Disinfection Byproducts Rule*; U.S. Environmental Protection Agency: 2005.
9. Kurokawa, Y.; Hayashi, Y.; Maekawa, A.; Takahashi, M.; Kokubo, T.; Odashima, S., Carcinogenicity of Potassium Bromate Administered Orally to F344 Rats. *J Natl Cancer I* **1983,** *71* (5), 965-972.
10. Couri, D.; Abdelrahman, M. S.; Bull, R. J., Toxicological Effects of Chlorine Dioxide, Chlorite and Chlorate. *Environ Health Persp* **1982,** *46* (Dec), 13-17.
11. Steffen, C.; Wetzel, E., Chlorate Poisoning - Mechanism of Toxicity. *Toxicology* **1993,** *84* (1-3), 217-231.
12. Siglin, J. C.; Mattie, D. R.; Dodd, D. E.; Hildebrandt, P. K.; Baker, W. H., A 90-day drinking water toxicity study in rats of the environmental contaminant ammonium perchlorate. *Toxicol Sci* **2000,** *57* (1), 61-74.
13. USEPA, Method 300.1: Determination of Inorganic Anions in Drinking Water by Ion Chromatography. Cincinnati, OH, 1997.

14. Tyrrell, E.; Shellie, R. A.; Hilder, E. F.; Pohl, C. A.; Haddad, P. R., Fast ion chromatography using short anion exchange columns. *Journal of Chromatography A* **2009,** *1216*, 8512-8517.

15. Salhi, E.; von Gunten, U., Simultaneous determination of bromide, bromate and nitrite in low mu g 1(-1) levels by ion chromatography without sample pretreatment. *Water Res* **1999,** *33* (15), 3239-3244.

16. USEPA, Method 317.0: Determination of Inorganic Oxyhalide Disinfection By-products in Drinking Water Using Ion Chromatography with the Addition of a Postcolumn reagent for the Trace Bromate Analysis. Cincinnati, OH, 2001.

17. USEPA, Method 326.0: Determination of Iorganic Oxyhalide Disinfection By-products in Drinking Water using Ion Chromatography Incorporating the Addition of a Suppressor Acidified Postcolumn Reagent for Trace Bromate Analysis. Cincinnati, OH, 2002.

18. USEPA, Method 314.2: Determination of perchlorate in drinking water using two-dimensional ion chromatography with suppressed conductivity detection. Cincinnati, OH, 2008.

19. USEPA, Method 557: Determination of haloacetic acids, bromate, and dalapon in drinking water by ion chromatography electrospray ionization tandem mass spectrometry (IC-ESI-MS/MS). Cincinnati, OH, 2009.

20. Hautman, D. P.; Munch, D. J.; Frebis, C.; Wagner, H. P.; Pepich, B. V., Review of the methods of the US Environmental Protection Agency for bromate determination and validation of Method 317.0 for disinfection by-product anoins and low-level bromate. *Journal of Chromatography A* **2001,** *920*, 221-229.

21. Wagner, H. P.; Pepich, B. V.; Hautman, D. P.; Munch, D. J., US Environmental Protection Agency Method 326.0, a new method for monitoring inorganic oxyhalides and optimization of the postcolumn derivatization for the selective determination of trace levels of bromate. *Journal of Chromatography A* **2002,** *956*, 93-101.

22. Joyce, R. J.; Dhillon, H. S., Trace level determination of bromate in ozonated drinking water using ion chromatography. *Journal of Chromatography A* **1994,** *671*, 165-171.

23. Zhu, B.; Zhong, Z.; Yao, J., Ion chromatographic determination of trace iodate, chlorite, chlorate, bromate, and nitrite in drinking water using suppressed conductivity detection in visible detection. *Journal of Chromatography A* **2006,** *1118*, 106-110.

24. Nowack, B.; von Gunten, U., Determination of chlorate at low ug/L levels by ion-chromatography with postcolumn reaction. *Journal of Chromatography A* **1999,** *849*, 209-215.

25. USEPA, Method 331.0: Determination of perchlorate in drinking water by liquid chromatography electrospray ionization mass spectrometry. Cincinnati, OH, 2005.

26. USEPA, Method 332.0: Determination of perchlorate in drinking water by ion chromatography with suppressed conductivity and electrospray ionization mass spectrometry. Cincinnati, OH, 2005.

27. Aribi, H. E.; Le Blanc, Y. J. C.; Antonsen, S.; Sakuma, T., Analysis of perchlorate in foods and beverages by ion chromatography coupled with tandem mass spectrometry (IC-ESI-MS/MS). *Analytica Chimica Acta* **2006,** *567*, 39-47.

28. Pisarenko, A. N.; Stanford, B. D.; Quinones, O.; Pacey, G. E.; Gordon, G.; Snyder, S. A., Rapid analysis of perchlorate, chlorate and bromate ions in concentrated sodium hypochlorite solutions. *Anal Chim Acta* **2010,** *659* (1-2), 216-223.

29. Cavalli, S.; Polesello, S.; Valsecchi, S., Chloride interference in the determination of bromate in drinking water by reagent free ion chromatography with mass spectrometry detection. *Journal of Chromatography A* **2005,** *1085*, 42-46.

30. Snyder, S. A.; Vanderford, B. J.; Rexing, D. J., Trace analysis of bromate, chlorate, iodate, and perchlorate in natural and bottled waters. *Environ Sci Technol* **2005,** *39* (12), 4586-4593.

31. West, D. M.; Mu, R.; Gamagedara, S.; Ma, Y.; Adams, C.; Eichholz, T.; Burken, J. G.; Shi, H., Simultaneous detection of perchlorate and bromate using rapid high-performance ion exchange chromatography - tandem mass spectrometry and perchlorate removal in drinking water. *Environmental Science and Pollution Research* **2015,** *22*, 8594-8602.

32. Wu, Q.; Zhang, T.; Sun, H.; Kannan, K., Perchlorate in tap water, groundwater, surface waters, and bottled water from China and its association with other inorganic anions and with disinfection byproducts. *Archives of Environmental Contamination and Toxicology* **2010,** *58*, 543-550.

33. Wilkin, R. T.; Fine, D. D.; Burnett, N. G., Perchlorate behavior in a municipal lake following fireworks displays. *Environmental Science and Technology* **2007,** *41*, 3966-3971.

34. Charles, L.; Pepin, D., Electrospray ion chromatography tandem mass spectrometry of oxyhalides at sub-ppb levels. *Analytical Chemistry* **1998,** *70* (2), 353-359.

35. von Gunten, U.; Oliveras, Y., Advanced Oxidation of Bromide-Containing Waters - Bromate Formation Mechanisms. *Environmental Science and Technology* **1998,** *32*, 63-70.

36. Buckingham, D. A.; Keene, F. R.; Sargeson, A. M., Base Hydrolysis of Coordinated Acetonitrile. *J Am Chem Soc* **1973,** *95* (17), 5649-5652.

37. APHA/AWWA/WEF, *Standard Methods: 4500-Cl G. DPD Colormetric Method*. 22 ed.; American Public Health Association: Washington D.C., 2012.

38. Forsyth, J. E.; Zhou, P. R.; Mao, Q. X.; Asato, S. S.; Meschke, J. S.; Dodd, M. C., Enhanced Inactivation of Bacillus subtilis Spores during Solar Photolysis of Free Available Chlorine. *Environmental Science & Technology* **2013,** *47* (22), 12976-12984.

39. Zhou, P.; Di Giovanni, G. D.; Meschke, J. S.; Dodd, M. C., Enhanced inactivation of Cryptosporidium parvum oocysts during solar photolysis of free available chlorine. *Environmental Science & Technology Letters* **2014,** *1* (11), 453-458.

40. Weinberg, H. S.; Yamada, H.; Joyce, R. J., New, sensitive and selective method for determining sub-mu g/l levels of bromate in drinking water. *J Chromatogr A* **1998,** *804* (1-2), 137-142.

41. Gilchrist, E. S.; Healy, D. A.; Morris, V. N.; Glennon, J. D., A review of oxyhalide disinfection byproducts determination in water by ion chromatography and ion chromatography-mass spectroscopy. *Analytica Chemica Acta* **2016,** *942*, 12-22.

42. Subirats, X.; Roses, M.; Bosch, E., On the effect of organic solvent composition on the pH of buffered HPLC mobile phases and the pK(a) of analytes - A review. *Sep Purif Rev* **2007,** *36* (3-4), 231-255.

43. Rabin, S.; Stillian, J., Practical Aspects on the Use of Organic-Solvents in Ion Chromatography. *Journal of Chromatography A* **1994,** *671* (1-2), 63-71.

44. Rossini, E.; Bochevarov, A. D.; Knapp, E. W., Empirical Conversion of pK(a) Values between Different Solvents and Interpretation of the Parameters: Application to Water, Acetonitrile, Dimethyl Sulfoxide, and Methanol. *Acs Omega* **2018,** *3* (2), 1653-1662.

45. Gilchrist, E. S.; Nesterenko, P. N.; Smith, N. W.; Barron, L. P., Organic solvent and temperature-enhanced ion chromatography-high resolution mass spectrometry for the determination of low molecular weight organic and inorganic anions. *Analytica Chimica Acta* **2015,** *865*, 83-91.

46. Stanford, B. D., Perchlorate, Bromate, and Chlorate in Hypochlorite Solutions: Guidelines for Utilities (vol 103, pg 71, 2011). *J Am Water Works Ass* **2011,** *103* (8), 100-100.

47. Taylor, M. C.; White, J. F.; Vincent, G. P.; Cunningham, G. L., Sodium chlorite - Properties and reactions. *Ind Eng Chem* **1940,** *32*, 899-903.

48. Liimatainen, H.; Visanko, M.; Sirvio, J. A.; Hormi, O. E. O.; Niinimaki, J., Enhancement of the Nanofibrillation of Wood Cellulose through Sequential Periodate-Chlorite Oxidation. *Biomacromolecules* **2012,** *13* (5), 1592-1597.

49. Zehavi, D.; Rabani, J., Oxidation of aqueous bromide ions by hydroxyl radicals. Pulse radiolytic investigation. *The Journal of Physical Chemistry* **1972,** *76* (3), 312-319.

50. Deborde, M.; Von Gunten, U. R. S., Reactions of chlorine with inorganic and organic compounds during water treatment—kinetics and mechanisms: a critical review. *Water research* **2008,** *42* (1-2), 13-51.

51. Hua, G.; Reckhow, D. A.; Kim, J., Effect of bromide and iodide ions on the formation and speciation of disinfection byproducts during chlorination. *Environmental Science & Technology* **2006,** *40* (9), 3050-3056.

52. Ike, I. A.; Karanfil, T.; Cho, J.; Hur, J., Oxidation byproducts from the degradation of dissolved organic matter by advanced oxidation processes–A critical review. *Water research* **2019**, 114929.

53. Klaning, U. K.; Sehested, K.; Holeman, J., Standard Gibbs energy of formation of the hydroxyl radical in aqueous solution. *Journal of Physical Chemistry* **1985,** *89*, 760-763.

54. Land, M.; Reichard, E. G.; Crawford, S. M.; Everett, R. R.; Newhouse, M. W.; Williams, C. F. *Ground-water quality of coastal aquifer systems in the West Coast Basin, Los Angeles County, California, 1999-2002*; U.S. Geological Survey and U.S. Department of the Interior: Sacramento, CA, 2004.

55. Orr, L., Is seawater intrusion affecting ground water on Lopez Island, Washington. *US Geological Survey Fact Sheet* **2000**, 057-00.

56. Soltermann, F.; Abegglen, C.; Gotz, C.; Von Gunten, U., Bromide sources and loads in Swiss surface waters and their relevance for bromate formation during wastewater ozonation. *Environmental Science & Technology* **2016,** *50*, 9825-9834.

2.6. Supporting Information for Chapter 2

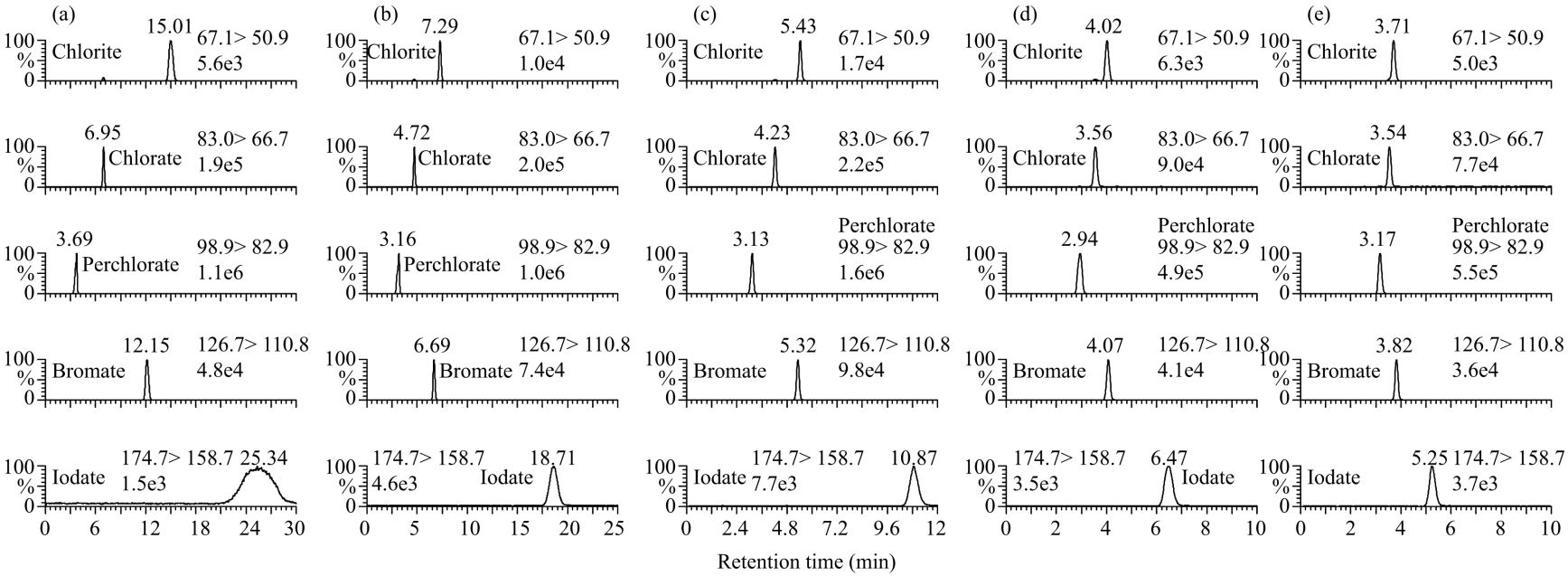

Figure S2.1. Oxyhalide chromatographs after isocratic IC-ESI-MS/MS analysis (channel A is 1 M methylamine and channel B is pure acetonitrile) with a.) 15% A (85% acetonitrile, mobile phase = 150 mM methylamine), b.) 20% A (80% acetonitrile, mobile phase = 200 mM methylamine), c.) 25% A (75% acetonitrile, mobile phase = 250 mM methylamine), d.) 30% A (70% acetonitrile, mobile phase = 300 mM methylamine), and e.) 35% A (65% acetonitrile, mobile phase = 350 mM methylamine).

Chapter 3. Characterization of Disinfection Byproduct Formation and Associated Changes to Dissolved Organic Matter During Solar Photolysis of Free Available Chlorine

Abstract

Solar irradiation of chlorine-containing waters enhances inactivation of chlorine-resistant pathogens (e.g., *Cryptosporidium* oocysts), through in situ formation of ozone, hydroxyl radical, and other reactive species during photolysis of free available chlorine (FAC) at UVB-UVA wavelengths of solar light (290-400 nm). However, corresponding effects on regulated disinfection byproduct (DBP) formation and associated dissolved organic matter (DOM) properties remain unclear. In this work, when compared to dark chlorination, sunlight-driven FAC photolysis over a range of conditions was found to yield higher DBP levels, depletion of DOM chromophores and fluorophores, preferential removal of phenolic groups versus carboxylic acid groups, and degradation of larger humic substances to smaller molecular weight compounds. Control experiments showed that increased DBP levels were not due to direct DOM photolysis and subsequent dark reactions with FAC, but to co-exposure of DOM to FAC and reactive species (e.g., O_3, $HO^{\bullet}$, $Cl^{\bullet}$, $Cl_2^{\bullet-}$, $ClO^{\bullet}$) generated by FAC photolysis. Because solar chlorine photolysis can enable inactivation of chlorine-resistant pathogens at far lower CT_{FAC} values than chlorination alone, the increases in DBP formation inherent to this approach can likely be offset to some extent by the ability to operate at significantly decreased CT_{FAC}. Nonetheless, these findings demonstrate that applications of solar chlorine photolysis will require careful attention to potential impacts on DBP formation.

3.1. Introduction

Free available chlorine (FAC) is the most commonly applied chemical disinfectant worldwide.[1] However, some important waterborne microorganisms are chlorine-resistant and persist after disinfection with FAC. For instance, highly chlorine-resistant oocysts of the protozoan parasites *Cryptosporidium hominis* and *Cryptosporidium parvum* are a frequent cause of waterborne illness in the United States and worldwide.[2, 3] Ultraviolet (UV) irradiation and ozonation are both recognized alternative disinfection strategies that can be applied to achieve inactivation of protozoan (oo)cysts and other chlorine-resistant microorganisms; nevertheless, monetary and energy expenses may prevent their use in small-scale drinking water treatment applications.[4, 5]

Exposing chlorinated water to sunlight has been reported to dramatically enhance inactivation of chlorine-resistant *Bacillus subtilis* endospores and highly-chlorine resistant *Cryptosporidium* oocysts when compared to chlorination alone.[6, 7] Photolysis of free available chlorine (FAC) by solar wavelengths of UV light (i.e., UVB and UVA wavelengths from 290-400 nm, which overlap with the absorption spectra for HOCl and OCl^-; Figure S3.2a) produces hydroxyl radical ($HO^\bullet$), chlorine atom ($Cl^\bullet$), and atomic oxygen ($O^3(P)$); the latter of which reacts with dissolved oxygen (O_2) to form ozone (O_3) (Table 3.1, Equations 3.1–3.4).[6-15] O_3 and $HO^\bullet$ in particular are strong oxidants that can enhance disinfection during chlorination by damaging or penetrating protective spore and cyst coats.[6, 7, 16, 17] Considering the low cost and widespread availability of FAC and sunlight, solar FAC photolysis could provide a uniquely effective option for enhancing disinfection in decentralized and point-of-use treatment, especially in low-resource settings – for example, by combining chlorination with conventional solar disinfection (SODIS)[18].

Table 3.1. Summary of chlorine photolysis reactions and quantum yields

		Φ(254 nm)	Φ(313 nm)	Φ(365 nm)
$HOCl + h\nu \rightarrow HO^{\bullet} + Cl^{\bullet}$	(3.1a)	0.46-1.4 [12,13,15]	1 [14*]	N/A
$OCl^{-} + h\nu \rightarrow O^{\bullet -} + Cl^{\bullet}$	(3.1b)	0.278 [11]	0.127 [11]	0.08 [11]
$OCl^{-} + h\nu \rightarrow O(^3P) + Cl^{-}$	(3.2)	0.074 [11]	0.075 [11]	0.28 [11]

*at approximately 310 nm, N/A = not available

$$HOCl \rightleftarrows H^{+} + OCl^{-} \quad (pK_a = 7.5, \text{ at } 25^{\circ}C) \tag{3.3}$$

$$O(^3P) + O_2 \rightarrow O_3 \tag{3.4}$$

While the potential of solar FAC photolysis for mitigating acute health risks (by enabling inactivation of chlorine-susceptible *and* chlorine-resistant pathogens) has been demonstrated,[6, 7] its possible long-term health implications (e.g., effects on disinfection byproduct formation) must also be explored before recommending its use.

FAC and the various oxidants generated during FAC photolysis also react with inorganic and organic water constituents, such as bromide and dissolved organic matter (DOM), that can serve as disinfection byproduct (DBP) precursors. An abundance of investigations have evaluated DBP formation in DOM-containing waters during UVC-driven (200-280 nm) FAC photolysis – in which HOCl and OCl^{-} undergo primarily homolytic cleavage to form $HO^{\bullet}$ and $Cl^{\bullet}$ (Eqs. 3.1a,b). However, conflicting results have been reported regarding whether FAC+UVC treatment leads to *increased* DBP formation (e.g., due to precursor formation via hydroxylation and aromatic ring opening by hydroxyl radical or other radical species)[19-21] or decreased DBP formation due to precursor degradation,[22, 23] when compared to chlorination alone.[24-26]

Comparatively little information is available regarding the potential impacts of sunlight-driven FAC photolysis on DBP formation.[8, 10, 20, 27] In comparison to UVC-driven FAC

photolysis, solar FAC photolysis ($\lambda > 290$ nm) proceeds to a much greater extent through OCl^- heterolysis (particularly at pH above the pK_a of HOCl; Eq. 3.3) – yielding ground-state atomic oxygen (Eq. 3.2), in addition to O_3 under oxic conditions (Eq. 3.4)[11]. Previous work investigating sequential exposure of DOM to O_3 and chlorine has shown that *high* O_3 doses can *decrease* DBP formation by degrading DBP precursors, whereas *low* O_3 doses can actually result in *increased* DBP formation, especially under conditions favoring $HO^\bullet$ formation.[28-30] The impacts of simultaneous DOM exposure to FAC, O_3, and $HO^\bullet$ or other radicals during solar FAC photolysis are less clear, and to the authors' knowledge, a comprehensive evaluation of this reaction chemistry has yet to be undertaken. Several groups have noted decreases in total organic halogens (TOX) within reclaimed water,[31] and degradation of naphthenic acids within oil sand process water[32] after sunlight-driven FAC photolysis. Others have reported increasing formation of organochlorine, trihalomethanes (THMs), and haloacetic acid (HAAs), coupled with significant degradation of chromophores and fluorophores, during treatment of organic precursors with FAC and artificial UVA light sources ($\lambda_{peak} \sim 350$-365 nm) when compared to dark chlorination.[10, 20] However, there is limited information on formation of specific classes of DBPs during broadband simulated or natural solar irradiation of chlorinated water, or the corresponding impacts on DOM and DBP precursors during the application of this process for drinking water treatment.

Furthermore, available data on DBP formation during UV or sunlight-driven FAC photolysis has generally been reported only for conditions in which water samples were subjected to either (i) varying initial FAC concentrations for fixed irradiation times, or (ii) fixed initial FAC concentrations for variable irradiation times, without accounting for variations in FAC concentration and consequent effects on cumulative FAC exposure ($CT_{FAC} = \int_0^t [\text{FAC}]dt$)

during irradiated and dark treatment. This is an important limitation, as DBP formation is dependent on both FAC concentration *and* reaction time and is expected to be strongly influenced by variations in FAC concentrations during irradiation. Without the availability of measurements of CT_{FAC} (which normalizes for variations in FAC concentration *and* reaction time) from the prior studies, it remains unclear how CT_{FAC}-*specific* DBP formation potentials are affected by sunlight-driven FAC photolysis, in turn hindering direct comparison of DBP formation under dark and light conditions.

The principal objectives of this work were to (a) quantify formation of regulated organic DBPs (THMs and HAAs) during sunlight-driven FAC photolysis, and (b) correlate DBP formation with characteristic changes to DOM during dark chlorination, solar irradiation, and sunlight-driven FAC photolysis. DBP formation was investigated under a variety of conditions (e.g., varying pH, temperature, bromide concentration, or O_2 concentration; w/ and w/o added oxidant scavengers; etc.). The effects of variations in FAC exposure were normalized to CT_{FAC} to enable comparison of CT_{FAC}-specific DBP formation under the range of conditions investigated. Corresponding changes in DOM character were investigated by monitoring changes in DOC, fluorescence excitation-emission matrices (EEMs), UV absorbance (UV_{254} specifically), differential absorbance spectra, and size-exclusion chromatographs of the DOM present in treated solutions. An overarching objective of this work was to utilize these analyses to provide an improved understanding of how DOM modifications resulting from solar irradiation in the presence of FAC influence DBP yields, and how this knowledge may be applied to mitigate such impacts during the use of this approach to enhance inactivation of chlorine-resistant microorganisms for drinking water treatment applications.

3.2. Materials and Methods

3.2.1. Materials. The reverse osmosis isolate of Suwannee River NOM (SRNOM) was obtained from the International Humic Substance Society (batch number 2R101N). All other chemicals, unless specified otherwise, were obtained from Sigma Aldrich and were of at least reagent-grade purity. All aqueous stock solutions were prepared in Milli-Q ultrapure water with resistivity ≥18.2 MΩ cm. Detailed descriptions of chemical and natural water sample sources and stock solution preparation are provided in the Supplementary Material, Text S3.1.

3.2.2. Chlorine and Simulated Sunlight Treatment Procedures. Experiments were undertaken in duplicate using buffered reagent water solutions (10mM phosphate unless otherwise specified, at pH 8.0 or 6.0) or natural water samples (details and characterization in Text S3.1 and Table S3.1) according to four treatment protocols: (i) dark chlorination (FAC only), (ii) simulated solar irradiation without FAC followed by a dark FAC period (Light only/FAC only), (iii) simulated solar irradiation of FAC-containing water for varying times followed by dark FAC treatment (FAC+light/FAC only), and (iv) simulated solar irradiation of FAC-containing water for varying times *without* subsequent dark FAC treatment (FAC+light). All simulated solar irradiations were conducted within an Atlas Material Testing Solutions SUNTEST XLS+ solar simulator equipped with a 1700-W, O_3-free, Xe arc lamp with daylight filter (cutoff below 290 nm) and infrared radiation filter. Irradiations of samples in quartz reactor tubes were undertaken at either 10 or 25 °C (maintained by means of a recirculating water bath). Detailed descriptions of reactor configurations and experimental procedures (including rationale for selection of FAC concentrations, irradiation times, and CT_{FAC} values utilized in experiments) are provided in Text S3.2-S3.3 and Figure S3.1.

Chemical actinometry experiments, using *para*-nitroanisole and pyridine,[33, 34] were

performed in quartz reactor tubes alongside sample irradiation experiments (Text S3.4). Periodic spectral irradiance measurements were obtained using a USB2000+ XR spectroradiometer (Ocean Optics) equipped with a 200 μm × 2 m optical fiber and CC-3-UV-S cosine corrector (see Figure S3.2b for representative spectral irradiance curves).

3.2.3. Natural Sunlight Experiments. Experiments using natural sunlight followed the same general procedures as simulated sunlight experiments, except that samples were exposed to sunlight on the roof of More Hall at the University of Washington. Incident fluence data is included in Figure S3.3, and a representative spectral irradiance curve is included in Figure S3.2b.

3.2.4. Ozone Experiments. One-hundred mL of 2 mg/L SRNOM solutions (pH 8, 0.5 mM phosphate buffer, w/ or w/o 50-mM *tert*-butanol (*t*-BuOH)) were dosed in duplicate with aqueous O_3 at concentrations ranging from 0.25 – 1 g O_3/g DOC, and allowed to react to complete O_3 consumption prior to analyses. See Text S3.1 for details on O_3 stock solution preparation.

3.2.5. Analytical Methods. *3.2.5.1. DBP Extraction and Analysis*. Twenty mL volumes of $Na_2S_2O_3$-quenched sample were acidified to pH < 2 with 98% purity H_2SO_4. After increasing the aqueous ionic strength with sodium sulfate, THMs and protonated HAAs were then extracted into 4 mL of MTBE amended with internal standards (100 μg/L 1,2,3-trichloropropane and 2,3-dibromopropanoic acid) via vigorous mixing. Subsequently, the supernatant MTBE layer containing THMs and HAAs was separated from the underlying aqueous phase via pipetting and transferred into a separate conical-bottom borosilicate glass vial. HAAs were esterified by adding 1 mL of acidified methanol (10% volume H_2SO_4) to 3 mL of the MTBE extract and heating at 50 °C for 2 hours. After esterification, excess acid was neutralized with 4 mL of

saturated aqueous sodium bicarbonate, and 1mL of neutralized MTBE supernatant was transferred to autosampler vials for analysis.[35] THMs and HAAs were analyzed using a Shimadzu GC-2010 with HP-1MS U column and electron-capture detector.

3.2.5.2. Absorbance and Fluorescence Measurements. Samples quenched with As(III), a fast-reacting[36] inorganic FAC quencher with negligible UV absorbance at $\lambda > 220$ nm, were analyzed by UV and fluorescence spectrophotometry. UV-Vis absorbance spectra were recorded from 224 – 800 nm and fluorescence EEMs recorded over an excitation range of 240 – 600 nm and an emission range of 245.2 – 826.6 nm. Both measurements were collected within a 1 cm quartz cuvette using a HORIBA Aqualog 800-C spectrofluorometer (details in Text S3.5).

3.2.5.3. UV-Vis Differential Absorbance Spectrophotometry (DAS). As per established methods,[37, 38] after completion of experiments 40 mL of 0.5 mM phosphate-buffered samples were quenched with $Na_2S_2O_3$ in two-fold excess of FAC and acidified to pH ~ 2.9 by addition of 1 M $HClO_4$. Samples were gradually titrated with NaOH (1 M) at 0.5-unit pH intervals, and absorbance spectra recorded in a 5 cm quartz cell within a Shimadzu UV2700 spectrophotometer (details in Text S3.6). DAS spectra were obtained using Equation 3.5, where $A_{pH(\lambda)}$ is the absorbance (measured between 200 to 600 nm) at varied pH, $A_{pH\_Ref(\lambda)}$ is the reference absorbance acquired at pH ~2.9, and l_{cell} is the quartz cell path length.

$$\Delta A_{pH(\lambda)} = \frac{A_{pH(\lambda)} - A_{pH\_Ref(\lambda)}}{l_{cell} \times DOC};\ \text{units of } L/(mg \cdot cm) \tag{3.5}$$

3.2.5.4. Size Exclusion Chromatography (SEC). As(III)-quenched samples were also analyzed by SEC with inline UV, fluorescence, and DOC detection. One-hundred μL injection volumes of each sample were resolved by size/molecular weight using a Tosoh Toyopearl HW-50S (250 mm x 20 mm, 3 μm) column installed on a Dionex UltiMate3000 HPLC operated at 1

mL/min with a mobile phase of 13.8 mM phosphate buffer at pH 6.8 and 0.1 M ionic strength (with ionic strength adjustment using $NaClO_4$). The HPLC-SEC system was equipped with a UV diode array detector, fluorescence detector, and GE Sievers 900 Series Turbo online organic carbon detector equipped with an inline inorganic carbon remover (additional details in Text S3.7).

3.3. Results and Discussion

3.3.1. Disinfection Byproduct Formation. *3.3.1.1. General effects of FAC photolysis on DBP formation*. Figure 3.1 compares concentrations of HAA5 (mono-, di-, and trichloroacetic acids, and mono- and dibromoacetic acids) and TTHM (chloroform, bromodichloromethane, dibromochloromethane, and bromoform) formed during exposure of phosphate buffered solutions containing 2 mg/L of SRNOM and 8 mg/L as Cl_2 of FAC to varying irradiation times (0, 15, 30, and 45 minutes of simulated sunlight, equal to 0, 6.2, 12.4, and 18.6 J/cm^2 fluence), coupled with post-irradiation dark FAC exposure up to a cumulative CT_{FAC} of 400 (mg/L)×min. As shown in Figure 3.1, there is a clear increase in DBP formation during FAC+light/FAC only treatment when compared to FAC only treatment for all conditions. Elevated temperature resulted in further increases in DBP formation at each condition (Figure 3.1), which appears to be due primarily to increased rates of dark DOM chlorination (Text S3.8). Direct solar irradiation (and hence direct DOM photolysis) did not appear to be an important contributor to DBP formation. Even at the highest fluence investigated (18.6 J/cm^2) HAA5 and TTHM yields after light only/FAC only treatment were similar to those measured following FAC only treatment (Table S3.3). Similar trends were also observed when using natural sunlight to photolyze FAC (Figure S3.3).

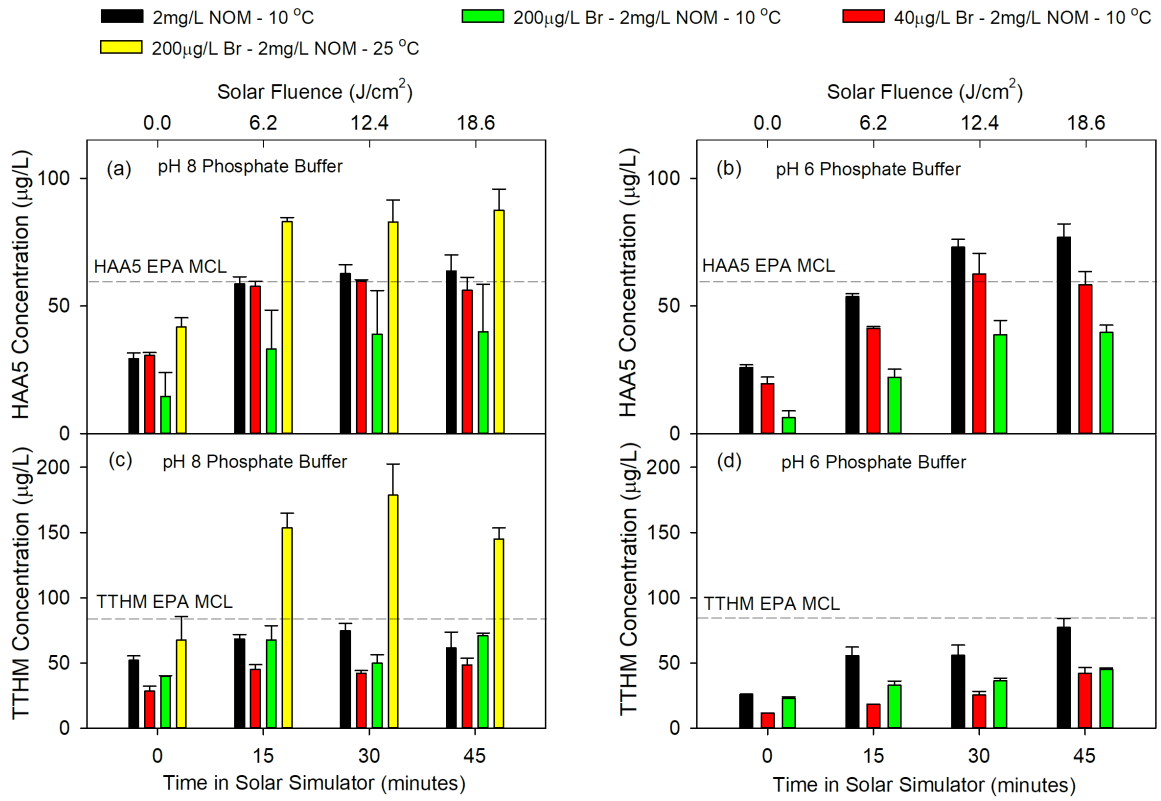

Figure 3.1. (a) HAA5; and **(c)** TTHM formation in pH 8 (10 mM) phosphate buffer with 2 mg/L SRNOM comparing FAC only treatment (0 minutes in the solar simulator) with FAC+light/FAC only treatment at varying bromide concentration (0-200 µg/L) and temperature (10°C or 25°C); and **(b)** HAA5; and **(d)** TTHM formation in pH 6 (10 mM) phosphate buffer with 2 mg/L SRNOM at 10 °C comparing FAC only treatment with FAC+light/FAC only treatment at varying bromide concentration (0-200 µg/L). All samples utilized $[FAC]_0 \sim 8$ mg/L as Cl_2 and targeted $CT_{FAC} = 400$ (mg/L)×min.

As discussed in more detail below, the increases in THM and HAA formation during solar FAC photolysis may result from DOM modifications predisposing certain DBP precursor constituents to increased halogenation during co-exposure to FAC, O_3, and various reactive oxygen or halogen species (ROS or RHS) generated by FAC photolysis. While prior work has shown that pre-ozonation of DOM at ~0.4 – 1 mg O_3/mg C and circumneutral pH can *decrease* THM formation during chlorination,[39, 40] pre-oxidative treatment at lower O_3 exposures and/or elevated $HO^{\bullet}$ exposures (e.g., during O_3 treatment at high pH or AOPs such as UV/H_2O_2) —

similar to the conditions of solar FAC photolysis — has actually been shown to *increase* THM formation during chlorination.[28-30, 41] This is thought to be due to degradation of higher molecular weight humic-like substances to smaller, chlorine-reactive alcohol or ketone-containing aromatic or aliphatic groups.[28-30, 41]

In additional experiments, bromide was added to reaction solutions at concentrations of 40 or 200 μg/L, in order to evaluate formation of brominated DBPs under conditions representative of relatively pristine or human-influenced surface waters.[42, 43] Addition of bromide led to suppression of HAA5 and TTHM yields during both FAC only and FAC+light/FAC only treatments (Figure 3.1). In contrast, HAA9 – which includes additional mixed Cl- and Br-containing HAAs not captured by HAA5 – remained relatively constant at elevated bromide levels during FAC only treatment (Figure S3.6a) (consistent with prior observations)[44, 45], and increased at elevated bromide levels during FAC+light/FAC only treatment (Figure S3.6a). In addition, bromine substitution factor (BSF) – a measure of the fraction of total DBP halogen content attributable to bromine (Text S3.9) – increased for TTHM *and* HAA9 during FAC only and FAC+light/FAC only treatments at elevated bromide levels, with a relatively larger increase in BSF observed during FAC+light/FAC only treatment (Figure S3.6). This suggests increased bromination during FAC+light/FAC only treatment compared to FAC only treatment – potentially due to modifications to DOM during FAC photolysis (leading to greater susceptibility of DBP precursors to bromination), or direct bromination of DBP precursors by photochemically-generated reactive bromine species such as $Br^{\bullet}$ or $BrCl^{\bullet-}$.

pH effects on FAC speciation or photolysis pathway (Eq. 3.1 – 3.4) did not seem to have a clear influence on HAA formation, as variation of pH did not have a strong effect on HAA5 (Figure 3.1a,b) or HAA9 (Figure S3.6a) yields during either FAC only or FAC+light/FAC only

treatment. Prior investigations have also reported variability in the pH-dependence of overall HAA formation during dark chlorination and FAC photolysis processes, though trihaloacetic acid formation appears to correlate inversely with pH during dark chlorination.[21, 24, 46, 47] In contrast, TTHM yields in the present work increased with increasing pH for both FAC only and FAC+light/FAC only treatment (Figure 3.1c,d), consistent with prior observations.[20, 39, 48] In addition to an increased importance of OH^- in the haloform reaction at higher pH, increased TTHM yields during FAC+light/FAC only treatment may be in part related to solar FAC photolysis kinetics, as the rate of FAC photolysis increases with pH at wavelengths above 260 nm due to increased UV absorbance by FAC with the shift in speciation from HOCl to OCl^- (Eqs. 3.1 – 3.4, Figure S3.2a).[8, 9]

3.3.1.2. Effects of dissolved O_2 removal and radical scavenger addition. In order to evaluate the relative importance of O_3 and radical species in driving DBP formation during FAC+light/FAC only treatment, concentrations of O_2 were varied from ~0 to 1.6 mmol/L and the radical scavengers *t*-BuOH or carbonate (as $NaHCO_3$) were added separately at concentrations of 50 mM to selected reaction solutions (Figure 3.2).

Initially anoxic conditions are expected to limit formation of O_3 by preventing the reaction of photochemically-generated $O(^3P)$ with O_2, whereas saturation with O_2 is anticipated to increase O_3 formation relative to ambient conditions (as per Eq. 3.4). Addition of 50 mM concentrations of *t*-BuOH or carbonate is anticipated to lead to 97% or 41% scavenging of $HO^\bullet$, 95% or 88% scavenging of $Cl^\bullet$, and 53% or 4% scavenging of $O(^3P)$ under the experimental conditions investigated here (Text S3.10 and Table S3.4).

The absence of O_2 did not appear to lead to significant differences in HAA5 yields, whereas O_2 saturation led to moderate decreases in HAA5 yields, indicating that O_3 may

contribute to destruction of HAA precursors during FAC photolysis (Figure 3.2a). Figure 3.2b shows that the absence of O_2 resulted in a small increase in TTHM yields during FAC+light/FAC only treatment, possibly due to decreased destruction of THM precursors (e.g., dihydroxybenzenes) by O_3.[39, 40] O_2 saturation had no clear effect on THM yields during FAC+light/FAC only treatment.

Addition of *t*-BuOH and carbonate each appeared to result in modest decreases in HAA5 yields (Figure 3.2a) during FAC+light/FAC only treatment, due in large part to decreases in di- and trichloroacetic acid formation (Figure 3.2a and Figure S3.6a). This indicates that radical reactions with DOM may contribute to HAA precursor formation. Carbonate and *t*-BuOH addition did not have a clear effect on TTHM yields during FAC+light/FAC only treatment (Figure 3.2b). Overall, variations in dissolved O_2 concentrations and addition of radical scavengers resulted in at most modest changes to organic DBP formation, making it difficult to distinguish direct effects of O_3 and radical species (e.g., $HO^{\bullet}$, $Cl^{\bullet}$, $Cl_2^{\bullet-}$, $ClO^{\bullet}$, $O(^3P)$) on DBP precursors.

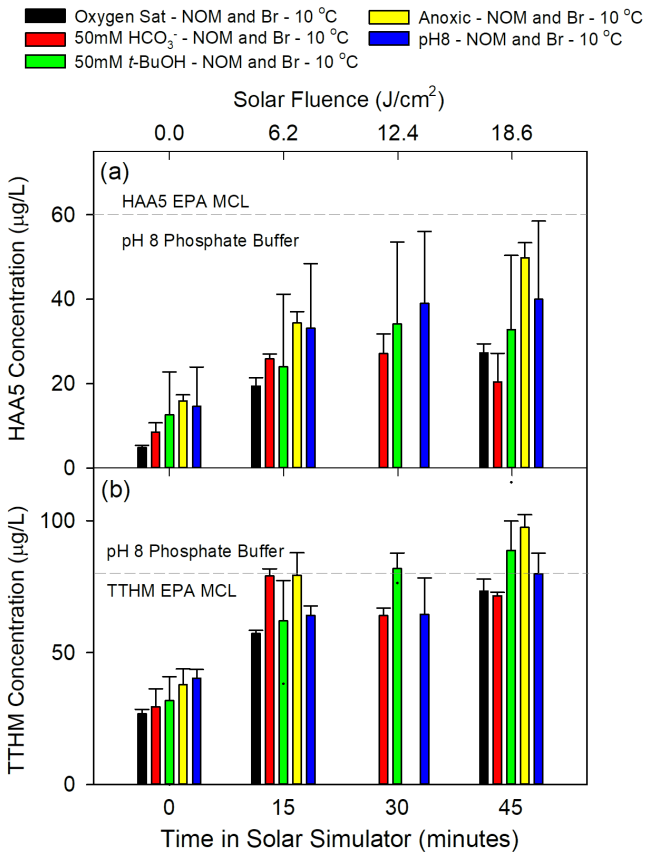

Figure 3.2. (a) HAA5 and **(b)** TTHM formation with saturated (1.6mM) dissolved O_2 (black), 50 mM HCO_3^- (red), 50 mM *t*-BuOH (green), initially anoxic conditions (yellow), or no alteration (blue) after exposure to FAC only or varied FAC+light/FAC only treatment. All solutions were prepared in 10 mM phosphate buffer at pH 8 at 10 °C with 2 mg/L SRNOM, 200 µg/L bromide, and $[FAC]_0 \sim 8$ mg/L as Cl_2, and targeted $CT_{FAC} = 400$ (mg/L)×min.

3.3.1.3. Importance of photochemical versus dark reactions in driving DBP formation.

Figure 3.3 compares DBP formation versus CT_{FAC} during FAC only treatment and FAC+light treatment (labeled 15, 30, and 45 minutes) *without* and *with* post-irradiation dark FAC treatment. Compared to FAC only treatment, FAC+light treatment resulted in substantially greater yields of THM and HAA5 at a given CT_{FAC} value, confirming that yields of DBPs are elevated *during* sunlight-driven FAC photolysis. Figure 3.3 also highlights the change in DBP formation resulting from continued FAC only treatment *after* sunlight-driven FAC photolysis by comparing

the results for FAC+light treatment (open symbols) with those for FAC+light/FAC only treatment (half-filled symbols), with the same irradiation times used in each case. It appears that the CT_{FAC}–normalized rate of HAA5 formation during dark chlorination (Figure 3.3, solid lines) increases modestly after FAC+light treatment (regression slopes increase by factors of 2 and 3 for pH 8 and 6, respectively), whereas the rate of TTHM formation during dark chlorination (Figure 3.3, dashed lines) is similar after FAC+light and FAC only pretreatment when normalized by CT_{FAC}. Taken together, these data indicate that most (if not all) of the *relative increases* in DBP yields observed during FAC+light/FAC only experiments are due to DBP formation during FAC photolysis, rather than to post-irradiation reactions in the dark. This in turn suggests that increases in DBP formation during sunlight-driven FAC photolysis are driven primarily by halogenation reactions *during* irradiation (consistent with Oliver and Cary (1977)[10]), though it is unclear if this is due to (i) direct halogenation of DOM by RHS (e.g., $Cl^{\bullet}$, $Br^{\bullet}$, $BrCl^{\bullet-}$, $Cl_2^{\bullet-}$, $ClO^{\bullet}$), (ii) oxidative modifications to DOM resulting in generation of precursor moieties with higher susceptibility toward halogenation by FAC (or RHS), or (iii) a combination of both.

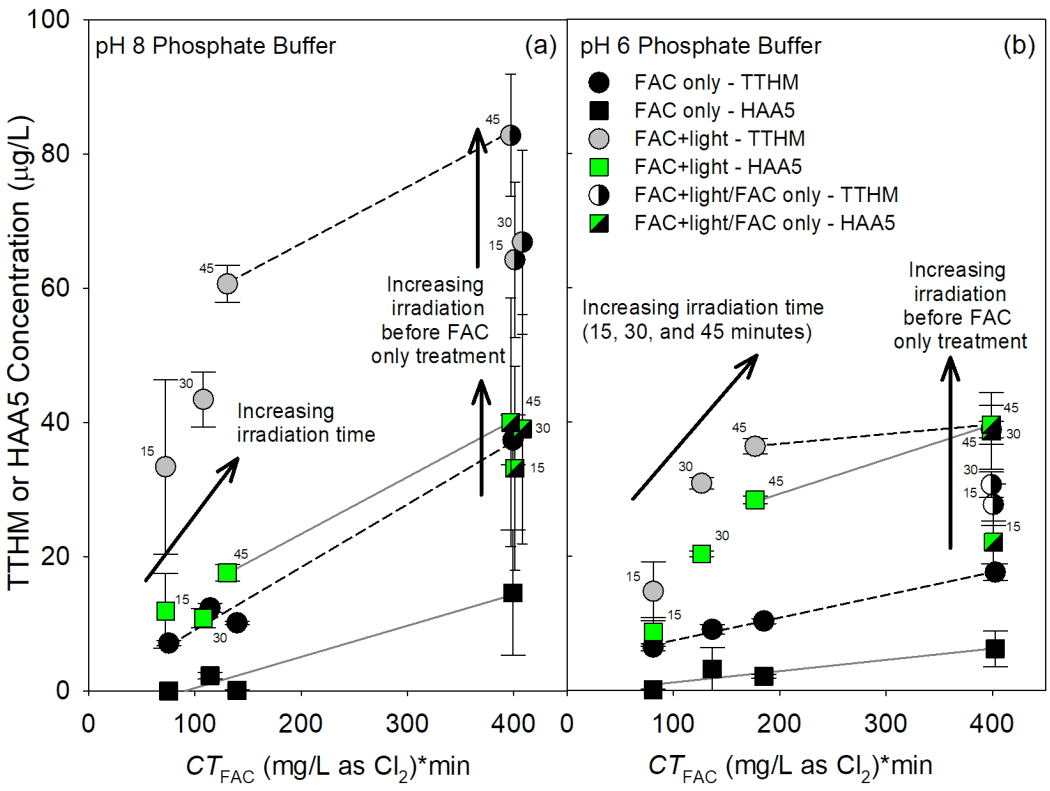

Figure 3.3. Comparison of TTHM and HAA5 formation during FAC only, FAC+light, and FAC+light/FAC only treatment targeting CT_{FAC} = 400 (mg/L)×min at 10 °C for **(a)** pH 8; and **(b)** pH 6. All samples were prepared in 10 mM phosphate buffer with 2 mg/L SRNOM, 200 µg/L bromide, and $[FAC]_0$ ~ 8 mg/L as Cl_2.

3.3.1.4. DBP formation during treatment of natural waters. Figure 3.4 shows HAA5 and TTHM yields in two natural freshwaters – Lake Washington and a local reservoir; with and without addition of 200 µg/L of bromide – subjected to (i) FAC only, (ii) Light only/FAC only, and (iii) FAC+light/FAC only treatment. FAC only and Light only/FAC only treatment (at fluences up to 18.6 J/cm^2) resulted in similar DBP yields, indicating that direct photolysis of the DOM does not impact DBP formation during chlorination. HAA5 concentrations associated with Lake Washington remained well below the EPA MCL of 60 µg/L and were not detected within the local reservoir water. TTHM formation was compliant with the EPA MCL of 80 µg/L at

natural bromide concentrations for each water, though at higher bromide concentrations, formation of bromodichloromethane and dibromochloromethane increased during solar FAC photolysis, and TTHM levels exceeded the MCL. These results indicate that sunlight-driven FAC photolysis can likely be applied for disinfection of natural waters with relatively low DOM and bromide concentrations, though further work is needed to evaluate its applicability over a wider range of water qualities.

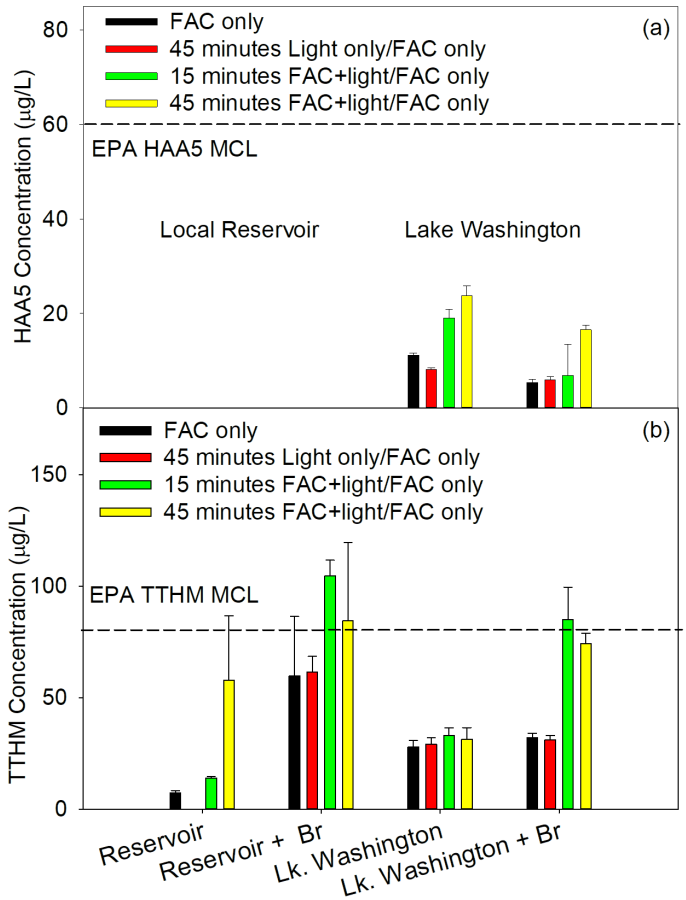

Figure 3.4. **(a)** HAA5; and **(b)** TTHM formation in natural waters during FAC only, Light only/FAC only, and FAC+light/FAC only treatment. For all samples the temperature was 10 °C, $[FAC]_0 \sim 8$ mg/L as Cl_2, and $CT_{FAC} = 400$ (mg/L)×min. Local Reservoir – pH = 8.05, 0.5 mg/L as C with 24.5 µg/L bromide and 30.7 mg/L as $CaCO_3$ alkalinity. Lake Washington – pH = 8.10, 2.4 mg/L as C with 23.7 µg/L bromide and 38.0 mg/L as $CaCO_3$ alkalinity. Samples labeled "+ Br" included an additional 200 µg/L of bromide in excess of natural levels.

3.3.2. Analyses of Changes to Dissolved Organic Matter. *3.3.2.1. UV-Vis Absorbance and Fluorescence.* The results summarized in Figure 3.5a, Figure S3.7a, and Table S3.5 show that SRNOM after FAC+light treatment has substantially lower 254 nm UV absorbance than after FAC only treatment. Addition of *t*-BuOH results in preservation of chromophores during solar FAC photolysis (31% and 51% losses in 254 nm absorbance with and without *t*-BuOH respectively, after 45 minutes of FAC+light). Anoxic conditions also result in preservation of chromophores during solar FAC photolysis treatment, but to a lesser extent than *t*-BuOH addition (40% loss after 45 minutes of FAC+light); indicating that radical species *and* O_3 contribute to decreases in absorbance and destruction of associated aromatic compounds.

Untreated SRNOM has characteristic fluorescence features, including two peaks located near 250 nm_{Ex} / 450 nm_{Em} and 330 nm_{Ex} / 450 nm_{Em}, that are typically associated with terrestrial humic constituents.[49, 50] DOM with high fluorescence intensity in these regions has been positively correlated to THM formation during chlorination.[22, 49] Figure S3.8 depicts the change to fluorescence EEMs after FAC only, Light only, Light only/FAC only, FAC+light, and FAC+light/FAC only treatment. FAC+light and FAC+light/FAC only treatments resulted in significantly greater losses in the fluorescence signals associated with humic constituents when compared to FAC only, Light only, or Light only/FAC only treatments (Figure 3.5a, S3.7a). Previous research also observed greater fluorophore destruction during FAC-UVA treatment when compared to FAC-UVC AOP treatment[20] and FAC-only treatment.[32]

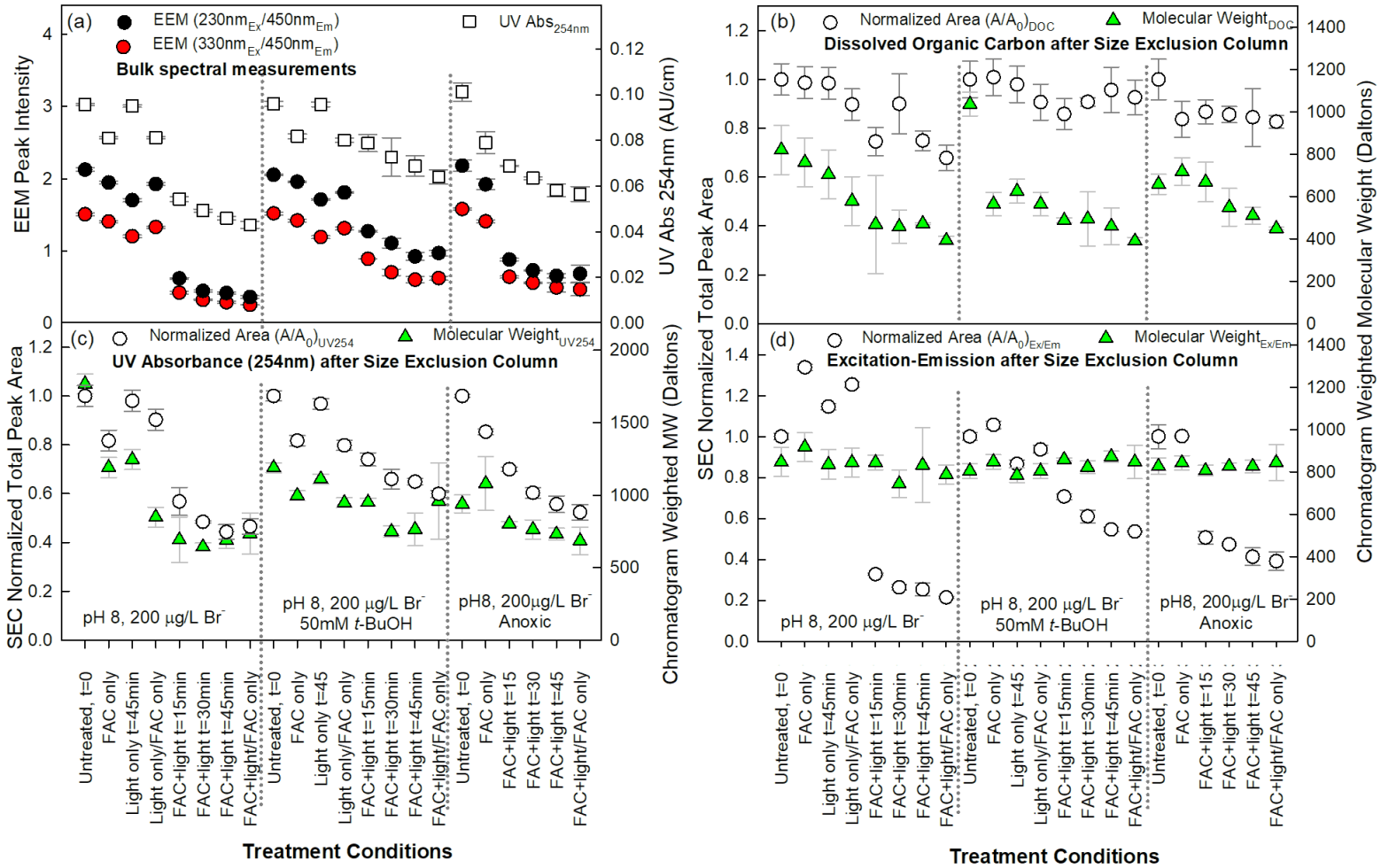

Figure 3.5. **(a)** Bulk UV absorbance at 254 nm (white squares) and fluorescence (filled circles). **(b)-(d)** SEC data for **(b)** DOC, **(c)** UV absorbance at 254 nm, and **(d)** fluorescence (Ex: 320 nm, Em: 450 nm), summarizing total chromatographic peak areas normalized by untreated samples (white circles), and MW estimated from signal intensity-weighted retention times (green triangles; Text S3.7 for details). Data is from experiments with pH 8, 10mM phosphate buffered solutions containing 2 mg/L SRNOM and 200 µg/L Br^- at 10 °C, after Light only, FAC only, Light only(45 min. irr.)/FAC only, FAC+Light, and FAC+Light(45 min. irr.)/FAC only treatment (x-axis represents treatment conditions, not time series). FAC only, Light only/FAC only, and FAC+light/FAC only experiments targeted CT_{FAC} = 400 (mg/L)×min.

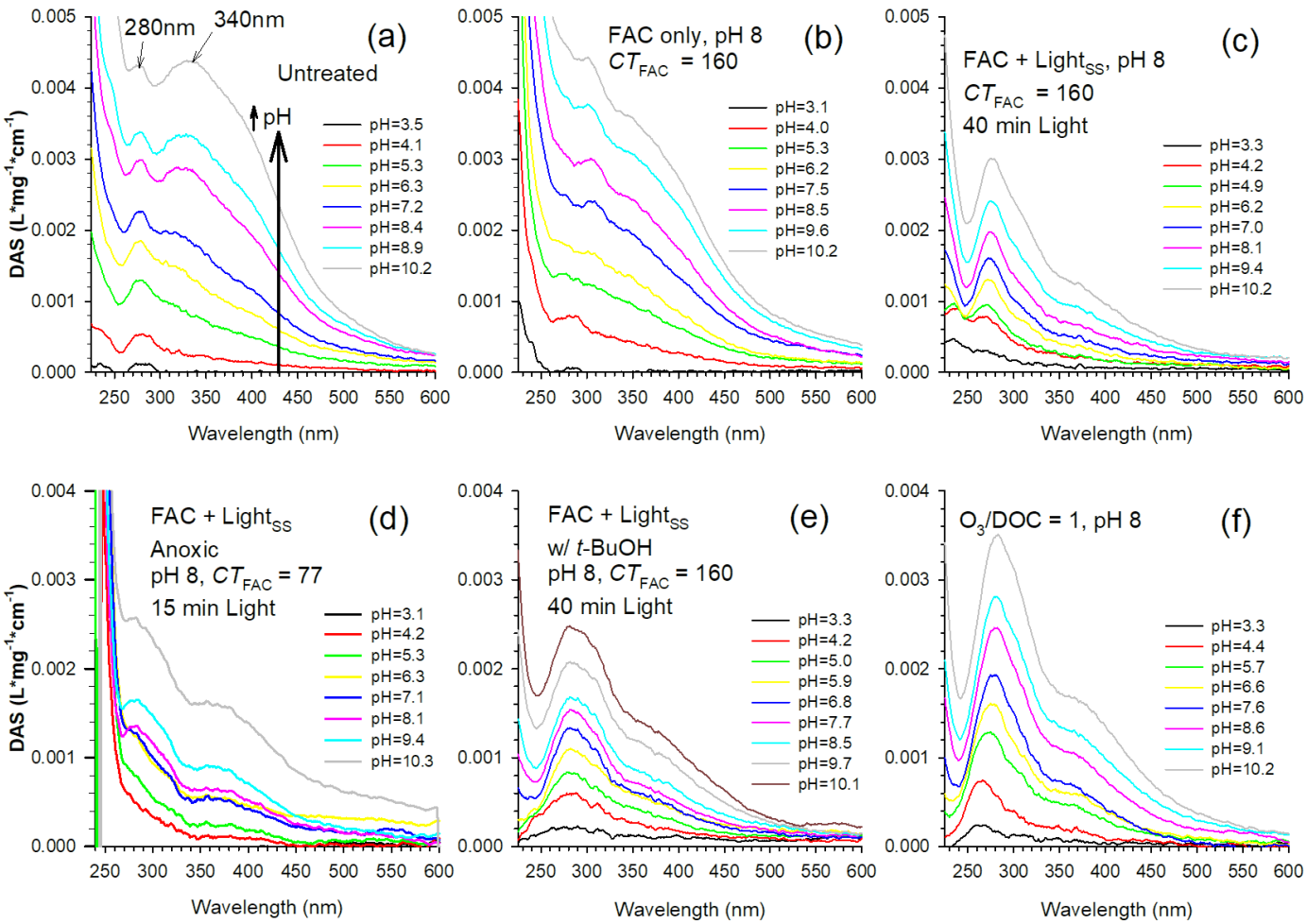

Figure 3.6. Sample DAS spectra for 2 mg/L SRNOM in 0.5 mM phosphate buffer subjected to **(a)** no treatment; **(b)** FAC only treatment at pH 8 to CT_{FAC} =160 (mg/L)×min; **(c)** FAC+light treatment at pH 8 to CT_{FAC} =160 (mg/L)×min; **(d)** FAC+light treatment at pH 8 with initially anoxic conditions, CT_{FAC} = 77 (mg/L)×min; **(e)** FAC+light treatment at pH 8 with 50mM *tert*-butanol to CT_{FAC} =160 (mg/L)×min; and **(f)** O_3 only treatment at pH 8. All solutions prepared in of 0.5 mM phosphate buffer at 25 °C with 2 mg/L SRNOM and $[FAC]_0$ ~ 8 mg/L as Cl_2.

Introducing *t*-BuOH as a radical scavenger during solar chlorine photolysis significantly inhibited degradation of humic-like fluorophores, to an extent greater than observed by limiting O_3 formation under anoxic conditions (Figure 3.5a, S3.7a and Table S3.5). These trends indicate that photochemically-generated $HO^{\bullet}$, $Cl^{\bullet}$, or other ROS/RHS, and – to a lesser degree – O_3, all play important roles in the degradation of fluorophores during FAC+light treatment.

3.3.2.2. UV-Vis Differential Absorbance Spectra (DAS). The pH titration DAS analysis method provides an in situ approach to quantifying behavior of ionizable chromophores, which reflects contributions of carboxylic and phenolic functional groups in DOM.[37, 38] A monotonic increase in UV absorbance (240-450 nm) of DOM is typically observed with increasing pH, which is primarily associated with deprotonation of aromatic DOM chromophores.[51] From the DAS results of raw SRNOM (Figure 3.6a) there are two prominent feature bands: a narrow band centered at ~280 nm (DA280) associated with carboxylic acid groups, and a broad band centered at ~340 nm (DA340) associated with phenolic groups.[37, 38]

FAC only treatment of SRNOM-containing solutions at pH 8 and 6 resulted in moderate decreases in sample absorbance (Figure 3.6b, S3.9a,b), indicating that FAC reacted directly with chromophores within the DOM. The DA340/DA280 ratio for samples subjected to FAC only treatment at pH 8 and 6 did not change during titration from pH 6 to 10, indicating suppression of the phenol deprotonation feature compared to the untreated sample (Figure S3.9a,b). Light only treatment had no significant impact on DAS spectra (Figure S3.9a,b).

Exposing SRNOM-containing solutions to FAC+light treatment using natural (FAC+$light_{NS}$) or simulated sunlight (FAC+$light_{SS}$) at pH 6 and 8 resulted in substantially greater bleaching of UV absorbance compared to FAC only treatment, and particularly enhanced removal at 340 nm, indicating preferential modification of phenolic groups (Figures 3.6c,

S3.9a,b). FAC+light treatment at pH 8 resulted in a lower average DA340/DA280 ratio than at pH 6, likely due to increased deprotonation of phenolic groups to more reactive phenolate forms and higher FAC photolysis rates at pH 8 (Figure S3.9a,b). The addition of bromide was found to have no significant effect on changes to the DA340/DA280 ratio before or after treatment (Figure S3.9b,c).

Changes in DAS spectra observed during FAC+light treatment at pH 8 were similar to those observed during treatment of samples with increasing O_3 doses (O_3/DOC > 0.75) (Figure 3.6c,f), where addition of *t*-BuOH had little effect on DAS changes during direct O_3 treatment (Figure S3.9e). This is consistent with the proposed role of O_3 in contributing to direct degradation of phenolic groups in DOM during FAC+light treatment. However, purging O_2 from solution to limit the formation of O_3 during FAC+light treatment at pH 8 did not have a significant effect on DA340/DA280 ratios in comparison to FAC+ $light_{SS}$ treatment at ambient O_2 levels (Figures 3.6d and S3.9d), suggesting either that O_3 plays a significantly less important role in driving phenol degradation compared to $O(^3P)$, $HO^{\bullet}$, $Cl^{\bullet}$, and other radical species, or that increased degradation of phenols by $O(^3P)$ (which would be elevated in the absence of O_2, as per Eq. 3.4) compensates for the absence of O_3. Adding *t*-BuOH as a radical scavenger limited decreases in DA340/DA280 ratios during FAC+light treatment to a moderate extent (Figure 3.6e and S3.9d), indicating some preservation of phenol groups due to suppression of ROS, RHS, and/or O_3 (via scavenging of $O(^3P)$).[7]

3.3.2.3. Size Exclusion Chromatography with UV-fluorescence-DOC detection (SEC-UV-FLD-DOC). Size exclusion chromatography enables fractionation of DOM by size and/or molecular weight (MW), resulting in discrimination of two major peaks in the SRNOM comprising (1) a larger peak (Peak 1 here) assigned to higher MW humic substances and (2) a

second, smaller peak (Peak 2 here) generally assigned to lower MW acidic compounds[52, 53] (see Figure S3.10 for example chromatograms). Figures 3.5b-d and S3.7b-d summarize results from chromatographic analyses of treated samples, including normalized total chromatogram area ($(\text{Peak 1 + Peak 2})_{area}/(\text{Peak 1 + Peak 2})_{area,untreated}$) and average DOM MW estimates – each obtained using UV, fluorescence, and DOC detection (see Text S3.7 for analytical details and MW calculations and Figure S3.11 for plots of fractional peak areas).

FAC only treatment generally resulted in a decrease of <20% for UV chromatogram areas and 5-10% for total DOC areas, while a slight (~5%) increase in total fluorescence was visible – an effect associated with halogenation of DOM.[54] Increasing periods of irradiation during FAC+light treatment resulted in decreases in overall MW as measured by UV and DOC detection, as well as 40-60% decreases in total UV chromatogram areas and up to 25% decreases in DOC chromatogram areas (Figures 3.5b,c, S3.7b-d). By comparison, fluorescence peak area decreased 20-80% with minimal changes to overall MW as measured by fluorescence (Figures 3.5d, S3.7d). These observations for FAC+light treatment are likely attributable to degradation of higher MW humic substances comprising Peak 1 to lower MW byproducts comprising Peak 2 (with little corresponding mineralization of DOC to CO_2), coupled with degradation of chromophores associated primarily with higher MW humic substances, and degradation of fluorophores associated with both higher and lower MW organics. Low MW byproducts that contribute to Peak 2 in DOC chromatograms after treatment appear to have a modest UV signal and very little fluorescence character (Figure S3.10).

Changes observable by DOC and UV detection were similar for each treatment at pH 8 and 6 (Figures 3.5b,c, S3.7b,c). Similar to bulk sample fluorescence and UV absorbance measurements, addition of *t*-BuOH resulted in preservation of chromophores and fluorophores

and appeared to hinder degradation of larger MW compounds to lower MW compounds. This implies that $HO^{\bullet}$, $Cl^{\bullet}$, and other RHS species likely play an important role in breaking down aromatic molecules contained within larger DOM size fractions, though it should be noted that *t*-BuOH also scavenges $O(^3P)$ to a limited extent,[7] so some of the decreases in chromophore and fluorophore destruction may also have been due to blockage of reactions between $O(^3P)$ or O_3 and DOM. Suppressing O_3 formation by deoxygenation of reaction solutions prior to FAC+light treatment also resulted in decreased destruction of chromophores and fluorophores, but not to the same extent as *t*-BuOH addition. This suggests that O_3 may target a subset of primarily electron-rich aromatic functional groups such as phenols and activated aromatic rings, whereas $HO^{\bullet}$, $Cl^{\bullet}$, and other radical species may less selectively attack a larger pool of aromatic components within the DOM.

3.3.3. Linkages Between Observed DOM Modifications and Increased DBP Formation during Sunlight-driven FAC Photolysis. Decreases in fluorescence and UV absorbance of SRNOM exhibited clear correlations with THM and HAA9 yields during FAC+light treatment (Figure S3.12), whereas correlations for HAA5 yields were weaker (likely due to the smaller group of HAAs encompassed by HAA5 relative to HAA9). There were no clear trends between DBP formation and fluorescence or absorbance changes during FAC only treatment, providing additional evidence that modifications of DOM by ROS, RHS, and/or O_3 produced during FAC photolysis are associated with the observed increases THM and HAA yields.

The findings discussed to this point suggest that O_3 generated during solar FAC photolysis contributes to preferential elimination of SRNOM's humic-like fluorescence properties, which are likely attributable in part to activated/electron-rich aromatic rings (e.g.,

phenolic groups).[55, 56] Similarities in DA340/DA280 losses during FAC+light treatment and O_3 only treatment also indicate a role for O_3 in preferential phenolic degradation during FAC photolysis. Previous work has shown that treatment of DOM by O_3 results in degradation of aromatics within DOM (e.g., ring cleavage of dihydroxybenzenes and phenolic-like compounds) and to decreased DBP formation during subsequent chlorination, highlighting the role of phenolic moieties in DOM as DBP precursors.[22, 39] However, it is possible that under the conditions of FAC+light treatment, O_3 levels are low enough relative to DOM concentrations that activated aromatic DBP precursors are *generated* by oxygenation and/or hydroxylation reactions to a greater extent than they are *destroyed.*[28, 29] In this work, HAA and THM formation during FAC+light/FAC only treatment seemed to correlate negatively with conditions favoring higher in situ O_3 levels, supporting the hypothesis that increasing O_3 exposure contributes to the net degradation of organic DBP precursors.

Experiments undertaken here with added radical scavengers indicate that ROS and RHS contribute to both chromophore and fluorophore destruction and non-selective attack and degradation of high molecular weight humic-like substances to form lower molecular weight organic acids. $HO^{\bullet}$ has been found to react rapidly via hydroxylation of olefins and aromatic compounds and hydrogen abstraction from aliphatic compounds.[41, 57-59] $Cl^{\bullet}$ may also react with a variety of aliphatic, aromatic, and olefinic moieties, as well as alcohol groups in DOM via addition, electron-transfer, and/or H-abstraction.[23, 57, 60, 61] Overall, ROS and/or RHS reactions appear to contribute to the generation of additional DBP precursors. It is hypothesized that $HO^{\bullet}$ in particular activates aromatic groups by hydroxylation and generates lower MW aldehydes, ketones, and carboxylic acids as transformation products after reacting with higher MW fractions of DOM.[23, 57] HAA formation increases moderately during FAC only treatment *after* FAC+light

pretreatment when compared to FAC only treatment at equivalent CT_{FAC}, supporting the hypothesis that molecules generated via ROS and RHS reactions with DOM act as HAA precursors (specifically for DCAA and TCAA) during the residual dark chlorination period of FAC+Light/FAC only experiments. Increased THM and HAA formation *during* FAC+light treatment may also be due to direct attack of DOM by radical species such as $HO^{\bullet}$, $Cl^{\bullet}$, $Br^{\bullet}$, $BrCl^{\bullet-}$, $Cl_2^{\bullet-}$, or $ClO^{\bullet}$ – initiating radical chain reactions leading to Cl-addition or C-centered radical recombination with $Cl^{\bullet}$ or other halogen radicals.[21, 22, 60, 61]

One possible explanation for the increases in DBP yields observed during FAC+light treatment, even in the presence of added radical scavengers or under anoxic conditions, is that O_3 *and* radical species contribute to varying degrees to both degradation *and* generation of DBP precursors,[28, 30] with precursor generation generally outweighing precursor degradation. Consequently, limiting O_3 formation does not prevent increases in DBP formation due to radical reactions,[22] and limiting $HO^{\bullet}$ and $Cl^{\bullet}$ levels does not prevent increases in DBP formation due to $O(^3P)$ and/or O_3 reactions.[28, 29]

3.4. Conclusions

- Application of simulated and natural sunlight-driven FAC photolysis in SRNOM solutions and natural waters resulted in increased yields of regulated organic DBPs (THMs and HAAs), degradation of DOM chromophores and fluorophores, and decreases in average DOM MW due to degradation of higher MW humic substances to lower MW organic acids with minimal mineralization of DOC.
- Subjecting DOM-containing solutions to FAC+light treatment resulted in substantial changes in the ratios of differential absorbances at 280 and 340 nm (corresponding to carboxylic and

phenolic DOM moieties), with preferential removal of the 340 nm band, indicating depletion of phenol groups relative to carboxylic groups in the bulk DOM.

- Taken together, these results indicate that FAC+light treatment results in enhanced degradation of UV-absorbing and fluorescent aromatic constituents (phenolic moieties in particular) of higher MW humic substances by photochemically-generated oxidants including O_3, $HO^{\bullet}$, and possibly $Cl^{\bullet}$, $ClO^{\bullet}$, $Cl_2^{\bullet-}$, and $O(^3P)$. Oxidants are expected to participate in aromatic and aliphatic electron transfer, addition, and H-abstraction reactions, in addition to aromatic ring cleavage, resulting in formation of lower MW organic acid byproducts. This process likely results in enhanced formation of DBPs through (a) increased dark halogenation of DBP precursors derived from aromatic ring-cleavage and other DOM degradation pathways; (b) direct halogenation of DBP precursors by RHS such as $Cl^{\bullet}$, $Br^{\bullet}$, $BrCl^{\bullet-}$, $Cl_2^{\bullet-}$, or $ClO^{\bullet}$; or (c) a combination of the two. The fact that DBP formation during FAC only treatment subsequent to FAC+light treatment was only moderately higher (for HAAs) than during FAC only treatment suggests that direct halogenation by photochemically-generated RHS may contribute substantially to the enhanced DBP yields observed during sunlight-driven FAC photolysis. It is recommended that future investigations expand on these findings by utilizing model compounds representing various types of DOM constituent groups to evaluate the relative importance of reaction pathways involving ROS, RHS, and O_3 in driving DBP formation during solar FAC photolysis (and UV-driven FAC photolysis in general).
- Application of sunlight-driven FAC photolysis for disinfection is anticipated to lead to increased DBP formation, and will require careful attention to potential impacts on THM and HAA levels. However, because this process can enable inactivation of chlorine resistant

pathogens (e.g., *Cryptosporidium* oocysts) at far lower CT_{FAC} values than chlorination alone, the increases in DBP formation inherent to FAC+light treatment may be offset by the ability to operate at significantly decreased CT_{FAC}. In addition, risks of increased DBP formation could be mitigated by limiting applications of sunlight-driven FAC photolysis to short-term (e.g., emergency) use and/or to appropriate source waters (e.g., those with low DOM and bromide levels, as observed here for treatment of two samples collected from natural surface water sources).

Acknowledgements

This material is based upon work supported by the National Science Foundation under Grant No. CBET-1236303. Additional support from a National Science Foundation Graduate Research Fellowship (ID: 2015177669) for T.R.Y., the National Science Foundation of China (51708279) for W.L., and the University of Washington Mary Gates Research Scholarship for A.G. is gratefully acknowledged. Two anonymous reviewers are thanked for their helpful comments.

3.5. References

1. WHO *Guidelines for drinking-water quality: fourth edition incorporating the first addendum*; License: CC BY-NC-SA 3.0 IGO; World Health Organization (WHO): Geneva, 2017.
2. Painter, J. E.; Hlavsa, M. C.; Collier, S. A.; Xiao, L. H.; Yoder, J. S., Cryptosporidiosis Surveillance - United States, 2011-2012. *Mmwr Surveill Summ* **2015,** *64* (3), 1-13.
3. Medema, G. T., P., Blokker,M.; Deere,D.; Davidson,A.; Charles,P.; and Loret, J.F., Risk Assessment of Cryptosporidium in Drinking Water. Public Health and Environment: Water, S., Hygiene and Health, Ed. WHO Press: Geneva, Switzerland, 2009.
4. Cho, M.; Kim, J. H.; Yoon, J., Investigating synergism during sequential inactivation of Bacillus subtilis spores with several disinfectants. *Water Res* **2006,** *40* (15), 2911-2920.
5. EPA, U. S., Technologies and Cost Document for the Final Long Term 2 Enhanced Surface Water Treatment Rule and Final Stage 2 Disinfectants and Disinfection Byproducts Rule. Water, O. o., Ed. National Service Center for Environmental Publications: 2005.
6. Forsyth, J. E.; Zhou, P. R.; Mao, Q. X.; Asato, S. S.; Meschke, J. S.; Dodd, M. C., Enhanced Inactivation of Bacillus subtilis Spores during Solar Photolysis of Free Available Chlorine. *Environ Sci Technol* **2013,** *47* (22), 12976-12984.
7. Zhou, P.; Di Giovanni, G. D.; Meschke, J. S.; Dodd, M. C., Enhanced Inactivation of Cryptosporidium parvum Oocysts during Solar Photolysis of Free Available Chlorine. *Environ Sci Tech Let* **2014,** *1* (11), 453-458.
8. Nowell, L. H.; Hoigne, J., Photolysis of Aqueous Chlorine at Sunlight and Ultraviolet Wavelengths .2. Hydroxyl Radical Production. *Water Res* **1992,** *26* (5), 599-605.
9. Nowell, L. H.; Hoigne, J., Photolysis of Aqueous Chlorine at Sunlight and Ultraviolet Wavelengths .1. Degradation Rates. *Water Res* **1992,** *26* (5), 593-598.
10. Oliver, B. G.; Carey, J. H., Photochemical Production of Chlorinated Organics in Aqueous-Solutions Containing Chlorine. *Environ Sci Technol* **1977,** *11* (9), 893-895.
11. Buxton, G. V.; Subhani, M. S., Radiation-Chemistry and Photochemistry of Oxychlorine Ions .2. Photodecomposition of Aqueous-Solutions of Hypochlorite Ions. *J Chem Soc Farad T 1* **1972,** *68*, 958-&.
12. Watts, M. J.; Linden, K. G., Chlorine photolysis and subsequent OH radical production during UV treatment of chlorinated water. *Water Research* **2007,** *41*, 2871-2878.
13. Wang, D.; Bolton, J.; Hofmann, R., Medium pressure UV combined with chlorine advanced oxidation for trichloroethylene destruction on a model water. *Water Research* **2012,** *46*, 4677-4686.
14. Molina, M.; Ishiwata, T.; Molina, L. T., Production of OH radical from photolyssi of HOCl at 307 - 309 nm. *Journal of Physical Chemistry* **1980,** *84*, 821-826.

15. Jin, J.; El-Din, M.; Bolton, R. G., Assessment of the UV/Chlorine process as an advanced oxidation process. *Water Research* **2011,** *45*, 1890-1896.

16. Cho, M.; Yoon, J., Measurement of OH radical CT for inactivating Cryptosporidium parvum using photo/ferrioxalate and photo/TiO2 systems. *J Appl Microbiol* **2008,** *104* (3), 759-766.

17. Cho, M.; Yoon, J., Quantitative evaluation and application of Cryptosporidium parvum inactivation with ozone treatment. *Water Sci Technol* **2007,** *55* (1-2), 241-250.

18. McGuigan, K. G.; Conroy, R. M.; Mosler, H. J.; du Preez, M.; Ubomba-Jaswa, E.; Fernandez-Ibanez, P., Solar Water Disinfection (SODIS): A review from bench-top to roof-top. *Journal of Hazardous Materials* **2012,** *7* (53), 29-46.

19. Xiang, Y.; Fang, J.; Shang, C., Kinetics and pathways of ibuprofen degradation by the UV/Chlorine advanced oxidation. *Water Res* **2016,** *90*, 301-308.

20. Pisarenko, A. N.; Stanford, B. D.; Snyder, S. A.; Rivera, S. B.; Boal, A. K., Investigation of the use of Chlorine Based Advanced Oxidation in Surface Water: Oxidation of Natural Organic Matter and Formation of Disinfection Byproducts. *J Adv Oxid Technol* **2013,** *16* (1), 137-150.

21. Wang, D.; Bolton, J. R.; Andrews, S. A.; Hofmann, R., Formation of disinfection by-products in the ultraviolet/chlorine advanced oxidation process. *Sci Total Environ* **2015,** *518*, 49-57.

22. Li, T.; Jiang, Y.; An, X. Q.; Liu, H. J.; Hu, C.; Qu, J. H., Transformation of humic acid and halogenated byproduct formation in UV-chlorine processes. *Water Res* **2016,** *102*, 421-427.

23. Wang, W. L.; Zhang, X.; Wu, Q. Y.; Du, Y.; Hu, H. Y., Degradation of natural organic matter by UV/chlorine oxidation: Molecular decomposition, formation of oxidation byproducts and cytotoxicity. *Water Res* **2017,** *124*, 251-258.

24. Remucal, C. K.; Manley, D., Emerging investigators series: the efficacy of chlorine photolysis as an advanced oxidation process for drinking water treatment. *Environ Sci-Wat Res* **2016,** *2* (4), 565-579.

25. Yang, X.; Sun, J.; Fu, W.; Shang, C.; Li, Y.; Chen, Y.; Gan, W.; Fang, J., PPCP degradation by UV/chlorine treatment and its impact on DBP formation potential in real waters. *Water Res* **2016,** *98*, 309-318.

26. Liu, W.; Zhang, Z.; Yang, X.; Xu, Y.; Liang, Y., Effects of UV irradiation and UV/chlorine co-exposure on natural organic matter in water. *Sci Total Environ* **2012,** *414*, 576-584.

27. Simard, S.; Tardif, R.; Rodriguez, M. J., Variability of chlorination by-product occurrence in water of indoor and outdoor swimming pools. *Water Res* **2013,** *47* (5), 1763-1772.

28. Mao, Y. Q.; Wang, X. M.; Yang, H. W.; Wang, H. Y.; Xie, Y. F. F., Effects of ozonation on disinfection byproduct formation and speciation during subsequent

chlorination. *Chemosphere* **2014,** *117*, 515-520.

29. Riley, T. L.; Mancy, K. H., *The effect of preozonation on chloroform production in the chlorine disinfection processes*. Ann Arbor Science: Ann Arbor, MI, 1978; Vol. 2.

30. De Vera, G. A.; Stalter, D.; Gernjak, W.; Weinberg, H. S.; Keller, J.; Farre, M. J., Towards reducing DBP formation potential of drinking water by favouring direct ozone over hydroxyl radical reactions during ozonation. *Water Res* **2015,** *87*, 49-58.

31. Lv, X. T.; Zhang, X.; Du, Y.; Wu, Q. Y.; Lu, Y.; Hu, H. Y., Solar light irradiation significantly reduced cytotoxicity and disinfection byproducts in chlorinated reclaimed water. *Water Res* **2017,** *125*, 162-169.

32. Shu, Z. Q.; Li, C.; Belosevic, M.; Bolton, J. R.; El-Din, M. G., Application of a Solar UV/Chlorine Advanced Oxidation Process to Oil Sands Process-Affected Water Remediation. *Environ Sci Technol* **2014,** *48* (16), 9692-9701.

33. Laszakovits, J. R.; Berg, S. M.; Anderson, B. G.; O'Brien, J. E.; Wammer, K. H.; Sharpless, C. M., p-Nitroanisole/Pyridine and p-Nitroacetophenone/Pyridine Actinometers Revisited: Quantum Yield in Comparison to Ferrioxalate. *Environ Sci Tech Let* **2017,** *4* (1), 11-14.

34. Dulin, D.; Mill, T., Development and Application of Chemical Actinometers for Solar Irradiance. *Abstr Pap Am Chem S* **1981,** *181* (Mar), 82-Envr.

35. Munch, D. J. M., J.W.; and Pawlecki, A.M., Method 552.2, Determination of Haloacetic acids and Dalapon in Drinking Water by Liquid-Liquid Extraction, Derivatization and Gas Chromatography with Electron Capture Detection. Laboratory, N. E. R., Ed. Cincinnati, OH, 1995.

36. Dodd, M. C.; Vu, N. V.; Le, V. C.; Kissner, R.; Pham, H. V.; Cao, T. H.; Berg, M.; Von Gunten, U., Kinetics and mechanistic aspects of As(III) oxidation by chlorine, chloramines, and ozone: Relevance to drinking water treatment. *Environmental Science and Technology* **2006,** *40* (10), 3285-3292.

37. Dryer, D. J.; Korshin, G. V.; Fabbricino, M., In situ examination of the protonation behavior of fulvic acids using differential absorbance spectroscopy. *Environ Sci Technol* **2008,** *42* (17), 6644-6649.

38. Gao, Y.; Korshin, G., Effects of NOM properties on copper release from model solid phases. *Water Res* **2013,** *47* (14), 4843-4852.

39. Gallard, H.; von Gunten, U., Chlorination of natural organic matter: kinetics of chlorination and of THM formation. *Water Res* **2002,** *36* (1), 65-74.

40. Hua, G. H.; Reckhow, D. A., Effect of pre-ozonation on the formation and speciation of DBPs. *Water Res* **2013,** *47* (13), 4322-4330.

41. Dotson, A. D.; Keen, V. S.; Metz, D.; Linden, K. G., UV/H2O2 treatment of drinking water increases post-chlorination DBP formation. *Water Res* **2010,** *44* (12), 3703-3713.

42. Soltermann, F.; Abegglen, C.; Gotz, C.; Von Gunten, U., Bromide sources and loads in

Swiss surface waters and their relevance for bromate formation during wastewater ozonation. *Environ Sci Technol* **2016,** *50*, 9825-9834.

43. Flury, M.; Papritz, A., Bromide in the natural enviroment: Occurence and Toxicity. *Journal of Environmental Quality* **1993,** *22*, 747-758.

44. Chellam, S.; Krasner, S. W., Disinfection byproduct relationships and speciation in chlorinated nanofiltered waters. *Environ Sci Technol* **2001,** *35* (19), 3988-3999.

45. Cowman, G. A.; Singer, P. C., Effect of bromide ion on haloacetic acid speciation resulting from chlorination and chloramination of aquatic humic substances. *Environ Sci Technol* **1996,** *30* (1), 16-24.

46. Korshin, G. V.; Wu, W. W.; Benjamin, M. M.; Hemingway, O., Correlations between differential absorbance and the formation of individual DBPs. *Water Res* **2002,** *36* (13), 3273-3282.

47. Liang, L.; Singer, P. C., Factors influencing the formation and relative distribution of haloacetic acids and trihalomethanes in drinking water. *Environ Sci Technol* **2003,** *37* (13), 2920-2928.

48. Rook, J. J., Chlorination Reactions of Fulvic Acids in Natural-Waters. *Environ Sci Technol* **1977,** *11* (5), 478-482.

49. Hua, B.; Veum, K.; Yang, J.; Jones, J.; Deng, B. L., Parallel factor analysis of fluorescence EEM spectra to identify THM precursors in lake waters. *Environ Monit Assess* **2010,** *161* (1-4), 71-81.

50. Ishii, S. K. L.; Boyer, T. H., Behavior of Reoccurring PARAFAC Components in Fluorescent Dissolved Organic Matter in Natural and Engineered Systems: A Critical Review. *Environ Sci Technol* **2012,** *46* (4), 2006-2017.

51. Korshin, G. V.; Li, C. W.; Benjamin, M. M., The decrease of UV absorbance as an indicator of TOX formation. *Water Res* **1997,** *31* (4), 946-949.

52. Her, N.; Amy, G.; McKnight, D.; Sohn, J.; Yoon, Y. M., Characterization of DOM as a function of MW by fluorescence EEM and HPLC-SEC using UVA, DOC, and fluorescence detection. *Water Res* **2003,** *37* (17), 4295-4303.

53. Huber, S. A.; Balz, A.; Abert, M.; Pronk, W., Characterisation of aquatic humic and non-humic matter with size-exclusion chromatography - organic carbon detection - organic nitrogen detection (LC-OCD-OND). *Water Res* **2011,** *45* (2), 879-885.

54. Korshin, G. V.; Kumke, M. U.; Li, C. W.; Frimmel, F. H., Influence of chlorination on chromophores and fluorophores in humic substances. *Environ Sci Technol* **1999,** *33* (8), 1207-1212.

55. Cory, R. M.; McKnight, D. M., Fluorescence spectroscopy reveals ubiquitous presence of oxidized and reduced quinones in dissolved organic matter. *Environ Sci Technol* **2005,** *39* (21), 8142-8149.

56. Sharpless, C. M.; Blough, N. V., The importance of charge-transfer interactions in

determining chromophoric dissolved organic matter (CDOM) optical and photochemical properties. *Environ Sci-Proc Imp* **2014,** *16* (4), 654-671.

57. Varanasi, L.; Coscarelli, E.; Khaksari, M.; Mazzoleni, L. R.; Minakata, D., Transformations of dissolved organic matter induced by UV photolysis, hydroxyl radicals, chlorine radicals, and sulfate radicals in aqueous-phase UV-based advanced oxidation processes. *Water Res* **2018,** *135*, 22-30.

58. Mvula, E.; von Sonntag, C., Ozonolysis of phenols in aqueous solution. *Org Biomol Chem* **2003,** *1* (10), 1749-1756.

59. Pan, X. M.; Schuchmann, M. N.; Vonsonntag, C., Oxidation of Benzene by the Oh Radical - a Product and Pulse-Radiolysis Study in Oxygenated Aqueous-Solution. *J Chem Soc Perk T 2* **1993,** (3), 289-297.

60. Martire, D. O.; Rosso, J. A.; Bertolotti, S.; Le Roux, G. C.; Braun, A. M.; Gonzalez, M. C., Kinetic study of the reactions of chlorine atoms and Cl(2)(center dot-)radical anions in aqueous solutions. II. Toluene, benzoic acid, and chlorobenzene. *J Phys Chem A* **2001,** *105* (22), 5385-5392.

61. Alegre, M. L.; Gerones, M.; Rosso, J. A.; Bertolotti, S. G.; Braun, A. M.; Martire, D. O.; Gonzalez, M. C., Kinetic study of the reactions of chlorine atoms and Cl-2(center dot-) radical anions in aqueous solutions. 1. Reaction with benzene. *J Phys Chem A* **2000,** *104* (14), 3117-3125.

62. Bader, H.; Hoigne, J., Determination of Ozone in Water by the Indigo Method. *Water Res* **1981,** *15* (4), 449-456.

63. Kumar, K.; Day, R. A.; Margerum, D. W., Atom-Transfer Redox Kinetics - General-Acid-Assisted Oxidation of Iodide by Chloramines and Hypochlorite. *Inorg Chem* **1986,** *25* (24), 4344-4350.

64. Huber, M. M. Elimination of pharmaceuticals during oxidative treatment of drinking water and wastewater: application of ozone and chlorine dioxide. ETH Zurich, 2004.

65. APHA/AWWA/WEF, *Standard Methods: 4500-Cl G. DPD Colormetric Method*. 22 ed.; American Public Health Association: Washington D.C., 2012.

66. EPA, U. S., Disinfection Profiling and Benchmarking Guidance Manual, Part 4. Water, O. o., Ed. 1999.

67. Internation, A., Standard Tables for Reference Solar Spectral Irradiances: Direct Normal and Hemispherical on 37deg; Tilted Surface. West Conshohocken, PA, 2012.

68. Bahnmuller, S.; von Gunten, U.; Canonica, S., Sunlight-induced transformation of sulfadiazine and sulfamethoxazole in surface waters and wastewater effluents. *Water Res* **2014,** *57*, 183-192.

69. Buxton, G. V.; Dainton, F. S., Radical and Molecular Yields in Gamma-Radiolysis of Water .V. Sodium Hypobromite System. *Proc R Soc Lon Ser-A* **1968,** *304* (1479), 441-&.

70. Buxton, G. V.; Greenstock, C. L.; Helman, W. P.; Ross, A. B., Critical-Review of Rate

Constants for Reactions of Hydrated Electrons, Hydrogen-Atoms and Hydroxyl Radicals (.Oh/.O-) in Aqueous-Solution. *J Phys Chem Ref Data* **1988,** *17* (2), 513-886.

71. Zuo, Z. H.; Katsumura, Y.; Ueda, K.; Ishigure, K., Reactions between some inorganic radicals and oxychlorides studied by pulse radiolysis and laser photolysis. *J Chem Soc Faraday T* **1997,** *93* (10), 1885-1891.

72. Klaning, U. K.; Wolff, T., Laser Flash-Photolysis of Hclo, Clo-, Hbro, and Bro- in Aqueous-Solution - Reactions of Cl-Atoms and Br-Atoms. *Ber Bunsen Phys Chem* **1985,** *89* (3), 243-245.

73. Westerhoff, P.; Mezyk, S. P.; Cooper, W. J.; Minakata, D., Electron pulse radiolysis determination of hydroxyl radical rate constants with Suwannee river fulvic acid and other dissolved organic matter isolates. *Environ Sci Technol* **2007,** *41* (13), 4640-4646.

74. Mertens, R.; Vonsonntag, C., Photolysis (Lambda=254 Nm) of Tetrachloroethene in Aqueous-Solutions. *J Photoch Photobio A* **1995,** *85* (1-2), 1-9.

75. Alfassi, Z. B.; Mosseri, S.; Neta, P., Reactivities of Chlorine Atoms and Peroxyl Radicals Formed in the Radiolysis of Dichloromethane. *J Phys Chem-Us* **1989,** *93* (4), 1380-1385.

76. Sauer, M. C.; Brown, W. G.; Hart, E. J., O(3P) atom formation by the photolysis of hydrogen peroxide in alkaline aqueous solutions. *J Phys Chem-Us* **1984,** *88*, 1398-1400.

77. Amichai, O.; Treinin, A., Chemical reactivity of O(P-3) atoms in aqeous solution. *Chem Phys Lett* **1969,** *3* (8), 611-613.

78. Buxton, G. V.; Bydder, M.; Salmon, G. A.; Williams, J. E., The reactivity of chlorine atoms in aqueous solution. Part III. The reactions of Cl-center dot with solutes. *Physical Chemistry Chemical Physics* **2000,** *2* (2), 237-245.

3.6. Supporting Information for Chapter 3

Characterization of Disinfection Byproduct Formation and Associated Changes to Dissolved Organic Matter During Solar Photolysis of Free Available Chlorine

10 narratives, 5 tables, 12 figures

Text S3.1. Chemical Reagent Sources, Natural Water Samples, and Preparation of Stock Solutions. *Chemical reagents and stock solution preparation.* Stock solutions of Suwannee River Natural Organic Matter (SRNOM) were prepared by dissolving the isolate in ultrapure water. HAA and THM standards (Supelco) were diluted from EPA 552.2 HAAs mix and EPA 501/601 THMs calibration mix ($CHCl_3$, $CHBrCl_2$, $CHBr_2Cl$, and $CHBr_3$) respectively. Polystyrene sulfonate molecular weight (MW) standards were purchased from Polymer Standard Solutions (15,000, 7,450 and 5,160 Dalton MW) and Polymer Standards Service USA (1,000 Dalton MW). FAC stock solutions were prepared by dilution of ~5% reagent grade sodium hypochlorite (NaOCl) (Sigma Aldrich) in ultrapure water. Aqueous O_3 stock solutions were prepared by bubbling O_3 though chilled ultrapure water immediately prior to use according to previously published procedures,[62] using an O_2-fed AC-2025 air-cooled O_3 generator (IN USA). Working FAC and O_3 stock solutions were standardized spectrophotometrically at λ = 292 nm and 258 nm, respectively, using $\varepsilon_{292nm,OCl^-} = 350\ M^{-1}\ cm^{-1}$ [63] and $\varepsilon_{258nm,O3} \cong 3000\ M^{-1}\ cm^{-1}$.[64]

Natural water sources and characterization. Four-liter samples were collected from (i) a local reservoir within a protected watershed that serves as a potable water source to nearby communities, and (ii) the exit of Lake Washington at the Montlake Cut near the University of Washington. The water samples were collected in glass bottles and stored at 4 °C prior to vacuum filtration through a 0.45 μm polyethersulfone membrane (SterliTech). Before collection of a natural water filtrate, the membrane was flushed with at least one liter of nanopore Milli-Q water followed by 0.5 L of natural water (which was discarded) to prevent filtrate contamination by carbon originating from the filter. DOC concentrations were determined using a Shimadzu TOC-L_{CSH} high-temperature catalytic combustion analyzer. Prior to use in experiments, the water samples were buffered with 10 mM phosphate targeting the native pH of the samples.

Water quality parameters are summarized in Table S3.

Text S3.2. Detailed Description of Experimental Setup and Reactor Configurations for FAC only, FAC+light, FAC+light/FAC only, and Light only/FAC only Treatments.

Simulated sunlight experiments. Experiments were undertaken under headspace-free conditions in 28-mL quartz tubes in duplicate, and thermostated at 10 or 25 °C in a circulating water bath below the light source. Samples were irradiated using an Atlas Material Testing Solutions Suntest XLS+ with 1700-W, O_3-free, Xe arc lamp with daylight filter (cutoff below 290 nm) and infrared radiation filter. Sample tubes were positioned 35° from the horizontal in a rack that can hold 10 tubes; two racks are able to fit within the water bath such that tubes are angled outward from the center to prevent overlap and shadowing, see Figure S3.1 for an image of the reactor configuration.

Phosphate buffer (10 mM, except for 0.5 mM DAS-analyzed samples) was used to control pH at either pH 6.00 or 8.00±0.02 in ultrapure reagent water, or at the native pH of natural water samples (Table S3.1). SRNOM was the organic matter source for all phosphate-buffered reagent water experiments (added at 2 mg/L as C). Bromide concentrations in phosphate-buffered reagent waters were varied at 0, 40 and 200 μg/L, and specified natural water samples were amended with an additional 200 μg/L of bromide beyond native concentrations. For initially anoxic experiments, solutions were sparged with high-purity N_2 gas to remove dissolved O_2, and for O_2-saturated experiments, solutions were sparged with high purity O_2 (details in Text S3.3).

Free available chlorine (FAC) only, FAC+light, and FAC+light/FAC only experiments were initiated by adding $[FAC]_0 \sim 8$ mg/L as Cl_2 into quartz tubes containing the prepared water matrix. Solutions within quartz tubes were mixed manually by inverting the tubes three times

such that a small PTFE-coated magnetic stir bar added to the tubes passed through the length of the tubes six times. After chlorine addition and mixing, FAC+light and FAC+light/FAC only experiments were immediately placed in one of the two racks (angling up to 20 tubes 35° from the horizontal) submerged in the thermostated water bath within the solar simulator. FAC concentration was monitored in dedicated tubes run in parallel with tubes reserved for DBP analyses (which were kept sealed) throughout the irradiation period by means of DPD colorimetry.[65]

For FAC+light/FAC only experiment sets irradiation ceased after a pre-defined irradiation time (0, 15, 30, or 45 minutes) and the quartz tubes were wrapped in aluminum foil to block further light exposure, initiating a post-irradiation dark FAC period where FAC concentration monitoring continued. Irradiation times and FAC concentrations were selected to reflect conditions previously found to yield 1- to 3-$\log_{10}$ inactivation of *Cryptosporidium* spp. oocysts and/or *Bacillus subtilis* spores during sunlight-driven FAC photolysis[6,7]. Experiments proceeded until a target cumulative FAC exposure was met, at which point FAC in all tubes was quenched with two-fold excess $Na_2S_2O_3$ or ten-fold excess arsenous acid ((As(III)), prepared from $NaAsO_2$), with most DBP experiments targeting a cumulative exposure of 400 (mg/L as Cl_2)×min. This cumulative CT_{FAC} target was selected to provide an exposure representative of the highest exposure levels likely to be utilized in applications of drinking water chlorination for primary disinfection.[66] Cumulative FAC exposures (CT_{FAC}) were calculated as $CT_{FAC} = \int_0^t [\mathrm{FAC}]\,dt$ (using trapezoidal Riemann summation) during the course of experiments, on the basis of FAC concentrations measured at defined reaction times.

FAC+light samples were exposed to FAC and simulated sunlight as above without a post-irradiation dark phase, with FAC quenched as above immediately after cessation of

irradiation.

Samples subjected to Light only/FAC only treatment were placed in the solar simulator without FAC for a specified irradiation time (0, 15, 30, or 45 minutes). Then, after the irradiation period elapsed, the samples were shielded from light and FAC was added to initiate the dark chlorination period. The FAC concentration was monitored by DPD colorimetry and used to determine CT_{FAC} throughout the dark chlorination period as above. Reaction solutions were quenched with two-fold excess of $Na_2S_2O_3$ or ten-fold excess of As(III) once the target CT_{FAC} was reached.

FAC only experiments. Dark FAC only experiments were conducted under headspace-free conditions in the same quartz reactor tubes as used for irradiation experiments, but wrapped in aluminum foil, or in borosilicate amber glass vials to prevent exposure to light. FAC only experiments were conducted to match the same target CT_{FAC} as in the corresponding FAC+light, FAC+light/FAC only, and Light only/FAC only experiments. Samples analyzed for DBP formation remained capped throughout experiments to prevent volatilization of THMs and parallel tubes were used to monitor chlorine concentration and estimate CT_{FAC} for the DBP reactors.

Natural sunlight experiments. Natural sunlight experiments were undertaken in duplicate 28-mL quartz test tubes thermostated at 10 °C or 25 °C, in accord with the above procedures and the general procedures described in Forsyth et al.[6] Samples were irradiated by placing them on the roof of the More Hall Civil and Environmental Engineering building on the University of Washington campus under clear skies on 9/12/2016, 9/22/2016, and 9/30/2016. Temperature was monitored by means of a thermometer in a control tube containing nanopore water adjacent to the experimental tubes in the water bath. Sample tubes were inclined at an angle of 35° from the

horizontal and reaction solutions were mixed before each experiment using the same protocol described for simulated sunlight experiments. Dark control (FAC only) experiments were undertaken in the same manner as for simulated sunlight experiments.

A summary of the experimental conditions applied, including solution conditions, dates of completion, and analyses undertaken is provided in Table S3.2.

Text S3.3. Gas Sparging Setup. Rubber septa (Ace glass sleeve-type precision seal septa) were used to seal the tops of the same 28 mL quartz tubes described in Text S3.2 during sparging and experimentation. The septa were fitted with a PTFE sparging/sampling tube extending to the bottom of the quartz reactor (with a gas-tight two-way valve fitted to the inlet end of the tube on the outside of the septa) and a one-way pressure relief valve inserted through the septa (but remaining above the liquid level) to prevent pressure build-up during sparging. Samples were adjusted to experimentation temperatures via water bath during sparging. Gas sparging occurred for 40 minutes; with either high purity 99.998% N_2 (30 ccm gas flow rate per reactor) for initially anoxic conditions or ultra-high purity 99.993% O_2 (27 ccm gas flow rate per reactor) for oxygen-saturated conditions. After completion of sparging, the two-way valve on the inlet end of the PTFE sparging/sampling was closed to maintain gas-tight conditions in the tube. Oxygen concentrations were measured with an MI-8-730 Flow-Thru O_2 electrode probe (Microelectrodes Inc.; Bedford, NH) before experiments, which were initiated by dosing chlorine through the sealed septa via syringe. Experiments then proceeded in the same fashion as described in Text S3.2 within the Atlas solar simulator.

Text S3.4. Spectroradiometry and *para*-Nitroanisole and Pyridine Actinometry Measurements. Incident spectral irradiance measurements for direct simulated and natural sunlight were obtained using a USB2000+ XR spectroradiometer (Ocean Optics; Dunedin, FL)

equipped with a 200 μm x 2 m optical fiber and a CC-3-UV-S cosine corrector. Representative incident spectral irradiance curves are depicted for each light source in Figure S3b in comparison to the ASTM standard G173-03 for solar radiation (hemispherical on a 37º tilted surface) at sea level (ASTM).[67] Measured incident irradiance spectra were obtained in each case at the surface of the reaction solutions contained within quartz tubes, with the plane of the spectroradiometer's cosine corrector facing directly toward the light source. Integration of the areas under the resulting incident spectral irradiance curves for simulated and natural sunlight yielded overall incident irradiances, $W_{tot,\lambda=290\text{-}400nm}$, of 65-75 W/m^2 and 44.2 W/m^2, respectively, between 290 and 400 nm (i.e., the region of overlap between FAC and the solar spectra). Although irradiance was higher overall for simulated sunlight, the spectral shapes for each light source were similar, with negligible output below 300 nm, as shown in Figure S3.2b.

Effective in situ fluence rates, $F_{tot,\lambda}$, from 290-400 nm were determined by means of *para*-nitroanisole (PNA)/pyridine actinometry for simulated sunlight and natural sunlight experiments.[33, 34] Actinometer solutions containing 1 μM PNA and 10 mM pyridine were prepared in nanopure Milli-Q water. These actinometer solutions were then transferred into the same 28-mL quartz tubes as used for irradiation experiments under simulated or natural sunlight. The actinometer solutions were kept in the dark until the start of each experiment, after which they were exposed to light for similar durations as utilized in the FAC+light, FAC+light/FAC only, and Light only/FAC only experiments. Samples were obtained from the irradiated actinometer solutions at pre-defined time intervals for PNA analysis. PNA concentrations were measured on an UltiMate3000 HPLC-UV system (Thermo Scientific/Dionex), using isocratic elution (0.2 mL/min) on a Supelco Ascentis C18 column (150 × 2.1 mm, 3 μm), with 50:50 CH_3CN:10-mM H_3PO_4 as mobile phase. Values of $F_{tot,\lambda}$ (in units of J m^{-2} s^{-1}, or W m^{-2}) were

determined from PNA degradation rates in accord with established procedures,[68] using the revised quantum yield for PNA photolysis from.[33]

Text S3.5. Fluorescence Excitation-Emission Matrix (EEM) Collection and Analyses. Fluorescence EEMs were collected for all samples that were also subjected to size exclusion chromatography (SEC) analyses (see Text S3.7 for the discussion of SEC analyses). EEMs and UV absorbance were collected immediately after experiments were finished by quenching FAC with arsenite and adjusting sample pH to a uniform value of 6.8, to be comparable with SEC analyses. Samples were brought to room temperature before analysis. An example EEM collected from the Horiba Aqualog Fluorometer (number J810012) is depicted in Figure S8. Nanopure water (18.2 MΩ cm resistivity, Milli-Q) was used to collect blank files in 1-cm path 4-way clear quartz cuvettes. Excitation wavelengths ranged from 240 – 600 nm (2 nm increments) and collected emission spectra ranged from 245.15 – 826.66 nm (2.33 nm increments). After collection, the sample EEMs were processed to correct for Rayleigh-scattering features and the water Raman scattering line. Blank EEMs were subtracted from sample EEMs to remove the water Raman scatter line. A Rayleigh-masking algorithm within the Aqualog software package nullified the first and second order Rayleigh lines. Inner filter effects were also corrected for using an Aqualog software algorithm and EEM intensity was normalized by the water-Raman scattering unit adjusted area (collected from the nanopore water blank). Processed EEM files were exported and compared using MATLAB software to identify peak local maxima which were also confirmed visually with each plotted EEM. Maxima in untreated samples were compared with those in treated samples to determine fractional decreases of the EEM peaks (Figure S3.8).

Text S3.6. Differential Absorbance Spectra (DAS) Analyses. Example DAS spectra

are included in Figure 3.6 in the main text. In addition to changes in ratios of differential absorbance at 340 nm and 280 nm, there are qualitative changes to the spectral shape that support the idea that O_3 and FAC react with different components of the SRNOM and perhaps form different organic products. O_3 only and FAC+light treatments show some preferential breakdown of higher wavelength absorbing chromophores and a decrease in absorbance above 350 nm when compared to FAC only treatment. Overall, however, the DAS spectra show that a range of chromophores within the SRNOM are reactive O_3 itself, and with ROS, RHS, and/or O_3 generated during FAC+light treatment. Addition of *tert*-butanol during O_3 only and FAC+light treatments attenuated some minor changes to the resulting spectra, but overall, the spectra obtained for O_3 only and FAC+light treatment with added *t*-BuOH maintained shapes similar to spectra obtained in the absence of *t*-BuOH.

Bromide Effects. Addition of bromide was also evaluated to determine its impacts on DAS analyses before and after FAC and FAC+light treatment. The presence of bromide (and by inference, the presence of HOBr and OBr^- formed via oxidation of bromide by FAC), did not appear to have a significant impact on DAS spectra following each type of treatment. The ratios of DA340nm to DA280nm depicted in Figure S3.9b,c show the equivalence in DAS results obtained with and without bromide.

Text S3.7. SEC-UV-Fluorescence-DOC Data Collection and Analyses. UV absorbance measurements were collected at 205, 225, 254, 280, and 320 nm and fluorescence measurements at 320 nm/450 nm Ex/Em. Molecular weights (MWs) of the separated carbon fractions were estimated using polystyrene sulfonate standards with MWs ranging between 1,000 and 16,000 Daltons. PSS peak maximum retention times were used to develop a calibration of retention time vs. log(MW). Dissolved organic carbon (DOC), UV and fluorescence

chromatographs were analyzed by integrating peak areas with a peak split between the primary humic and fulvic acid peak and a prominent shoulder peak that is referenced as low molecular weight organic acids and humic substances (Figure S3.10). Chromatographic data (DOC, UV, and fluorescence) were also used to determine intensity-weighted retention times for each detection method, which were calculated according to Equation S3.1, in which *rt* is the retention time at a discrete time point, *Δrt* is the time-step between data points, and $Intensity_{SECi}$ is the signal intensity value at a discrete time point. The intensity-weighted retention times were then input into PSS calibration curves to obtain the corresponding MW values.

$$rt_w = \frac{\int_{x=0}^{rt} x * f_{SEC}(x)dx}{\int_{x=0}^{rt} f_{SEC}(x)dx} \approx \frac{\sum(\Delta rt \times Intensity_{SEC,i} \times rt_i)}{\sum \Delta rt \times Intensity_{SEC,i}} \quad \text{(S3.1)}$$

Text S3.8. Temperature Effects on DBP formation during FAC only and FAC+Light/FAC only Treatment. Experiments were undertaken at 10 °C and 25 °C to evaluate the effect of temperature on DBP formation within realistic environmental ranges. As shown in Figure 3.1, experiments at 25 °C resulted in nearly a doubling of HAA5 (86% increase for FAC only and 83% increase for 45 minutes of FAC+light) and TTHM (70% increase for FAC only and 105% increase for 45 minutes of FAC+light) yields. The temperature increase did not affect chlorine photolysis rates without DOM (data not shown). Thus, increased DBP formation appears to be due primarily to increases in the rates of dark DOM chlorination reactions.

Text S3.9. Calculation of Bromine Substitution Factor. Bromine substitution factor (BSF) is calculated using Equations S3.2 and S3.3 (Hua and Reckhow 2012).

$$\mathrm{BSF_{HAA}} = \frac{\sum(\#\ \text{Bromine atoms/HAA}_i) \times [\mathrm{HAA}_i]}{\sum(\text{Total \# Br or Cl atoms/HAA}_i) \times [\mathrm{HAA}_i]} \quad \text{(S3.2)}$$

$$BSF_{THM} = \frac{\sum(\#\ \text{Bromine atoms/THM}_i) \times [\text{THM}_i]}{\sum(3\ \text{Br or Cl atoms/THM}_i) \times [\text{THM}_i]} \quad \text{(S3.3)}$$

Figure S3.6 shows that as the experimental bromide concentrations utilized in experiments were raised, the BSFs for TTHMs and HAAs following FAC only and FAC+light/FAC only treatments increased substantially due to preferential formation of brominated products in lieu of chlorinated products.

Text S3.10. Radical Scavenging Calculations. The fractions of $HO^{\bullet}$, $Cl^{\bullet}$, and $O(^3P)$ scavenged by the addition of *t*-BuOH or HCO_3^-/CO_3^{2-} were estimated on the basis of calculated pseudo-first-order rate constants determined using concentrations of HOCl/OCl^-, OH^-, HOBr/OBr^-, and other key constituents expected to be present in reaction solutions at initial conditions at pH 8. Table S3.4 outlines the constituents, initial concentrations, and rate constants included in these calculations.[7, 11, 69-78] Pseudo-first-order scavenging rate constants, $k_{scav,i}$, were calculated for each scavenger, *i*, by multiplying scavenger concentrations, $[C]_0$, at initial conditions (with the exception of HOBr/OBr-, which was taken as $[Br^-]_0$, assuming 100% oxidation of Br^- by FAC) by the corresponding second-order rate constants, k_i, for reaction of the radical of interest with each scavenger. Scavenging fractions were then calculated as the ratio of $k_{scav,i}$ to the total scavenging rate constant, $k_{scav,t}$, for reaction of the radical of interest with all scavengers listed (equal to the sum of $k_{scav,i}$ values calculated for that radical).

Table S3.1. Characteristics of natural water samples.

Parameter	Local Reservoir	Lake Washington
pH	8.15	8.10
DOC (mg C L^{-1})	0.5	2.4
Bromide (μg L^{-1})	24.5	23.7
Alkalinity (mg L^{-1} as $CaCO_3$)	30.7	38.0
$SUVA_{254}$ (L mg^{-1} m^{-1})	1.40	2.39

Table S3.2. Experimental conditions, dates, and analyses undertaken

pH	SRNOM (mg/L)	Bromide (µg/L)	Modifications	THM/HAA[a]	Fluorescence, UV Abs, and SEC-UV-FLD-DOC[a]	DAS[b]
8	2	0	-	1/12/2015		9/22/2016, 11/08/2016, 7/07/2017
8	2	40	-	2/5/2015		
8	2	200	-	9/22/16 and 7/28/17	3/1/2017 and 6/29/2017	7/07/2017
8	2	200	Natural Sunlight	9/30/2016		
8.05	2.4	23.7	Lake Washington	11/11/2016		
8.05	2.4	223.7	Lake Washington	11/11/2016		
8.1	0.5	24.5	Local Reservoir	11/23/2016		
8.1	0.5	224.5	Local Reservoir	11/23/2016		
8	2	200	25 °C	12/1/2017		
8	2	200	Initially Anoxic	12/19/2016	5/5/2017 and 7/5/2017	
8	2	0	Initially Anoxic, 25 °C			11/08/2016, 7/07/2017
8	2	200	50 mM *t*-BuOH	9/16/2016 and 6/28/2017	3/31/2017 and 6/28/2017	
8	2	200	50mM HCO_3^-	2/1/2017		
8	2	200	O_2 saturation	2/10/2017		
8	2	200	Kinetic exp. (no post photolysis dark period)	4/28/2017	4/28/2017 [a]	
6	2		-	1/28/2015		9/12/2016, 9/23/2016
6	2	40	-	4/15/2015		
6	2	200	-	5/19/2016	3/1/2017 and 6/29/2017	
6	2	200	Natural Sunlight	9/30/2016		
6	2	200	Kinetic exp. (no post photolysis dark period)	4/28/2017	4/28/2017 [a]	

[a] Experiments run in 10 mM phosphate buffer containing SRNOM at 10 °C unless specified otherwise; [b]Experiments run in 0.5 mM phosphate buffer containing SRNOM at 25 °C

Table S3.3. Comparing disinfection byproduct formation during FAC only treatment and Light only/FAC only treatment of phosphate-buffered solutions containing SRNOM

	TTHMs				**HAA5**			
		Light only / FAC only Treatment				*Light only / FAC only Treatment*		
Experimental Condition	FAC only	15 mins (6.2 J/cm^2)	30 mins (12.4 J/cm^2)	45 mins (18.6 J/cm^2)	FAC only	15 mins (6.2 J/cm^2)	30 mins (12.4 J/cm^2)	45 mins (18.6 J/cm^2)
pH 6 - SRNOM - 10 °C	25.8	21.9	25.0	18.7	25.9	27.1	26.8	33.5
pH 6 - SRNOM - 40 μg/L Br - 10 °C	11.6	11.6	14.3	11.2	19.5	20.9	21.9	19.5
pH 6 - SRNOM - 200 μg/L Br - 10 °C	22.9	19.9	20.9	17.0	6.2	4.5	4.7	3.0
pH 8 - SRNOM - 10 °C	52.0	48.2	48.7	52.5	29.4	32.3	31.0	30.1
pH 8 - SRNOM - 40 μg/L Br - 10 °C	28.4	21.8	35.2	33.0	30.6	29.7	36.2	35.6
pH 8 - SRNOM - 200 μg/L Br - 10 °C	39.9	43.7	54.9	33.3	22.5	25.9	21.5	23.1
pH 8 - 50 mM HCO_3^- - SRNOM 200 μg/L Br - 10 °C	29.5	30.1	39.1	37.2	8.5	8.1	9.7	10.1
pH 8 - 50 mM *t*-BuOH - SRNOM 200 μg/L Br - 10 °C	42.2	43.7	49.7	47.7	24.3	27.3	33.0	30.4

Table S3.4. Estimation of radical scavenging fractions for solutions amended with 50 mM *tert*-BuOH or $NaHCO_3$ (pH 8)

Compound	50 mM *tert*-butanol addition				50 mM bicarbonate addition		
	k_i 1/(M×s)	$[C]_0$ mol/L	$k_{scav,i}$ 1/s	$k_{scav,i}/k_{scav,t}$	$[C]_0$ mol/L	$k_{scav,i}$ 1/s	$k_{scav,i}/k_{scav,t}$
Reactions with hydroxyl radical							
tert-Butanol	6.00E+08[a]	5.00E-02	3.00E+07	9.73E-01	0	0	0.00E+00
HOCl	1.40E+08[b]	2.71E-05	3.79E+03	1.23E-04	2.71E-05	3.79E+03	2.66E-03
OCl^-	8.80E+09[c]	8.56E-05	7.53E+05	2.44E-02	8.56E-05	7.53E+05	5.29E-01
HOBr	2.00E+09[d]	2.00E-06	4.00E+03	1.30E-04	2.00E-06	4.00E+03	2.81E-03
OBr^-	4.20E+09[e]	5.03E-07	2.11E+03	6.84E-05	5.03E-07	2.11E+03	1.48E-03
HCO_3^-	8.50E+06[a]	2.01E-05	1.71E+02	5.54E-06	4.87E-02	4.87E+05	3.42E-01
CO_3^{-2}	3.90E+08[a]	9.40E-08	3.67E+01	1.19E-06	2.28E-04	9.11E+04	6.40E-02
DOC	5.00E+08[f]	1.67E-04	8.33E+04	2.70E-03	1.67E-04	8.33E+04	5.85E-02
Reactions with chlorine radical							
tert-Butanol	6.20E+08[g]	5.00E-02	3.10E+07	9.54E-01	0	0	0.00E+00
HOCl	3.00E+09[d]	2.71E-05	8.12E+04	2.50E-03	2.71E-05	8.12E+04	6.61E-03
OCl^-	8.20E+09[d]	8.56E-05	7.02E+05	2.16E-02	8.56E-05	7.02E+05	5.71E-02
HCO_3^-	2.20E+08[h]	2.01E-05	4.42E+03	1.36E-04	4.87E-02	1.07E+07	8.71E-01
CO_3^{-2}	5.00E+08[h]	9.40E-08	4.70E+01	1.45E-06	2.28E-04	1.14E+05	9.27E-03
DOC	4.17E+09[i]	1.67E-04	6.94E+05	2.14E-02	1.67E-04	6.94E+05	5.65E-02
Reactions with atomic oxygen $O(^3P)$							
tert-Butanol	3.80E+07[j]	5.00E-02	1.90E+06	5.33E-01	0	0	0.00E+00
OCl^-	3.50E+09[c]	8.56E-05	3.00E+05	8.41E-02	8.56E-05	3.00E+05	1.73E-01
OBr^-	1.10E+09[k]	5.03E-07	5.53E+02	1.55E-04	5.03E-07	5.53E+02	2.92E-04
HCO_3^-	1.10E+06[k*]	2.01E-05	2.21E+01	6.20E-06	4.87E-02	5.36E+04	3.10E-02
CO_3^{-2}	4.40E+07[k]	9.40E-08	4.14	1.16E-06	2.28E-04	1.00E+04	5.29E-03
O_2	4.00E+09[d]	3.39E-04	1.36E+06	3.81E-01	3.39E-04	1.36E+06	7.86E-01
OH^-	4.20E+08[l]	1.00E-06	4.20E+02	1.18E-04	1.00E-06	4.20E+02	2.22E-04
DOC	3.80E+07[j†]	1.67E-04	6.33E+03	1.78E-03	1.67E-04	6.33E+03	3.35E-03

[a]Buxton et al. 1988; [b]Zuo et al. 1997; [c]Buxton and Subhani 1972; [d]Klaning and Wolff 1985; [e]Buxton and Dainton 1968; [f]Westerhoff et al. 2007; [g]Buxton et al. 2000; [h]Mertens and von Sonntag 1995; [i]Alfassi et al 1989; [j]Zhou et al. 2014; [k]Amichai and Treinin 1969; [l]Sauer et al. 1984, *HCO_3^- rate constant estimated as 1/40 of the CO_3^{2-} rate constant – a ratio consistent with second-order rate constants for reactions of $HO^\bullet$ and $Cl^\bullet$ with HCO_3^- and CO_3^{2-}, †DOM rate constants are unavailable, so second-order rate constants for *tert*-butanol were used to estimate scavenging.

Table S3.5. Changes in bulk fluorescence and UV absorbance in phosphate-buffered samples during FAC only, Light only/FAC only, FAC+light, and FAC+light/FAC only treatment of phosphate-buffered solutions containing SRNOM

Fractional Value (normalized by untreated NOM)	pH 6, 2 mg/L SRNOM, 200 µg/L Br^-			pH 8, 2 mg/L SRNOM, 200 µg/L Br^-			pH 8, 2 mg/L SRNOM, 200 µg/L Br^-, 50mM *t*-BuOH			pH 8, 2 mg/L SRNOM, 200 µg/L Br, $Anoxic_{Initially}$		
	Ex/Em: 250/450	Ex/Em: 330/450	Abs 254nm	Ex/Em: 250/450	Ex/Em: 330/450	Abs 254nm	Ex/Em: 250/450	Ex/Em: 330/450	Abs 254nm	Ex/Em: 250/450	Ex/Em: 330/450	Abs 254nm
FAC only 400 (mg/L)×min *CT*	0.887	0.927	0.876	0.916	0.933	0.847	0.953	0.936	0.852	0.881	0.892	0.780
Light only time = 45min	0.886	0.840	1.034	0.801	0.798	0.993	0.832	0.784	0.998	-	-	-
Light only/FAC only 400 (mg/L)×min *CT*	0.908	0.863	0.844	0.906	0.882	0.848	0.880	0.865	0.835	-	-	-
FAC+light time = 15 mins	0.396	0.433	0.634	0.304	0.281	0.573	0.614	0.587	0.790	0.427	0.411	0.707
FAC+light time = 30 mins	0.310	0.342	0.541	0.219	0.214	0.520	0.535	0.465	0.728	0.354	0.359	0.652
FAC+light time = 45 mins	0.263	0.297	0.493	0.205	0.192	0.485	0.446	0.397	0.690	0.317	0.317	0.597
FAC+light/FAC only time = 45 mins 400 (mg/L)×min *CT*	0.255	0.272	0.499	0.177	0.168	0.454	0.468	0.410	0.642	0.332	0.300	0.581

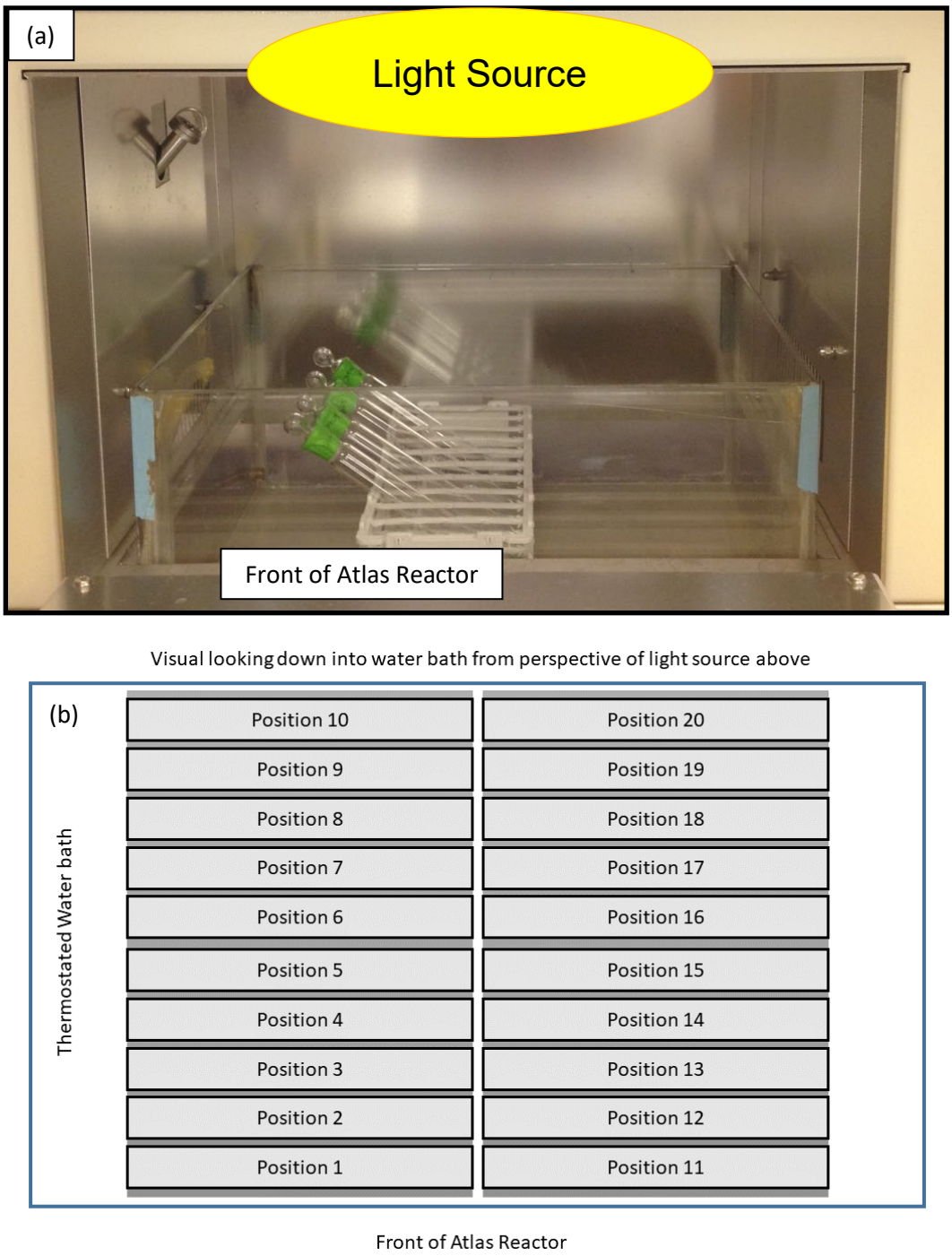

Figure S3.1. (a) Image of reactor setup within the Atlas SunTest Solar Simulator and associated water bath (drained in the photo) with one tube rack and quartz tubes in position; (b) rack positions (with two racks) and reactor tube numbering from a vertical perspective looking down from the light source.

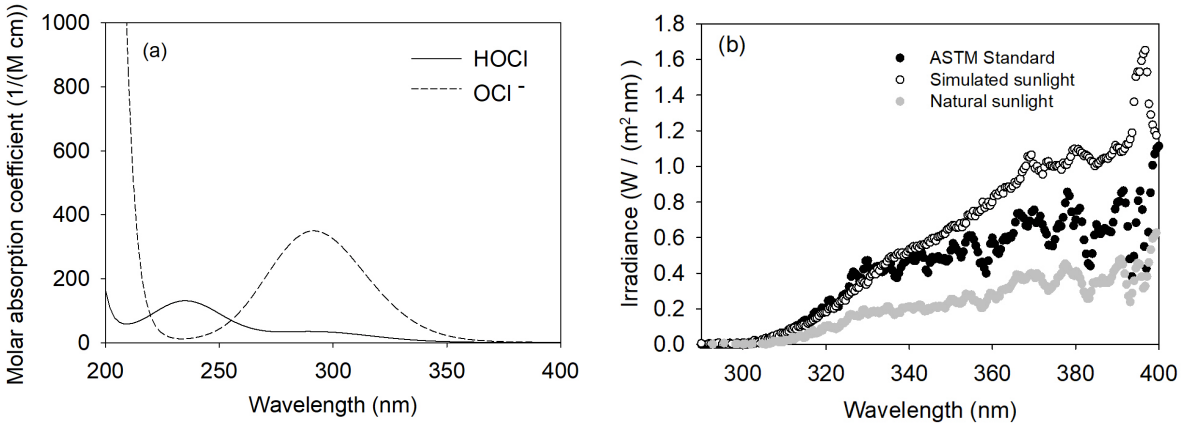

Figure S3.2. (a) Molar extinction coefficients of hypochlorous acid and hypochlorite [6]; (b) direct incident spectral irradiance curves between 290 and 400 nm for to the ASTM G173-03 solar irradiance standard (hemispherical on a 37º tilted surface); the Atlas SunTest Solar Simulator (with atmospheric filter and infrared radiation filter) centered and at the surface of irradiated reactor solutions, directly facing the light source; and natural sunlight on the roof of More Hall (Seattle, WA) at 3:00PM on 09/30/2016, at an angle of 45º from the horizontal facing the sun. Spectroradiometric measurements were taken using an Ocean Optics USB2000+ XR spectroradiometer equipped with a 200 μm × 2 m optical fiber and a CC-3-UV-S cosine corrector.

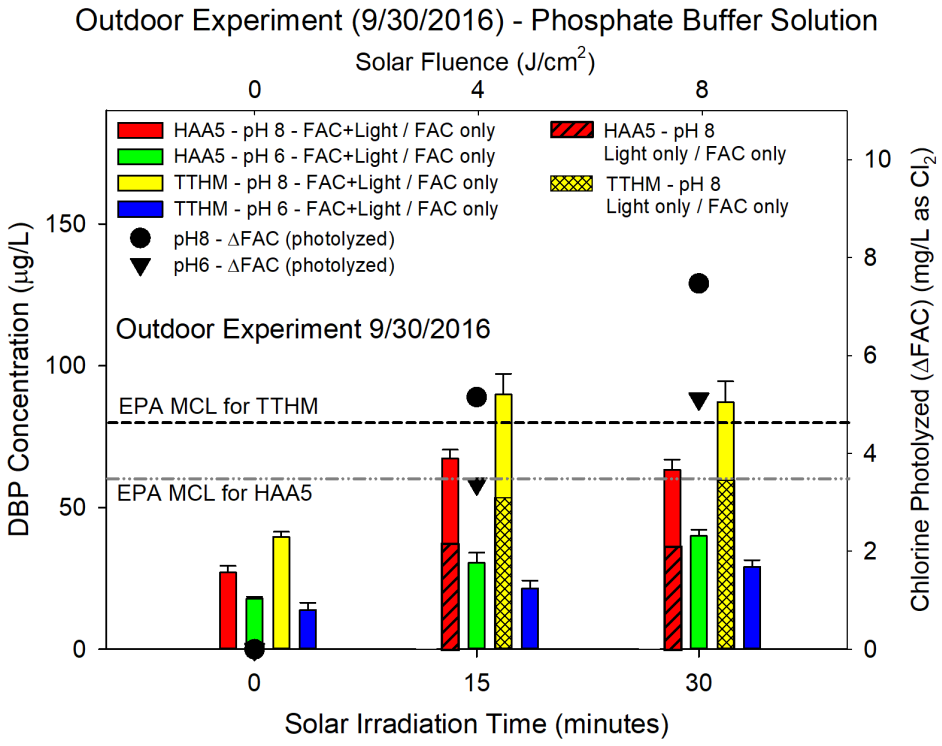

Figure S3.3. TTHM and HAA5 formation in pH 6 and pH 8 phosphate buffer (200 µg/L bromide, 2 mg/L as C SRNOM, 10 °C) during FAC only and FAC+light/FAC only experiments conducted under natural sunlight on the roof of More Hall (47.6525° N, 122.3048° W) on September 30th, 2016. Samples were angled at 35° from the horizontal. $[FAC]_0$ = 8 mg/L as Cl_2 and CT_{FAC} = 400 (mg/L)×min.

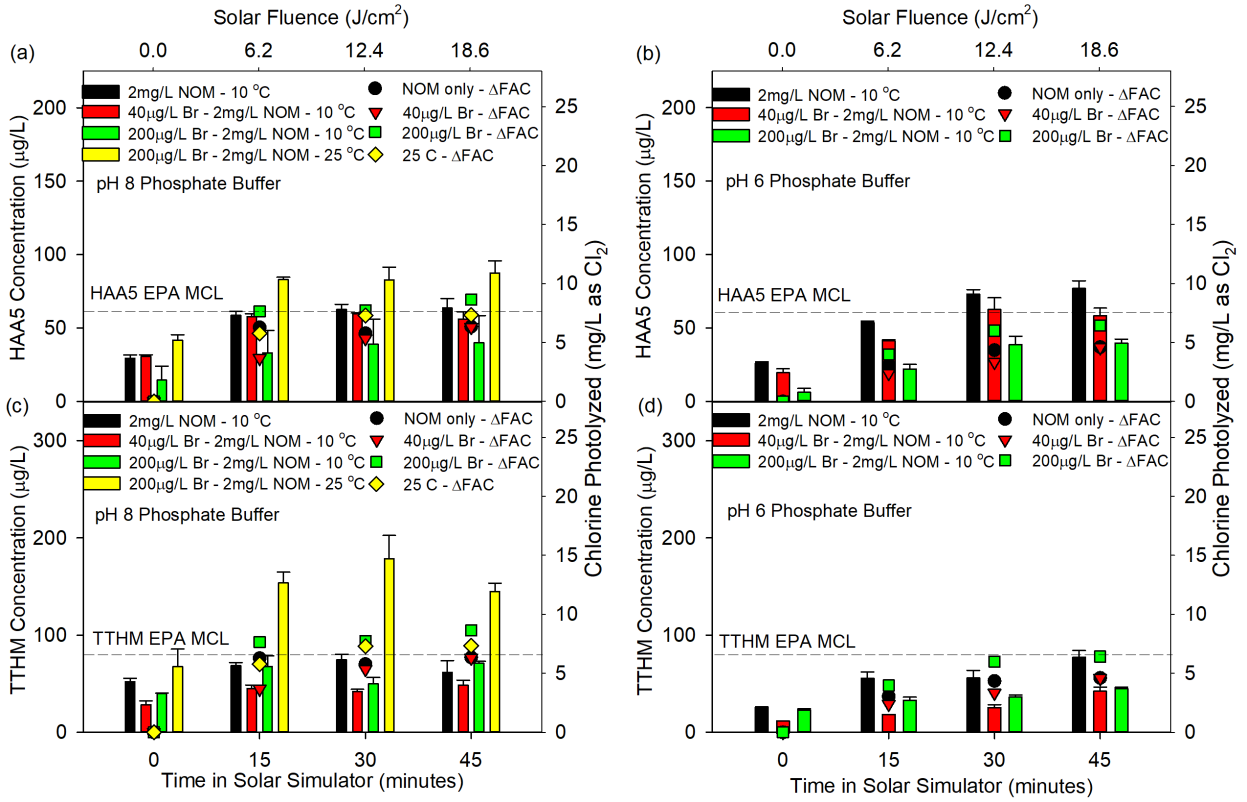

Figure S3.4. Modified version of Figure 3.1 from the main text (a) HAA5; and (c) TTHM formation in pH 8 (10 mM) phosphate buffer with 2 mg/L SRNOM comparing FAC only treatment (0 minutes in the solar simulator) with FAC+light/FAC only treatment at varying bromide concentration (0-200 µg/L) and temperature (10°C or 25°C); and (b) HAA5; and (d) TTHM formation in pH 6 (10 mM) phosphate buffer with 2 mg/L SRNOM at 10 °C comparing FAC only treatment with FAC+light/FAC only treatment at varying bromide concentration (0-200 µg/L). ΔFAC is the change in chlorine during photolysis. All samples utilized an initial chlorine concentration of 8 mg/L as Cl_2 and targeted CT_{FAC} = 400 (mg/L)×min.

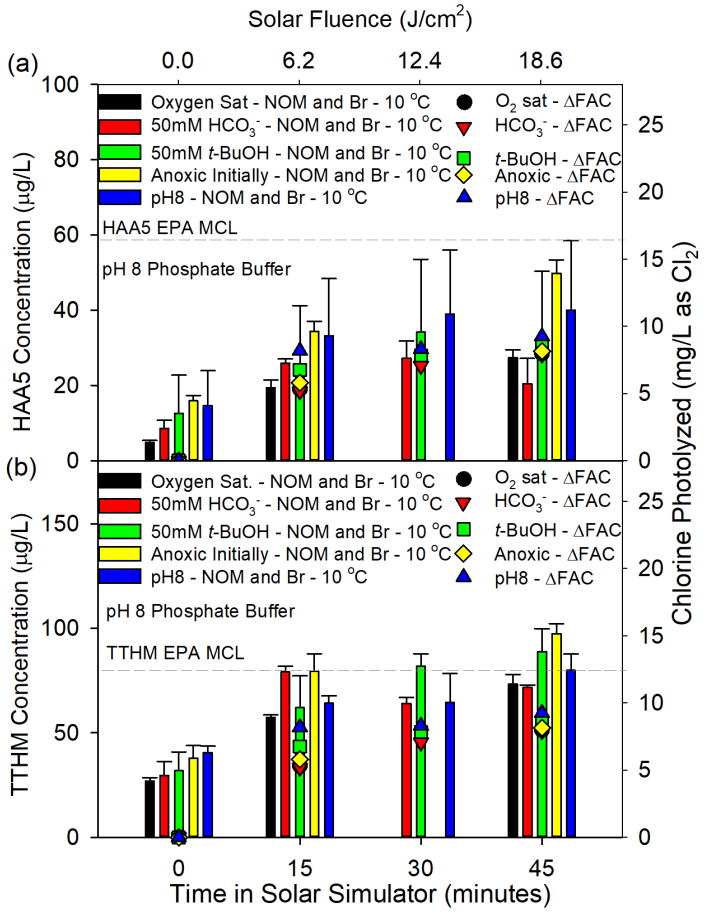

Figure S3.5. Modified version of Figure 3.2 from the main text (a) HAA5 formation and (b) TTHM formation with saturated (1.6 mM) dissolved O_2 (black), 50 mM HCO_3^- (red), 50 mM *t*-BuOH (green), initially anoxic conditions (yellow), or no alteration (blue), after exposure to FAC only or varied FAC+light/FAC only treatment. ΔFAC is the change in chlorine during photolysis. All solutions were prepared in 10 mM phosphate buffer at pH 8 and 10°C with 2 mg/L SRNOM, 200 µg/L bromide, and $[FAC]_0 \sim 8$ mg/L as Cl_2, and targeted $CT_{FAC} = 400$ (mg/L)×min.

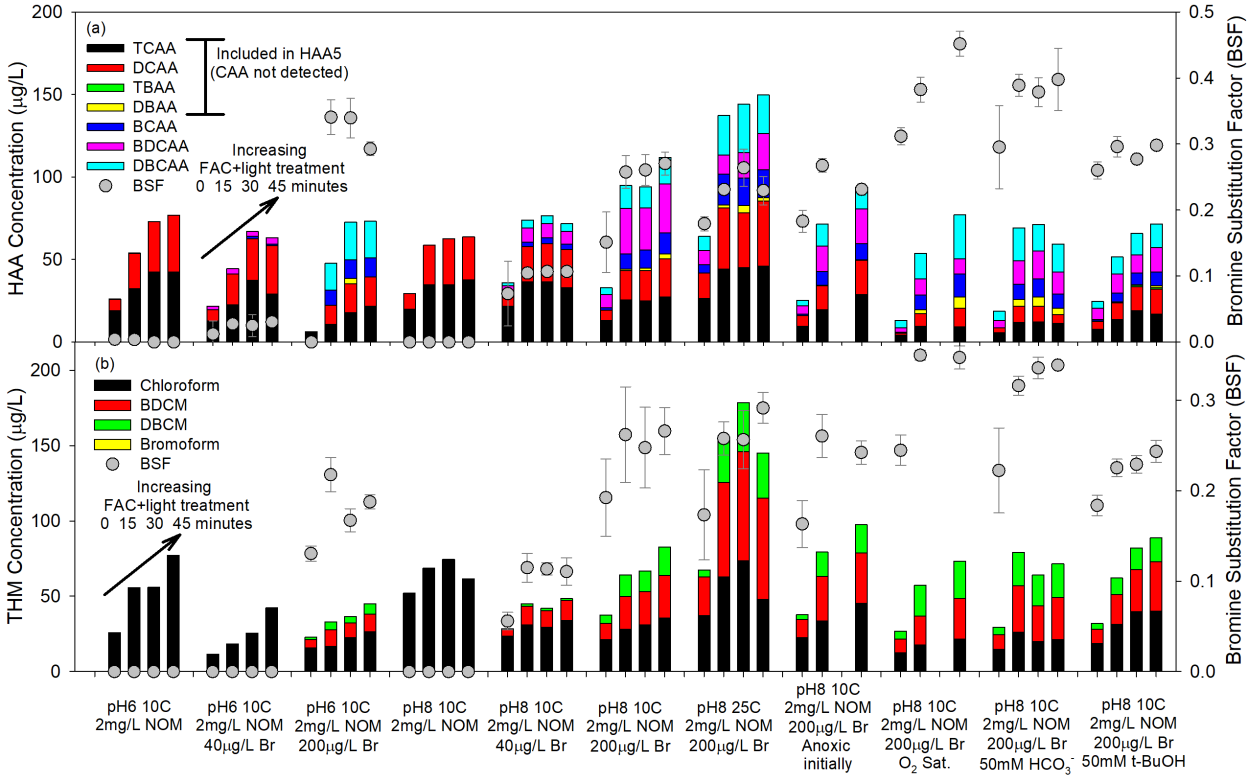

Figure S3.6. (a) Individual HAAs, HAA9, and bromine substitution factor (BSF) of HAA9 and (b) individual THMs, TTHM, and BSF of TTHMs, during FAC and FAC+light/FAC only experiments. Experiments were undertaken at pH 6 or 8 with varied bromide concentration (0-200 µg/L); at pH 8 with varied temperature (10 or 25 °C); at pH 8 in the presence of 50 mM HCO_3^-/CO_3^{2-} or *tert*-Butanol (*t*-BuOH), and at pH 8 under anoxic or O_2-supersaturated conditions. All solutions utilized $[FAC]_0 \sim 8$ mg/L as Cl_2 and targeted $CT_{FAC} = 400$ (mg/L)×min.

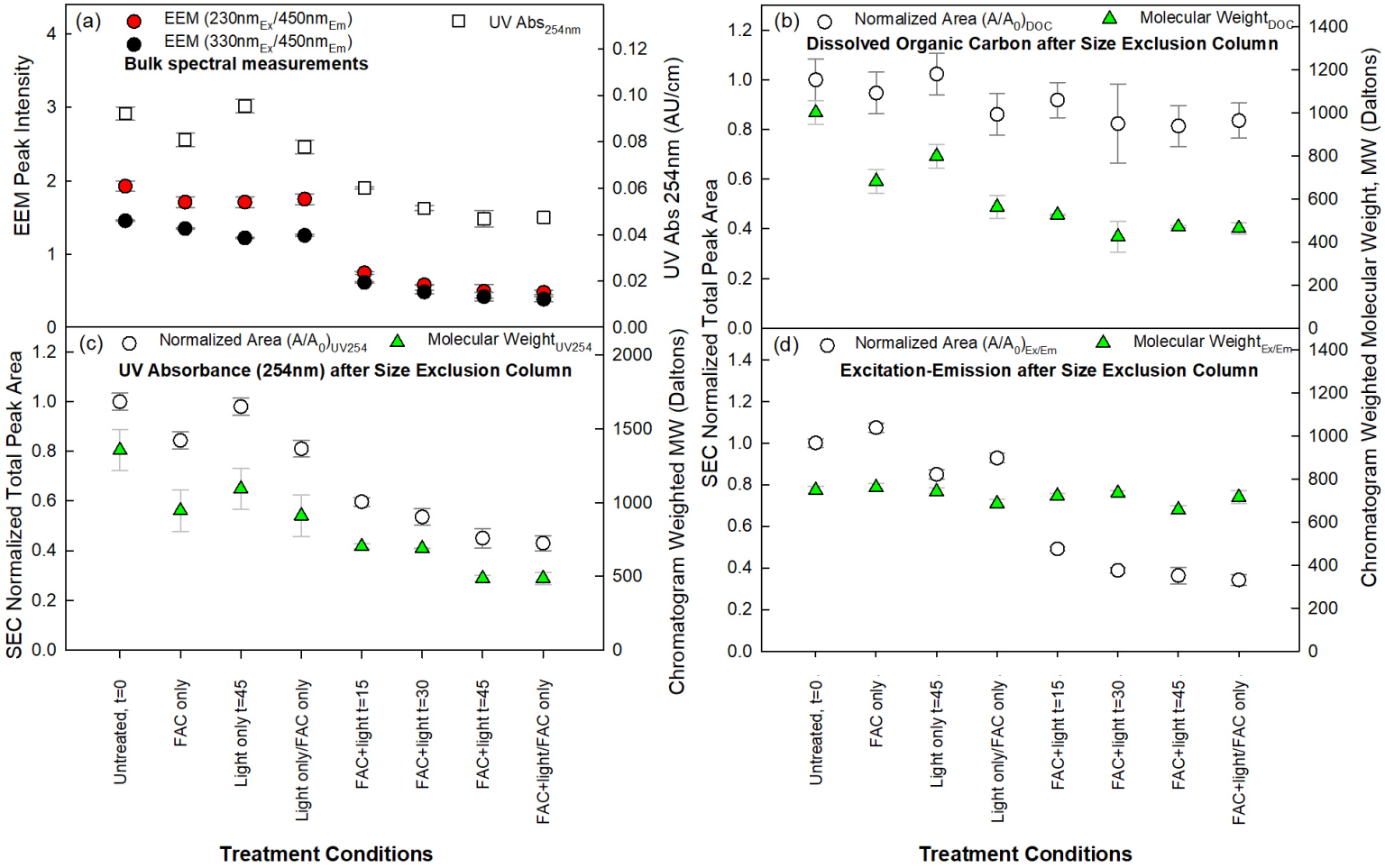

Figure S3.7. (a) Bulk UV absorbance at 254 nm (white squares) and fluorescence (filled circles). (b)-(d) SEC data for (b) DOC, (c) UV absorbance at 254 nm, and (d) fluorescence (Ex: 320 nm, Em: 450 nm), summarizing total chromatographic peak areas normalized by untreated samples (white circles), and MW estimated from signal intensity-weighted retention times (green triangles; see Text S3.7 for details). Data is from experiments with pH 6, 10mM phosphate buffered solutions containing 2 mg/L SRNOM and 200 µg/L Br^- at 10 °C, after Light only, FAC only, Light only(45 min. irr.)/FAC only, FAC+Light, and FAC+Light(45 min. irr.)/FAC only treatment (x-axis represents treatment conditions, not time series). FAC only, Light only/FAC only, and FAC+light/FAC only experiments targeted CT_{FAC} = 400 (mg/L)×min.

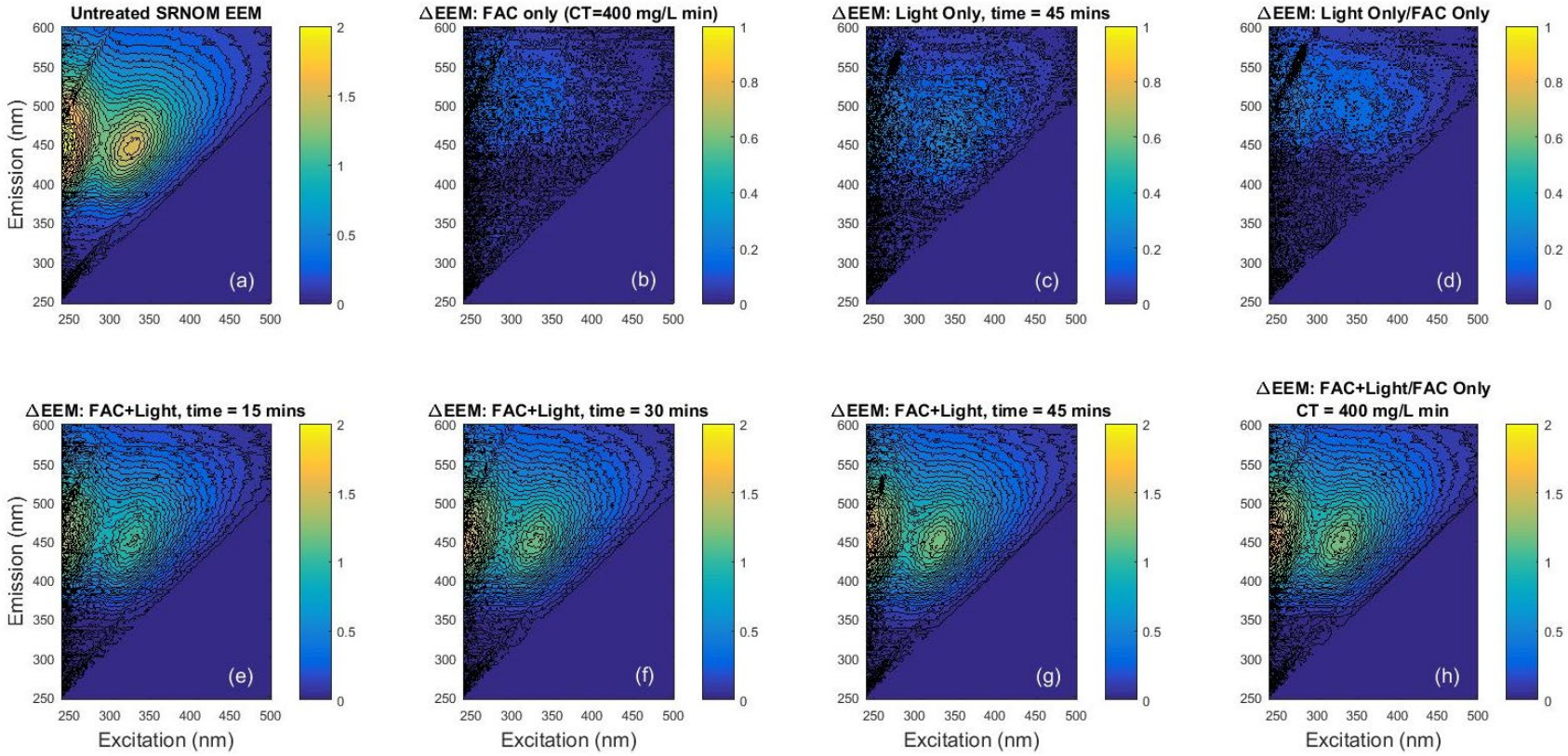

Figure S3.8. Sample EEM and differential EEMs for pH 8 phosphate buffer with 2 mg/L SRNOM and 200 µg/L bromide treated at 10 °C, with $[FAC]_0$ ~ 8 mg/L as Cl_2 (except in panels (a) and (c), for which FAC was not present); (a) depicts the untreated sample EEM that was used to calculate the differential change after treatment for the following EEMs; (b) FAC only treatment targeting CT_{FAC} = 400 (mg/L)×min; (c) Light only treatment for 45 minutes (18.6 J/cm^2 fluence); (d) Light only/FAC only treatment targeting CT_{FAC} = 400 (mg/L)×min for the same fluence (18.6 J/cm^2) as in the Light only treatment; (e) FAC+light treatment for 15 minutes (6.2 J/cm^2 fluence); (f) FAC+light treatment for 30 minutes (12.4 J/cm^2 fluence); (g) FAC+light treatment for 45 minutes (18.6 J/cm^2 fluence); (h) FAC+light/FAC only treatment (18.6 J/cm^2 fluence) with 45 minutes of irradiation and a cumulative CT_{FAC} = 400 (mg/L)×min.

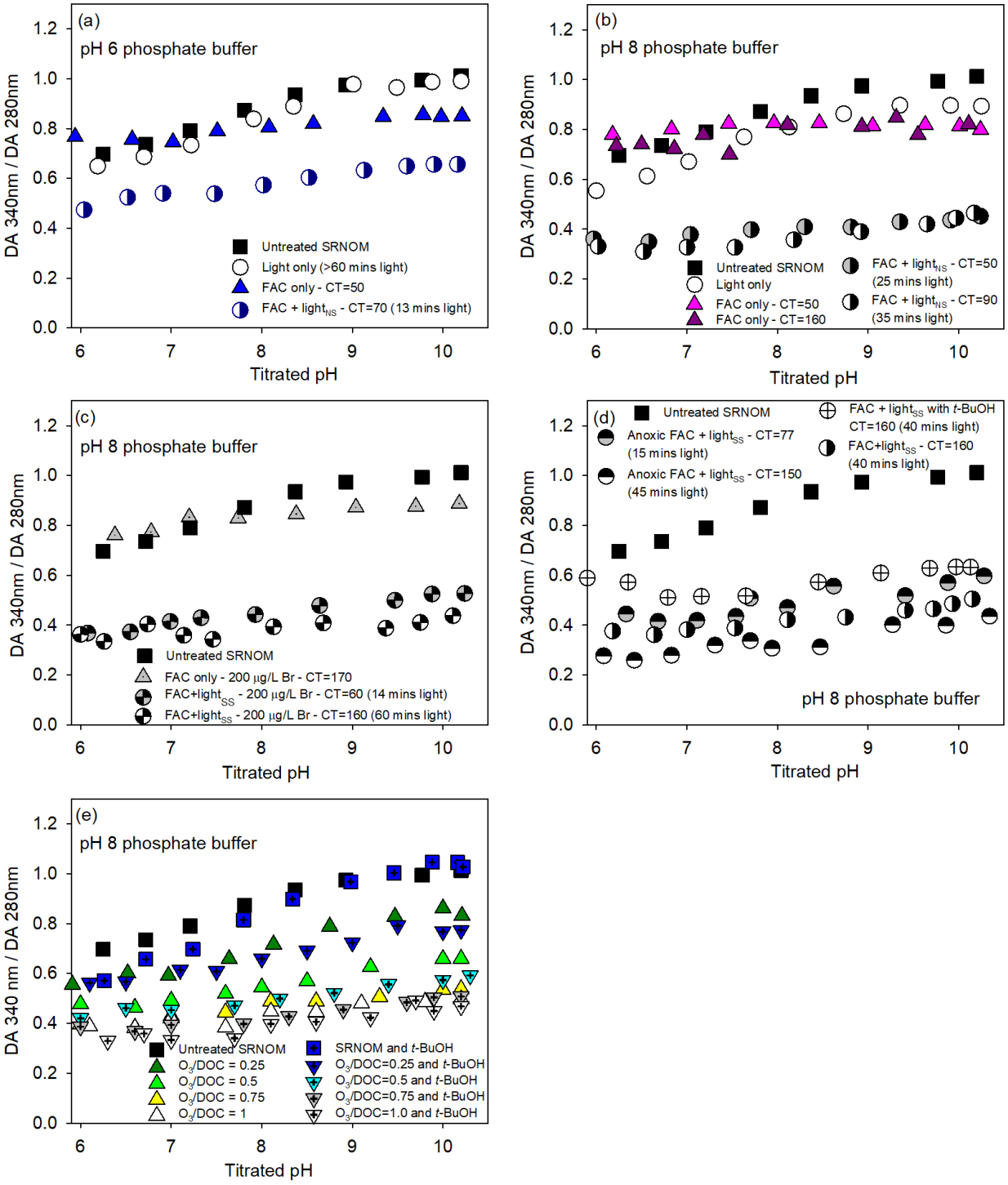

Figure S3.9. Ratios of differential absorbance at 340 nm band (phenolic groups) and 280 nm band (carboxylic acid groups) as the titrated pH is increased from 6 - 10.2 for: (a) Light Only, FAC only, and FAC+light$_{NS}$ treatment in pH 6 and (b) pH 8 buffer; (c) FAC only and FAC+light$_{SS}$ treatment with 200 µg/L bromide in pH 8 buffer; (d) FAC+light$_{SS}$ treatment under oxic and anoxic conditions (decreased O_3 formation) and radical quenching with 50 mM *t*-BuOH in pH 8 buffer; and (e) O_3 treatment with and without 50 mM *t*-BuOH at pH 8.

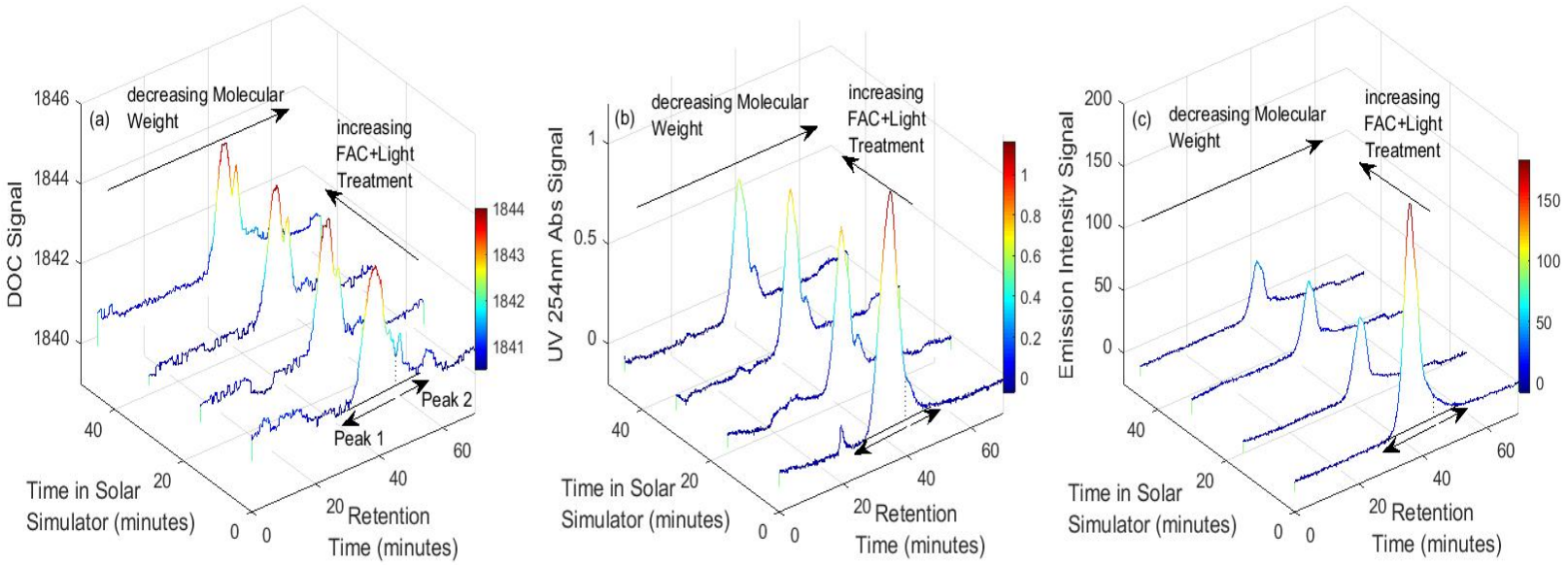

Figure S3.10. SEC chromatographs for (a) DOC; (b) UV absorbance (254 nm); (c) and fluorescence (320 nm/450 nm $\lambda_{Ex}/\lambda_{Em}$) of FAC+light treated samples containing 200 μg/L bromide, 2 mg/L Suwannee River NOM, and $[FAC]_0$ = 8 mg/L as Cl_2 in pH 8 (10 mM) phosphate buffer at 10 °C.

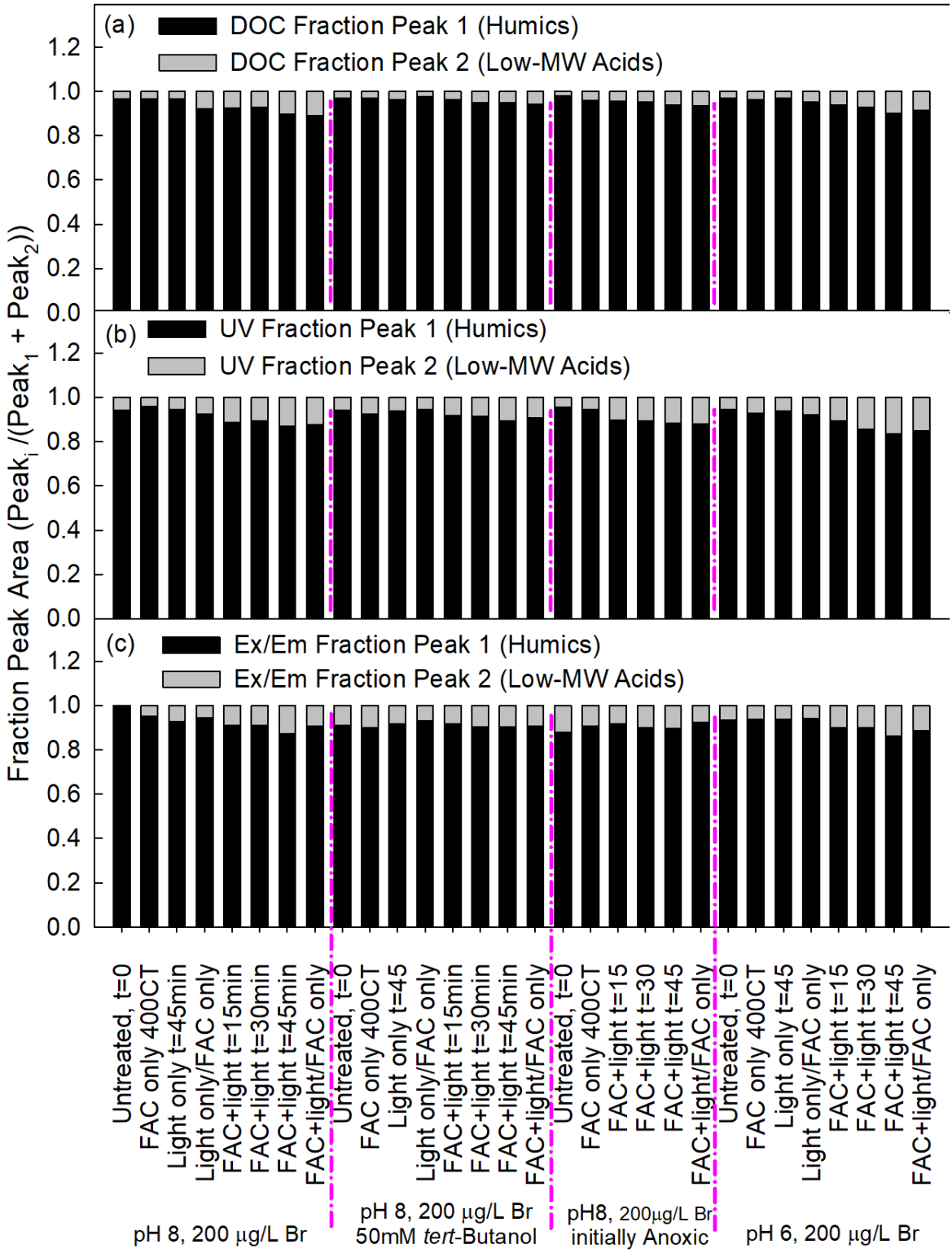

Figure S3.11. Size-exclusion chromatography data for (a) DOC, (b), UV absorbance at 254 nm and (c) fluorescence (Ex: 320 nm, Em: 450 nm), summarizing fractional chromatographic peak areas for humic (black) and lower molecular weight acid (grey) peaks.

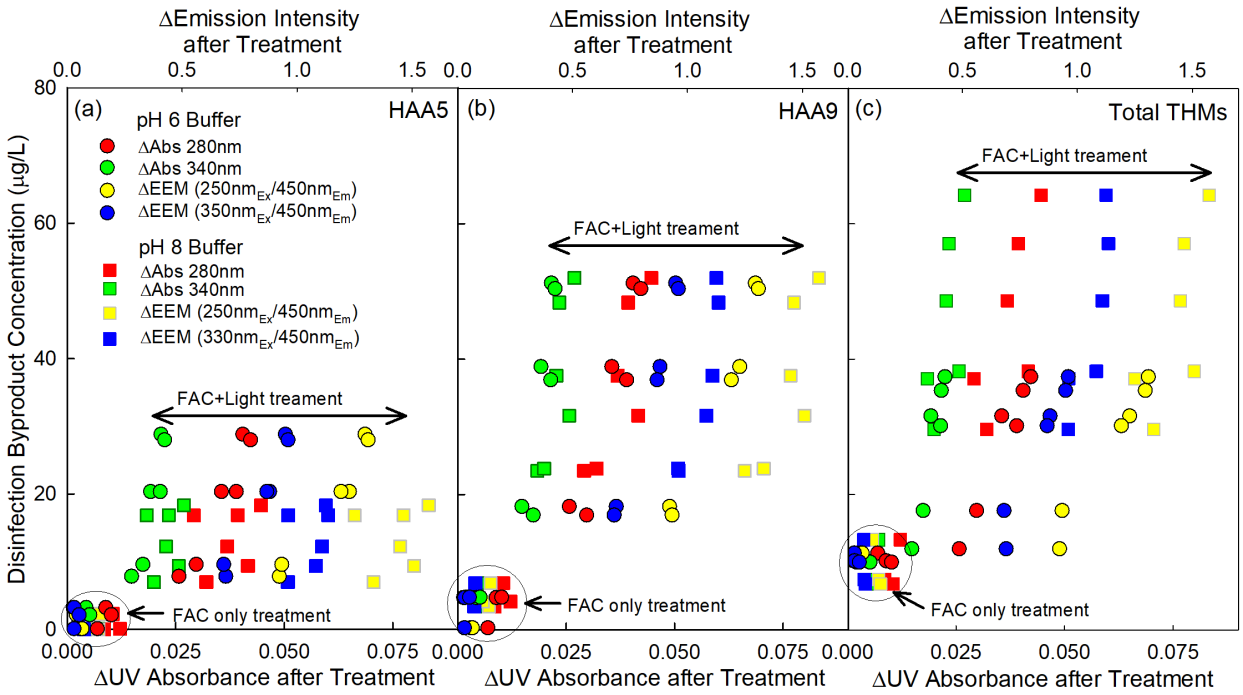

Figure S3.12. Trends comparing (a) HAA5 formation; (b) HAA9 formation; and (c) TTHM formation vs. changes in UV absorbance (270 nm or 340 nm) and fluorescence (λ_{ex} = 250 nm / λ_{em} = 450 nm and λ_{ex} = 330 nm / λ_{em} = 450 nm) during FAC+light treatment (15, 30, and 45 minutes of irradiation) and equivalent CT_{FAC} FAC only treatment (CT_{FAC} = 81, 136, and 185 (mg/L)×min for pH 6 and 75, 114, and 140 (mg/L)×min for pH 8). All pH 6 or 8 phosphate buffered (10 mM) samples contained 200 μg/L bromide and 2 mg/L as C of Suwannee River NOM. $[FAC]_0$ ~ 8 mg/L as Cl_2, and temperature was maintained at 10 °C.

Chapter 4. Modifications to Dissolved Organic Matter Structure, Redox Properties, and Disinfection Byproduct Formation Potential during Chlorination, Solar Chlorine Photolysis, Ozonation, and Advanced Oxidation Processes

Abstract

This work investigated modifications to the structural and redox properties of dissolved organic matter (DOM) and model compounds during solar irradiation of free available chlorine (FAC) and the influence of organic matter modifications on DBP yields. The stable radical cation $[ABTS^{\cdot+}]^-$ was used to estimate the electron donating capacity (EDC) of natural organic matter isolates and model compounds. FAC, which can quickly oxidize or halogenate activated aromatic constituents of organic matter (such as phenolic or resorcinol moieties), was found to rapidly decrease the measurable EDC of DOM and phenol (reactive model compound), and only moderately decrease UV absorbance (fluorescence was unaffected). Ozone contributes to cleavage of aromatic rings and as a result, UV absorbance loss was greater than EDC loss when compared to chlorination treatment alone. Hydroxyl radical addition to benzoic acid (model compound, not reactive with FAC or O_3) and DOM during advanced oxidation treatment was found to increase the measured EDC, and increased DBP formation when normalizing by chlorine exposure – CT_{FAC}. Low exposures of hydroxyl radical ($CT_{HO\cdot} < 1.5 \times 10^{-10}$ M×sec) during solar chlorine photolysis are suspected to be a primary factor responsible for increased trihalomethane and haloacetic acid formation during chlorine photolysis. In contrast, electron transfer by $Cl^{\cdot}$ and $ClO^{\cdot}$ appears to contribute primarily to oxidation of phenolic groups in organic matter to less reactive quinones, with lesser impact on DBP formation. These findings provide an improved understanding of the processes leading to increased DBP formation potential during application of solar FAC photolysis, and may be useful in mitigating DBP formation during practical drinking water treatment application of solar FAC photolysis (or other combinations of chlorine and reactive oxygen species such as UVC/FAC photolysis or AOPs followed by chlorination).

4.1. Introduction

Identification and quantification of halogenated disinfection byproducts (DBP) has been a focus of drinking water and wastewater treatment for decades, starting with identification of haloforms in chlorinated drinking water.[1, 2] Due to the frequent use of chlorine in the United States, DBP mitigation has focused on removing or oxidizing natural organic matter (NOM) prior to chlorination or replacing free-available chlorine (FAC) with chloramine as the secondary disinfectant within the distribution systems. Chloramine is a weaker oxidant, but its use may pose additional risks, as it has been associated with formation of unregulated nitrogenous disinfection byproducts.[3, 4] While DBP yields may be lower, there is growing concern that the emerging class of nitrogenous DBP may be more toxic than currently regulated DBPs.[5] Oxidation of disinfection byproduct precursors is an inviting alternative as radical species, ozone, or chlorine dioxide may provide additional benefits of degrading nuisance organic contaminants.

Research applying advanced oxidation processes (AOPs) to drinking and wastewater treatment is growing and radical species have been utilized to degrade a range of target organic compounds, including pharmaceuticals,[6, 7] taste and odor compounds,[8] and algal toxins.[9, 10] With a focus on target-compound degradation, concurrent changes to water matrix constituents due to unselective reactions with radical species can be easily overlooked. Pretreatment of dissolved organic matter (DOM) via hydrogen peroxide photolysis – an AOP yielding highly reactive hydroxyl radical – was found to increase chlorine demand[11] and TTHM yields[11, 12] when dissolved organic carbon (DOC) did not decrease due to DOM mineralization. At higher fluences (>1000 mJ/cm^2), observations of DOM mineralization were reported with decreased THM and HAA formation potential when compared to chlorination alone.[13] Ozonation treatment that favors hydroxyl radical production (e.g., addition of H_2O_2 or destabilizing ozone at elevated pH)

was observed to increase THM formation potential after low exposures when compared to chlorination controls.[14-16] Ozone treatment alone has been observed to degrade spectral properties of DOM[17] and decrease DBP yields upon chlorination. This may indicate the ozonation products of these chromophores are not forming chlorine-reactive DBP precursors.[15, 18, 19] Comparing ozone and ozone AOPs suggests selective ozone reactions may degrade DBP precursors while non-selective hydroxyl radical reactions may result in DBP formation (especially at lower O_3/ $HO^{\cdot}$ exposures). UVC (100 – 280 nm) photolysis of free chlorine (UVC/FAC) is an advanced oxidation processes that produces reactive chlorine species (RCS), such as $Cl^{\cdot}$, $Cl_2^{\cdot -}$ and $ClO^{\cdot}$, and hydroxyl radical in situ. UVC/FAC treatment of DOM has been reported to increase HAA[20] and THM[21] formation in some cases, while other studies have observed decreased TCAA yields at neutral[21] and acidic[22] pH (with low pH favoring $Cl^{\cdot}$ yields) during UVC/FAC treatment. These discrepancies in the literature indicate that operational parameters and source water characteristics have a substantial impact on DBP formation. Reactions between RCS and DOM are difficult to evaluate independently, as hydroxyl radical is typically present to generate RCS ($Cl^{\cdot}$ and $Cl_2^{\cdot -}$ via $HO^{\cdot}$ reaction with chloride,[23, 24] $ClO^{\cdot}$ via $HO^{\cdot}$ reaction with OCl^-,[25] or $Cl^{\cdot}$ and $HO^{\cdot}$ generated in situ during FAC photolysis,[26, 27] etc.) or is formed after $Cl^{\cdot}$ reacts with water or hydroxide.[28] Therefore, it is difficult to determine if these radical species react with natural organic matter to form DBP precursors synergistically or competitively, due to the combined presence of hydroxyl radical and RCS during chlorine-based AOP treatment.

Solar irradiation of chlorinated water is a novel water treatment option that has been reported to increasing the yield of halogenated organic disinfection byproducts (DBP) while enhancing inactivation of chlorine-resistant pathogens and *Bacillus subtilis* endospores when

compared to chlorination alone.[29-31] Chlorine disinfection is aided by oxidants formed during solar chlorine photolysis,[29, 30] particularly reactive oxygen species (ROS) – such as hydroxyl radical ($HO^{\cdot}$) and atomic oxygen ($O(^3P)$) which can react with dissolved oxygen (O_2) to form ozone (O_3) – and possibly reactive chlorine species (RCS) – such as chlorine atom ($Cl^{\cdot}$) and chlorine oxide radical ($ClO^{\cdot}$) (Equations 4.1–4.7)[25-27, 32-35]. Photolysis quantum yields for hypochlorous acid and hypochlorite are detailed in Table S4.1.

$$HOCl \rightleftharpoons H^+ + OCl^- \quad (pK_a = 7.5, \text{ at } 25\ ^\circ C) \tag{4.1}$$

$$HOCl/OCl^- \xrightarrow{h\nu} HO^{\bullet} / O^{\bullet -} + Cl^{\bullet} \tag{4.2}$$

$$OCl^- \xrightarrow{h\nu} O(^3P) + Cl^- \tag{4.3}$$

$$O(^3P) + O_2 \rightarrow O_3 \tag{4.4}$$

$$Cl^{\bullet} + Cl^- \rightarrow Cl_2^{\bullet -} \tag{4.5}$$

$$HO^{\bullet} + HOCl/OCl^- \rightarrow ClO^{\bullet} + H_2O / OH^- \tag{4.6}$$

$$Cl^{\bullet} + HOCl/OCl^- \rightarrow ClO^{\bullet} + Cl^- \tag{4.7}$$

Addition of humic-rich Suwannee River natural organic matter (SRNOM) to phosphate buffer treated via solar chlorine photolysis yielded increased DBP formation (when compared to dark chlorination), particularly in the absence of *tert*-butanol (an effective $HO^{\cdot}$ and $Cl^{\cdot}$ scavenger).[31] Simultaneously, spectral properties – such as UV absorbance and fluorescence – decreased after exposure to reactive oxygen and chlorine species, such as $HO^{\cdot}$ and $Cl^{\cdot}$.[15, 16, 31] One study targeting microcystin-LR degradation in natural water reported an increase in

trihalomethane (THM) and haloacetic acid (HAA) formation after chlorination and sunlight pretreatment followed by chlorination, and a decrease in DBPs after solar chlorine photolysis.[9] However, these THM and HAA formation experiments were initiated with a fixed initial chlorine concentration (rather than a target final residual), and did not account for variation in chlorine concentration in solar chlorine photolysis samples (FAC concentration decreases during photolysis), which may contribute to the reported decrease in DBP yields during solar chlorine photolysis.

Measurement of DOM redox properties – such as the electron donating capacity (EDC) – can provide insight into the inherent reactivity of DOM toward oxidants such as chlorine, chlorine dioxide, and ozone.[17] The stable radical cation of 2,2'-azino-bis(3-ethylbenzothiazoline-6-sulfonate) ($[ABTS^{\cdot+}]^-$) has been used to measure antioxidants in food science[36] and to estimate the redox properties of humic substances by means of mediated electrochemical oxidation.[37, 38] The stable radical cation $[ABTS^{\cdot+}]^-$ (detected at the 405 nm absorption shoulder and observed as green/blue in color) can react with the dissolved organic matter, accept an electron, and form a clear $ABTS^{2-}$ solution[39] (non-absorbing at 405nm) enabling simple colorimetric measurement of $[ABTS^{\cdot+}]^-$ to estimate EDC of DOM. $[ABTS^{\cdot+}]^-$ was selected for this study because its standard one-electron reduction potential ($E_H^0([ABTS^{\cdot+}]^- / ABTS^{2-}) = 0.7$ V) is sufficient to react with a significant fraction of phenolic moieties that contribute to the electron donating capacity in humic substances.[37, 40, 41] Phenolic moieties are frequently cited as a contributors to the aromatic structure in humic substances.[42, 43] This colorimetric approach can also be implemented with size exclusion chromatography to separate DOM and remove interfering dissolved ions, thus improving the reliability of the method.[19, 44, 45] DOM also contains moieties that are unreactive with $[ABTS^{\cdot+}]^-$ within the selected reaction time, though transformation may increase reactivity.

The principal objectives of this work were threefold: (i) to quantify changes to DOM isolates and simple model compounds (spectral and redox properties and identify products) during the application of individual oxidants or mixtures of oxidants; including free-available chlorine (FAC), ozone, $HO^{\cdot}$, $O(^3P)$, $Cl^{\cdot}$, and $ClO^{\cdot}$; (ii) to compare with modifications to DOM measured during solar chlorine photolysis (FAC+Light) treatment of DOM isolates and simple organic model compounds; and (iii) to relate disinfection byproduct formation to changes to DOM properties (normalized by chlorine exposure, $CT_{FAC} = \int[FAC]\,dt$). DOM oxidation and DBP formation were investigated under a variety of conditions (e.g., varying DOM source, pH, or O_2 concentration; with and without added oxidant scavengers; etc.). Monitored DOM characteristics included EDC, fluorescence excitation-emission matrices (EEMs), and UV absorbance (A_{254}). Including two model compounds (phenol and benzoic acid) in disinfection experiments enabled identification of oxidant products and comparison to DOM components facilitated identification of possible reaction pathways. Benzoic acid was selected as a simple model compound for oxidant-recalcitrant DOM moieties, as it has a negligible measurable electron donating capacity with $[ABTS^{\cdot+}]^-$ and is essentially unreactive with FAC and O_3. An overarching objective of this work was to leverage these analyses to identify DOM modifications due to solar chlorine photolysis or AOPs that result in increased DBP yields, and identify how to mitigate DBP formation while maintaining enhanced disinfection.

4.2. Materials and Methods

4.2.1. Materials. Commercially available isolates of Suwannee River NOM (SRNOM), Suwannee River Humic Acid (SRHA), Suwannee River Fulvic Acid (SRFA), and Upper

Mississippi River NOM (UMNOM) were obtained from the International Humic Substances Society (properties summarized in Table S4.2). All other chemicals, unless specified otherwise, were obtained from Sigma Aldrich and were of at least reagent-grade purity. All aqueous stock solutions were prepared in Milli-Q ultrapure water with resistivity ≥18.2 MΩ cm. Haloacetic acid (HAA) and trihalomethane (THM) standards (Supelco) were diluted in MTBE from EPA 552.2 HAAs mix and EPA 501/601 THMs calibration mix respectively. FAC stock solutions were prepared by dilution of ~5% reagent grade sodium hypochlorite (Sigma Aldrich) in ultrapure water. FAC stock solutions were standardized spectrophotometrically (at pH 11) at λ = 292 nm using $\varepsilon_{292nm,OCl^-} = 350\ M^{-1}\ cm^{-1}$.[46]

4.2.2. Ozone and Ozone-Superoxide Treatment. Ozone gas was produced from high purity oxygen, using either an Innovatec, Rheinbach model CMG 3-3 (location: Eawag), or an IN USA, model AC-2025 (location: University of Washington) ozone generator. Stock solutions were prepared by bubbling the ozone-oxygen gas mixture through ultrapure water cooled in an ice bath. O_3 stock solutions were standardized spectrophotometrically at λ = 260 nm using ε_{260} = 3200 $M^{-1}\ cm^{-1}$.[18] Ozone experiments were initiated by transferring ozone stock via syringe (Hamilton, Switzerland) into experimental solutions (10 mM phosphate buffer, with or without 50 mM *tert*-butanol (*t*BuOH)), with aqueous O_3 concentrations ranging from 0.05–1.0 g O_3 / g DOC. Solutions were rapidly mixed and then allowed to react for 24 hours at 25 °C, ensuring complete consumption of O_3 prior to analyses. Selected samples were also chlorinated after ozone treatment (designated as O_3/FAC), according to the same conditions for FAC only treatment described in Section 4.2.4.

Superoxide and ozone flow-through experiments were designed to optimize hydroxyl radical yields and minimize ozone reactions with DOM. Superoxide was sourced from KO_2 and

stabilized in an alkaline solution (100mM NaOH). However, concentrations still degraded quickly, so mixing with ozone and sample solutions was initiated within 10 minutes of dissolution. Superoxide ($O_2^{\cdot-}$) concentration was estimated by monitoring UV absorbance at 240 and 260 nm and decoupling the contributions from $O_2^{\cdot-}$ ($\varepsilon_{O2-,240nm}$ = 2173 $M^{-1}cm^{-1}$, $\varepsilon_{O2-,260nm}$ = 1850 $M^{-1}cm^{-1}$, at pH 13)[47] and ionized hydrogen peroxide, HO_2^- ($\varepsilon_{H2O2,240nm}$ = 354 $M^{-1}cm^{-1}$, $\varepsilon_{H2O2,260nm}$ = 192 $M^{-1}cm^{-1}$, at pH 13)[48]. Diluted ozone stocks were stabilized under acidic conditions (10 mM H_2SO_4) and solutions containing probes and SRNOM were also acidified (~40 mM H_2SO_4) such that the final mixed pH was 5.0±0.2. Three syringe pumps were used to mix the three reagents at a four-way mixing cross, each reagent flowrate was set to 15 mL min^{-1} and resulted in an exit flowrate of 45 mL min^{-1}. Hydrogen peroxide was quenched with catalase prior to DOM analysis or chlorination.

4.2.3. X-ray Irradiation. All X-ray irradiations were performed in an NSI X5000 CT scanner with a 450 kV broad focal-spot source. The dose rate was calculated as 0.22 kGy hr^{-1}, in a position 21 cm from the source, via hydrogen peroxide formation (determined via colorimetry)[49] during irradiation of air saturated solutions with 1 mM formate (pH = 6.7). The ionizing radiation resulted in radiolysis of water, producing H_2O_2, $HO^{\cdot}$, $H^{\cdot}$, and $e^-_{(aq)}$. All experiments (unless otherwise specified) were saturated with a mixture of N_2O and O_2 (4/1 v/v), with N_2O added to convert $H^{\cdot}$ and $e^-_{(aq)}$ into hydroxyl radical (reactions listed in the Appendix, Table A.2). Direct radiolysis of the solutes was assumed to be negligible. Hydroxyl radical yields in N_2O/O_2 saturated samples were estimated by measuring the buildup of formaldehyde during radiolysis of tert-butanol (0.05 M, pH 7)[50, 51]. Formaldehyde was determined using the Hantzsch method (ε_{412nm} = 7700 M^{-1} cm^{-1})[52]. Select X-ray irradiation experiments also included addition of chloride (5.0×10^{-3} M) or hypochlorite (1.1×10^{-4} M) to produce $Cl^{\cdot}/Cl_2^{\cdot-}$ and $ClO^{\cdot}$ respectively

(Eq. 4.5 and 4.6). Steady state radical concentrations were estimated from assumed pseudo-first order losses of select probes including nitrobenzene, benzoic acid, phenol, and/or 1,4-dimethoxybenzene (reaction rate constants are listed in the Appendix Table A.2 and steady-state radical calculations are detailed in Text S4.5). Residual hydrogen peroxide was removed with catalase prior to DOM analysis and sequential chlorination.

4.2.4. Chlorine and Simulated Sunlight Treatment. Photolysis experiments and controls were buffered (10mM phosphate unless otherwise specified, at pH 8.0 or 6.0) and treated according to four treatment protocols: (i) dark chlorination (FAC only), (ii) simulated solar irradiation without FAC followed by a dark FAC period (Light only / FAC only), (iii) simulated solar irradiation of chlorine containing water (FAC+light) as previously described,[31] and (iv) simulated solar irradiation of hydrogen peroxide containing water (H_2O_2+UV) followed by a dark FAC period (H_2O_2+UV/FAC only). All simulated solar irradiations were conducted at 25 °C (maintained via recirculating water bath) within a Heraeus AG SUNTEST CPS+ (Eawag) or Atlas XLS+ (University of Washington) solar simulator, each equipped with a O_3-free, Xe arc lamp with daylight filter (cutoff below 290 nm) and infrared radiation filter, see Text S4.1 and Figure S4.2 for reactor configuration details. FAC concentration was monitored using DPD colorimetry,[53] and chlorine exposure ($CT_{FAC} = \int[FAC]\, dt$) was approximated by using trapezoidal Riemann summation of FAC concentrations during the course of experiments. In selected experiments, solutions were sparged with high purity nitrogen to create initially anoxic conditions (procedures are outlined in Text S4.2). H_2O_2 concentration was monitored before and after irradiation using Allen reagent.[49]

Chemical actinometry experiments, using *p*-nitroanisole and pyridine,[54] were performed in quartz reactor tubes alongside sample irradiation experiments (details provided in Text S4.3).

Spectral irradiance measurements were obtained using an ILT950-UV spectroradiometer (SpectriLight III) or a USB2000+XR1 extended range spectroradiometer (see Figure S4.1 for representative spectral irradiance curves). Steady-state radical concentrations were estimated using a combination of nitrobenzene and benzoic acid or *p*-chlorobenzoic acid as probes. Concentrations were monitored via HPLC (see Text S4.4 and S4.5 for HPLC method and steady-state radical concentration calculations).

4.2.5. Analytical Methods. *4.2.5.1. HAA Extraction and Analysis*. HAAs were extracted into MTBE from 20 mL aqueous samples quenched with sodium thiosulfate ($Na_2S_2O_3$), amended with internal standards (100 μg/L 1,2,3-trichloropropane and ^{13}C isotope CAA, DCAA, and BAA standards), and esterified by means of acidified methanol following standard EPA Methods 551.1.[55] Further details for the extraction procedure were detailed by Young et al. (2018). Extracted and esterified HAAs were analyzed using a Thermo Scientific Trace GC Ultra with HS-DB-624 column and DSQ II MS detector (Eawag) or Shimadzu GC-2010 with HP-1MS U column and electron-capture detector (University of Washington).

4.2.5.2. THM Analysis. THMs in samples quenched with $Na_2S_2O_3$ were measured either by headspace GC-MS within 24 hours of experimentation (Eawag) or extracted into MTBE with HAAs as described in Section 4.2.5.1 (University of Washington). 1,2,3-trichloropropane was used as an internal standard in both cases, either added to samples in glass headspace vials or in the MTBE phase. Headspace vials were heated to 80°C, shaken for 30 minutes, and gases in the headspace were injected, separated, and analyzed on a Thermo Scientific Trace GC Ultra with RTX-VMS GC column and DSQ II MS detector.

4.2.5.3. Fluorescence Measurements. Samples containing chlorine were quenched with As(III)[31] prior to analysis by fluorescence spectrometry. Fluorescence excitation emission

matrices (EEM) were collected using a HORIBA FluoroMax (ETH-Zurich) or a HORIBA Aqualog (University of Washington) spectrofluorometer and processed as described previously.[31] Regional maxima at Ex/Em = 350 nm/450 nm were monitored (see Figure S4.3 for example EEM).

4.2.5.4. Electron Donating Capacity. Treated and untreated samples (samples containing chlorine were quenched with As(III), or containing H_2O_2 were quenched with catalase) were mixed with the stable radical cation of 2,2'-azino-bis(3-ethylbenzothiazoline-6-sulfonate) ($[ABTS^{\cdot+}]^-$) to estimate the electron donating capacity (EDC). The stable radical $[ABTS^{\cdot+}]^-$ (absorbing at 405 nm) reacts as an electron acceptor with the dissolved organic matter, and reforms $ABTS^{2-}$ (non-absorbing at 405nm), see Scheme 4.1. The $[ABTS^{\cdot+}]^-$ reagent solution was prepared by oxidizing $ABTS^{2-}$ (stabilized in 50mM H_2SO_4) with sub-stoichiometric concentrations of FAC and mixing vigorously for at least ten minutes to ensure complete reaction (targeting 20μM $[ABTS^{\cdot+}]^-$). $[ABTS^{\cdot+}]^-$ stock solutions were standardized spectrophotometrically at λ = 405 nm using $\varepsilon_{405nm,ABTS^{\cdot+}} = 31600\ M^{-1}\ cm^{-1}$.[56] Untreated and treated samples (2.5 mL injection volume) were analyzed using a high-performance liquid chromatography system (Ultimate 3000) with an SEC column (8mm × 300 mm, Toyopearl HW50S), installed before a post-column reactor that introduced $[ABTS^{\cdot+}]^-$ reagent.[44, 45] The eluent consisted of 25 mM phosphate buffer, to maintain a pH of 7.8, pumped at a flow rate of 0.2 mL min^{-1}. After exiting the SEC column, the solution passes through a UV detector (monitor A_{254}), then mixes with the $[ABTS^{\cdot+}]^-$ reagent solution (50 μL min^{-1}) and passes through a PTFE reaction coil (Dionex, USA; internal volume of 1.75 mL, corresponding to a retention time of 7 min), in which $[ABTS^{\cdot+}]^-$ is reduced by electron-donating moieties of DOM. The extent of $[ABTS^{\cdot+}]^-$ reduction was quantified spectrophotometrically at 405nm (A_{405}) in an UltiMate 3100

VWD UV-detector following the post-column reactor.

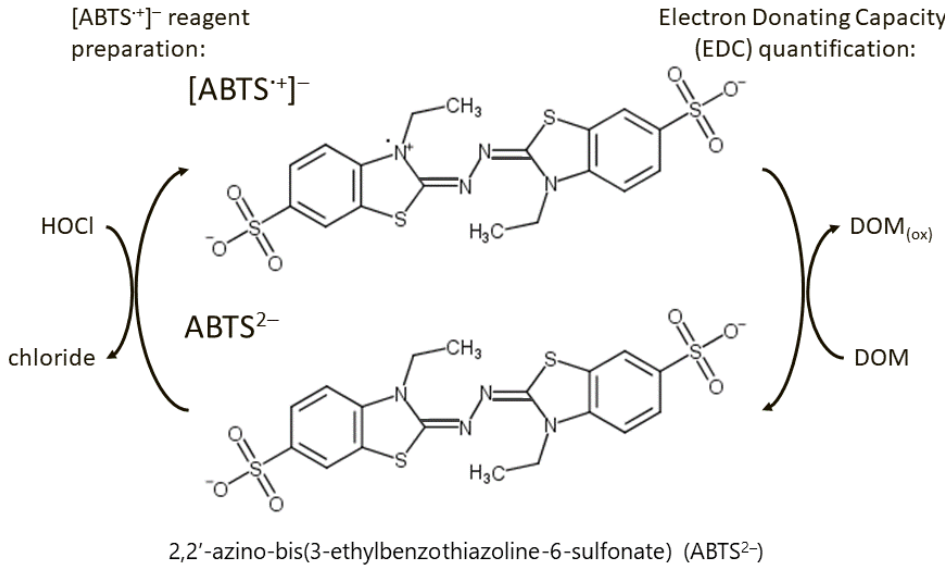

Scheme 4.1. Preparation of $[ABTS^{\cdot+}]^-$ via reaction with free chlorine and $[ABTS^{\cdot+}]^-$ oxidation of dissolved organic matter (DOM) to quantify electron donating capacity.

Model compounds and treated DOM samples were also measured using a batch setup. In the batch setup, 1.4mL phosphate buffer (25 mM) is mixed with 1 mL of sample and 0.6 mL $[ABTS^{\cdot+}]^-$ reagent (prepared as described above and maintaining a mixed pH of 7.8), and A_{405} was recorded after 7 minutes. Sample EDC was calculated as $\Delta A_{405} = A_{405,blank} - A_{405,sample}$, with blank samples prepared with phosphate buffer and $[ABTS^{\cdot+}]^-$. Additional instrumentation details are provided in Text S4.6.

4.3. Results and Discussion

4.3.1. Chlorine Treatment. *4.3.1.1. DOM Variation.* Chlorination of DOM resulted in a rapid decrease in the measured EDC (>35 % decrease for SRNOM, Figure 4.1a), even at low chlorine exposures ($CT_{FAC} \geq 3$ mg/L×min). Following the initial rapid drop in measured EDC, increasing CT_{FAC} during dark chlorination resulted in a more gradual decrease in EDC. For the

studied DOM isolates (SRNOM, SRHA, SRFA, and UMNOM), the normalized EDC of the FAC treated DOM is well correlated to the normalized A_{254} (R^2 = 0.977). However, EDC is more sensitive to chlorination than A_{254}, as indicated by the slope of the regression line in Figure 4.1b (A_{254} vs EDC, slope = 2.96±0.16, R^2 = 0.94). The addition of electron withdrawing functional groups (such as Cl) to phenol decreases the measured EDC, particularly when substituted in the

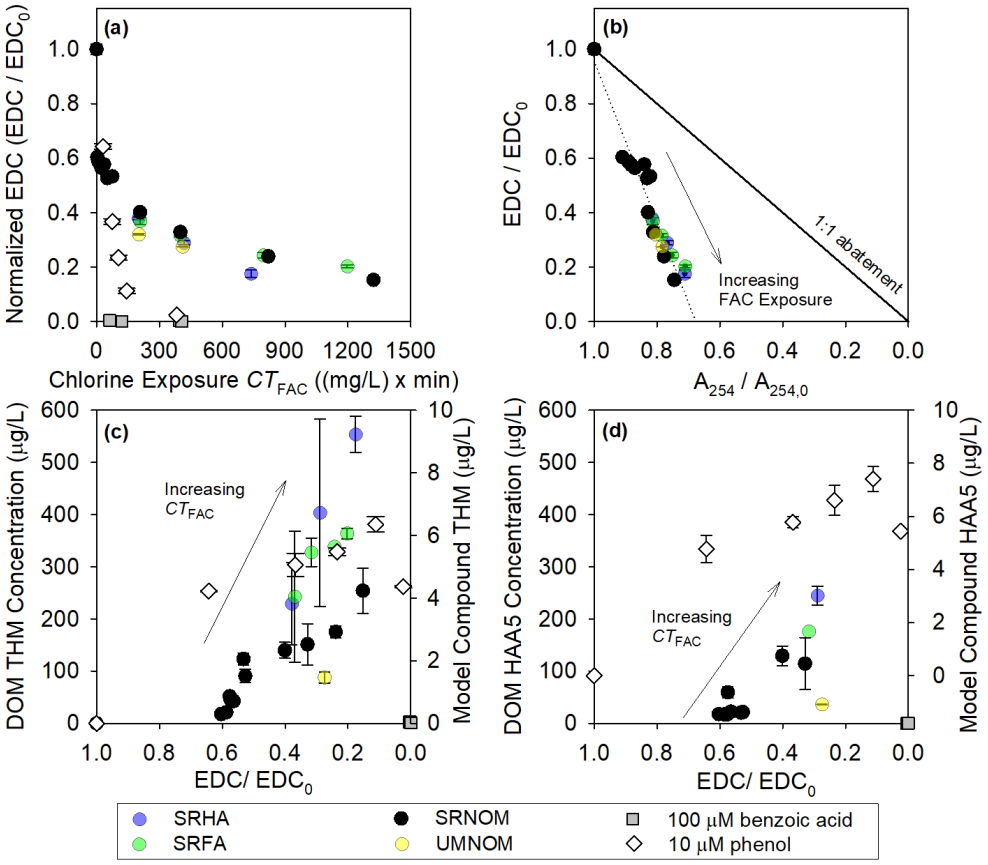

Figure 4.1. Dark chlorine treatment (FAC only) with **(a)** normalized EDC ($\Delta A_{405}/\Delta A_{405,t=0}$) versus chlorine exposure (CT_{FAC}); **(b)** normalized EDC versus normalized UV absorbance (A_{254}), slope of 2.96±0.16 ; **(c)** total trihalomethane (TTHM) yields versus normalized EDC; and **(d)** HAA5 yields versus normalized EDC. Experiments were run at 25 °C, pH 8, and concentrations of SRNOM, SRHA, SRFA, and UMNOM were 5 mg/L as C, $[BA]_0$ = 100 µM, and $[phenol]_0$ = 10 µM. Note: DBPs from model compound experiments are plotted on secondary y-axis in panels (c) and (d).

para-position (Figure S4.4). Therefore, the sudden decrease in EDC during chlorination is theorized to be due to rapid halogenation of activated aromatics within the DOM[19, 57] (e.g., phenol-like moieties with $k_{phenol,FAC(pH\ 8)} \sim 90\ M^{-1}s^{-1}$)[42].

4.3.1.2. DBP formation. EDC loss appeared to correlate with THM and HAA formation following DOM chlorination, and each was driven by increasing chlorine exposure. Elevated EDC and aromatic content of untreated DOM appeared to result in elevated formation of chloroform, dichloroacetic acid, and trichloroacetic acid during chlorination (normalizing for CT_{FAC}, Figure S4.5). For example, SRHA has the highest initial EDC, highest percentage aromatic carbon (Table S4.2, data sourced from International Humic Substances Society)[58], and highest THM and HAA5 yields upon chlorination when compared to SRNOM and UMNOM. Our observations of significant EDC loss and modest changes to absorbance during chlorination of SRHA and SRFA are consistent with previously reported data, accounting for variation in chlorination dose and reaction times.[17, 19] Ultimately, chlorination impacted this suite of DOM isolates similarly and halogenation of aromatic-moieties of DOM is suspected of decreasing the measurable EDC.[19, 57] DBP yields are likely attributable to chlorination of a fraction of highly-reactive aromatics, hypothesized to be phenolic or resorcinol-like moieties.

4.3.1.3. Model Compounds. The complex and heterogeneous structure of DOM makes it very difficult to identify mechanisms for DOM oxidation and DBP formation during combined, sequential, or individual treatment with FAC, O_3, ROS, and RCS. Therefore, experiments were also conducted with simpler model compounds (phenol and benzoic acid), facilitating identification of reaction mechanisms that may be occurring in natural water systems. Benzoic acid was included as a model compound to probe radical reactions, as it is essentially unreactive with chlorine or ozone, and phenol was included as a reactive aromatic model compound.

Benzoic acid is unreactive with FAC (for $CT_{FAC} \leq 400$ mg/L×min) and does not have a measurable EDC before or after FAC treatment. Phenol is reactive with chlorine and has been used as a model for DOM for conventional drinking water treatment.[42] Initial chlorination of phenolate is driven primarily by reactions with HOCl (second-order reaction rate constant $k_{phenol,FAC(pH\ 8)} \sim 90\ M^{-1}s^{-1}$)[42]. The only quantifiable halogenated product identified after FAC only treatment of phenol was 2,4,6-trichlorophenol (Figure 4.2). Low concentrations of mono and dichlorophenols, which are anticipated to precede trichlorophenol formation, could be transformed due to rapid halogenation after initial chlorine substitution (accumulating 2,4,6-trichlorophenol as the primary product). Concentrations appeared to be below our method detection limits. DBP yields remain low (Figure 4.1 c and d, secondary y-axis), indicating that residual chlorine concentrations and reaction times were not sufficient to initiate ring cleavage of trichlorophenol and subsequent chlorination of DBP precursors. DBP yields from DOM may be elevated after these low chlorine exposures due to contributions from activated aromatic groups within the DOM that are more reactive with FAC than phenol (e.g., resorcinol-like moieties $k_{resorcinol,FAC(pH8)} \sim 10{,}000\ M^{-1}s^{-1}$)[59].

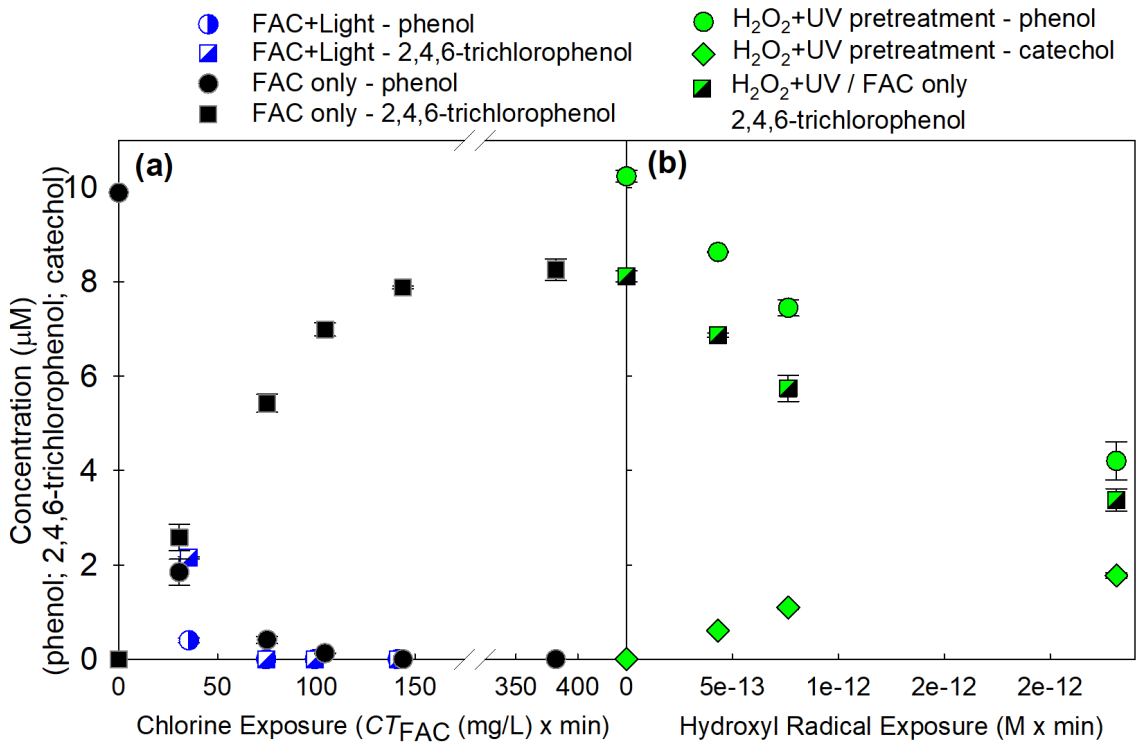

Figure 4.2. Concentrations of phenol, catechol, and 2,4,6-trichlorophenol after **(a)** dark chlorination (FAC only) and solar chlorine photolysis (FAC+Light) treatment (no detected catechol) and; **(b)** hydrogen peroxide photolysis (H_2O_2 + UV) treatment (1 mM H_2O_2). $[FAC]_0$ ~ 8 mg/L as Cl_2, 25 °C in 10 mM phosphate buffer (pH 8). Note the break in the x-axis for panel A.

4.3.2. Ozone Treatment. *4.3.2.1. DOM treatment.* Figure 4.3a displays normalized EDC data after increasing ozone doses ("O_3 only") and post ozonation-chlorination ("O_3/FAC only", CT_{FAC} = 400 mg/L×min) treatment for a fixed DOC concentration with and without radical scavenging (50mM *t*BuOH). Addition of *t*BuOH is necessary to evaluate the effect of ozone independently, as ozone decomposition will result in $HO^{\cdot}$ formation in parallel. Ozone decomposition is accelerated at elevated pH (via reaction with hydroxide) resulting in greater influence from $HO^{\cdot}$ and other ROS. The EDC for SRNOM decreased slowly with low ozone doses (molar ratio $[O_3]/[DOC] \leq 0.1$) and decreased more substantially with increasing ozone doses. Degradation of A_{254} was consistent with increasing ozone dose and did not include a slow

initial phase, as observed with EDC. These findings indicate that at the lowest ozone doses investigated here, ozonation (and ROS derived from O_3 decomposition) resulted in oxidation of UV-absorbing moieties while forming or maintaining electron donating moieties. This resulted in data trends above the A_{254} vs EDC 1:1 abatement line, slope = 0.592±0.08 (Figure 4.3b).

Pretreatment with low ozone exposures resulted in increased chloroform and HAA formation after chlorination (Figure 4.3c and d) followed by decreases in chloroform and HAA formation with increasing O_3 ($[O_3]/[DOC] > 0.25$, molar basis). Our DBP observations with varied O_3 are consistent with observed increases in organic DBP formation after low ozone exposures at elevated pH,[15, 16] favoring hydroxyl radical formation at these conditions. The ozone oxidation trends indicate that ozone is degrading DOM chromophores (which have a measurable EDC) and hydroxyl radical may be initially activating some recalcitrant moieties (benzoic acid-like) while degrading reactive moieties (phenol-like).

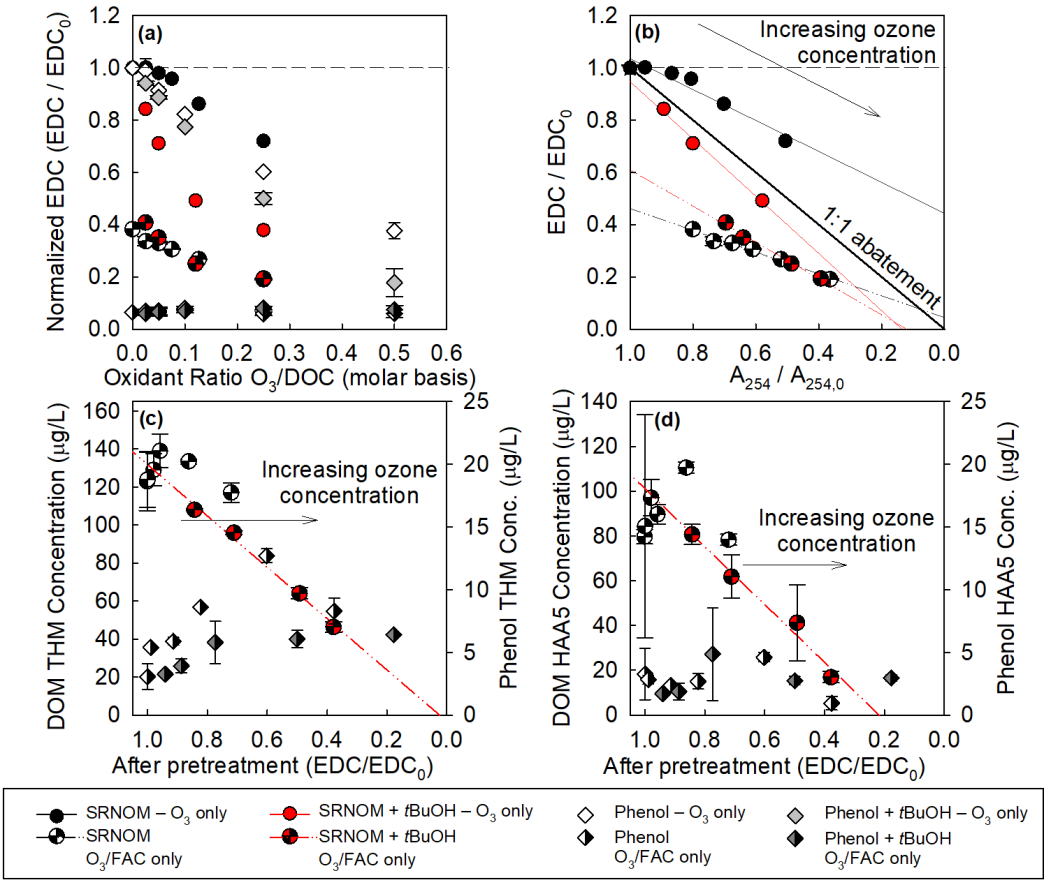

Figure 4.3. (a) Changes to normalized EDC after ozone (O_3 only) or sequential (O_3/FAC only) treatment; and correlations between; **(b)** normalized EDC and UV absorbance (254nm); **(c)** THM yields versus EDC (EDC_t/EDC_0) after ozone pretreatment; and **(d)** HAA5 yields versus EDC (EDC_t/EDC_0) after ozone pretreatment. Experiments were run at 25 °C, pH 8, initial SRNOM, SRHA, SRFA, and UMNOM concentrations are 5 mg/L as C and $[phenol]_0$ = 10 µM. Note: DBPs from model compound experiments are plotted on secondary y-axis in panels (c) and (d).

Radical scavenging by *t*BuOH will suppress hydroxyl radical generated during ozone decomposition, which may also result in higher O_3 exposures by limiting $HO^{\cdot}$ reactions with O_3 at the same time. Addition of *t*BuOH during ozonation resulted in decreases in SRNOM EDC, to a greater extent than ozonation without the radical scavenger. O_3/FAC only treatment resulted in significant decreases in SRNOM EDC, as expected from chlorination data described in Section 4.3.1. Increasing the ozone concentration resulted in a diminishing pool of electron donating moieties that persist after O_3/FAC only treatment. The loss of EDC after chlorination was not

influenced by *t*BuOH addition. The similarities between datasets with and without radical scavenging indicate that ozone may degrade DOM moieties that are slow reacting with FAC but measurable via EDC. THM and HAA yields decrease with increasing ozone dose and appear to correlate with EDC loss following ozonation of SRNOM with *t*BuOH (THM slope of 135±8 with $R^2 = 0.992$, HAA5 slope of 129±14 with $R^2 = 0.977$). These DBP trends are distinctly different than those observed following ozonation without *t*BuOH addition. The combination of ozonation and $HO^{\cdot}$ hydroxylation (occurring without addition of *t*BuOH) of DOM simultaneously activate and degrade EDC moieties. The hydroxylation reactions are believed to result in the slowed EDC loss and increased DBP formation at low O_3 doses.

4.3.2.2. Model Compounds. Phenol was also sequentially treated with ozone (with and without *t*BuOH) and chlorine (Figure 4.6). Benzoic acid was not included in this experiment set due to its low reaction rate with O_3. In general, the EDC trends during ozone treatment of phenol were similar to SRNOM trends, with EDC decreasing with increasing O_3 concentration and a significant decrease observed after chlorination. One difference observed in the phenol experiments was that radical scavenging had a lesser influence on EDC degradation of phenol during ozonation when compared to SRNOM, likely due to fast reactions between ozone and phenol. Hydroxyl radical (produced from direct ozone reactions with phenol and ozone autodecomposition)[60] also reacts with phenol directly and likely forms dihydroxybenzenes initially and then O_3 and $HO^{\cdot}$ further degrade the oxidized phenolate products.

HAA formation was minimal following O_3/FAC only treatment of phenol and ozone dose did not appear to impact these low yields (Figure 4.3d). Low ozone dose (without *t*BuOH) also resulted in minor increases to chloroform formation after sequential O_3/FAC only treatment of phenol (CT_{FAC} ~ 400 mg/L×min) (Figure 4.3c). There is a decrease in the measured chloroform

for the highest ozone dose, similar to THM trends following SRNOM ozonation. Addition of a radical scavenger during ozonation of phenol also eliminates the apparent increase in chloroform formation. Similar to SRNOM, this may be due to suppression of hydroxyl radical reaction with phenol.

4.3.3. Hydroxyl Radical Treatment. Three hydroxyl radical AOPs were investigated: X-ray radiolysis, ozone-superoxide, and hydrogen peroxide solar photolysis. Solar photolysis of hydrogen peroxide was utilized to limit direct photolysis of target compounds. However, SRNOM was photolyzed directly[61] such that its chlorine reactivity was altered following irradiation with solar fluences required for hydrogen peroxide photolysis (25 – 139 J/cm^2). To minimize SRNOM transformation by side reactions, only probes were treated by hydrogen peroxide photolysis. The other two alternative hydroxyl radical treatments were necessary to remove the impact of photodegradation and direct alteration of DOM.

4.3.3.1. X-Ray Radiolysis. Hydroxyl radical treatment of SRNOM was implemented via X-ray radiolysis of N_2O/O_2 (4/1 v/v) saturated water. Increasing irradiation time (resulting in increased hydroxyl radical exposures, determined by nitrobenzene loss) resulted in increased EDC for treated SRNOM (Figure 4.4a). Additionally, these hydroxyl radical exposures ($< 2\times10^{-10}$ M×s) appear to have a minimal impact on A_{254}, resulting in poorly correlated trends for A_{254} vs EDC ($R^2 = 0.001$, and a slope of –0.1±1.4) in Figure 4.4b. The negative slope indicates EDC is formed, though this appears to be independent to changes to A_{254}. The observed increase in EDC with minimal A_{254} degradation provides some evidence that hydroxyl radical is participating in hydroxyl-addition reactions, activating aromatic rings, while hydroxyl radical exposures are not sufficient to cause ring cleavage or degradation of chromophores.[62] The activated SRNOM (pretreated with hydroxyl radical) also yielded increased DBP formation upon chlorination when

compared to chlorination alone (plotted as normalized pretreatment EDC = 1). The THM and HAA formation also appeared to correlate positively with the normalized pretreatment EDC (THM $R^2 = 0.728$, HAA $R^2 = 0.818$). This provides some striking evidence that hydroxyl radical treatment is modifying DOM such that DBP formation increases upon chlorination. These increased DBP formation trends are similar to the initial increase observed for O_3 treatment without *t*BuOH, indicating hydroxyl addition may be an important mechanism during AOP treatment of SRNOM.

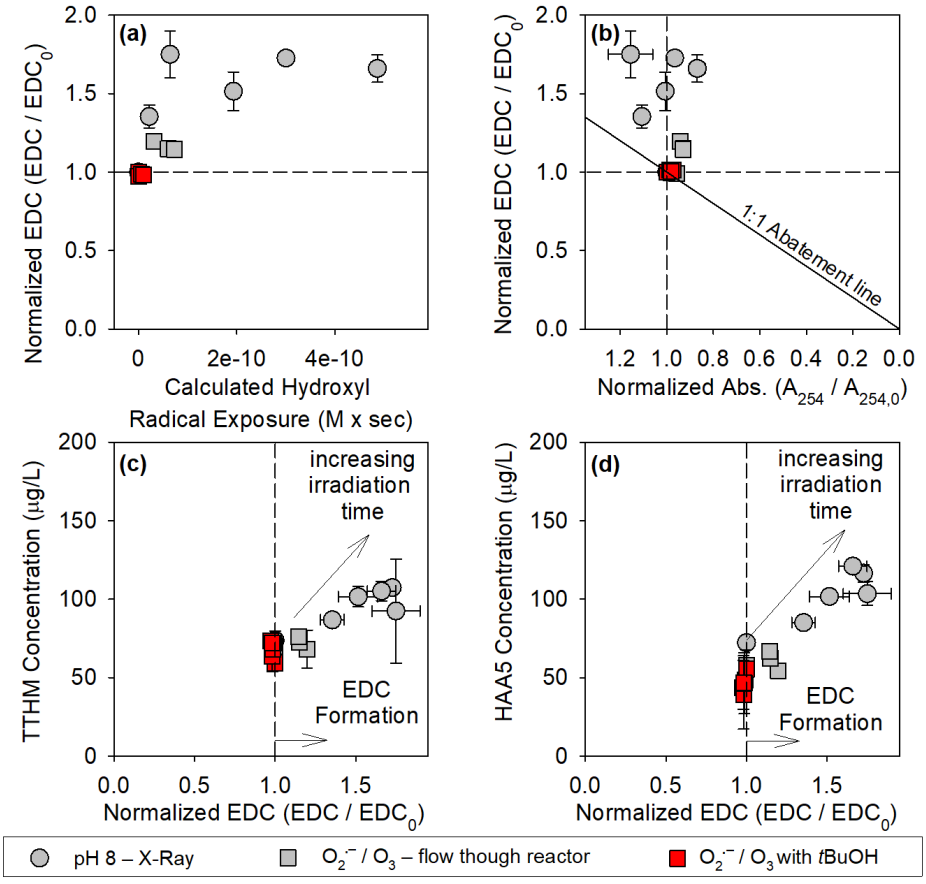

Figure 4.4. (a) Normalized EDC (EDC/ EDC_0) of SRNOM with varied hydroxyl radical exposure; **(b)** Normalized EDC formation versus normalized UV absorbance ($A_{254}/A_{254,0}$); **(c)** TTHM yields versus normalized EDC following Xray radiolysis pretreatment (Formation: EDC/ $EDC_0 > 1$); and **(d)** HAA5 yields versus normalized EDC following Xray radiolysis pretreatment. Experiments run at 25 °C, pH 8, initial SRNOM concentration of 5mg/L as C, and saturated with (4:1) N_2O:O_2. $O_2^{\cdot-}$/O_3 experiments targeted a mixed pH = 5.

4.3.3.2. Ozone-superoxide AOP. As an alternative to X-ray radiolysis, the reaction of ozone and superoxide (O_3/ $O_2^{\cdot-}$) was investigated as a clean source of $HO^{\cdot}$, as previous studies have demonstrated that hydroxyl radical is formed in reactions between O_3 and $O_2^{\cdot-}$ at neutral pH.[63] In mixtures which maintained excess superoxide ($1.5 < [O_2^{\cdot-}]/[O_3] < 2.5$), phenol loss (added as a probe, 1μM upon mixing) appeared to be dictated by hydroxyl radical exposures calculated by degradation of benzoic acid (added as a probe, 1 μM upon mixing). This would indicate that residual ozone concentrations are low upon mixing due to rapid reaction with the excess superoxide, otherwise phenol loss would be greater due to direct reactions with residual ozone. Moreover, experiments with added tert-butanol (150mM in sample solution, 50 mM after mixing) resulted in no net loss of organic probes (benzoic acid, dimethoxybenzene, or phenol) when compared to blanks mixed without superoxide or ozone.

Similar to X-ray irradiation, increasing ozone concentrations (while maintaining superoxide ratios) resulted in an increase in the EDC of SRNOM. Following chlorination, THM and HAA formation increased modestly. The minimal impact on DBP formation (when compared to X-ray radiolysis) is anticipated to be due to low hydroxyl radical exposures associated with this method ($CT_{HO\cdot} < 1\times10^{-10}$). The stability of superoxide limits the concentration of ozone that can be utilized, hence the radical yields are also limited. With increased superoxide stability this method could be expanded to target a larger range of hydroxyl radical exposures, though this was not pursued in this study. While the ionic strength of the final mixture is high, this method could be utilized as an alternative hydroxyl radical source for research laboratories that desire to work with photosensitive compounds without access to ^{60}Co-gamma radiation or X-ray radiation sources.

4.3.3.3. Hydrogen peroxide photolysis AOP. Experiments treating benzoic acid and phenol via hydrogen peroxide photolysis (with simulated sunlight) were included to investigate hydroxyl radical reactions with simpler model compounds. Both model compounds were unaffected by extended solar fluences required for hydrogen peroxide photolysis. Phenol concentrations decreased with increasing steady-state hydroxyl radical exposures (Figure 4.2). Catechol was the primary stable hydroxylated product identified after H_2O_2+UV treatment of phenol (Figure 4.2). Hydrogen peroxide photolysis resulted in decreased EDC with increasing $HO^{\cdot}$ exposure (Figure 4.5), in contrast with increasing EDC trends observed for SRNOM. Phenol and phenolate are susceptible to hydroxyl radical oxidation and their degradation is suspected to be driven by hydroxylation[43] and ring cleavage. Both mechanisms are likely occurring and may explain the modest net loss of EDC during pretreatment: a proportion of the initial phenol is degraded and undergoes ring opening reactions, resulting in EDC loss, but some products (such as hydroquinone and catechol) are formed and have a higher EDC than phenol (Figure S4.4).

Chlorination following H_2O_2+UV pretreatment resulted nearly 80% of the measured phenol forming 2,4,6-trichlorophenol when treated with equivalent chlorine exposures, CT_{FAC} = 400 mg/L×min (Figure 4.2). EDC was not detected following H_2O_2+UV/FAC only treatment, which is consistent with the EDC profiles for trichlorophenol (Figure S4.4). HAA formation, and to a lesser degree THM formation, increased with increasing hydroxyl radical treatment of phenol. Hydroxylation of phenol is likely contributing to the pool of DBP precursors (catechol and hydroquinone formation). DBP formation from phenol may be rate limited by ring cleavage,[42] and dihydroxybenzenes may react to form ring-opening products, such as lower molecular weight aldehydes and carboxylic acids (i.e., muconic acid)[64]. These ring-opening products are suspected to be the primary DBP precursors upon chlorination. In brief, DBP

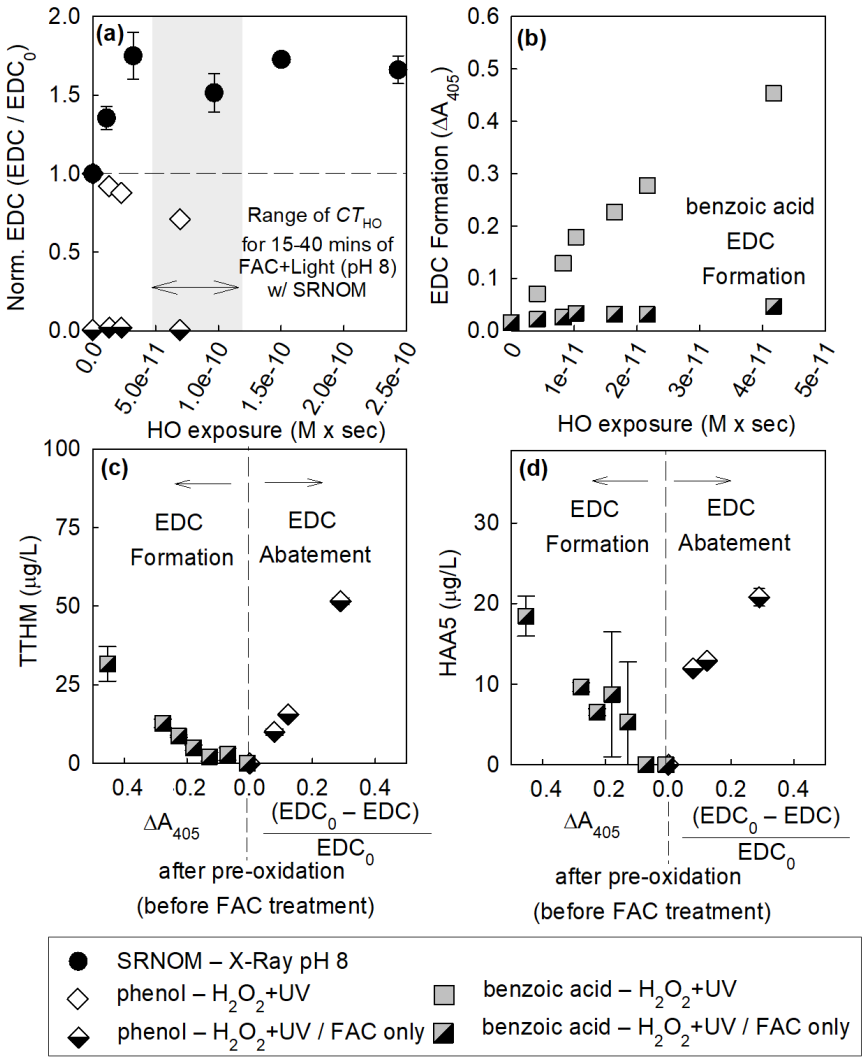

Figure 4.5. (a) Normalized EDC (EDC/EDC$_0$) of phenol and SRNOM with varied hydroxyl radical exposure; **(b)** EDC formation (ΔA_{405}) of benzoic acid with increasing hydroxyl radical exposure; **(c)** TTHM yields versus EDC formation (ΔA_{405}) or EDC abatement (EDC$_0$ – EDC)/ EDC$_0$); and **(d)** HAA5 yields versus EDC formation or EDC abatement. Experiments were run at 25 °C, pH 8, DOM concentrations were [SRNOM]$_0$ = 5mg/L as C, [BA]$_0$ = 100 μM and [phenol]$_0$ = 10 μM.

formation did increase after phenol pretreatment with hydroxyl radical and adds additional evidence that radical reactions, specifically product hydroxylation, increased chlorine consumption and contribute to EDC (though oxidation/degradation of the pool of phenol resulted in a net EDC loss).

Sequential hydrogen peroxide photolysis (H_2O_2+UV) treatment confirmed that hydroxyl radical reactions contribute to benzoic acid degradation and formation of hydroxylated products. In Figure 4.6, salicylic acid (2-hydroxybenzoic acid) and 4-hydroxybenzoic acid were the two stable hydroxylated byproducts identified after H_2O_2+UV. As expected, addition of a radical scavenger halts benzoic acid transformation to hydroxylated products. In Figure 4.5b, the EDC (measured as ΔA_{405}) increases during H_2O_2+UV treatment, while benzoic acid does not have a detectable EDC (hence the EDC cannot be normalized by the initial value). The trend of increasing EDC follows similar trends as the normalized EDC treated via X-ray radiolysis. Sequential chlorination resulted in complete loss of the EDC formed during H_2O_2+UV treatment of benzoic acid and all identified hydroxylated products were transformed to products lacking EDC during FAC treatment. Hydroxylation of benzoic acid increased chlorine reactivity and resulted in formation of chloroform and HAAs (Figure 4.5 c and d). Hydroxylation of benzoic acid compounds confirms that chlorine recalcitrant compounds can be activated by AOPs and contribute to DBP formation upon chlorination.

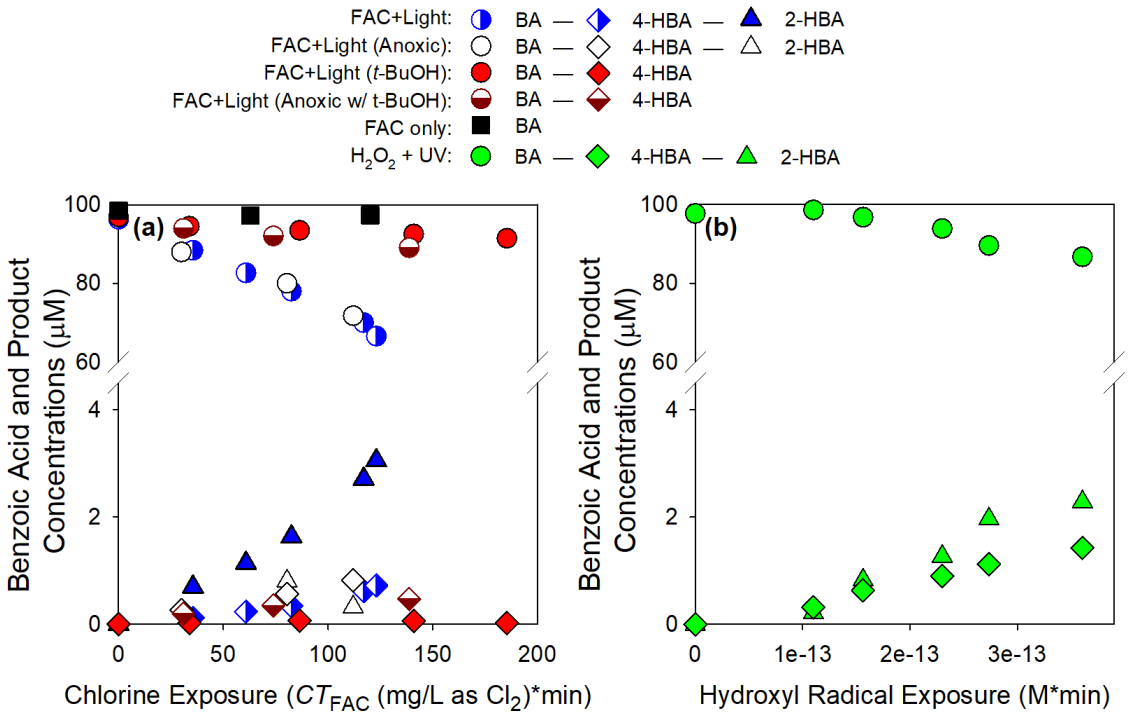

Figure 4.6. Concentrations of benzoic acid (BA), 2-hydroxybenzoic acid (2-HBA), and 4-hydroxybenzoic acid (4-HBA) after **(a)** dark chlorination (FAC only) and solar chlorine photolysis (FAC+Light) treatment and; **(b)** hydrogen peroxide photolysis (H_2O_2 + UV) treatment (1 mM H_2O_2). Modifications to FAC+Light treatment include initially anoxic conditions (Anoxic), 50 mM *tert*-butanol (*t*BuOH) as a radical scavenger and the combination of the two conditions (Anoxic w/ *t*BuOH). $[FAC]_0$ ~ 8 mg/L as Cl_2, 25 °C in 10 mM phosphate buffer (pH 8). Note the break in the y-axis for figure (a) and (b).

4.3.4. Reactive Chlorine Species Treatment. *4.3.4.1. Chlorine oxide radical.*

Hypochlorite was added to X-ray irradiated alkaline (pH 10) solutions to promote chlorine oxide radical ($ClO^{\cdot}$) formation via reaction of hydroxyl radical with OCl^- (reaction 4.5). The reactivity of SRNOM with hypochlorite constrained the hypochlorite concentration utilized, as increasing the concentration would favor $ClO^{\cdot}$ formation and decrease $[HO^{\cdot}]_{ss}$ but high OCl^- concentrations would exceed realistic CT_{FAC}. Ultimately 0.11 mM OCl^- was selected to maintain the same [FAC]/[DOC] ratio as is present initially in chlorination experiments and modelled results indicate this concentration is sufficient to scavenge ~90% of the estimated hydroxyl radical yield. Similar to chlorination experiments, the EDC of SRNOM after treatment decreased rapidly

(Figure 4.7). Again, the sudden decrease in SRNOM EDC is suspected to be due to halogenation of phenolic-moieties by FAC. In previous studies, degradation of personal care products by $ClO^{\cdot}$ were not negatively impacted by alkaline conditions,[65] but hydroquinone autoxidation[66] may be occurring in the oxygenated solutions at pH 10 and contribute to the decrease in EDC as well.

THM and HAA formation increased with increasing X-ray irradiation, implying $ClO^{\cdot}$ may oxidize DOM and contribute to DBP precursor formation. Hydroxyl radical was still formed in this system and could contribute to direct hydroxylation and activation of DOM, resulting in increased DBP formation, as seen with sequential hydroxylation and chlorination. However, controls irradiating alkaline solutions (without OCl^{-}) followed by sequential chlorination confirm that DBP formation is higher with hypochlorite and $ClO^{\cdot}$ present with lower $[HO^{\cdot}]_{ss}$ (Figure 4.7 c and d). $ClO^{\cdot}$ has been identified as a single electron oxidizer,[35, 65, 67] and is anticipated to react with aromatic and alkene organic bonds, which may react further with dissolve oxygen to form hydroquinones.[68] This co-exposure of $ClO^{\cdot}$, $HO^{\cdot}$, and OCl^{-} in oxygenated solutions appear to be contributing to increased THM and HAA formation when compared to sequential hydroxyl radical and chlorination treatment or chlorination alone. This may be due to $ClO^{\cdot}$ oxidation of aromatic moieties within the DOM, which contributes to the pool of DBP precursors that are susceptible to halogenation by FAC, also present in solution.

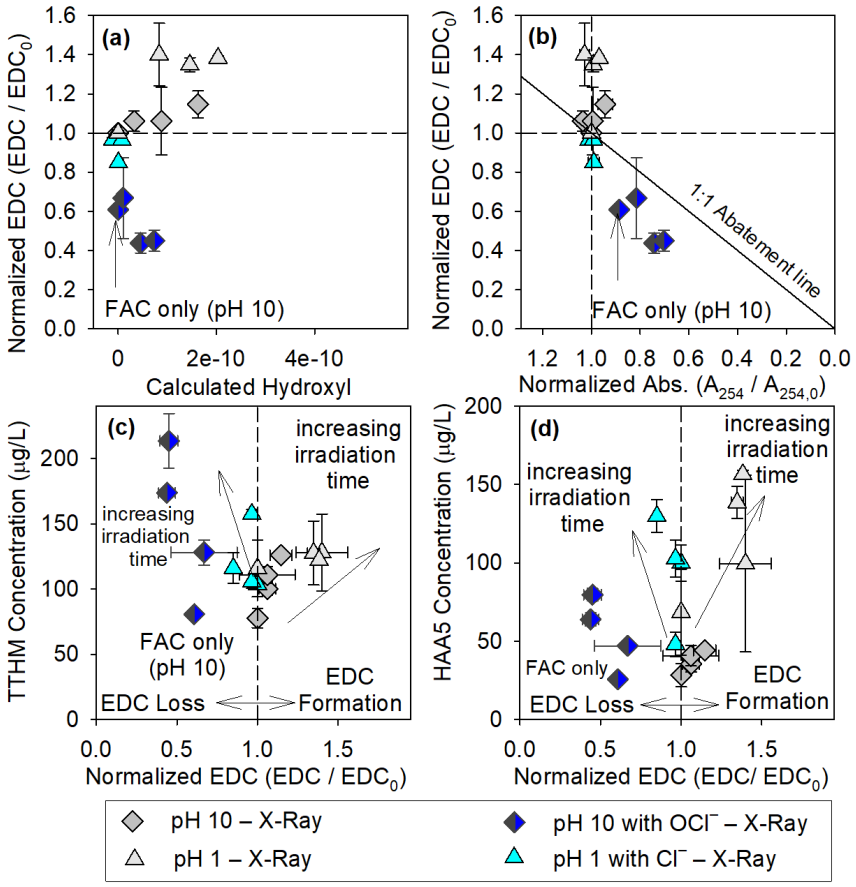

Figure 4.7. (a) Normalized EDC (EDC/ EDC_0) of SRNOM with varied hydroxyl radical exposure; **(b)** Normalized EDC formation versus normalized UV absorbance ($A_{254}/A_{254,0}$); **(c)** TTHM yields versus normalized EDC (Abatement: EDC / EDC_0 < 1; Formation: EDC / EDC_0 > 1); and **(d)** HAA5 yields versus normalized EDC. Experiments run at 25 °C, initial SRNOM concentration of 5mg/L as C, and saturated with 4/1 N_2O/O_2. pH 1 samples were brought to pH 8 prior to chlorination.

4.3.4.2. Chlorine atom and dichloride radical anion. Chloride was added during X-ray radiolysis experiments to produce chlorine atom ($Cl^{\cdot}$) (via $HO^{\cdot}$ reaction with Cl^-)[69] and dichloride radical anion ($Cl_2^{\cdot-}$) (via $Cl^{\cdot}$ reaction with Cl^-, Equation 4.4). Experimental conditions were selected from Kintecus[70] modelling results to favor RCS formation (included equations and reaction rate constants are listed in the Appendix, Table A.2). Acidic pH (pH 1.0 ± 0.05, >100 mM $HClO_4$) was selected to lower the steady-state hydroxyl radical concentrations (modelled $[HO^{\cdot}]_{ss} \sim 3\times10^{-14}$ M) by favoring $Cl^{\cdot}$ formation from $ClOH^{\cdot}$ reaction with H^+. Chloride

concentrations (5mM Cl^-) were selected to optimize formation of chlorine atom (modelled $[Cl^\cdot]_{ss}$ ~ 4×10^{-13} M) and avoid depleting $Cl^\cdot$ via reactions with Cl^-, favoring $Cl_2^{\cdot-}$ formation (modelled $[Cl_2^{\cdot-}]_{ss}$ ~ 1×10^{-10} M). Other kinetic studies focusing on $Cl^\cdot/Cl_2^{\cdot-}$ reactions have utilized higher chloride concentrations to minimize direct impacts from hydroxyl or sulfate radical.[23, 71, 72] After X-ray irradiation under these conditions (pH 1.0±0.05 and $5x10^{-3}$ M Cl^-), the EDC did decrease though the change was modest (Figure 4.7a). A decrease in EDC could be driven by DOM oxidation by $Cl^\cdot$ or $Cl_2^{\cdot-}$, or formation of low concentrations of Cl_2 which can also react with DOM. A_{254} and EEM did not appear to be modified during radiolysis treatment (Figure 4.7b and Figure S4.6C). This could indicate $Cl^\cdot/Cl_2^{\cdot-}$ did not efficiently degrade chromophores and fluorophores at these their respective exposures. Chloroform, DCAA, and TCAA were not directly formed during X-ray radiolysis pretreatment with chloride, which indicated Cl_2 yields are low during radiolysis and DOM was not chlorinated by chlorine. Because DBP formation does not occur during radiolysis of chloride, $Cl^\cdot/Cl_2^{\cdot-}$ is assumed to engage primarily in electron transfer or H-abstraction reactions with DBP precursors and not halogen addition, as theorized in previous RCS studies.[35, 65, 73, 74]

Following radiolysis treatment, samples were adjusted to pH 8 with NaOH and sequentially treated with free chlorine. HAA yields may increase slightly with increasing irradiation (Figure 4.7 d), though trends in DBP formation were less conclusive than was observed during ROS or $ClO^\cdot$ pretreatment. Even with the selected concentration of chloride, our probes indicated the system was dominated by $Cl_2^{\cdot-}$ which is selectively reactive; potentially halogenating alkene bonds or abstracting electrons from hydroxylated aromatic rings.[75, 76] $Cl^\cdot$ may preferentially react via electron transfer at oxygen-containing functional groups, though under these conditions $Cl^\cdot$ yields were low and acidic pH conditions are expected to decrease the

reactivity of protonated acidic DOM functional groups.[77] Normalizing DBP formation by chlorination controls and plotting versus calculated RCS exposures confirm that $Cl_2^{\cdot-}$ has a minimal impact on THM and HAA formation under these conditions (Figure S4.7 d and e). Therefore, $Cl_2^{\cdot-}$ is not anticipated to be a major contributor to DBP formation during AOPs with significant chlorine or chloride concentrations in solution. $Cl^{\cdot}$ oxidation is suspected to contribute to DOM oxidation via electron transfer, but chlorine addition and H-abstraction cannot be ruled out definitively as $Cl^{\cdot}$ yields were low during this experimental condition.

4.3.5. Solar Chlorine Photolysis. *4.3.5.1. DOM Variation.* Solar chlorine photolysis (referred to as "FAC+Light" throughout the text and figures) combines free chlorine, RCS, O_3 and other ROS, where each type of oxidant may exhibit a wide range of reactivities toward various types of constituent groups present in DOM. A_{254} degradation was enhanced during FAC+Light treatment when compared to chlorination alone (Figure S4.5a). Changes to A_{254} during solar chlorine photolysis of SRNOM are suspected to be driven by ozone reactions with chromophores, as these trends were also observed following ozonation pretreatment with and without *t*BuOH addition. Simultaneously, FAC+Light treatment of DOM resulted in further decreases in EDC when compared to FAC only treatment with equivalent CT_{FAC} (Figure S4.5b). THM and HAA yields for each DOM increased with longer FAC+Light treatment. Solar chlorine photolysis of SRNOM resulted in DBP formation that appears to correlate with changes to normalized EDC variation (THM $R^2 = 0.95$ and HAA $R^2 = 0.73$), as seen in Figure 4.8 c and d. With FAC in solution, halogenation of DOM is expected to result in a decrease in measured EDC[19, 57] due to the electron withdrawing properties of Cl substituents (Figure S4.4). During solar chlorine photolysis of DOM, FAC is suspected to be the dominant halogenating oxidant,[73] though Cl-addition from $Cl^{\cdot}$ cannot be ruled out definitively. Hydroxyl radical generated during

photolysis can react with DOM via addition, electron transfer, or H-abstraction reactions. ROS reactions may activate aromatic and phenolic-moieties through hydroxyl addition as observed during hydroxyl radical pretreatment, or degrade DOM (e.g., cleavage of alkyl bonds or oxidized ring species, such as benzoquinone moieties).[78]

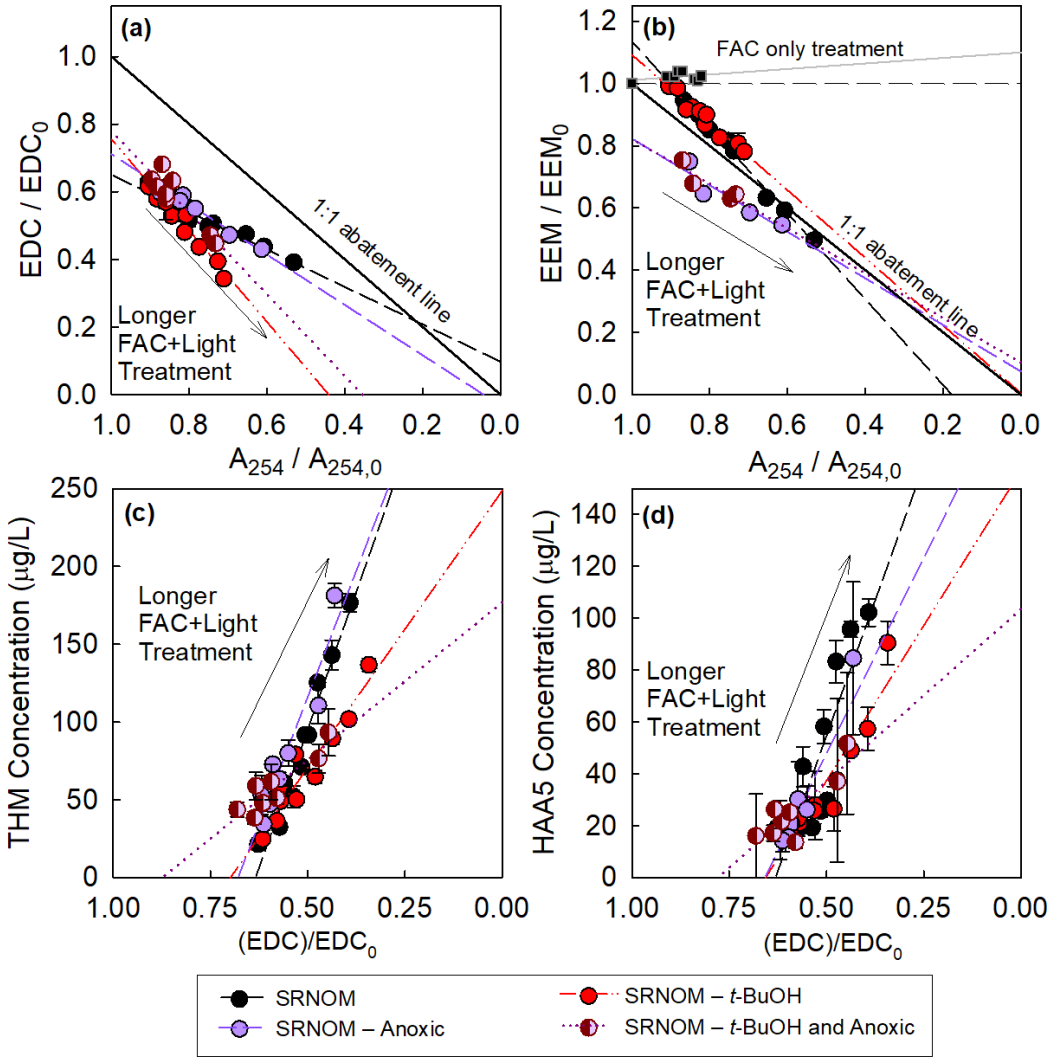

Figure 4.8. Suwannee River NOM, humic acid, fulvic acid (SRNOM, SRHA, SRFA), and upper Mississippi NOM (UMNOM) after solar chlorine photolysis with or without 50mM tert-butanol (*t*BuOH) and nitrogen sparging (Anoxic). Subpanels include **(a)** normalized EDC versus chlorine exposure (CT_{FAC}); and correlations between **(b)** normalized EDC and UV absorbance (254nm); **(c)** THM yields versus normalized EDC; and **(d)** HAA5 yields versus normalized EDC. Experiments were run at 25 °C, pH 8, initial DOC concentrations were 5 mg/L as C.

4.3.5.2. Reactive Oxygen Species (ROS) Variation. Anoxic conditions (solutions sparged with N_2 gas) in select samples labeled "Anoxic" limited ozone formation initially during FAC+Light treatment. 50mM tert-butanol (*t*BuOH) was added as a radical scavenger to select samples, and one set included anoxic conditions with *t*BuOH addition. As shown in Figure 4.8, the similar EDC profiles for modified (w/ *t*BuOH or anoxic conditions) and unmodified FAC+Light treatment confirm that FAC rapidly reacts with electron-rich moieties of the SRNOM and decreases the measured EDC initially. Anoxic sample solutions limited initial ozone formation but did not affect RCS and ROS production during FAC+Light treatment. Anoxic conditions alone did not appear to significantly impact DBP yields or spectral DOM modifications (Figure 4.8). This resulted in similar linear slopes for EDC vs. DBP correlations between the unmodified and anoxic FAC+Light treatment of SRNOM (unmodified THM slope = –709±59, R^2 = 0.94, and HAA5 slope = –418±90, R^2 = 0.72; Anoxic conditions THM slope = –649±88, R^2 = 0.90, and HAA5 slope = –302±60, R^2 = 0.81). Lower linear slopes for EDC vs. DBP correlations were observed for *t*BuOH and Anoxic+*t*BuOH modified FAC+Light treatment of SRNOM (*t*BuOH THM slope = –356±43, R^2 = 0.90, and HAA5 slope = –239±34, R^2 = 0.86; Anoxic+*t*BuOH conditions THM slope = –202±38 R^2 = 0.83, and HAA5 slope = –133±32 R^2 = 0.74). Addition of *t*BuOH to FAC+Light treatment of SRNOM resulted in preservation of A_{254} and a decrease in DBP yields when compared to unmodified FAC+Light treatment. Similar to A_{254}, fluorescence (EEM intensity in Figure S4.8c) was preserved during FAC+Light conditions with *t*BuOH addition. This would indicate that radicals formed during FAC+Light treatment (e.g., $HO^{\cdot}$, $Cl^{\cdot}$, and $ClO^{\cdot}$ which are effectively scavenged by *t*BuOH) are involved in degradation of chromophores and fluorophores.

As shown in Figure 4.8c and d, DBP yields increased with increasing CT_{FAC} and solar

fluence during FAC+Light treatment of SRNOM. THM and HAA5 yields are lower for FAC+Light conditions modified by *t*BuOH addition when compared to unmodified or anoxic FAC+Light treatment; however, all FAC+Light conditions yield elevated DBP concentrations when compared to chlorination alone (Figure 4.1 and 4.8). This indicates ROS and RCS produced during solar chlorine photolysis are contributing to increased formation of DBPs. Solar chlorine photolysis of anoxic solutions with *t*BuOH will still yield atomic oxygen, $O(^3P)$, as an oxidant. Atomic oxygen is suspected to react with alkanes via H-abstraction[79] and is capable of oxidizing phenols.[80] Increased DBP yields during anoxic FAC+Light treatment with *t*BuOH may be driven by $O(^3P)$ oxidation reactions with natural organic matter when compared to chlorination alone.

There is a portion of SRNOM that is recalcitrant to chlorination, and these structures may become more reactive with FAC following reaction with radical species and result in increased DBP formation upon chlorination, as observed during sequential $HO^{\cdot}$ treatment. This DOM activation is likely due to hydroxyl addition which increases reactivity with FAC, as discussed further with respect to benzoic acid (see Section 4.3.2.3). Hydroxyl radical and RCS (such as, $Cl^{\cdot}/Cl_2^{\cdot-}$) are both scavenged by *t*BuOH, therefore the experiment sets with *t*BuOH highlighted the importance of radical reactions in DBP formation but cannot distinguish the effects of hydroxyl radical from chlorine atom, though $Cl_2^{\cdot-}$ is not anticipated to increase DBP formation.

4.3.5.3. Model Compounds. Phenol was degraded faster during FAC+Light treatment when compared to chlorination alone and yielded increased THM and HAA formation (Figure 4.1 and 4.9). 2,4,6-trichlorophenol was identified after brief solar irradiation (fluence ~ 1.3 J/cm^2) during FAC+Light treatment (Figure 4.2), and increasing solar fluences during FAC+Light treatment (increasing ROS *and* FAC exposures) resulted in complete degradation of phenol and chlorinated

phenols. Phenol may form dihydroxybenzenes after hydroxyl addition or electron transfer, forming carbon-centered radicals which can react further with dissolved oxygen during FAC+Light treatment. FAC in solution is then expected to rapidly react with the formed resorcinol, catechol, or hydroquinone and result in chloroform and TCAA formation. The higher second order reaction rate constants for dihydroxybenzene with FAC may explain why negligible concentrations of dihydroxybenzenes were identified during FAC+Light treatment. Phenol transformation is likely due to ring opening and formation of smaller MW organics (e.g., aldehyde and carboxylic acid groups), which have been identified as precursors for chloroform, dichloroacetic acid, and trichloroacetic acid[42] (Figure 4.5).

As discussed earlier, benzoic acid is essentially unreactive with free chlorine, but was reactive with radical species formed in situ during FAC+Light treatment. Hydroxylated products such salicylic acid and 4-hydroxybenzoic acid were identified during FAC+Light treatment and result after $HO^{\cdot}$ reacts with benzoic acid (see Figure 4.6). Chlorinated benzoic acid products were not identified, indicating $Cl^{\cdot}$ is not likely directly halogenating benzoic acid during solar chlorine photolysis but rather participating in electron transfer and formation of cyclohexadienyl radical (or peroxyl radical after reaction with dissolved oxygen)[72]. Hydroxylation of benzoic acid during FAC+Light treatment resulted in a measurable EDC and formation of chloroform and trichloroacetic acid. Untreated benzoic acid does not react with $[ABTS^{\cdot+}]^{-}$; therefore, EDC measurements for benzoic acid are reported as ΔA_{405} and are not normalized by the untreated EDC in Figure 4.9. Addition of *t*BuOH disrupts chloroform and TCAA formation during FAC+Light treatment of benzoic acid and confirms that radical reactions were contributing to increased DBP formation.

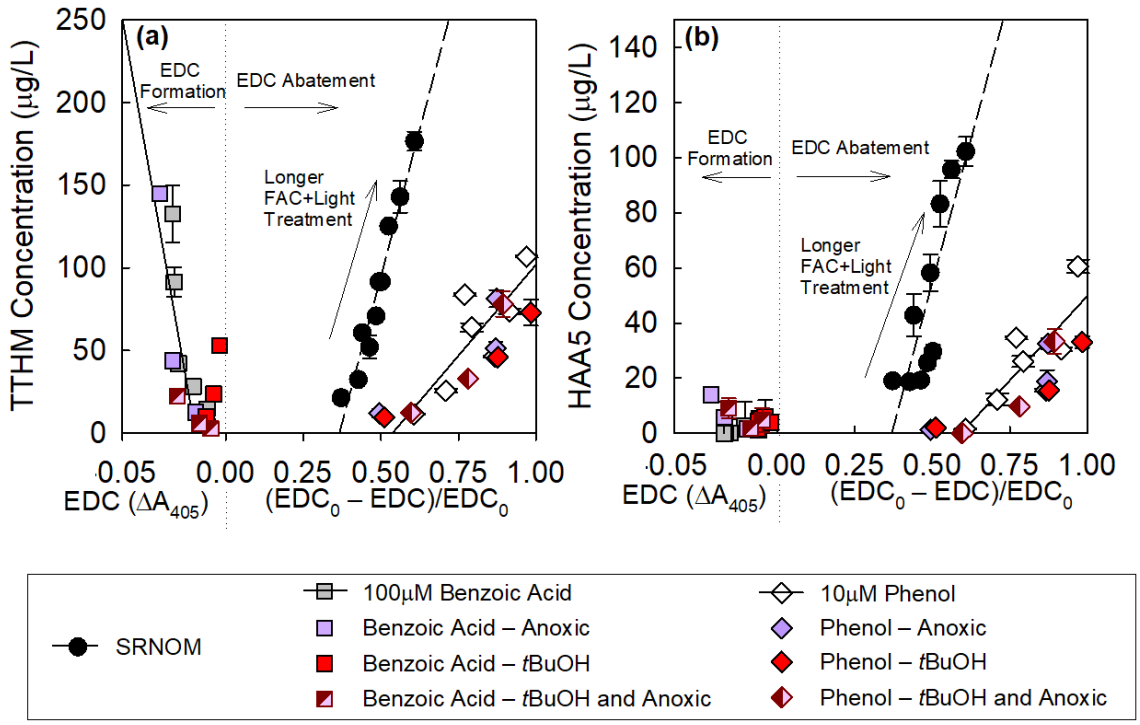

Figure 4.9. Correlations after solar chlorine photolysis treatment between **(a)** THM yields versus EDC formation (EDC = $A_{405} - A_{405,blank}$) or EDC abatement ($EDC_0 - EDC$)/ EDC_0; and **(b)** HAA5 yields versus EDC formation (ΔA_{405}) or EDC abatement ($EDC_0 - EDC$)/ EDC_0 . Experiments at 25 °C, pH 8, $[FAC]_0$ = 4 or 8 mg/L as Cl_2, initial DOM concentrations were $[SRNOM]_0$ = 5 mg/L as C, $[BA]_0$ = 100 µM , and $[phenol]_0$ = 10 µM.

DOM oxidation indicates that reactive moieties such as phenol and resorcinol – reacting rapidly with free chlorine and ozone – are present in a mixture with diverse aromatic structures that have slower reaction rates with oxidants such as FAC that are commonly implemented as disinfectants. These less reactive constituents of DOM do not contribute to the measurable EDC or DBP formation after chlorination alone, however, they may be altered via electron transfer or hydroxylation via $HO^{\bullet}$ – similar to $HO^{\bullet}$ and/or $Cl^{\bullet}$ oxidation of benzoic acid or persistent pollutants.[9, 81] Increased reactivity due to hydroxylation of previously unreactive DOM could be the primary driver for increased DBP formation during FAC+Light treatment when compared to FAC only treatment.

4.3.6. Implications for Solar Chlorine Photolysis and AOP Application. While the mechanism for THM and HAA formation from natural organic matter after advanced oxidation and chlorination is not precisely understood, the data collected in this study emphasizes the role of hydroxyl radical (and perhaps $ClO^{\cdot}$) in activating natural organic matter. Sequential AOP and FAC treatment of a humic-rich DOM (such as Suwannee River NOM isolate) can result in increased DBP formation following low $HO^{\cdot}$ exposures, though higher $HO^{\cdot}$ exposures would eventually result in DOM mineralization and anticipated decreases in DBP yields upon chlorination.[73] Hydroxylation (from $HO^{\cdot}$) in the presence of free chlorine (e.g., during solar chlorine photolysis or UVC chlorine photolysis) activates aromatic DOM, increasing reactivity with FAC. $HO^{\cdot}$ oxidation also likely cleaves aromatic rings to form lower molecular weight aldehydes and carboxylic acid (similar to observations following treatment of phenol in AOPs),[43] ultimately contributing to elevated DBP yields. $ClO^{\cdot}$ may also contribute to DBP formation in the presence of FAC, as seen in the X-ray irradiation experiments. $ClO^{\cdot}$ may transfer an electron from an aromatic bond,[76] forming a carbon-centered radical that could react with dissolved oxygen or RCS and contribute to chloroform and TCAA formation. While $ClO^{\cdot}$ could contribute to increased DBP formation during solar chlorine photolysis, more research is needed in this area as some bimolecular rate constants for $ClO^{\cdot}$ with relevant inorganic and organic water constituents are unknown, and kinetic models may overestimate steady-state yields in complex oxidation and photooxidation systems.[82] Ozone (and to a lesser degree $Cl_2^{\cdot-}$) appears to oxidize SRNOM, resulting in a decrease in EDC. Ozone also degrades chromophores and decreases DBP formation potential in the presence of a radical scavenger (which precludes parallel reactions resulting from hydroxyl radical activation of SRNOM).

In this work, co-exposure of SRNOM and/or model compounds to ROS, RCS, and free chlorine consistently resulted in increased DBP formation, either due to the opportunity for all activated DOM moieties to react with FAC before being further oxidized by radical species or ozone, or formation of reactive RCS which contribute to direct DBP formation. Regardless, water treatment applications should be designed with caution when combining FAC simultaneously or in sequence with advanced oxidation to minimize the potential for enhanced formation of regulated DBPs such as THMs and HAAs, as well as various unregulated DBPs that may also result from similar mechanisms as those discussed here.

Advanced oxidation processes are typically designed to meet removal efficiency targets for micropollutants, which require high radical exposures ($HO^{\cdot}$ and/or $Cl^{\cdot}$) and so will likely yield decreases in DBP formation. However, low exposures of hydroxyl radical – suspected to be encountered in disinfection applications or in treating waters containing high levels of natural radical scavengers, e.g., DOM and carbonate – are more likely to increase organic DBP formation upon chlorination. These findings highlight the need to evaluate the impacts of a wide range of hydroxyl radical exposures on DBP formation potentials before applying AOPs or conventional O_3-based pre-oxidation processes for municipal water treatment.

Acknowledgements

We would like to thank Elisabeth Salhi, Jakov Bolotin, and Jacqueline Traber at the Swiss Federal Institute of Aquatic Science and Technology (Eawag) in Dübendorf, Switzerland and Gordon Getzinger and Kris McNeill at ETH-Zurich for assisting in sample analysis and method development. This material is based upon work supported by the National Science Foundation under Grant No. CBET-1236303. Additional support for T.R.Y. from a National

Science Foundation Graduate Research Fellowship (ID: 2015177669) and Graduate Opportunities Worldwide support from the U.S. National Science Foundation and Swiss National Science Foundation (SNSF) is gratefully acknowledged.

4.4. References

1. Rook, J. J., Haloforms in Drinking Water. *Journal American Water Works Association* **1976,** *68* (3), 168-172.

2. Bellar, T. A.; Lichtenberg, J. J.; Kroner, R. C., The Occurrence of Organohalides in Chlorinated Drinking Waters. *Journal (American Water Works Association)* **1974,** *66* (12), 703-706.

3. Shah, A. D.; Krasner, S. W.; Lee, C. F. T.; von Gunten, U.; Mitch, W. A., Trade-Offs in Disinfection Byproduct Formation Associated with Precursor Preoxidation for Control of N-Nitrosodimethylamine Formation. *Environmental Science & Technology* **2012,** *46* (9), 4809-4818.

4. Yang, X.; Fan, C.; Shang, C.; Zhao, Q., Nitrogenous disinfection byproducts formation and nitrogen origin exploration during chloramination of nitrogenous organic compounds. *Water Research* **2010,** *44* (9), 2691-2702.

5. Muellner, M. G.; Wagner, E. D.; McCalla, K.; Richardson, S. D.; Woo, Y.-T.; Plewa, M. J., Haloacetonitriles vs. Regulated Haloacetic Acids: Are Nitrogen-Containing DBPs More Toxic? *Environmental Science & Technology* **2007,** *41* (2), 645-651.

6. Klavarioti, M.; Mantzavinos, D.; Kassinos, D., Removal of residual pharmaceuticals from aqueous systems by advanced oxidation processes. *Environment International* **2009,** *35* (2), 402-417.

7. Wols, B. A.; Hofman-Caris, C. H. M.; Harmsen, D. J. H.; Beerendonk, E. F., Degradation of 40 selected pharmaceuticals by UV/H2O2. *Water Research* **2013,** *47* (15), 5876-5888.

8. Ferguson, D. W.; McGuire, M. J.; Koch, B.; Wolfe, R. L.; Aieta, E. M., Comparing PEROXONE and ozone for controlling taste and odor compounds, disinfection by-products, and microorganisms. *Journal-American Water Works Association* **1990,** *82* (4), 181-191.

9. Zhang, X.; He, J.; Lei, Y.; Qiu, Z.; Cheng, S.; Yang, X., Combining solar irradiation with chlorination enhances the photochemical decomposition of microcystin-LR. *Water research* **2019,** *159*, 324-332.

10. He, X.; de la Cruz, A. A.; Hiskia, A.; Kaloudis, T.; O'Shea, K.; Dionysiou, D. D., Destruction of microcystins (cyanotoxins) by UV-254 nm-based direct photolysis and advanced oxidation processes (AOPs): Influence of variable amino acids on the degradation kinetics and reaction mechanisms. *Water Research* **2015,** *74*, 227-238.

11. Dotson, A. D.; Keen, V. S.; Metz, D.; Linden, K. G., UV/H2O2 treatment of drinking water increases post-chlorination DBP formation. *Water Research* **2010,** *44* (12), 3703-3713.

12. Metz, D. H.; Meyer, M.; Dotson, A.; Beerendonk, E.; Dionysiou, D. D., The effect of UV/H2O2 treatment on disinfection by-product formation potential under simulated distribution system conditions. *Water Research* **2011,** *45* (13), 3969-3980.

13. Ike, I. A.; Lee, Y.; Hur, J., Impacts of advanced oxidation processes on disinfection byproducts from dissolved organic matter upon post-chlor (am) ination: A critical review. *Chemical Engineering Journal* **2019**, 121929.

14. Mao, Y. Q.; Wang, X. M.; Yang, H. W.; Wang, H. Y.; Xie, Y. F. F., Effects of ozonation on disinfection byproduct formation and speciation during subsequent chlorination. *Chemosphere* **2014,** *117*, 515-520.

15. Riley, T. L.; Mancy, K. H., *The effect of preozonation on chloroform production in the chlorine disinfection processes*. Ann Arbor Science: Ann Arbor, MI, 1978; Vol. 2.

16. de Vera, G. A.; Stalter, D.; Gernjak, W.; Weinberg, H. S.; Keller, J.; Farre, M. J., Towards reducing DBP formation potential of drinking water by favouring direct ozone over hydroxyl radical reactions during ozonation. *Water Research* **2015,** *87*, 49-58.

17. Wenk, J.; Aeschbacher, M.; Salhi, E.; Canonica, S.; von Gunten, U.; Sander, M., Chemical oxidation of dissolaved organic matter by chlorine dioxide, chlorine, and ozone - effect on its optical and antioxidant properties. *Environmental Science and Technology* **2013,** *47*, 11147-11156.

18. von Sonntag, C.; von Gunten, U., *Chemistry of Ozone in Water and Wastewater Treatment: From Basic Principles to Applications*. IWA Publishing: London, 2012.

19. Önnby, L.; Salhi, E.; McKay, G.; Rosario-Ortiz, F. L.; von Gunten, U., Ozone and chlorine reactions with dissolved organic matter - Assessment of oxidation-reactive moieties by optical measurements and the electron donating capacities. *Water Research* **2018,** *144*, 64-75.

20. Wang, D.; Bolton, J. R.; Andrews, S. A.; Hofmann, R., Formation of disinfection by-products in the ultraviolet/chlorine advanced oxidation process. *Science of the Total Environment* **2015,** *518*, 49-57.

21. Liu, W.; Zhang, Z.; Yang, X.; Xu, Y.; Liang, Y., Effects of UV irradiation and UV/chlorine co-exposure on natural organic matter in water. *Science of the Total Environment* **2012,** *414*, 576-584.

22. Li, T.; Jiang, Y.; An, X. Q.; Liu, H. J.; Hu, C.; Qu, J. H., Transformation of humic acid and halogenated byproduct formation in UV-chlorine processes. *Water Research* **2016,** *102*, 421-427.

23. Alegre, M. L.; Gerones, M.; Rosso, J. A.; Bertolotti, S. G.; Braun, A. M.; Martire, D. O.; Gonzalez, M. C., Kinetic study of the reactions of chlorine atoms and Cl-2(center dot-) radical anions in aqueous solutions. 1. Reaction with benzene. *Journal of Physical Chemistry A* **2000,** *104* (14), 3117-3125.

24. Buxton, G. V.; Bydder, M.; Salmon, G. A., The reactivity of chlorine atoms in aqueous solution Part II. The equilibrium SO 4-+ Cl-Cl Nsbd+ SO 4 2. *Physical Chemistry Chemical Physics* **1999,** *1* (2), 269-273.

25. Buxton, G. V.; Subhani, M. S., Radiation chemistry and photochemistry of oxychlorine ions. Part 1.—Radiolysis of aqueous solutions of hypochlorite and chlorite ions. *Journal of the Chemical Society, Faraday Transactions 1: Physical Chemistry in Condensed Phases* **1972,** *68*, 947-957.

26. Nowell, L. H.; Hoigne, J., Photolysis of Aqueous Chlorine at Sunlight and Ultraviolet Wavelengths .1. Degradation Rates. *Water Res* **1992,** *26* (5), 593-598.

27. Nowell, L. H.; Hoigne, J., Photolysis of Aqueous Chlorine at Sunlight and Ultraviolet Wavelengths .2. Hydroxyl Radical Production. *Water Res* **1992,** *26* (5), 599-605.

28. Kläning, U. K.; Wolff, T., Laser Flash Photolysis of HClO, ClO−, HBrO, and BrO− in Aqueous Solution. Reactions of Cl-and Br-Atoms. *Berichte der Bunsengesellschaft für physikalische Chemie* **1985,** *89* (3), 243-245.

29. Forsyth, J. E.; Zhou, P. R.; Mao, Q. X.; Asato, S. S.; Meschke, J. S.; Dodd, M. C., Enhanced Inactivation of Bacillus subtilis Spores during Solar Photolysis of Free Available Chlorine. *Environ Sci Technol* **2013,** *47* (22), 12976-12984.

30. Zhou, P.; Di Giovanni, G. D.; Meschke, J. S.; Dodd, M. C., Enhanced Inactivation of Cryptosporidium parvum Oocysts during Solar Photolysis of Free Available Chlorine. *Environ Sci Tech Let* **2014,** *1* (11), 453-458.

31. Young, T. R.; Li, W.; Guo, A.; Korshin, G.; Dodd, M. C., Characterization of disinfection byproduct formation and associated changes to dissolved organic matter during solar chlorine photolysis of free available chlorine. *Water Research* **2018,** *146* (1), 318-327.

32. Oliver, B. G.; Carey, J. H., Photochemical Production of Chlorinated Organics in Aqueous-Solutions Containing Chlorine. *Environ Sci Technol* **1977,** *11* (9), 893-895.

33. Buxton, G. V.; Subhani, M. S., Radiation-Chemistry and Photochemistry of Oxychlorine Ions .2. Photodecomposition of Aqueous-Solutions of Hypochlorite Ions. *J Chem Soc Farad T 1* **1972,** *68*, 958-&.

34. Buxton, G. V.; Greenstock, C. L.; Helman, W. P.; Ross, A. B., Critical-Review of Rate Constants for Reactions of Hydrated Electrons, Hydrogen-Atoms and Hydroxyl Radicals (.Oh/.O-) in Aqueous-Solution. *Journal of Physical and Chemical Reference Data* **1988,** *17* (2), 513-886.

35. Bulman, D. M.; Mezyk, S. P.; Remucal, C. K., The impact of pH and irradiation wavelength on the production of reactive oxidants during chlorine photolysis. *Environmental science & technology* **2019,** *53* (8), 4450-4459.

36. Re, R.; Pellegrini, N.; Proteggente, A.; Pannala, A.; Yang, M.; Rice-Evans, C., Anitoxidant Activity Applying an Improved ABTS Radical Cation Decolorization Assay. *Free Radical Biology and Medicine* **1999,** *26*, 1231-1237.

37. Aeschbacher, M.; Sander, M.; Schwarzenbach, R. P., Novel Electrochemical Approach to Assess the Redox Properties of Humic Substances. *Environmental Science and Technology* **2010,** *44*, 87-93.

38. Aeschbacher, M.; Vergari, D.; Schwarzenbach, R.; Sander, M., Electrochemical Analysis of Proton and Electron Transfer Equilibria of the Reducible Moieties in Humic Acids. *Environmental Science and Technology* **2011,** *45*, 8385-8394.

39. Soltermann, F.; Widler, T.; Canonica, S.; von Gunten, U., Comparison of a novel extraction-based colorimetric (ABTS) method with membrane introduction mass spectrometry (MIMS): Trichloramine dynamics in pool water. *Water Research* **2014,** *58*, 258-268.

40. Aeschbacher, M.; Graf, C.; Schwarzenbach, R. P.; Sander, M., Antioxidant properties of humic substances. *Environmental Science and Technology* **2012,** *46*, 4916-4925.

41. de Vera, G.; Gernjak, W.; Radjenovic, J., Predicting reactivity of model DOM compounds towards chlorine with mediated electrochemical oxidation. *Water Research* **2017,** *114*, 113-121.

42. Gallard, H.; von Gunten, U., Chlorination of Phenols: Kinetics and formation of Chloroform. *Environmental Science and Technology* **2002,** *36*, 884-890.

43. Mvula, E.; von Sonntag, C., Ozonolysis of phenols in aqueous solution. *Organic & Biomolecular Chemistry* **2003,** *1* (10), 1749-1756.

44. Chon, K.; Salhi, E.; von Gunten, U., Combination of UV absorbance and electron donating capacity to assess degradation of micropollutants and formation of bromate during ozonation of wastewater effluents. *Water Research* **2015,** *81*, 388-397.

45. Önnby, L.; Walpen, N.; Salhi, E.; Sander, M.; von Gunten, U., Two analytical approaches quantifying the electron donating capacities of dissolved organic matter to monitor its oxidation during chlorination and ozonation. *Water Research* **2018,** *44*, 677-689.

46. Kumar, K.; Day, R. A.; Margerum, D. W., Atom-Transfer Redox Kinetics - General-Acid-Assisted Oxidation of Iodide by Chloramines and Hypochlorite. *Inorg Chem* **1986,** *25* (24), 4344-4350.

47. Bielski, B. H. J.; Cabelli, D. E.; Arudi, R. L.; Ross, A. B., Reactivity of HO2/O− 2 radicals in aqueous solution. *Journal of physical and chemical reference data* **1985,** *14* (4), 1041-1100.

48. Bielski, B. H. J.; Allen, A. O., Mechanism of the disproportionation of superoxide radicals. *The Journal of Physical Chemistry* **1977,** *81* (11), 1048-1050.

49. Allen, N., Quantitative determination of small amounts of hydrogen peroxide and of ozone. *Industrial and Engineering Chemistry* **1930,** *2*, 55-56.

50. Schuchmann, M. N.; Von Sonntag, C., Hydroxyl radical-induced oxidation of 2-methyl-2-propanol in oxygenated aqueous solution. A product and pulse radiolysis study. *Journal of Physical Chemistry* **1979,** *83* (7), 780-784.

51. Nöthe, T.; Fahlenkamp, H.; Sonntag, C. v., Ozonation of wastewater: rate of ozone consumption and hydroxyl radical yield. *Environmental Science & Technology* **2009,** *43* (15), 5990-5995.

52. Nash, T., The colorimetric estimation of formaldehyde by means of the Hantzsch reaction. *Biochemical Journal* **1953,** *55* (3), 416.

53. APHA/AWWA/WEF, *Standard Methods: 4500-Cl G. DPD Colormetric Method*. 22 ed.; American Public Health Association: Washington D.C., 2012.

54. Laszakovits, J. R.; Berg, S. M.; Anderson, B. G.; O'Brien, J. E.; Wammer, K. H.; Sharpless, C. M., p-Nitroanisole/Pyridine and p-Nitroacetophenone/Pyridine Actinometers Revisited: Quantum Yield in Comparison to Ferrioxalate. *Environ Sci Tech Let* **2017,** *4* (1), 11-14.

55. Munch, D. J.; Munch, J. W.; and Pawlecki, A. M., Method 552.2, Determination of Haloacetic acids and Dalapon in Drinking Water by Liquid-Liquid Extraction, Derivatization and Gas Chromatography with Electron Capture Detection. Laboratory, N. E. R., Ed. Cincinnati, OH, 1995.

56. Pinkernell, U.; Luke, H. J.; Karst, U., Selective photometric determination of peroxycarboxylic acids in the presence of hydrogen peroxide. *Analyst* **1997,** *122* (6), 567-571.

57. Wenk, J.; Aeschbacher, M.; Salhi, E.; Canonica, S.; von Gunten, U.; Sander, M., Chemical oxidation of dissolved organic matter by chlorine dioxide, chlorine, and ozone - effect on its optical and antioxidant properties. *Environmental Science and Technology* **2013,** *47*, 11147-11156.

58. Thorn, K. A.; Folan, D. W.; MacCarthy, P. *Characterization of the International Humic Substances Society Standard and Reference Fulvic and Humic Acids by Solution State Carbon-13 (13 C) and Hydrogen-1 (1 H) Nuclear Magnetic Resonance Spectrometry*; U.S. Geologic Survey: Denver, CO, 1989; pp 1-93.

59. Rebenne, L. M.; Gonzalez, A. C.; Olson, T. M., Aqueous Chlorination Kinetics and Mechanism of Substituted Dihydroxybenzenes. *Environmental Science & Technology* **1996,** *30* (7), 2235-2242.

60. Staehelin, J.; Hoigne, J., Decomposition of ozone in water in the presence of organic solutes acting as promoters and inhibitors of radical chain reactions. *Environmental Science and Technology* **1985,** *19* (12), 1206-1213.

61. Sharpless, C. M.; Aeschbacher, M.; Page, S. E.; Wenk, J.; Sander, M.; McNeill, K., Photooxidation-Induced Changes in Optical, Electrochemical, and Photochemical Properties of Humic Substances. *Environmental Science & Technology* **2014,** *48* (5), 2688-2696.

62. Gierer, J.; Reitberger, T., The reactions of hydroxyl radicals with aromatic rings in lignins, studied with creosol and 4-methylveratrol. *Holzforschung-International Journal of the Biology, Chemistry, Physics and Technology of Wood* **1992,** *46* (6), 495-504.

63. Sehested, K.; Holcman, J.; Hart, E. J., Rate constants and products of the reactions of e-aq, dioxide (1-)(O2-) and proton with ozone in aqueous solutions. *The Journal of Physical Chemistry* **1983,** *87* (11), 1951-1954.

64. Singer, P. C.; Gurol, M. D., Dynamics of the ozonation of phenol. Part 1: Experimental observations. *Water Research* **1983,** *17* (9), 1163-1171.

65. Guo, K.; Wu, Z.; Shang, C.; Yao, B.; Hou, S.; Yang, X.; Song, W.; Fang, J., Radical chemistry and structural relationships of PPCP degradation by UV/chlorine treatment in simulated drinking water. *Environmental science & technology* **2017,** *51* (18), 10431-10439.

66. Roginsky, V.; Barsukova, T., Kinetics of oxidation of hydroquinones by molecular oxygen. Effect of superoxide dismutase. *Journal of the Chemical Society, Perkin Transactions 2* **2000,** (7), 1575-1582.

67. Alfassi, Z. B.; Huie, R. E.; Mosseri, S.; Neta, P., Kinetics of one-electron oxidation by the ClO radical. *International Journal of Radiation Applications and Instrumentation. Part C. Radiation Physics and Chemistry* **1988,** *32* (1), 85-88.

68. Schuchmann, M. N.; von Sonntag, C., Oxidation of benzene by the OH radical. A product and pulse radiolysis study in oxygenated aqueous solution. *Journal of the Chemical Society, Perkin Transactions 2* **1993,** (3), 289-297.

69. Anbar, M.; Thomas, J. K., Pulse Radiolysis Studies of Aqueous Sodium Chloride Solutions1. *The Journal of Physical Chemistry* **1964,** *68* (12), 3829-3835.

70. Ianni, J. C. Kintecus.

71. Yang, Y.; Pignatello, J. J.; Ma, J.; Mitch, W. A., Comparison of halide impacts on the efficiency of contaminant degradation by sulfate and hydroxyl radical-based advanced oxidation processes (AOPs). *Environmental science & technology* **2014,** *48* (4), 2344-2351.

72. Martire, D. O.; Rosso, J. A.; Bertolotti, S.; Le Roux, G. C.; Braun, A. M.; Gonzalez, M. C., Kinetic study of the reactions of chlorine atoms and Cl(2)(center dot-)radical anions in aqueous solutions. II. Toluene, benzoic acid, and chlorobenzene. *Journal of Physical Chemistry A* **2001,** *105* (22), 5385-5392.

73. Ike, I. A.; Karanfil, T.; Cho, J.; Hur, J., Oxidation byproducts from the degradation of dissolved organic matter by advanced oxidation processes–A critical review. *Water research* **2019**, 114929.

74. Grebel, J. E.; Pignatello, J. J.; Mitch, W. A., Effect of halide ions and carbonates on organic contaminant degradation by hydroxyl radical-based advanced oxidation processes in saline waters. *Environmental science & technology* **2010,** *44* (17), 6822-6828.

75. Hasegawa, K.; Neta, P., Rate constants and mechanisms of reaction of chloride (Cl2-) radicals. *The Journal of Physical Chemistry* **1978,** *82* (8), 854-857.

76. Zhang, K.; Parker, K. M., Halogen Radical Oxidants in Natural and Engineered Aquatic Systems. *Environmental Science & Technology* **2018,** *52* (17), 9579-9594.

77. Buxton, G. V.; Bydder, M.; Salmon, G. A.; Williams, J. E., The reactivity of chlorine atoms in aqueous solution. Part III. The reactions of Cl-center dot with solutes. *Physical Chemistry Chemical Physics* **2000,** *2* (2), 237-245.

78. Wang, W.-L.; Wu, Q.-Y.; Huang, N.; Xu, Z.-B.; Lee, M.-Y.; Hu, H.-Y., Potential risks from UV/H2O2 oxidation and UV photocatalysis: A review of toxic, assimilable, and sensory-unpleasant transformation products. *Water Research* **2018,** *141*, 109-125.

79. Andresen, P.; Luntz, A. C., The chemical dynamics of the reactions of O (3 P) with saturated hydrocarbons. I. Experiment. *The Journal of Chemical Physics* **1980,** *72* (11), 5842-5850.

80. Sun, B.; Sato, M.; Clements, J. S., Use of a pulsed high-voltage discharge for removal of organic compounds in aqueous solution. *Journal of Physics D-Applied Physics* **1999,** *32* (15), 1908-1915.

81. Sun, P.; Lee, W.-N.; Zhang, R.; Huang, C.-H., Degradation of DEET and caffeine under UV/chlorine and simulated sunlight/chlorine conditions. *Environmental science & technology* **2016,** *50* (24), 13265-13273.

82. Chuang, Y.-H.; Chen, S.; Chinn, C. J.; Mitch, W. A., Comparing the UV/monochloramine and UV/free chlorine Advanced Oxidation Processes (AOPs) to the UV/hydrogen peroxide AOP under scenarios relevant to potable reuse. *Environmental science & technology* **2017,** *51* (23), 13859-13868.

83. Internation, A., Standard Tables for Reference Solar Spectral Irradiances: Direct Normal and Hemispherical on 37deg; Tilted Surface. West Conshohocken, PA, 2012.

84. Bahnmuller, S.; von Gunten, U.; Canonica, S., Sunlight-induced transformation of sulfadiazine and sulfamethoxazole in surface waters and wastewater effluents. *Water Res* **2014,** *57*, 183-192.

85. Molina, M.; Ishiwata, T.; Molina, L. T., Production of OH radical from photolyssi of HOCl at 307 - 309 nm. *Journal of Physical Chemistry* **1980,** *84*, 821-826.

4.5. Supplementary Information for Chapter 4

Text S4.1. Reactor Configuration. Two solar simulators were used throughout this study, as research was conducted at Eawag, located in Dübendorf, Switzerland and at the University of Washington, located in Seattle, WA, USA. Pictures of the solar simulators and associated water baths are included in Figure S4.2.

Text S4.2. Gas Sparging Setup. Rubber septa (Ace glass sleeve-type precision seal septa) were used to seal the tops of 28 mL quartz tubes during sparging and experimentation. For anoxic conditions septa were fitted with a PTFE sparging/sampling tube extending to the bottom of the quartz reactor (with a gas-tight two-way valve fitted to the inlet end of the tube on the outside of the septa) and a pressure relief valve inserted through the septa (but remaining above the liquid level) that connected to a N_2 gas reservoir to prevent pressure build-up during sparging or vacuum during sampling. N_2 sparging occurred for 40 minutes; with high purity 99.998% N_2 (30 ccm gas flow rate per reactor) for initially anoxic conditions. After completion of sparging, the valves on the inlet end of the PTFE sparging/sampling tube were closed to maintain gas-tight conditions in the reactor. Oxygen concentrations were measured with an MI-8-730 Flow-Thru O_2 electrode probe (Microelectrodes Inc.; Bedford, NH) before experiments, which were initiated by dosing chlorine through the sealed septa via syringe. Experiments then proceeded in the same fashion as described in the main text within the SunTest solar simulator.

For N_2O/O_2 sparging in preparation for X-ray radiolysis experiments, septa were fitted with glass frits and an ETFE sampling tube. Sparging occurred for 20-30 minutes with analytical grade N_2O/O_2 (4:1 N_2O:O_2) fitted with a granular activated carbon filter at the exit of the regulator. A gas reservoir of the nitrous oxide oxygen gas mix was attached to the quartz reactors to prevent vacuum build up during sampling.

Text S4.3. Spectroradiometry and *para*-Nitroanisole and Pyridine Actinometry Measurements. Incident spectral irradiance measurements for simulated sunlight with the Atlas system were obtained using a USB2000+ XR spectroradiometer (Ocean Optics; Dunedin, FL) equipped with a 200 μm x 2 m optical fiber and a CC-3-UV-S cosine corrector. Incident spectral irradiance measurements for simulated sunlight with the SunTest CPS+ Solar Simulator were obtained using an ILT950-UV spectroradiometer (SpectriLight III) spectroradiometer. Representative incident spectral irradiance curves are depicted for each light source in Figure S1 in comparison to the ASTM standard G173-03 for solar radiation (hemispherical on a 37º tilted surface) at sea level ASTM [83]. Measured incident irradiance spectra were obtained in each case at the surface of the reaction solutions contained within quartz tubes, with the plane of the spectroradiometer's cosine corrector facing directly toward the light source. Integration of the areas under the resulting incident spectral irradiance curves for simulated and natural sunlight yielded overall incident irradiances, $W_{tot,\lambda=290\text{-}400nm}$, of 65-75 W/m^2 and 44.2 W/m^2, respectively, between 290 and 400 nm (i.e., the region of overlap between FAC and the solar spectra). Although irradiance was higher overall for simulated sunlight, the spectral shapes for each light source were similar, with negligible output below 300 nm, as shown in Figure S2b.

Effective in situ fluence rates, $F_{tot,\lambda}$, from 290-400 nm were determined by means of *para*-nitroanisole (PNA)/pyridine actinometry for simulated sunlight and natural sunlight experiments.[54] Actinometer solutions containing 1 μM PNA and 10 mM pyridine were prepared in nanopure Milli-Q water. These actinometer solutions were then transferred into the same 28-mL quartz tubes as used for irradiation experiments under simulated or natural sunlight. The actinometer solutions were kept in the dark until the start of each experiment, after which they

were exposed to light for similar durations as utilized in the FAC+light, FAC+light/FAC only, and Light only/FAC only experiments. Samples were obtained from the irradiated actinometer solutions at pre-defined time intervals for PNA analysis. PNA concentrations were measured on an UltiMate3000 HPLC-UV system (Thermo Scientific/Dionex), using isocratic elution (0.2 mL/min) on a Supelco Ascentis C18 column (150 × 2.1 mm, 3 μm), with 50:50 CH_3CN:10-mM H_3PO_4 as mobile phase. Values of $F_{tot,\lambda}$ (in units of J m^{-2} s^{-1}, or W m^{-2}) were determined from PNA degradation rates in accord with established procedures,[84] using the revised quantum yield for PNA photolysis from.[54]

Text S4.4. HPLC analysis of probes and model compound products. All probe compounds were analyzed using an UltiMate3000 HPLC-UV system (Thermo Scientific/Dionex), using isocratic elution (0.2 mL/min) on a Supelco Ascentis C18 column (150 × 2.1 mm, 3 μm). The HPLC analysis of the probes and hydroxylated or chlorinated products of benzoic acid and phenol with gradient methods using 10-mM H_3PO_4 (A) and methanol (B). Phenol, benzoic acid, and nitrobenzene were separated with 65/35 A/B (hold 2 mins), 5 minute gradient to 15/85 A/B (hold 6.5 mins), 0.5 minute gradient to 65/35 A/B (hold 5 mins). Hydroxylated benzoic acid or phenol products were separated with 100% A (hold 2 mins), 15 minute gradient to 15/85 A/B (hold 10 mins), 1 minute gradient to 100% A (hold 5 mins). Chlorinated phenol products were separated with 55/45 A/B (hold 5 mins), 13 minute gradient to 100% B (hold 3 mins), 0.5 minute gradient to 55/45 A/B (hold 5 mins).

Text S4.5. Calculation of steady state radical concentrations using probe compounds. Steady state radical yields were estimated from the observed degradation rate of

probes compounds, with low initial concentrations (1μM) selected to prevent significant radical scavenging by the probes while monitor steady-state radical concentrations. Nitrobenzene is unreactive with many oxidants, but reacts with hydroxyl radical so it was leveraged as a hydroxyl radical specific probe. Steady state hydroxyl radical yields were estimated by solving for $[HO^{\cdot}]_{ss}$ in Equation S4.1 using the integrated form expressed in Equation S4.2.

$$k_{obs,NB} = k_{NB,HO^{\cdot}} \times [HO^{\bullet}]_{ss} \quad \text{(S4.1)}$$

$$[HO^{\bullet}]_{ss} = \frac{(-\ln([NB]/[NB]_0))}{k_{NB,HO^{\cdot}}} \quad \text{(S4.2)}$$

where $k_{obs,NB}$ is the observed rate constant for nitrobenzene loss and $k_{NB,HO\cdot}$ is the literature rate constant for nitrobenzene and hydroxyl radical (reaction 86, Appendix). For conditions with chlorine atom and $Cl_2^{\cdot-}$ a mix of three probes were utilized to estimate the steady state concentrations for these radical species. Hydroxyl radical concentration was estimated from nitrobenzene depletion kinetics alone, and then substituted into Equation S4.3, which describes the pseudo first-order depletion rate constant for benzoic acid. This was assumed to be degraded by both $HO^{\cdot}$ and $Cl^{\cdot}$, but not by $Cl_2^{\cdot-}$ ($k_{BA,Cl2\cdot} < 10^6\ M^{-1}\ s^{-1}$), so this contribution can be ignored.

$$k_{obs,BA} = k_{BA,HO^{\cdot}} \times [HO^{\bullet}]_{ss} + k_{BA,Cl^{\cdot}} \times [Cl^{\bullet}]_{ss} \quad \text{(S4.3)}$$

$$[Cl^{\bullet}]_{ss} = \frac{(-\ln([BA]/[BA]_0 - k_{BA,HO^{\cdot}} \times [HO^{\bullet}]_{ss})}{k_{BA,Cl^{\cdot}}} \quad \text{(S4.4)}$$

where $k_{obs,BA}$ is the observed rate constant for benzoic acid loss, $k_{BA,HO\cdot}$ is the literature rate constant for benzoic acid and hydroxyl radical (reaction 88, Appendix), and $k_{BA,Cl\cdot}$ is the literature rate constant for benzoic acid and chlorine atom (reaction 90, Appendix). Finally, the calculated $[HO^{\cdot}]_{ss}$ and $[Cl^{\cdot}]_{ss}$ values can be substituted into the Equation S4.5, which described the pseudo-first order depletion rate constant for phenol during the pH 1 X-ray irradiation

experiments with added chloride. Under this condition, ozone and free-chlorine are not present, and phenol is degraded by $HO^{\cdot}$, $Cl^{\cdot}$, and $Cl_2^{\cdot-}$.

$$k_{obs,PhOH} = k_{PhOH,HO^{\cdot}} \times [HO^{\bullet}]_{ss} + k_{PhOH,Cl^{\cdot}} \times [Cl^{\bullet}]_{ss} + k_{PhOH,Cl_2^{\cdot-}} \times [Cl_2^{\bullet-}]_{ss} \quad \text{(S4.5)}$$

$$[Cl_2^{\bullet-}]_{ss} = \frac{(-\ln([PhOH]/[PhOH]_0) - k_{PhOH,HO^{\cdot}} \times [HO^{\bullet}]_{ss} - k_{PhOH,Cl^{\cdot}} \times [Cl^{\bullet}]_{ss})}{k_{PhOH,Cl_2^{\cdot-}}} \quad \text{(S4.6)}$$

where $k_{obs,PhOH}$ is the observed pseudo-first order rate constant for phenol loss, $k_{PhOH,HO\cdot}$ is the literature second-order rate constant for the reaction of phenol with hydroxyl radical (reaction 97, Appendix), $k_{PhOH,Cl\cdot}$ is the literature second-order rate constant for the reaction of phenol with chlorine atom (reaction 99, Appendix), and $k_{PhOH,Cl2\cdot-}$ is the literature second-order rate constant for the reaction of phenol with $Cl_2^{\cdot-}$ (reaction 103, Appendix).

To estimate $ClO^{\cdot}$ steady-state concentrations during X-ray irradiation of pH 10 solution with hypochlorite addition, a combination of three probes was also used, with nitrobenzene and benzoic acid as probes for $HO^{\cdot}$ and $Cl^{\cdot}$ as described above (equation S4.1 and S4.3), but using the second-order reaction rate constants for deprotonated benzoate, pKa = 4.2 (reactions 89 and 91, Appendix). Psuedo-first order loss of 1,4-dimethoxybenzene (DMB) was assumed to be driven by the combined effect from $HO^{\cdot}$, $Cl^{\cdot}$, and $ClO^{\cdot}$. The determined steady-state concentrations of $HO^{\cdot}$ and $Cl^{\cdot}$ are then substituted into the following equation to estimate the steady-state concentrations of $ClO^{\cdot}$.

$$k_{obs,DMB} = k_{DMB,HO^{\cdot}} \times [HO^{\bullet}]_{ss} + k_{DMB,Cl^{\cdot}} \times [Cl^{\bullet}]_{ss} + k_{DMB,ClO^{\cdot}} \times [ClO^{\bullet}]_{ss} \quad \text{(S4.7)}$$

$$[ClO^{\bullet}]_{ss} = \frac{(-\ln([DMB]/[DMB]_0) - k_{DMB,HO^{\cdot}} \times [HO^{\bullet}]_{ss} + k_{DMB,Cl^{\cdot}} \times [Cl^{\bullet}]_{ss})}{k_{DMB,ClO^{\cdot}}} \quad \text{(S4.8)}$$

where $k_{obs,DMB}$ is the observed pseudo-first order rate constant for 1,4-dimethoxybenzene loss, $k_{DMB,HO\cdot}$ is the literature second-order rate constant for the reaction of 1,4-dimethoxybenzene with hydroxyl radical (reaction 83, Appendix), $k_{DMB,Cl\cdot}$ is the literature second-order rate constant for the reaction of 1,4-dimethoxybenzene with chlorine atom (reaction 84, Appendix), and $k_{DMB,ClO^{\cdot}}$ is the literature second-order rate constant for the reaction of 1,4-dimethoxybenzene with $ClO^{\cdot}$ (reaction 82, Appendix).

Text S4.6. HPLC-SEC-UV-PCR Analysis. A Toyopearl TOSOH, HW50S (8mm × 300 mm) size-exclusion column (SEC) was used to separate DOM samples (2.5mL inj.) on an HPLC system running with a 25 mM phosphate buffer eluent (pH = 7.8) running at a flowrate of 0.2 mL/min. After exiting the SEC column, the mobile phase and sample pass through a diode-array UV detector collecting data at 254, 280, and 405 nm wavelengths. After the UV detector the eluent passes through a mixing-T and 50 μL/min of the stable radical cation of 2,2'-azino-bis(3-ethylbenzothiazoline-6-sulfonate) ($[ABTS^{\cdot+}]^{-}$) reagent is added. The mixture then enters a post-column reactor (PCR) and is allowed to react for 7 minutes before subsequent analysis with a UV-Vis on-line detector collecting data at 405 nm. The $[ABTS^{\cdot+}]^{-}$ reagent was prepared by mixing neutral $ABTS^{2-}$ with sub-stoichiometric concentrations of free chlorine (20 μM target). The $[ABTS^{\cdot+}]^{-}$ reagent was purged with helium to remove dissolved gasses and was fed to the PCR using a positive pressure pneumatic delivery system, with helium gas providing the necessary driving pressure. Reagent flowrates would be monitored before and after sample analysis to confirm consistent flowrates throughout the HPLC analysis. As it is a decoloration reaction, it was critical to have a sufficient concentration of $[ABTS^{\cdot+}]^{-}$ to react with the pool of electron-rich organic moieties in the treated and untreated DOM.

Text S4.7. X-Ray Radiolysis Controls for RCS Experiments. Chlorination pH appeared to impact DBP speciation (with chloroform formation increasing at pH 10 when compared to chlorination at pH 5 or 8). Radiolysis experiments conducted at pH 1 and 10 without halogen addition were included as controls to identify alterations to the SRNOM driven by acidic or alkaline conditions or influences from buffer composition (borate versus phosphate) or ionic strength (from perchloric acid/perchlorate). DBP yields appear elevated in the samples prepared with >100mM $HClO_4$ without chloride (pH = 1.0 ±0.02), though the system also yielded lower $[HO^{\cdot}]_{ss}$ estimates than pH 8 and 10 after the same irradiation times which may be due to buffer solutes scavenging radical species during irradiation. With lower hydroxyl radical yields, one would expect a lessened increase in DBP formation across the range of X-ray irradiated samples, and this was observed for the X-ray radiolysis set at pH 1; though the DBP yields from chlorine controls without radical pretreatment were higher than FAC controls in pH 8 phosphate butter. The increased yields in chlorine only controls may be in part due to modification to DOM (cycling from pH 1 to 8) before FAC treatment or altered DOM surface properties/conglomerations within the high ionic strength solution (0.14 M, dominated by high $[Na^{+}]$ and $[ClO_4^{-}]$ in this system).

Table S4.1. Summary of direct chlorine photolysis reactions and quantum yields

		Φ(313 nm)	Φ(365 nm)
$HOCl + h\nu \rightarrow HO^{\bullet} + Cl^{\bullet}$	(2a)	1[a*]	N/A
$OCl^{-} + h\nu \rightarrow O^{\bullet -} + Cl^{\bullet}$	(2b)	0.127[b]	0.08[b]
$OCl^{-} + h\nu \rightarrow O(^3P) + Cl^{-}$	(3)	0.075[b]	0.28[b]

N/A = not available, [a*]measured at approximately 310 nm, [85], [b33]

Table S4.2. Natural organic matter isolate properties

Sample Name	Acronym	Catalog number[a]	Aromaticity[a] (%)	Titrated phenol content[a] meq/g_C	Elemental Composition[a] (%w/w) C	O	N	S	EDC[b] mol_e/g_C
Suwannee River aquatic NOM	SRNOM	2R101N	23	2.47	50.7	41.48	1.27	1.78	4.78
Suwannee River humic acid	SRHA	2S101H	31	3.72	52.63	42.04	1.17	0.54	6.99
Suwannee River fulvic acid	SRFA	2S101F	22	2.84	52.34	42.98	0.67	0.46	5.44
Upper Mississippi River aquatic NOM	UMNOM	1R110N	19	0.83	49.98	41.4	2.36	2.62	–

[a]From International Humic Substances Society (humic-substances.org), [b][40]

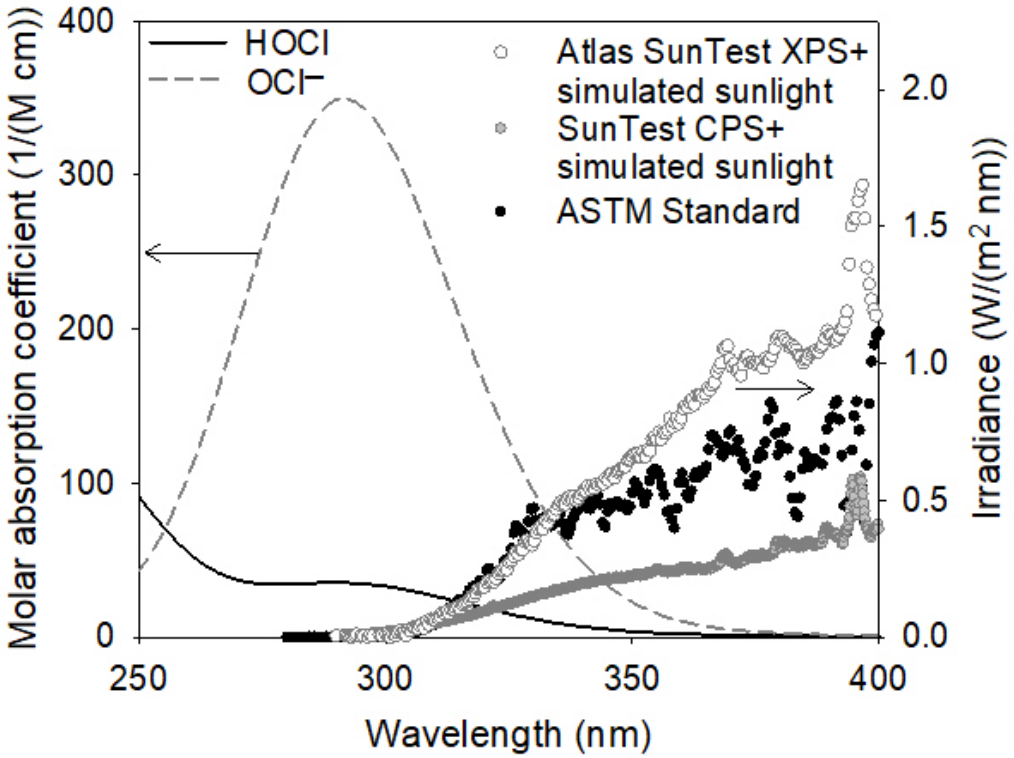

Figure S4.1. Molar extinction coefficients of hypochlorous acid and hypochlorite [29] and direct incident spectral irradiance curves between 290 and 400 nm for to the ASTM G173-03 solar irradiance standard (hemispherical on a 37º tilted surface) the SunTest CPS+ Solar Simulator (located at Eawag) and SunTest XLS+ Solar Simulator (located at University of Washington) (with atmospheric and infrared radiation filters) centered and at the surface of irradiated reactor solutions, directly facing the light source. Spectroradiometric measurements were taken using an ILT950-UV spectroradiometer (location: Eawag) or USB2000+ XR (Ocean Optics) spectroradiometer (location: University of Washington) equipped with a 200 μm × 2 m optical fiber and a CC-3-UV-S cosine corrector.

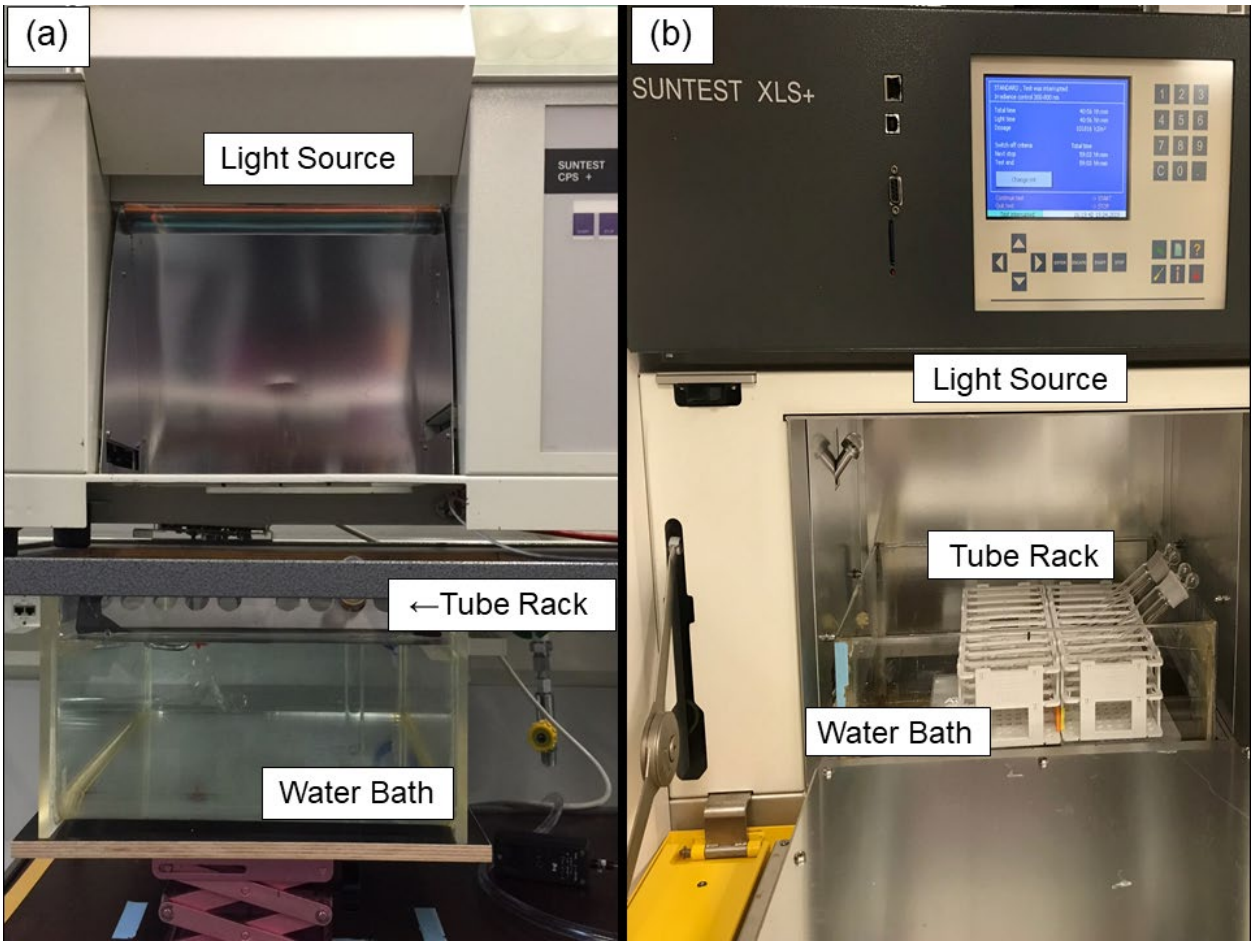

Figure S4.2. (a) Reactor configuration for the SunTest CPS+ (located at Eawag, Dübendorf, CH), and (b) Reactor configuration for the SunTest XLS+ (located at the University of Washington, Seattle, WA, USA).

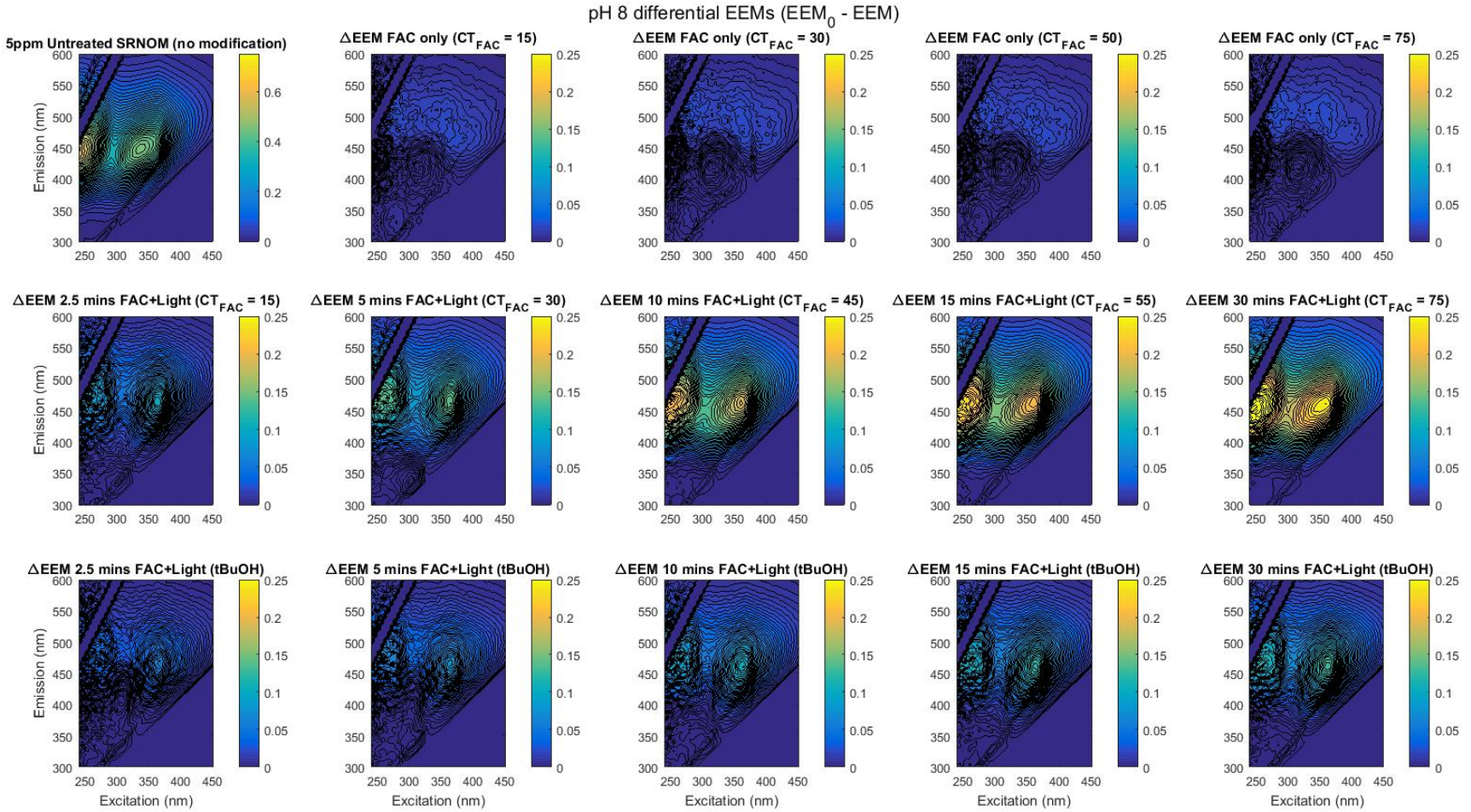

Figure S4.3. Example EEM of untreated SRNOM, and the change in EEM intensity (EEM_0-EEM) following FAC only treatment, FAC+Light, and FAC+Light with 50 mM *tert*-butanol (*t*BuOH). Conditions at pH 8, 25 °C, with 5 mg/L as C SRNOM and $[FAC]_0$ ~ 8 mg/L as Cl_2.

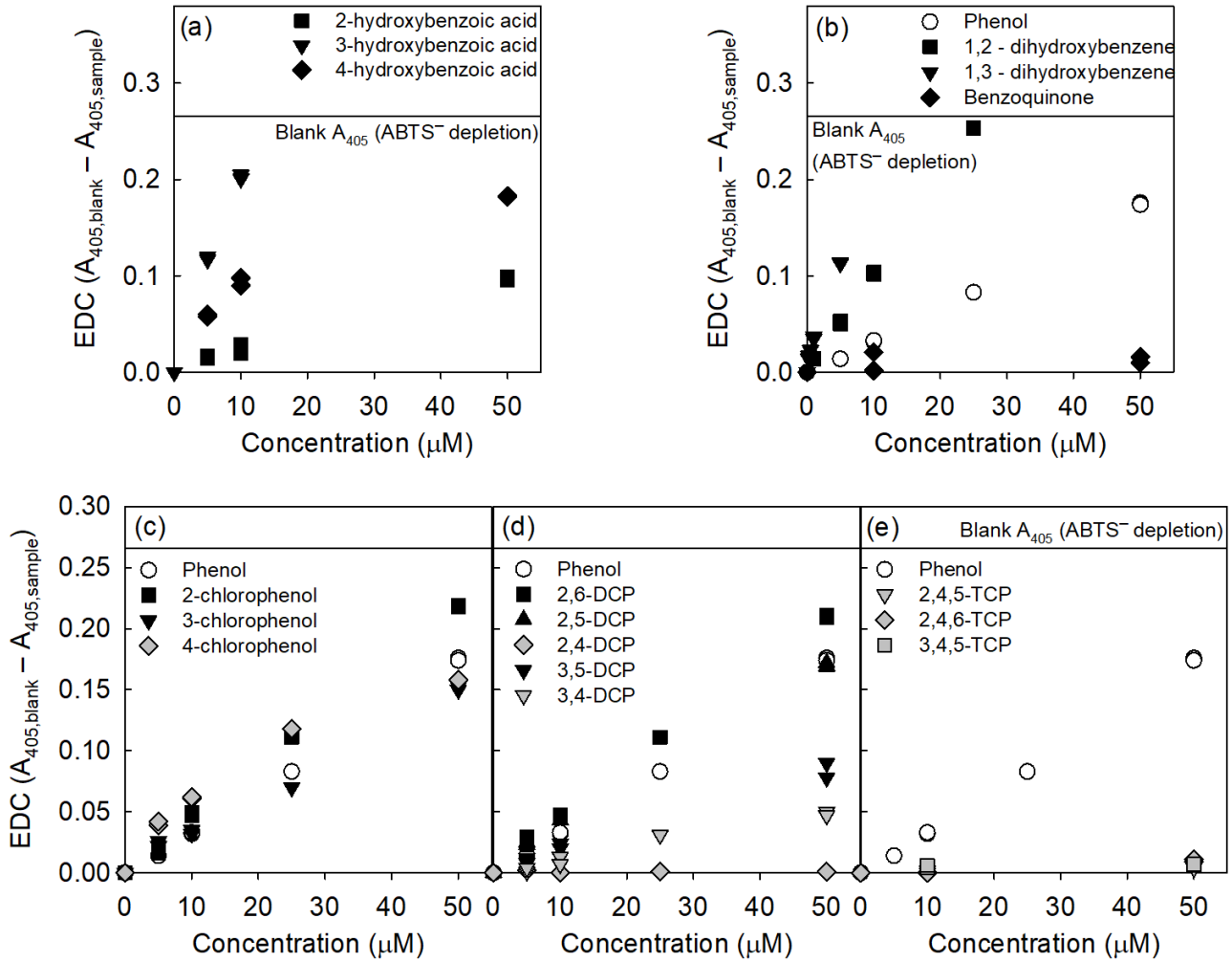

Figure S4.4. EDC measurements for calibrations of commercially available model compounds including: (a) hydroxy-substituted benzoic acid, (b) phenol and dihydroxybenzenes, (c) monochlorophenols, (d) dichlorophenols (DCP), and (e) trichlorophenols (TCP). Each model compound was analyzed via the batch cuvette reaction $[ABTS^{\cdot+}]^{-}$ method, mixing 0.6mL $[ABTS^{\cdot+}]^{-}$ reagent, 1.4mL 25mM phosphate buffer (pH 7.8), and 1mL sample diluted in ultrapure water with absorbance collected at 405nm after 7 minutes reaction time. The solid line on the figures provides reference to the blank absorbance in this experiment set (0.266, 1cm path length).

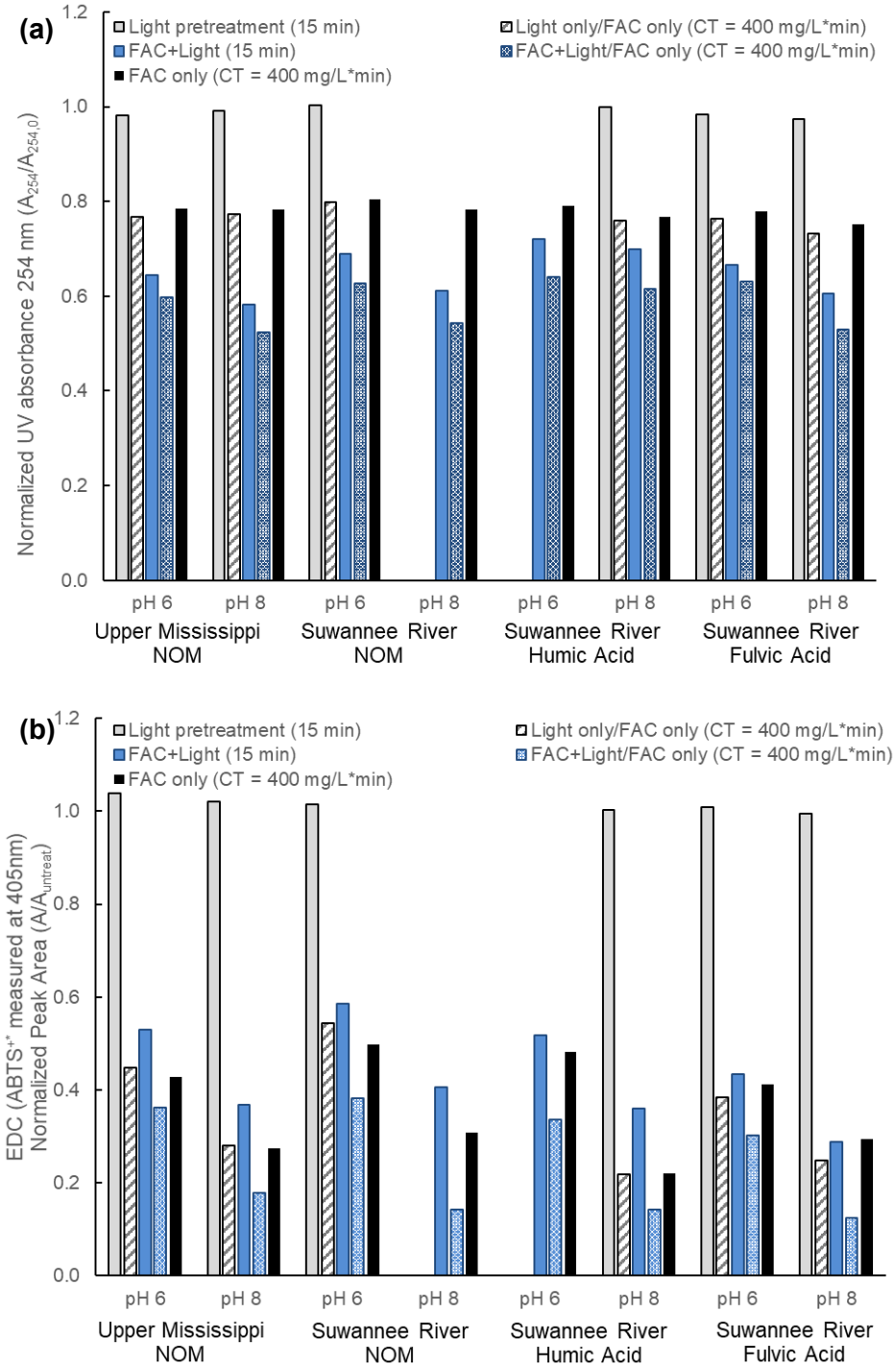
(a)
Light pretreatment (15 min)
FAC+Light (15 min)
FAC only (CT = 400 mg/L*min)
Light only/FAC only (CT = 400 mg/L*min)
FAC+Light/FAC only (CT = 400 mg/L*min)
Normalized UV absorbance 254 nm (A254/A254,0)
1.2
1.0
0.8
0.6
0.4
0.2
0.0
pH 6
pH 8
Upper Mississippi NOM
Suwannee River NOM
Suwannee River Humic Acid
Suwannee River Fulvic Acid
(b)
Light pretreatment (15 min)
FAC+Light (15 min)
FAC only (CT = 400 mg/L*min)
Light only/FAC only (CT = 400 mg/L*min)
FAC+Light/FAC only (CT = 400 mg/L*min)
EDC (ABTS+• measured at 405nm) Normalized Peak Area (A/Auntreat)
1.2
1.0
0.8
0.6
0.4
0.2
0.0
pH 6
pH 8
Upper Mississippi NOM
Suwannee River NOM
Suwannee River Humic Acid
Suwannee River Fulvic Acid

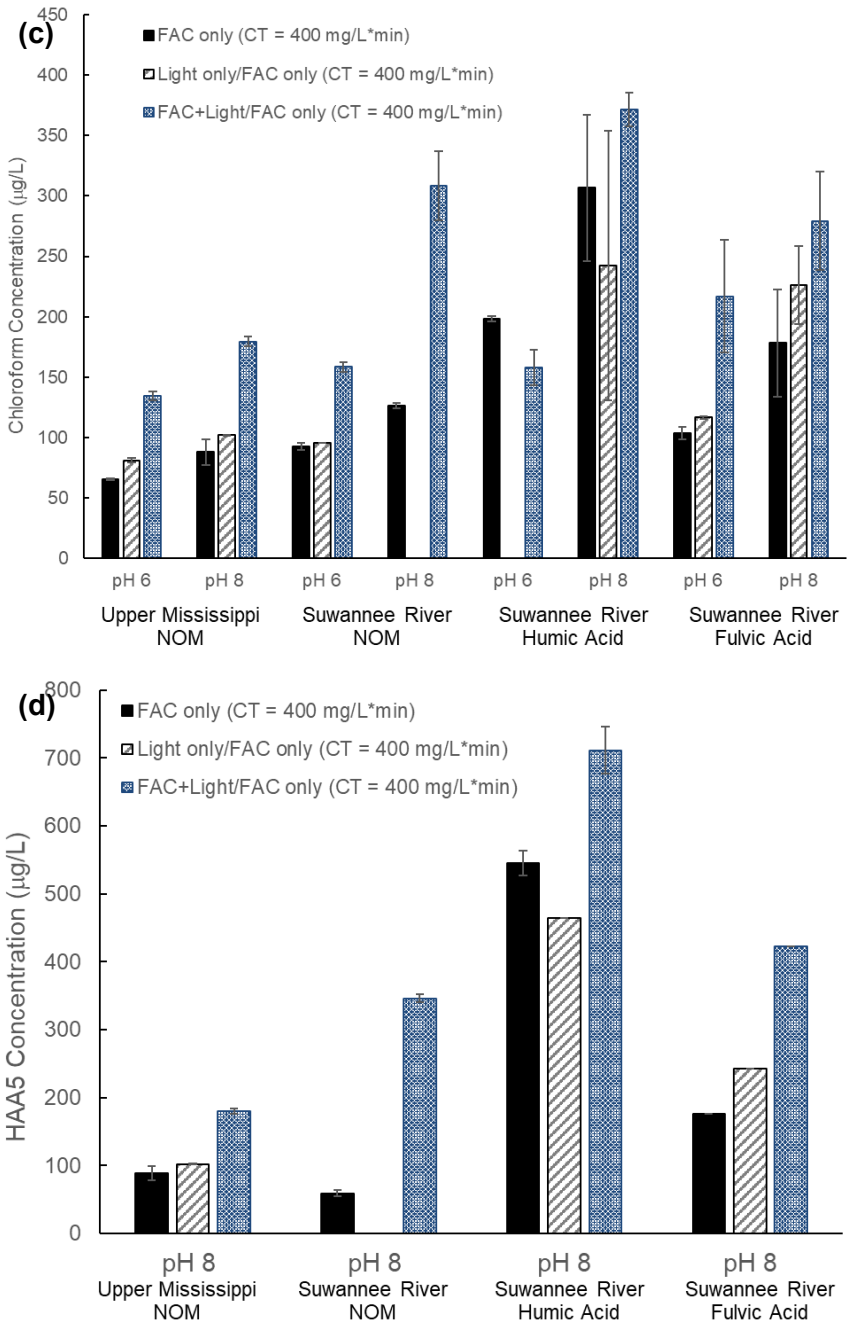

Figure S4.5. (a) UV Absorbance (A_{254}) normalized by the untreated absorbance for 4 carbon isolates; (b) EDC (ΔA405) normalized by the untreated EDC; (c) TTHM formation; and (d) HAA5 formation. Each sample was exposed to solar light pretreatment without chlorine (grey bars), light pretreatment with chlorine treatment after (white with striped bar), solar chlorine photolysis (FAC+Light) with CT_{FAC} for 15 minutes ranging between 35.9 – 105 (mg/L as Cl_2)*min (blue bars), FAC+light/FAC only with dark chlorination period targeting CT_{FAC} ~ 400 (mg/L as Cl_2)*min (blue dotted bars), and dark chlorine only treatment CT_{FAC} 400 (mg/L as Cl_2)*min (black bars). 25 deg C temperature, $[FAC]_0$ ~ 8 mg/L as Cl_2, pH 6.0 or 8.0.

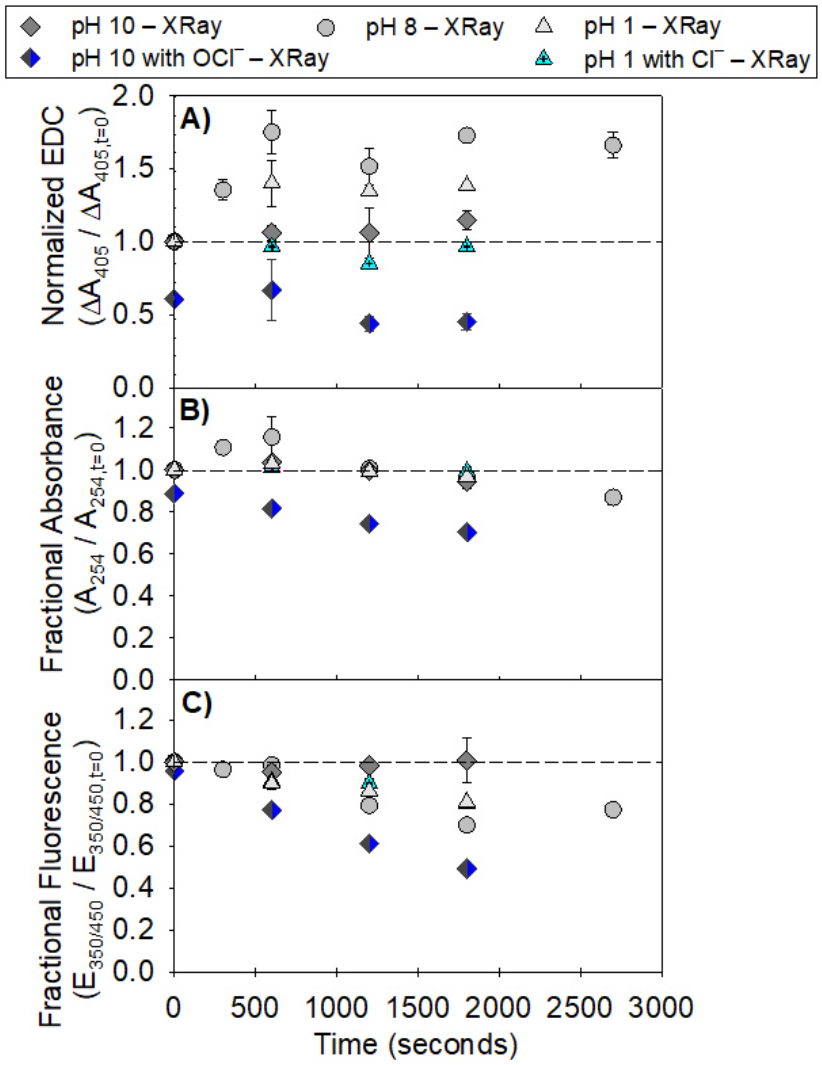

Figure S4.6. (a) Normalized EDC (EDC / $EDC_{,0}$); (b) normalized 254nm absorbance ($A_{254}/A_{254,0}$) and; (c) normalized EEM intensity (Ex/Em : 350/450nm) for 5 mg/L SRNOM with conditions exposed to X-ray radiolysis. Conditions include pH 8 (10 mM phosphate buffer), pH 10 (10 mM borate buffer) with and without hypochlorite $[OCl^-]_0 \sim 1.1\times10^{-4}$ M, and pH 1 (>100 mM $HClO_4$) with and without chloride $[Cl^-]_0 = 5\times10^{-3}$ M, irradiated at a temperature of 22 ℃.

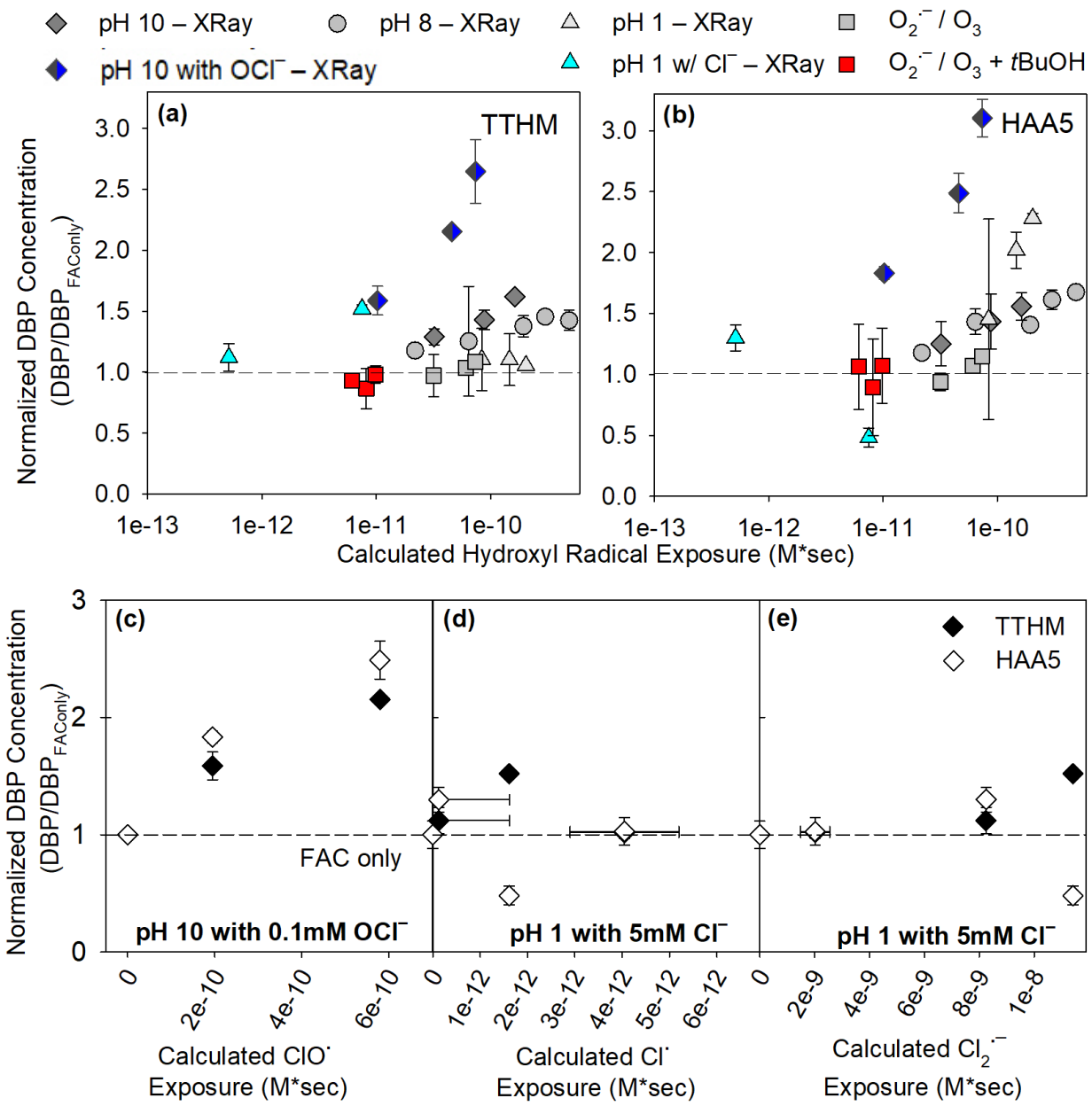

Figure S4.7. DBP concentration after X-ray radiation experiments normalized by chlorination controls prepared from the same DOM and buffer mixture for: (a) total trihalomethanes (TTHMs) versus estimated [$HO^{\cdot}$] exposures; (b) haloacetic acid (HAA) versus estimated [$HO^{\cdot}$] exposures; (c) THMs and HAAs versus estimated [$ClO^{\cdot}$] exposures; (d) THMs and HAAs versus estimated [$Cl^{\cdot}$] exposure; and (e) THMs and HAAs versus estimated [$Cl_2^{\cdot-}$] exposures calculated from probe compound degradation during irradiation (calculation outlined in Text S4.4).

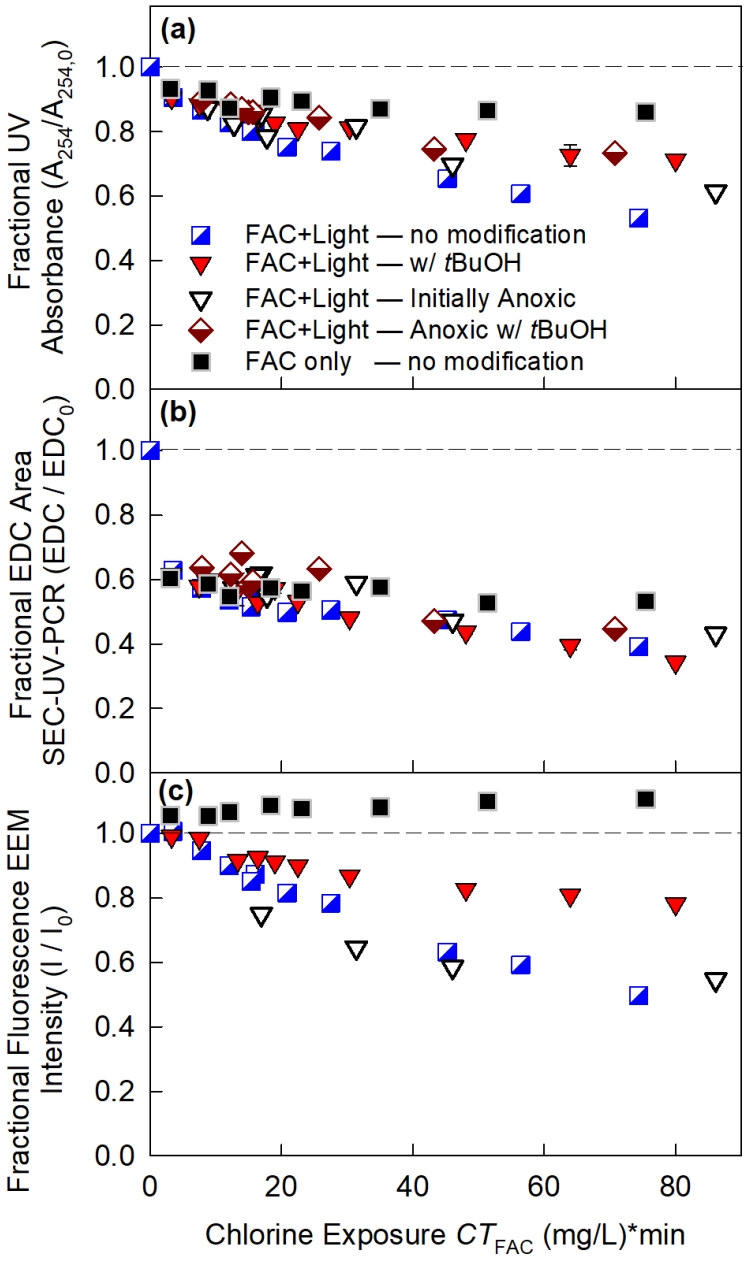

Figure S4.8. (a) Normalized 254nm absorbance (A_{254}); (b) normalized SEC-$[ABTS^{\cdot+}]^{-}$ absorbance peak area ($\Delta A_{405}/\Delta A_{405,0}$) and; (c) normalized EEM intensity (Ex/Em : 350/450nm) for 5 mg/L SRNOM with varied tert-butanol (0 or 50mM) and initial dissolved oxygen (anoxic or in equilibrium with atmosphere) concentration during solar chlorine photolysis (FAC+Light) and dark chlorination targeting CT_{FAC} equivalent to the measured value for the FAC+Light samples. $[FAC]_0 \sim 4$ or 8 mg/L as Cl_2, 25 deg C, in pH 8 (10 mM) phosphate buffer.

Chapter 5. General Conclusions

In the United States, chlorine or chloramine are ubiquitous disinfectants in drinking water treatment, due to the extended protection a residual concentration provides in the distribution system. Chlorine is inexpensive and provides sufficient protection against many pathogens. However, chlorine is responsible for the halogenation of natural organic matter (NOM) and formation of disinfection byproducts (DBP), and is not effective inactivating chlorine-resistant protozoan (oo)cysts. The shortcomings of chlorination treatment alone have been addressed by adding additional treatment prior to chlorination; such as filtration (to physically remove particles, cysts, and NOM), ozonation (to oxidize dissolved organic carbon (DOC) and enhance disinfection), UV irradiation (to enhance disinfection), or advanced oxidation processes (oxidize DOC and enhance disinfection). The multiple treatment trains create a redundant disinfection process, ensuring protection of the served public. However, worldwide too many people are drinking under-treated or untreated water, and construction or maintenance of advanced water treatment facilities may be out of reach. The combination of an inexpensive disinfectant (chlorine) with an abundant energy source (sunlight) to drive advanced oxidation and disinfection could improve health and sanitation conditions in decentralized treatment. However, the suite of byproduct analysis completed in this study identified conditions that could result in levels of halogenated byproducts that have the potential to be toxic for human consumption; i.e., increase incidence of cancer or other health aliments such as liver or nervous system damage. However, the potential benefits of solar chlorine photolysis as a water treatment alternative should be remain in focus, as vulnerable populations (such as children under 5) are at-risk of morbidity or mortality from waterborne diarrheal diseases.

This work has built upon previous research focused on the disinfection processes attributed to solar chlorine photolysis, with a focus on investigating oxidative reactions with

common water constituents and their associated byproducts, including disinfection byproducts regulated by the U.S. EPA. The project objectives included:

(i) Systematically quantify disinfection byproduct formation during solar chlorine photolysis, under ranges of relevant drinking water treatment conditions

(ii) Characterize changes to dissolved organic matter and model compounds during chlorination, ozonation, exposure to various ROS and RCS, solar irradiation, and combinations thereof reflective of conditions experienced during solar chlorine photolysis

(iii) Identify reactive species that contribute to disinfection byproduct formation

For the conditions evaluated, solar irradiation of chlorinated water resulted in increased yields of regulated disinfection byproducts when compared to chlorination alone (with the exception of chlorite); i.e., bromate, chloroform, total trihalomethanes, and HAA5 yields increased. Maximum contaminant level (MCL) exceedances were highly dependent on untreated water characteristics. Specific trends and optimal conditions are summarized below.

Solar chlorine photolysis of water with bromide resulted in bromate formation, due to reactions between hypobromous acid, ozone, and hydroxyl radical. Bromate and chlorate formation essentially doubled at pH 8 when compared to pH 6 (1.8× increase BrO_3^-, and 2.8× increase of formed ClO_3^-), likely due to increased in situ ozone formation from hypochlorite photolysis. Chlorate and chlorite were introduced initially from the chlorine stock, but chlorite was efficiently degraded during solar chlorine photolysis. Addition of humic-rich Suwannee River NOM (2 mg/L) completely interrupted bromate and chlorate formation mechanisms; other natural water sources also reduced formation, but to a lesser extent. Ultimately, bromate formation remains a concern for low DOC (or low reactivity DOM) and high bromide waters

treated via solar chlorine photolysis, though chlorite MCL exceedance is not anticipated.

While natural organic matter may decrease oxyhalide formation during solar chlorine photolysis, it introduces the formation of halogenated organic disinfection byproducts. DBP concentrations after chlorination and solar chlorine photolysis increased with increasing DOC concentrations and temperature. DBP speciation was influenced by both bromide – increasing bromine incorporation and forming high yields of unregulated mixed chloro- and bromo-halogenated HAAs – and treatment pH (6 or 8). Chlorine speciation varies with pH which directly influenced photolysis rates and product yields, while acidic groups within NOM, and protonated versus deprotonated reaction rates, certainly impacted reactivity and subsequent DBP formation; additionally, haloform formation is known to be favorable at alkaline conditions. The marked increase in DBP yields occurs during the chlorine photolysis period, and residual dark chlorination after photolysis yields incremental DBP formation with increasing CT_{FAC}, a similar rate to dark chlorination alone.

In addition to increased yields of regulated organic DBPs (THMs and HAAs), solar chlorine photolysis of Suwannee River NOM (and humic and fulvic acid isolates), Upper Mississippi NOM, and collected surface waters resulted in degradation of DOM chromophores and fluorophores, and decreases in average molecular weight due to degradation of higher molecular weight humic substances to lower molecular weight organic acids with minimal mineralization of DOC. Differential absorbance spectra analysis also revealed that phenolic moieties are degraded preferentially relative to carboxylic acid moieties. Phenolic and other reactive aromatic moieties contribute to the measured electron donating capacity of untreated natural organic matter. These redox properties are rapidly altered while chromophores are preserved upon chlorination (alone or during solar chlorine photolysis), which is proposed to be

due to halogenation of hydroxylated aromatics such as phenolic-moieties and dihydroxybenzenes (similar trends were observed treating phenol as a model DBP precursors within NOM). Oxidation of SRNOM via ozone degrades electron donating moieties within the DOM, and unlike chlorination, aromatic rings cleavage (likely forming carboxylic and carbonyl) is favorable during this process, resulting in a loss of UV absorbance. During solar chlorine photolysis, halogenation by free chlorine is happening simultaneously with oxidative ozone and radical reactions, resulting in decreased fluorescence, UV absorbance (A_{254}), and electron donating capacity of the natural organic matter.

Anoxic experiments (limiting ozone formation) and tert-butanol addition revealed that radical species (rather than ozone) were contributing to the increased THM and HAA formation during solar chlorine photolysis. Sequential AOP and chlorine treatment was evaluated to identify species that increase chlorine reactivity or form DBP precursors. Low hydroxyl radical exposures of SRNOM ($< 5\times10^{-10}$ M×sec $HO^{\cdot}$, prior to DOM mineralization) increased the measured electron donating capacity and resulted in increased DBP yields upon subsequent chlorination, similar to AOP treatment of benzoic acid. Hydroxyl radical and chlorine atom ($Cl^{\cdot}$) can react via addition, electron transfer, or H-abstraction. Hydroxylation of aromatics increased the electron donating capacity, as observed with model compounds (phenol vs dihydroxybenzene and benzoic acid versus 4-hydroxylbenxoic acid), and correlates with increased reactivity with free chlorine. Hydroxylation of slow reacting moieties (similar to benzoic acid) within NOM during AOP-FAC sequential treatment and solar chlorine photolysis is considered a source of increased THM and HAA formation. Chloride addition to favor $Cl^{\cdot}/Cl_2^{\cdot-}$ formation did not significantly alter the electron donating capacity or DBP yields, though the system was dominated by $Cl_2^{\cdot-}$, a weak oxidant. During solar chlorine photolysis $Cl^{\cdot}$ is anticipated to be a

more influential oxidant, and likely reacts via single electron transfer, though probing this oxidant individually (without $Cl_2^{\cdot-}$ or $HO^{\cdot}$) proved challenging. Conditions favoring $ClO^{\cdot}$ formation resulted in increased chloroform and HAA yields, indicating electron transfer oxidation may also contribute to increased reactivity with free chlorine in solution. However, nitrobenzene loss indicated hydroxyl radical could still be reacting with/modifying NOM directly and DBP increases could be due in part to synergistic modifications to the DOM via free chlorine and hydroxyl radical.

In summary, solar chlorine photolysis treatment does contribute to increased DBP formation, though yields may be acceptable for waters with low DOC and bromide concentrations with low alkalinity. Hydroxyl radical reactions with natural organic matter (particularly hydroxylation) result in increased disinfection byproduct formation during solar chlorine photolysis and could also be contributing to increased DBP formation in other advanced oxidation processes (e.g., UVC/chlorine or UV/H_2O_2) when DOM is either simultaneously or subsequently exposed to free chlorine, unless DOM mineralization occurs and degrades the reactive moieties formed during initial exposures. Hydroxylation and increased DBP formation upon chlorination may be less of a concern with lower concentrations (< 5 mg/L) or less reactive DOM, as observed with decreased DBP yields in tested natural waters.

Future studies should evaluate disinfection efficiency and DBP formation during simulated and natural solar chlorine photolysis of a diverse set of water sources (as NOM character impacts reactivity with chlorine and photooxidants), test reactor materials (such as durable plastics), and develop a simple actinometer to assist prescriptive treatment at a user level; all with the goal to facilitate implementing solar chlorine photolysis as a practical point-of-use drinking water treatment.

Appendix

Table A.1. Glossary of Abbreviations

$ABTS^{2-}$	2,2'-azino-bis(3-ethylbenzothiazoline-6-sulfonate)
$[ABTS^{\cdot+}]^{-}$	2,2'-azino-bis(3-ethylbenzothiazoline-6-sulfonate) radical cation
AOP	Advanced Oxidation Process
BAA	Bromoacetic Acid
BSF	Bromine Substitution Factor
CAA	Chloroacetic Acid
CCL	Contaminant Candidate List
DAS	Differential Absorbance Spectra
DBAA	Dibromoacetic Acid
DBP	Disinfection By-product
DCAA	Dichloroacetic Acid
DNA	Deoxyribonucleic Acid
DOC	Dissolved Organic Carbon
DOM	Dissolved Organic Matter
DPD	N,N-diethyl-p-phenylenediamine
EDA	Ethylene Diamine
EDC	Electron Donating Capacity
EEM	Excitation Emission Matrix
EPA	Environmental Protection Agency
FAC	Free-Available Chlorine
HAA	Haloacetic Acid
HPLC	High Performance Liquid Chromatography
ICR	Information Collection Rule
LOD	Limit of Detection
LOQ	Limit of Qualification
MCL	Maximum Contaminant Level
MTBE	Methyl tert-Butyl Ether
MW	Molecular Weight
NOM	Natural Organic Matter
PPCP	Pharmaceuticals and Personal Care Products
RCS	Reactive Chlorine Species
RHS	Reactive Halogen Species
RNA	Ribonucleic Acid
ROS	Reactive Oxygen Species
RSD	Relative Standard Deviation
SEC	Size-exclusion Chromatography
SODIS	Solar Disinfection
SRFA	Suwannee River Fulvic Acid
SRHA	Suwannee River Humic Acid
SRM	Selective Reaction Monitoring
SRNOM	Suwannee River Natural Organic Matter
SUVA	Specific Ultraviolet Absorbance
TBAA	Tribromoacetic Acid

TCAA	Trichloroacetic Acid
THM	Trihalomethane
TOX	Total Organic Halogen
UMNOM	Upper Mississippi Natural Organic Matter
UV	Ultraviolet

Table A2. Reactions and reaction rate constants summary table (used in Kintecus Modelling)

No.	Reaction	Reaction Rate Constant	Reference
	Direct Photolysis reactions		
1	$HOCl \xrightarrow{hv} HO^{\bullet} + Cl^{\bullet}$		1
2	$OCl^{-} \xrightarrow{hv} O^{\bullet -} + Cl^{\bullet}$		1
3	$OCl^{-} \xrightarrow{hv} O(^{3}P) + Cl^{-}$		1
4	$OCl^{-} \xrightarrow{hv} O(^{1}D) + Cl^{-}$		1
5	$H_2O_2 \xrightarrow{hv} 2\ HO^{\bullet}$		2
6	$HO_2^{-} \xrightarrow{hv} HO^{\bullet} + O^{\bullet -}$		2
	X-Ray Radiolysis reactions		
7	$H_2O \xrightarrow{X-Ray} H_2O^{+}$		
8	$4.8\ H_2O^{+} \rightarrow (2.8)HO^{\bullet},\ (0.6)H^{\bullet},\ (2.65)e_{aq}^{-},\ (0.45)H_2,\ (0.68)H_2O_2,\ (2.7)H^{+}$		3
9	$N_2O + e_{aq}^{-} \rightarrow N_2 + OH^{-} + HO^{\bullet}$	9.1 x 10^9 $M^{-1}s^{-1}$	3
10	$N_2O + H^{\bullet} \rightarrow N_2 + HO^{\bullet}$	2.1 x 10^6 $M^{-1}s^{-1}$	3
11	$H^{\bullet} + O_2 \rightarrow HO_2^{\bullet}$	2.1 x 10^{10} $M^{-1}s^{-1}$	3
	Hydroxyl Radical reactions		
12	$HO^{\bullet} + HOCl \rightarrow ClO^{\bullet} + H_2O$	1.2 x 10^9 $M^{-1}s^{-1}$	4
13	$HO^{\bullet} + OCl^{-} \rightarrow ClO^{\bullet} + OH^{-}$	6.4 x 10^9 $M^{-1}s^{-1}$	4
14	$O^{\bullet -} + OCl^{-} \rightarrow ClO^{\bullet} + OH^{-}$	2.3 x 10^8 $M^{-1}s^{-1}$	1
15	$HO^{\bullet} + O_3 \rightarrow HO_2^{\bullet} + O_2$	1.1 x 10^8 $M^{-1}s^{-1}$	5
16	$HO^{\bullet} + O_3^{\bullet -} \rightarrow HO_2^{\bullet} + O_2^{\bullet -}$	8.5 x 10^9 $M^{-1}s^{-1}$	5
17	$HO^{\bullet} + ClO_2 \rightarrow ClO_3^{-} + H^{+}$	4 x 10^9 $M^{-1}s^{-1}$	6
18	$HO^{\bullet} + ClO^{\bullet} \rightarrow ClO_2^{-} + H^{+}$	1.0 x 10^9 $M^{-1}s^{-1}$	7
19	$HO^{\bullet} + HO^{\bullet} \rightarrow H_2O_2$	4.2 x 10^9 $M^{-1}s^{-1}$	8

20	$HO^{\bullet} + OH^{-} \rightarrow O^{\bullet -} + H_2O$	1.2 x 10^{10} $M^{-1}s^{-1}$	9
21	$HO^{\bullet} + HO_2^{-} \rightarrow H_2O + O_2^{\bullet -}$	7.5 x 10^{9} $M^{-1}s^{-1}$	3
22	$HO^{\bullet} + H_2O_2 \rightarrow H_2O + O_2^{\bullet -}$	2.7 x 10^{7} $M^{-1}s^{-1}$	3
23	$HO^{\bullet} + HCO_3^{-} \rightarrow CO_3^{\bullet -} + H_2O$	8.5 x 10^{6} $M^{-1}s^{-1}$	3
24	$HO^{\bullet} + CO_3^{2-} \rightarrow CO_3^{\bullet -} + OH^{-}$	3.9 x 10^{8} $M^{-1}s^{-1}$	3
25	$HO^{\bullet} + CO_3^{\bullet -} \rightarrow CO_3^{2-} + OH^{-}$	3.0 x 10^{9} $M^{-1}s^{-1}$	10
26	$HO^{\bullet} + HO_2^{\bullet} \rightarrow H_2O + O_2$	3.5 x 10^{10} $M^{-1}s^{-1}$	11
27	$HO^{\bullet} + O_2^{\bullet -} \rightarrow OH^{-} + O_2$	2.8 x 10^{10} $M^{-1}s^{-1}$	11
28	$HO^{\bullet} + DOM \rightarrow DOM_{OH}$	1.5 x 10^{8} $M^{-1}s^{-1}$	12
Atomic oxygen reactions			
29	$O(^3P) + O_2 \rightarrow O_3$	4.0 x 10^{9} $M^{-1}s^{-1}$	13
30	$O(^3P) + OCl^{-} \rightarrow ClO_2^{-}$	3.0 x 10^{9} $M^{-1}s^{-1}$	1
31	$O(^3P) + OCl^{-} \rightarrow Cl^{-} + O_2$	5.08 x 10^{8} $M^{-1}s^{-1}$	1
32	$O(^3P) + H_2O_2 \rightarrow HO^{\bullet} + HO_2^{\bullet}$	1.6 x 10^{9} $M^{-1}s^{-1}$	14
33	$O(^3P) + HO_2^{-} \rightarrow HO^{\bullet} + O_2^{\bullet -}$	5.3 x 10^{9} $M^{-1}s^{-1}$	14
34	$O(^3P) + OH^{-} \rightarrow HO_2^{-}$	4.2 x 10^{8} $M^{-1}s^{-1}$	14
35	$O(^1D) + H_2O \rightarrow HO^{\bullet} + HO^{\bullet}$	1.2 x 10^{11} $M^{-1}s^{-1}$	1
Chlorine atom reactions			
36	$Cl^{\bullet} + HOCl \rightarrow ClO^{\bullet} + H^{+} + Cl^{-}$	3.0 x 10^{9} $M^{-1}s^{-1}$	6
37	$Cl^{\bullet} + OCl^{-} \rightarrow ClO^{\bullet} + Cl^{-}$	8.2 x 10^{9} $M^{-1}s^{-1}$	6
38	$Cl^{\bullet} + H_2O_2 \rightarrow HO_2^{\bullet} + Cl^{-} + H^{+}$	2.0 x 10^{9} $M^{-1}s^{-1}$	6
39	$Cl^{\bullet} + Cl_2^{\bullet -} \rightarrow Cl_2 + Cl^{-}$	2.1 x 10^{9} $M^{-1}s^{-1}$	6
40	$Cl^{\bullet} + Cl_2 \rightarrow Cl_3^{\bullet}$	5.3 x 10^{8} $M^{-1}s^{-1}$	6
41	$Cl^{\bullet} + H_2O \rightarrow HClO^{\bullet -} + H^{+}$	4.5 x 10^{3} $M^{-1}s^{-1}$	6
42	$Cl^{\bullet} + Cl^{\bullet} \rightarrow Cl_2$	8.8 x 10^{7} $M^{-1}s^{-1}$	6

43	$Cl^{\bullet} + Cl^{-} \rightarrow Cl_2^{\bullet-}$	6.5 x 10^9 $M^{-1}s^{-1}$	6
44	$Cl^{\bullet} + OH^{-} \rightarrow HClO^{\bullet-}$	1.8 x 10^{10} $M^{-1}s^{-1}$	6
45	$Cl^{\bullet} + HCO_3^{-} \rightarrow Cl^{-} + CO_3^{\bullet-} + H^{+}$	2.2 x 10^8 $M^{-1}s^{-1}$	15
46	$Cl^{\bullet} + CO_3^{2-} \rightarrow Cl^{-} + CO_3^{\bullet-}$	5.0 x 10^8 $M^{-1}s^{-1}$	15
	Chlorine radical anion reactions		
47	$Cl_2^{\bullet-} + HO_2^{\bullet} \rightarrow 2Cl^{-} + H^{+} + O_2$	3.0 x 10^9 $M^{-1}s^{-1}$	16
48	$Cl_2^{\bullet-} + O_2^{\bullet-} \rightarrow 2Cl^{-} + O_2$	1.0 x 10^9 $M^{-1}s^{-1}$	17
49	$Cl_2^{\bullet-} + OH^{-} \rightarrow ClOH^{\bullet-} + Cl^{-}$	4.5 x 10^7 $M^{-1}s^{-1}$	18
50	$Cl_2^{\bullet-} \rightarrow Cl^{\bullet} + Cl^{-}$	1.1 x 10^5 s^{-1}	6
51	$Cl_2^{\bullet-} + Cl_2^{\bullet-} \rightarrow Cl_2 + 2Cl^{-}$	8.3 x 10^8 $M^{-1}s^{-1}$	16
52	$Cl_2^{\bullet-} + H_2O \rightarrow HOCl^{\bullet-} + H^{+} + Cl^{-}$	23.4 $M^{-1}s^{-1}$	
53	$Cl_2^{\bullet-} + HO^{\bullet} \rightarrow HOCl + Cl^{-}$	1.0 x 10^9 $M^{-1}s^{-1}$	19
54	$Cl_2^{\bullet-} + HCO_3^{-} \rightarrow 2Cl^{-} + H^{+} + CO_3^{\bullet-}$	8.5 x 10^4 $M^{-1}s^{-1}$	15
55	$Cl_2^{\bullet-} + CO_3^{2-} \rightarrow 2Cl^{-} + CO_3^{\bullet-}$	3.9 x 10^6 $M^{-1}s^{-1}$	15
	$ClO^{\bullet}$ reactions		
56	$ClO^{\bullet} + ClO^{\bullet} + H_2O \rightarrow ClO_2^{-} + OCl^{-} + 2\ H^{+}$	4.5 x 10^7 $M^{-1}s^{-1}$	6
57	$ClO^{\bullet} + ClO_2 \rightarrow Cl_2O_3$	7.0 x 10^9 $M^{-1}s^{-1}$	20
58	$ClO^{\bullet} + O_3^{\bullet-} \rightarrow OCl^{-} + O_3$	1.0 x 10^9 $M^{-1}s^{-1}$	13
59	$ClO^{\bullet} + ClO_2^{-} \rightarrow OCl^{-} + ClO_2$	9.4 x 10^8 $M^{-1}s^{-1}$	21
	Ozone reactions		
60	$O_3 + OH^{-} \rightarrow HO_2^{-} + O_2$	70	22
61	$O_3 + HO_2^{-} \rightarrow O_2^{\bullet-} + O_2 + HO^{\bullet}$	2.8 x 10^6 $M^{-1}s^{-1}$	22
62	$O_3 + O_2^{\bullet-} \rightarrow O_3^{\bullet-} + O_2$	1.6 x 10^9 $M^{-1}s^{-1}$	23
63	$O_3 + OCl^{-} \rightarrow 2O_2 + Cl^{-}$	37	24
64	$O_3 + OCl^{-} \rightarrow O_2 + ClO_2^{-}$	10.1	24

65	$O_3 + ClO_2^- \rightarrow ClO_2 + O_3^{\bullet-}$	8.2 x 10^6 $M^{-1}s^{-1}$	25
66	$O_3 + ClO_2 \rightarrow O_2 + ClO_3$	1.4 x 10^3 $M^{-1}s^{-1}$	26
	Reactive Oxygen Species (ROS) reactions		
67	$HOCl + O_2^{\bullet-} \rightarrow O_2 + HO^{\bullet} + Cl^-$	7.5 x 10^6 $M^{-1}s^{-1}$	27
68	$O_3^{\bullet-} + H^+ \rightarrow HO_3^{\bullet}$	1.0 x 10^{10} $M^{-1}s^{-1}$	28
69	$HO_3^{\bullet} \rightarrow O_3^{\bullet-} + H^+$	1.0 x 10^{12} $M^{-1}s^{-1}$	29
70	$HO_3^{\bullet} \rightarrow HO^{\bullet} + O_2$	1.4 x 10^5 $M^{-1}s^{-1}$	28
71	$O_3^{\bullet-} \rightarrow O^{\bullet-} + O_2$	2.1 x 10^3 s^{-1}	30
72	$O^{\bullet-} + O_2 \rightarrow O_3^{\bullet-}$	3.3 x 10^9 $M^{-1}s^{-1}$	3
73	$O^{\bullet-} + H_2O \rightarrow HO^{\bullet} + OH^-$	1.7 x 10^6 $M^{-1}s^{-1}$	9
74	$O_3^{\bullet-} + ClO_2 \rightarrow O_3 + ClO_2^{\bullet-}$	1.8 x 10^5 $M^{-1}s^{-1}$	6
75	$O_3^{\bullet-} + ClO_2 \rightarrow O_2 + ClO_3^{\bullet-}$	1.8 x 10^5 $M^{-1}s^{-1}$	6
	Chlorine reactions		
76	$HOCl + HO_2^- \rightarrow O_2 + Cl^- + H_2O$	4.4 x 10^7 $M^{-1}s^{-1}$	31
77	$OCl^- + O^{\bullet-} \rightarrow ClO^{\bullet} + Cl^-$	2.3 x 10^8 $M^{-1}s^{-1}$	6
78	$ClO_2^{\bullet} + HO_2^- \rightarrow ClO_2^- + HO_2^{\bullet}$	1.3 x 10^5 $M^{-1}s^{-1}$	26
	Scavengers and Organic Probe reactions		
79	$HO^{\bullet} + t\text{BuOH} \rightarrow$ 0.241 formaldehyde + products	6.0 x 10^8 $M^{-1}s^{-1}$	3
80	$O(^3P) + t\text{BuOH} \rightarrow$ *products*	3.8 x 10^7 $M^{-1}s^{-1}$	32
81	$Cl^{\bullet} + t\text{BuOH} \rightarrow$ *products*	3.0 x 10^8 $M^{-1}s^{-1}$	15
82	$ClO^{\bullet} + t\text{BuOH} \rightarrow$ *products*	1.0 x 10^7 $M^{-1}s^{-1}$	estimated
83	$O_3 + \text{DMB} \rightarrow$ *products*	1.3 x 10^4 $M^{-1}s^{-1}$	33
84	$ClO^{\bullet} + \text{DMB} \rightarrow$ *products*	2.1 x 10^9 $M^{-1}s^{-1}$	21
85	$HO^{\bullet} + \text{DMB} \rightarrow$ *products*	7.0 x 10^9 $M^{-1}s^{-1}$	34
86	$Cl^{\bullet} + \text{DMB} \rightarrow$ *products*	1.8 x 10^{10} $M^{-1}s^{-1}$	35

87	$HO^{\bullet} + p\text{CBA} \rightarrow products$	5.0 x 10^9 $M^{-1}s^{-1}$	36
88	$HO^{\bullet} + NB \rightarrow n\text{-nitrophenol} + H^{\bullet}$	4.64 x 10^9 $M^{-1}s^{-1}$	37
89	$H^{\bullet} + NB \rightarrow NB^{\bullet} + H_2O$	4 x 10^9 $M^{-1}s^{-1}$	36
90	$HO^{\bullet} + BA \rightarrow products$	4.3 x 10^9 $M^{-1}s^{-1}$	37
91	$HO^{\bullet} + \text{benzoate} \rightarrow products$	5.27 x 10^9 $M^{-1}s^{-1}$	4
92	$Cl^{\bullet} + BA \rightarrow n\text{-chlorobenzoic acid} + H^{\bullet}$	1.8 x 10^{10} $M^{-1}s^{-1}$	38
93	$Cl^{\bullet} + \text{benzoate} \rightarrow products$	1.8 x 10^{10} $M^{-1}s^{-1}$	38
94	$Cl_2^{\bullet-} + BA \rightarrow products$	1.5 x 10^6 $M^{-1}s^{-1}$	39
95	$Cl_2^{\bullet-} + \text{benzoate} \rightarrow products$	2.0 x 10^6 $M^{-1}s^{-1}$	39
96	$H^{\bullet} + BA \rightarrow products$	9.2 x 10^8 $M^{-1}s^{-1}$	3
97	$H^{\bullet} + \text{benzoate} \rightarrow products$	1.08 x 10^9 $M^{-1}s^{-1}$	4
98	$ClO^{\bullet} + \text{benzoate} \rightarrow products$	3.0 x 10^6 $M^{-1}s^{-1}$	21
99	$HO^{\bullet} + \text{phenol} \rightarrow products$	6.6 x 10^9 $M^{-1}s^{-1}$	40
100	$HO^{\bullet} + C_6H_5O^- \rightarrow products$	9.6 x 10^9 $M^{-1}s^{-1}$	41
101	$Cl^{\bullet} + \text{phenol} \rightarrow products$	2.5 x 10^{10} $M^{-1}s^{-1}$	35
102	$Cl^{\bullet} + C_6H_5O^- \rightarrow products$	3.0 x 10^{10} $M^{-1}s^{-1}$	Est. from 35
103	$ClO^{\bullet} + \text{phenol} \rightarrow products$		35
104	$ClO^{\bullet} + C_6H_5O^- \rightarrow products$		35
105	$Cl_2^{\bullet-} + \text{phenol} \rightarrow products$	3.2 x 10^8 $M^{-1}s^{-1}$	35
106	$Cl_2^{\bullet-} + C_6H_5O^- \rightarrow products$	3.0 x 10^8 $M^{-1}s^{-1}$	35
Acid Base Equilibrium			
107	$H_2O_2 \rightleftarrows HO_2^- + H^+$	$pK_a = 11.6$	42
108	$HO_2 \rightleftarrows O_2^- + H^+$	$pK_a = 4.7$	43
109	$H_2CO_3 \rightleftarrows H^+ + HCO_3^- \rightleftarrows H^+ + CO_3^{2-}$	$pK_{a1} = 6.4$, $pK_{a2} = 10.3$	42
110	$HClO \rightleftarrows ClO^- + H^+$	$pK_a = 7.5$	44

111	$Cl_2 + H_2O \rightleftarrows HClO + Cl^- + H^+$	LogK = 3.43	45
112	$2\ HClO \rightleftarrows Cl_2O + H_2O$	LogK = 2.06	45
113	$C_6H_5COOH \rightleftarrows C_6H_5COO^- + H^+$	$pK_a = 4.2$	42
114	$C_6H_5OH \rightleftarrows C_6H_5O^- + H^+$	$pK_a = 10.0$	42

References

1. Buxton, G. V.; Subhani, M. S., Radiation chemistry and photochemistry of oxychlorine ions. Part 2.—Photodecomposition of aqueous solutions of hypochlorite ions. *Journal of the Chemical Society, Faraday Transactions 1: Physical Chemistry in Condensed Phases* **1972,** *68*, 958-969.

2. Baxendale, J. H.; Wilson, J. A., The photolysis of hydrogen peroxide at high light intensities. *Transactions of the Faraday Society* **1957,** *53*, 344-356.

3. Buxton, G. V.; Greenstock, C. L.; Helman, W. P.; Ross, A. B., Critical-Review of Rate Constants for Reactions of Hydrated Electrons, Hydrogen-Atoms and Hydroxyl Radicals (.Oh/.O-) in Aqueous-Solution. *Journal of Physical and Chemical Reference Data* **1988,** *17* (2), 513-886.

4. Bulman, D. M.; Mezyk, S. P.; Remucal, C. K., The impact of pH and irradiation wavelength on the production of reactive oxidants during chlorine photolysis. *Environmental science & technology* **2019,** *53* (8), 4450-4459.

5. Sehested, K.; Holcman, J.; Bjergbakke, E.; Hart, E. J., A pulse radiolytic study of the reaction hydroxyl+ ozone in aqueous medium. *The Journal of Physical Chemistry* **1984,** *88* (18), 4144-4147.

6. Kläning, U. K.; Wolff, T., Laser Flash Photolysis of HClO, ClO−, HBrO, and BrO− in Aqueous Solution. Reactions of Cl-and Br-Atoms. *Berichte der Bunsengesellschaft für physikalische Chemie* **1985,** *89* (3), 243-245.

7. Guo, K.; Wu, Z.; Shang, C.; Yao, B.; Hou, S.; Yang, X.; Song, W.; Fang, J., Radical chemistry and structural relationships of PPCP degradation by UV/chlorine treatment in simulated drinking water. *Environmental science & technology* **2017,** *51* (18), 10431-10439.

8. Elliot, A. J.; Chenier, M. P.; Ouellette, D. C., g-Values for γ-irradiated water as a function of temperature. *Canadian Journal of Chemistry* **1990,** *68* (5), 712-719.

9. Buxton, G. V., Pulse radiolysis of aqueous solutions. Rate of reaction of OH with OH–. *Transactions of the Faraday Society* **1970,** *66*, 1656-1660.

10. Holcman, J.; Bjergbakke, E.; Sehested, K. In *The importance of radical-radical reactions in pulse radiolysis of aqueous carbonate/bicarbonate*, 1987; Akadémiai Kiadó: pp 149-153.

11. Elliot, A. J.; Buxton, G. V., Temperature dependence of the reactions OH+ O–2 and OH+ HO 2 in water up to 200° C. *Journal of the Chemical Society, Faraday Transactions* **1992,** *88* (17), 2465-2470.

12. Westerhoff, P.; Mezyk, S. P.; Cooper, W. J.; Minakata, D., Electron pulse radiolysis determination of hydroxyl radical rate constants with Suwannee river fulvic acid and other dissolved organic matter isolates. *Environmental Science & Technology* **2007,** *41* (13), 4640-4646.

13. Klaning, U. K.; Sehested, K.; Holeman, J., Standard Gibbs energy of formation of the hydroxyl radical in aqueous solution. *Journal of Physical Chemistry* **1985,** *89*, 760-763.

14. Sauer, M. C.; Brown, W. G.; Hart, E. J., O(3P) atom formation by the photolysis of hydrogen peroxide in alkaline aqueous solutions. *Journal of Physical Chemistry* **1984,** *88*, 1398-1400.

15. Mertens, R.; von Sonntag, C., Photolysis (Lambda=254 Nm) of Tetrachloroethene in Aqueous-Solutions. *Journal of Photochemistry and Photobiology a-Chemistry* **1995,** *85* (1-2), 1-9.

16. Gogolev, A. V.; Makarov, I. E.; Pikaev, A. K., Pulse radiolysis of strong hydrochloric acid. *Khimiya Vysokikh Ehnergij* **1984,** *18* (6), 496-501.

17. Zhestkova, T. P.; Pikaev, A. K., Kinetics of Cl 2-anion-radicals decay in the pulse radiolysis of concentrated aqueous solutions of lithium chloride. *Izvestiya Akademii Nauk SSSR, Seriya Khimicheskaya* **1974**, 913-914.

18. Grigor'ev, A. E.; Makarov, I. E.; Pikaev, A. K., Formation of Cl 2-in the bulk of solution during radiolysis of concentrated aqueous solutions of chlorides. *Khimiya Vysokikh Ehnergij* **1987,** *21* (2), 123-126.

19. Wagner, H. P.; Pepich, B. V.; Hautman, D. P.; Munch, D. J.

20. Wang, L.; Margerum, D. W., Hypohalite ion catalysis of the disproportionation of chlorine dioxide. *Inorganic chemistry* **2002,** *41* (23), 6099-6105.

21. Alfassi, Z. B.; Huie, R. E.; Mosseri, S.; Neta, P., Kinetics of one-electron oxidation by the ClO radical. *International Journal of Radiation Applications and Instrumentation. Part C. Radiation Physics and Chemistry* **1988,** *32* (1), 85-88.

22. Staehelin, J.; Hoigne, J., Decomposition of ozone in water: rate of initiation by hydroxide ions and hydrogen peroxide. *Environmental Science & Technology* **1982,** *16* (10), 676-681.

23. Sehested, K.; Holcman, J.; Hart, E. J., Rate constants and products of the reactions of e-aq, dioxide (1-)(O2-) and proton with ozone in aqueous solutions. *The Journal of Physical Chemistry* **1983,** *87* (11), 1951-1954.

24. Haag, W. R.; Hoigné, J., Ozonation of water containing chlorine or chloramines. Reaction products and kinetics. *Water Research* **1983,** *17* (10), 1397-1402.

25. Nicoson, J. S.; Wang, L.; Becker, R. H.; Huff Hartz, K. E.; Muller, C. E.; Margerum, D. W., Kinetics and mechanisms of the ozone/bromite and ozone/chlorite reactions. *Inorganic chemistry* **2002,** *41* (11), 2975-2980.

26. Hoigné, J.; Bader, H., Kinetics of reactions of chlorine dioxide (OClO) in water—I. Rate constants for inorganic and organic compounds. *Water Research* **1994,** *28* (1), 45-55.

27. Long, C. A.; Bielski, B. H. J., Rate of reaction of superoxide radical with chloride-containing species. *The Journal of Physical Chemistry* **1980,** *84* (5), 555-557.

28. Buehler, R. E.; Staehelin, J.; Hoigné, J., Ozone decomposition in water studied by pulse radiolysis. 1. Perhydroxyl (HO2)/hyperoxide (O2-) and HO3/O3-as intermediates. *The Journal of Physical Chemistry* **1984,** *88* (12), 2560-2564.

29. Nöthe, T.; Fahlenkamp, H.; Sonntag, C. v., Ozonation of wastewater: rate of ozone consumption and hydroxyl radical yield. *Environmental Science & Technology* **2009,** *43* (15), 5990-5995.

30. Elliot, A. J.; McCracken, D. R., Effect of temperature on O⊘ reactions and equilibria: A pulse radiolysis study. *International Journal of Radiation Applications and Instrumentation. Part C. Radiation Physics and Chemistry* **1989,** *33* (1), 69-74.

31. Held, A. M.; Halko, D. J.; Hurst, J. K., Mechanisms of chlorine oxidation of hydrogen peroxide. *Journal of the American Chemical Society* **1978,** *100* (18), 5732-5740.

32. Zhou, P.; Di Giovanni, G. D.; Meschke, J. S.; Dodd, M. C., Enhanced inactivation of Cryptosporidium parvum oocysts during solar photolysis of free available chlorine. *Environmental Science & Technology Letters* **2014,** *1* (11), 453-458.

33. Muñoz, F.; von Sonntag, C., Determination of fast ozone reactions in aqueous solution by competition kinetics. *Journal of the Chemical Society, Perkin Transactions 2* **2000,** (4), 661-664.

34. O'Neill, P.; Steenken, S.; Schulte-Frohlinde, D., Formation of radical cations of methoxylated benzenes by reaction with OH radicals, Ti 2+, Ag 2+, and SO 4.-in aqueous solution. An optical and conductometric pulse radiolysis and in situ radiolysis electron spin resonance study. *Journal of Physical Chemistry* **1975,** *79* (25), 2773-2779.

35. Alfassi, Z. B.; Mosseri, S.; Neta, P., Reactivities of Chlorine Atoms and Peroxyl Radicals Formed in the Radiolysis of Dichloromethane. *Journal of Physical Chemistry* **1989,** *93* (4), 1380-1385.

36. Neta, P.; Dorfman, L. M., Pulse radiolysis studies: XIII. Rate constants for the reaction of hydroxyl radicals with aromatic compounds in aqueous solutions. *Advances in Chemistry Series* **1968,** *81*, 222-230.

37. Ashton, L.; Buxton, G. V.; Stuart, C. R., Temperature dependence of the rate of reaction of OH with some aromatic compounds in aqueous solution. Evidence for the formation of a π-complex intermediate? *Journal of the Chemical Society, Faraday Transactions* **1995,** *91* (11), 1631-1633.

38. Martire, D. O.; Rosso, J. A.; Bertolotti, S.; Le Roux, G. C.; Braun, A. M.; Gonzalez, M. C., Kinetic study of the reactions of chlorine atoms and Cl(2)(center dot-)radical anions in aqueous solutions. II. Toluene, benzoic acid, and chlorobenzene. *Journal of Physical Chemistry A* **2001,** *105* (22), 5385-5392.

39. Hasegawa, K.; Neta, P., Rate constants and mechanisms of reaction of chloride (Cl2-) radicals. *The Journal of Physical Chemistry* **1978,** *82* (8), 854-857.

40. Field, R. J.; Raghavan, N. V.; Brummer, J. G., Pulse radiolysis investigation of the reactions of BrO 2. with Fe (CN) 6 4-, Mn (II), phenoxide ion, and phenol. *Journal of Physical Chemistry* **1982,** *86* (13), 2443-2449.

41. Matthews, R. W.; Sangster, D. F., Measurement by benzoate radiolytic decarboxylation of relative rate constants for hydroxyl radical reactions. *The Journal of Physical Chemistry* **1965,** *69* (6), 1938-1946.

42. Lide, D. R., CRC handbook of physics and chemistry. *CRC Press, Boca Raton, USA* **2001,** *76*, 1995-1996.

43. Bielski, B. H. J.; Allen, A. O., Mechanism of the disproportionation of superoxide radicals. *The Journal of Physical Chemistry* **1977,** *81* (11), 1048-1050.

44. Morris, J. C., The acid ionization constant of HOCl from 5 to 35. *The Journal of Physical Chemistry* **1966,** *70* (12), 3798-3805.

45. Sivey, J. D.; Roberts, A. L., Assessing the reactivity of free chlorine constituents Cl2, Cl2O, and HOCl toward aromatic ethers. *Environmental science & technology* **2012,** *46* (4), 2141-2147.